

ACS SYMPOSIUM SERIES **766**

Green Engineering

Paul T. Anastas, EDITOR

White House Office of Science, Technology and Policy

Lauren G. Heine, EDITOR

International Sustainable Development Foundation

Tracy C. Williamson, EDITOR

U.S. Environmental Protection Agency



American Chemical Society, Washington, DC

In Green Engineering; Anastas, P., et al.;
ACS Symposium Series; American Chemical Society: Washington, DC, 2000.



Library of Congress Cataloging-in-Publication Data

Green engineering / Paul T. Anastas, editor, Lauren G. Heine [editor], Tracy C. Williamson, editor.

p. cm.—(ACS symposium series ; 766)

Includes bibliographical references and index.

ISBN 0-8412-3677-1

1. Environmental chemistry—Industrial applications—Congresses. 2. Environmental management—Congresses. I. Anastas, Paul T., 1962– II. Heine, Lauren G., 1957– III. Williamson, Tracy C., 1963– IV. Series.

TP155.2.E58 G76 2000
660'28'6—dc21

00-056579

The paper used in this publication meets the minimum requirements of American National Standard for Information Sciences—Permanence of Paper for Printed Library Materials, ANSI Z39.48–1984.

Copyright © 2001 American Chemical Society

Distributed by Oxford University Press

All Rights Reserved. Reprographic copying beyond that permitted by Sections 107 or 108 of the U.S. Copyright Act is allowed for internal use only, provided that a per-chapter fee of \$20.00 plus \$0.50 per page is paid to the Copyright Clearance Center, Inc., 222 Rosewood Drive, Danvers, MA 01923, USA. Republication or reproduction for sale of pages in this book is permitted only under license from ACS. Direct these and other permission requests to ACS Copyright Office, Publications Division, 1155 16th St., N.W., Washington, DC 20036.

The citation of trade names and/or names of manufacturers in this publication is not to be construed as an endorsement or as approval by ACS of the commercial products or services referenced herein; nor should the mere reference herein to any drawing, specification, chemical process, or other data be regarded as a license or as a conveyance of any right or permission to the holder, reader, or any other person or corporation, to manufacture, reproduce, use, or sell any patented invention or copyrighted work that may in any way be related thereto. Registered names, trademarks, etc., used in this publication, even without specific indication thereof, are not to be considered unprotected by law.

PRINTED IN THE UNITED STATES OF AMERICA

**American Chemical Society
Library**

1155 16th St., N.W.

Washington, D.C. 20036

ACS Symposium Series, American Chemical Society: Washington, DC, 2000.

Foreword

THE ACS SYMPOSIUM SERIES was first published in 1974 to provide a mechanism for publishing symposia quickly in book form. The purpose of the series is to publish timely, comprehensive books developed from ACS sponsored symposia based on current scientific research. Occasionally, books are developed from symposia sponsored by other organizations when the topic is of keen interest to the chemistry audience.

Before agreeing to publish a book, the proposed table of contents is reviewed for appropriate and comprehensive coverage and for interest to the audience. Some papers may be excluded in order to better focus the book; others may be added to provide comprehensiveness. When appropriate, overview or introductory chapters are added. Drafts of chapters are peer-reviewed prior to final acceptance or rejection, and manuscripts are prepared in camera-ready format.

As a rule, only original research papers and original review papers are included in the volumes. Verbatim reproductions of previously published papers are not accepted.

ACS BOOKS DEPARTMENT

Preface

The importance of protecting human health and the environment simply cannot be overstated at the dawn of the 21st century. The beginning of the new millennium comes with unparalleled opportunities and challenges. Science and technology are witnessing the explosion of knowledge and discovery in areas ranging from genomics to nanotechnology, to information technology. At the same time, the daunting threats to sustainability as the world passes a population of six billion people and the growing recognition of the realities of global climate change are enough to give even the most wide-eyed of optimists pause.

However, the work portrayed in this book will illustrate to the reader why some of the people most optimistic about the future are those involved with green engineering. The new perspectives, methodologies, and technologies of green engineering are demonstrating a capability of dealing with some of the greatest challenges to sustainability. Green Engineering is identifying methods of using renewable feedstocks, minimizing energy usage, and decreasing negative impacts on human health and the environment. It achieves these goals while increasing efficiency, productivity, and profitability. The dual goals of environmental and economic benefit are essential to any approach toward sustainability.

PAUL T. ANASTAS¹
White House Office of Science, Technology and Policy
1600 Pennsylvania Avenue
Washington, DC 20500

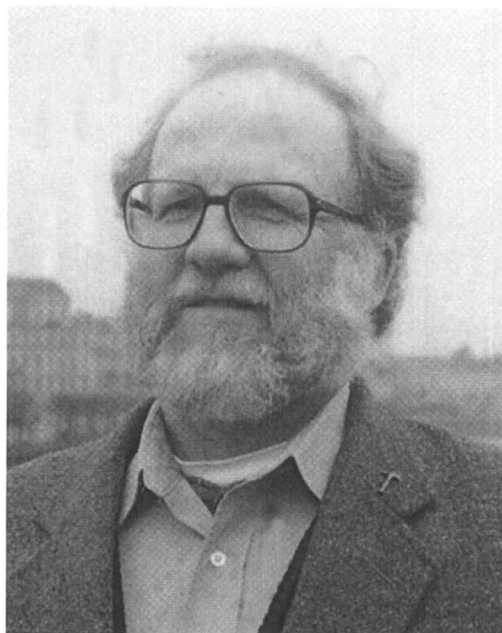
LAUREN G. HEINE
Zero Waste Alliance
International Sustainable Development Foundation
3624 S.W. 10th Avenue
Portland, OR 97201

TRACY C. WILLIAMSON
Industrial Chemicals Branch
U.S. Environmental Protection Agency
Waterside Mall, Mail Code 7406
401 M. Street, SW
Washington, DC 20460

¹Visiting Professor at Department of Chemistry, The University of Nottingham, University Park, Nottingham NG7 2RD, United Kingdom.

Green Engineering

Dedication



A founding co-chair, of the Green Chemistry and Engineering Conference, from which this book is derived, was named after Dr. Joseph J. Breen. Joe Breen was an inspiration to people around the world because of the passion and enthusiasm with which he articulated the need and the goals of green chemistry and engineering for sustainability. Joe's premature death in the summer of 1999 is a tragedy to all who knew him and a loss to the causes he championed. This book is dedicated to the memory of Dr. Joseph J. Breen.

Errata Sheet

ACS Symposium Series 766

Green Engineering

Paul T. Anastas, Lauren G. Heine, and Tracy C. Williamson

On page ii, the Dedication should read as follows: This book is dedicated to the memory of Dr. Joseph J. Breen. Joe Breen was a founding co-chair of the Green Chemistry and Engineering Conference from which this book is derived. He was an inspiration to people around the world because of the passion and enthusiasm with which he articulated the needs and goals of green chemistry and engineering for sustainability. Joe's premature death in the summer of 1999 is a tragedy to all who knew him and a loss to the causes he championed.

On pages xi and 1, the correct addresses for Paul Anastas and Lauren Heine should be the following: Dr. Paul Anastas, White House Office of Science and Technology Policy, Old Executive Office Building, Washington, DC 20502 and Lauren Heine, Zero Waste Alliance, International Sustainable Development Foundation, 121 SW Salmon Street, Suite 210, Portland, OR 97204.

The editors thank Larry Chalfan, Executive Director, Zero Waste Alliance for helping to design the cover.

Chapter 1

Green Engineering: Introduction

Paul T. Anastas¹, Lauren G. Heine², and Tracy C. Williamson³

¹White House Office of Science, Technology and Policy,
1600 Pennsylvania Avenue, Washington, DC 20500

²Zero Waste Alliance, International Sustainable Development Foundation,
3624 S.W. 10th Avenue, Portland, OR 97201

³Industrial Chemicals Branch, U.S. Environmental Protection Agency,
Waterside Mall, Mail Code 7406, 401 M Street, SW,
Washington, DC 20460

The field of engineering, especially chemical engineering, has led the development of environmental technology over the past two generations. The design and implementation of a wide range of treatment and control technologies ranging from smoke-stack scrubbers to water effluent treatment facilities has resulted in dramatic improvement in the quality of the air, water and land, especially in the past thirty years. As the approaches to environmental protection evolved to include pollution prevention, chemical engineering once again produced a wide range of technologies and process changes that allowed, not only the chemical industry, but all industrial sectors that use chemical processes to reduce pollution at the source. This again, resulted in large measurable reductions in releases of toxic substances to the environment.

Today, as environmental protection is continuing to evolve, chemical engineering is once again responding with the innovation and ingenuity that has become a tradition in this field for addressing environmental issues. *Green Engineering, defined as the design of systems and unit processes that obviate or reduce the need for the use of hazardous substances while minimizing energy usage and the generation of unwanted by-products*, is the next generation of environmental protection in chemical engineering. Using the wide array of technologies developed in the past and applying them in new ways to new problems, and inventing and developing new technologies, chemical engineers are not only preventing pollution but are also creating inherently safer chemical processes by reducing the presence of hazards wherever possible.

This book presents a number of the innovations that have been developed recently in the emerging area of green engineering. The chapters of the book are derived from presentations made at the Green Chemistry and Engineering Conference

¹Visiting Professor at Department of Chemistry, The University of Nottingham, University Park, Nottingham NG7 2RD, United Kingdom.

at the National Academy of Sciences, Washington, D.C. This conference was established to highlight the cutting edge science and engineering in this field being conducted in industry, academia and government.

Over the years, the Green Chemistry and Engineering Conference has had different themes. One of those themes was “Implementing Vision 2020 for the Environment”. This theme was based on the document produced by the chemical industry to provide goals for the next twenty years, entitled “Technology Vision 2020: the U.S. Chemical Industry”. Throughout this document, there was a common thread that was woven throughout the goals ranging from new chemical technologies to supply chain issues and this thread was the environment. Throughout all aspects of the chemical enterprise and all of the goals outlined in the report was the recurring and overarching recognition that the environmental impact of all activities must be among the fundamental considerations.

It is because of the ubiquitous need to consider environmental issues in all parts of the chemical industry that Vision 2020 was viewed as an appropriate theme for the conference. It was recognized that the science and technology of Green Chemistry and Engineering was, in real time, implementing or beginning to implement many of the stated goals of ‘Vision 2020’. By developing new separation techniques, new syntheses, new reaction processes, etc., and doing it while engaging in fundamental protection of human health and the environment, Green Chemistry and Engineering was accomplishing, or at least beginning to accomplish, those challenges outlined in ‘Vision 2020’.

Another theme of a Green Chemistry and Engineering Conference was “Global Perspectives”. This conference emphasized the fact that the science and engineering that are the topic of the conference know no boundaries. By featuring presentations from industry, academia, and government, the conference illustrated that Green Chemistry and Engineering is being actively pursued in both the public and private sectors. By featuring talks from disciplines ranging from organic synthesis to biology to electrical engineering and many others, it was demonstrated that this area is not limited by disciplinary bounds. The industrial sectors represented as well spanned well beyond the traditional chemical industry into electronics, pulp and paper, and pharmaceuticals, to name a few. Finally, it was shown that green chemistry and engineering know no national boundaries by representatives from eleven nations around the world taking part in the conference. Therefore, in several ways, one can see that a global perspective can be achieved through the practice of green chemistry and engineering.

Each year an organizing committee with representatives from all parts of the chemical and chemical engineering enterprise convene to construct a conference that will represent some of the most recent, innovative and topical advances in green chemistry and engineering. Those organizations, American Chemical Society, American Institute of Chemical Engineers, Chemical Manufacturers Association, Council for Chemical Research, U.S. Department of Energy, U.S. Environmental Protection Agency, National Academy of Sciences, National Research Council, National Institute of Standards and Technology, and Organization for Economic Cooperation and Development, represent a breadth of essential elements of the

discovery, demonstration, and commercialization of chemical technology. The fine work presented in this volume is a tribute to the work these organizations do in promoting, encouraging, funding, supporting and catalyzing the emerging area of Green Chemistry and Engineering.

Discussion

Green Processing

Source reduction has the highest priority in the Pollution Prevention Act's waste minimization hierarchy since it aims at solving environmental problems at the roots. Effective source reduction relies on a comprehensive and deep analysis of process operations and the development of new processes that reduce and/or eliminate the inherent hazard in processes and products as well as unwanted by-products and co-products. The research and development work presented in this section contributes to greener processing in several important areas of industrial manufacturing.

In the area of coatings, Dong et al. present their work as part of a wider effort to develop a new class of water-borne coatings. They target the use of hybrid miniemulsion polymerization with acrylic monomers in the presence of alkyd and oil-modified polyurethane resins as a replacement for solvent-based coatings.

Nikles et al. contribute to pollution prevention in the magnetic tape industry. Through their work, significant progress has been made toward identifying a binder materials package that enables solventless magnetic tape manufacturing and the subsequent elimination of air pollution from this process.

Bersin of Ulvac Technologies, Inc. describes a process methodology (ENVIRO™) that contributes toward eliminating organic solvents and acids in wafer processing. This technology uses deionized water to dissolve photoresist-ashing residues after plasma etching or ion implantation.

Lou and Huang introduce a novel approach for qualitative and quantitative analyses of clean electroplating operations. Using fundamental engineering principles and practical industrial experience, they developed a computer-aided tool to facilitate effective process analysis for waste reduction in electroplating operations.

Li and Paganessi of Air Liquide address the problem of using strong greenhouse gas, perfluorocompounds, in semiconductor manufacturing. They describe the development of a patented membrane-based recycle system that can capture and concentrate more than 95% of perfluorocompounds from the process exhausts.

Green Applications of Carbon Dioxide

The environmental benefits of using CO₂ as a solvent for processing are augmented by its tunability, the ability to control properties such as solubility, miscibility, rheology, viscosity, molecular density and reactivity. These special properties result in economic benefits as well. In this section, the use of both liquid and supercritical CO₂ are described in processing applications ranging from the

synthesis of chemicals and building materials to the formation of solvent-free drug coatings for pharmaceuticals.

Hâncu et al. describe the environmental and engineering benefits of using supercritical CO₂ as the sole process solvent in several combined reaction/separation processes. In each of the processes described, the use of CO₂ resulted in benefits such as increased product purity, better throughput, and reduced energy input.

Subramaniam et al. describe the benefits of using supercritical carbon dioxide (scCO₂) to produce drug particles and as the fluidizing medium for substrate coating. Coating with scCO₂ allows the use of traditional organic-soluble coatings with complete solvent recovery and virtually no atmospheric emissions.

Hobbs and Lesser describe the effects of drawing fibers of poly(ethylene terephthalate) using a two stage drawing technique. Significant impacts were obtained by drawing fibers first in liquid CO₂.

Roger Jones of Materials Technology Limited describes a manufacturing process by which carbon dioxide is recovered from flue gas, made supercritical, and used to treat pastes derived from fly ash and other dusty wastes to produce several valuable building products. Examples of these products include a lightweight roofing tile that resembles a cedar shake and fiberglass-reinforced ceramic wallboard.

Environmentally Benign Catalysis

One of the principles of Green Chemistry is that “catalytic reagents (as selective as possible) are superior to stoichiometric reagents” (1). The chapters in this section illustrate some of the advancements and challenges of engineering and processing using catalysts.

Chuang et al. probe the mechanism of catalysis for oxidative carbonylation as an alternative, low-pressure pathway for isocyanate synthesis that does not require the use of highly toxic phosgene. They describe catalyst screening studies and estimate the economic viability of the process.

Robert Farrauto of Engelhard Corporation discusses the promise and challenges of three catalyst-based technologies for generating power with improved fuel efficiency and decreased emissions for vehicular and stationary applications. These technologies include the lean burn gasoline and diesel internal combustion engines, the proton exchange membrane fuel cell, and stationary power generation using catalyst assisted thermal combustion.

Marcus and Cormier of PQ Corporation (Zeolyst International) describe the intensive development and commercialization of zeolites of aluminosilicate and other compositions in diverse areas due to their process and environmental advantages. They review the properties of zeolites, and some of the “green” application areas where zeolites are being used.

Flytzani-Stephanopoulos and Zhu describe a single-stage process of catalytic reduction of SO₂ to elemental sulfur as a promising new technology. This process is better suited to handle SO₂-laden streams generated in power plants and certain industries than the conventional multi-stage Claus process.

Ribeiro and Somorjai explore the kinetics for the hydrodechlorination of chlorofluorocarbons over model palladium catalysts. This chemistry is important in the manufacture of many new compounds that use hydrodechlorination as an intermediate step.

Separations

One area of opportunity for new chemical science and engineering technology which will help meet the goals of the U.S. Chemical Industry's *Technology Vision 2020*, and facilitate movement towards sustainability, is the development of new separations technologies that eliminate the use of flammable, toxic volatile organic compounds (VOCs) as industrial solvents. Spear et al. describe a portion of their work in the area of separation science and technology geared toward replacement of VOCs in industrial scale liquid/liquid or chromatographic separations using water-soluble polyethylene glycol polymers. They also discuss the use of air and moisture stable, water immiscible, room temperature ionic liquids.

Harten et al. at the National Risk Management Research Laboratory (NRMRL) of the U.S. Environmental Protection Agency describe new separations materials and processes for removal and recovery of VOCs and toxic metals from waste streams and industrial process streams. Such separations technologies enable process lines to more closely approach zero emission through in-process recycling and reuse of resources that would otherwise be emitted to air, water, and solid wastes.

Conclusion

The chapters in the book serve to illustrate some of the examples of green engineering that are being researched and developed in academia, as well as being developed in industry. Also recommended to the reader is an accompanying volume entitled, "Green Chemical Syntheses and Processes" that provides a complementary treatment of the area of green chemistry that works together integrally with green engineering.

Literature Cited

1. Anastas, P.T. and Warner, J.C. (1998). *Green Chemistry: Theory and Practice*. Oxford University Press, Oxford.

Chapter 2

Novel Waterborne Coatings via Hybrid Miniemulsion Polymerization

H. Dong¹, J. W. Gooch², G. W. Poehlein², S. T. Wang², X. Wu²,
and F. J. Schork^{2,3}

¹Schools of Textile & Fiber Engineering and ²Chemical Engineering,
Georgia Institute of Technology, Atlanta, GA 30332-0100

As part of a wider effort to develop a new class of water-borne coatings, hybrid miniemulsion polymerization was carried out with acrylic monomers (methyl methacrylate, butyl acrylate and acrylic acid) in the presence of alkyd and oil-modified polyurethane resins. Latexes with different ratios of resin to acrylic monomers were synthesized. The monomer emulsions prepared for hybrid miniemulsion polymerization showed excellent shelf-life stability (up to 5 months) and the polymerization was run free of coagulation. Solvent extraction indicated that the grafting efficiency of polyacrylics was greater than 20% for all the samples produced. ¹³C solution NMR spectrum showed that a substantial fraction of the original carbon double bonds (>60%) in the resin remained after polymerization for film curing. Films obtained from the latexes showed good adhesion and fair hardness properties. Alkyd/acrylate coatings are targeted as a replacement for solvent-based architectural coatings, and oil-modified polyurethane/acrylate coatings may provide a low VOC alternative to solvent-based clear coats.

Water-based coatings have become more widely used in the past several decades because they are environmentally friendly, offer easy clean up and, their properties and application performance characteristics have improved. Solvent based systems such as alkyd resins and polyurethanes have remained important for some applications because of superior properties such as gloss and hardness. This is due to curing mechanism of oil-based coatings in which the oils react with atmospheric oxygen to form very hard crosslinked materials. This mechanism is generally lacking in water-based coatings which tend to be soft and pliable, due to the fact that, the coatings are made soft to allow film formation, and, since there is no curing chemistry available, remain soft on drying. This work reports on the graft copolymerization of acrylic monomers in the presence of alkyd and polyurethane resins to develop alternative coatings which have the advantages

³Corresponding Author.

of water-based systems (low VOC, etc.) with the drying (air cure) properties of solvent-based systems. It has been shown that conventional emulsion polymerization cannot be used to produce these materials; it is necessary to employ a miniemulsion polymerization technique. Alkyd/acrylate coatings are targeted as a replacement for solvent-based architectural coatings, and oil-modified polyurethane (OMPU)/acrylate coatings may provide a low VOC alternative to solvent-based clear coats. Since U.S architectural coating sales in 1995 amounted to 625 million gallons, a conservative estimate of the VOC reduction if all of these coatings were water-based is approximately 500 million pounds of solvent that would not be released into the air.

Emulsion and miniemulsion polymerizations have many similarities, but particle nucleation and monomer transport are very different. Conventional emulsion polymerization is started with a monomer emulsion comprised of relatively large (in the range of 5-10 microns) monomer droplets and significant free or micellar surfactant. Particle nucleation takes place early in the reaction via homogeneous (water phase) polymerization followed by precipitation, or via free radical entry into monomer-swollen micelles. Radicals can enter the monomer droplets, but this phenomenon is generally discounted because of the relatively small droplet surface area. Nucleation stops or slows significantly after the surface area of the particles becomes sufficient to adsorb all of the surfactant from the micelles. The major locus of polymerization thereafter is in the nucleated particles. The monomer must move from the monomer droplets to the reaction sites in the particles by diffusion.

In miniemulsion polymerization, an effective surfactant/hydrophobe system is used to stabilize very small monomer droplets (50–500 nm). In order to break up monomer droplets to such size, high agitation is applied by sonication or homogenization. (1). The hydrophobe (also known as a cosurfactant) is a highly monomer-soluble, highly water-insoluble material added to increase diffusional stability of the emulsion. Usually long-chain alkanes such as hexadecane or long-chain alcohols such as cetyl alcohol are employed as hydrophobes (2,3). Because these hydrophobes cannot diffuse readily through the aqueous phase (due to their extremely low water solubility), removing monomer from a small monomer droplet will cause an increase in the concentration of the hydrophobe, with a resultant increase in the free energy. Therefore, the use of a hydrophobe will significantly retard, or even prevent Ostwald ripening (transfer of monomer from small droplets to large droplets to reduce the total surface energy of the system), and thus keep the small droplets stable during polymerization. For an ideal miniemulsion polymerization, there is no mass transport involved. The large droplet surface area in miniemulsions (because of small droplet size) results in most of the surfactant being adsorbed to the droplets with little free surfactant available to form micelles or stabilize aqueous phase polymerization. Therefore, the predominant nucleation mechanism in miniemulsion polymerization is droplet nucleation. This is exactly what is desired for the current application, since if there is significant micellar or homogeneous nucleation, particles will be formed which contain little or no resin. The total water-insolubility of the resin makes it difficult for diffusion of the resin from the monomer droplets to the particles that are the loci of polymerization. In contrast, in miniemulsion polymerization, polymerization takes place in the (very small) droplets,

in the presence of the resin, and without the need for diffusion of the resin across the aqueous phase. If a conventional emulsion polymerization were run in the presence of the water-insoluble resin, the result would be polyacrylic particles in a physical blend with dispersed resin, with very little chance of grafting between the two species. Miniemulsion polymerization in the presence of an additional resin for the purposes of grafting will be termed hybrid miniemulsion polymerization.

Wang et al. (4) have reported the grafting of alkyd resin into water-based acrylic coatings. Dong et al. (5) have reported the incorporation of oil modified polyurethane (OMPU) in a similar system. This paper will serve to compare and contrast these two works, and to draw some conclusions about the future of these hybrid materials.

Experimental

Materials

Alkyd resin was supplied by McWhorter Technologies as Durama 2768 which contains 80% durable medium soya-linseed alkyd and 20% solvents, i.e., 6.3% n-butyl acetate, 4.4% xylene, 2.9% solvent naphtha (petroleum), 5.2% trimethylbenzene, and 0.9% ethylbenzene. The solvents were removed by vacuum distillation before use. Oil-modified polyurethane 138-0634 supplied by McWhorter Technologies was used as the OMPU. This resin contains 60% solid linseed modified polyurethane, 20% solvent naphtha (heavy alkylate), 20% naphtha (hydrotreated heavy), 0.07% dibutyl tin oxide and 0.03% triphenyl phosphite. The polyurethane portion was made from TDI (toluene diisocyanate), and no free TDI was left unreacted. The solvents were removed by vacuum evaporation before use. Methyl methacrylate (MMA), butyl acrylate (BA), acrylic acid (AA), potassium persulfate (KPS) (all from Aldrich), sodium lauryl sulfate (SLS) (Fisher), and benzoyl peroxide (BPO) (Fisher) were used as supplied. The water is deionized.

Emulsion Preparation and Polymerization

The miniemulsions were prepared by dispersing the desired amount of monomer-resin solution in the aqueous SLS solution by mixing with a stirrer at room temperature. The resulting emulsion was sheared further by sonication. The monomer miniemulsion was transferred to a flask which was equipped with nitrogen inlet-outlet tube, condenser, and mechanical stirrer. The system was purged with nitrogen heated to 60 or 80 °C. Agitation was provided by a paddle stirrer. The polymerization was started by injection of KPS solution. When BPO was present in the monomer mixture the polymerization started during the heating period. The reaction was followed by determining the change in the fraction of volatiles in the emulsion as the (volatile) monomer is converted to (nonvolatile) polymer.

Table I. Recipe for Hybrid Miniemulsion Polymerizations Containing Alkyd

<i>Run</i>	<i>MMA</i> ¹	<i>BA</i> ¹	<i>AA</i> ¹	<i>Alkyd</i> ²
MA00	45	50	1.0	0.0
MA30	45	50	1.0	30
MA60	45	50	1.0	60
MA100	45	50	1.0	100

SLS: 0.02 mol/L water. KPS: 0.04 mol/L water. Total solids: 29 wt%. BPO: 0.5 wt% based on total acrylate.

1. %wt of total acrylate, including 4 wt% polymethyl methacrylate (PMMA) used as a cosurfactant.
2. %wt based on total acrylate.

Table II. Recipe for Hybrid Miniemulsion Polymerizations Containing Oil Modified Polyurethane

<i>Run</i>	<i>MMA</i> ¹	<i>BA</i> ¹	<i>AA</i> ¹	<i>OMPU</i> ²
1	49	50	1.0	100
2	49	50	1.0	60
3	49	50	1.0	30

SLS: 0.02 mol/L water. KPS: 0.04 mol/L water. Total solids: 33.3 wt%. BPO: 0.5 wt% based on total acrylate.

1. %wt of total acrylate.
2. %wt based on total acrylate.

Droplet and Particle Size

Monomer droplet and particle sizes were measured by quasi-elastic light scattering with a Malvern Autosizer IIc. The measurement process for monomer droplets involved dilution of the emulsion with a monomer-saturated solution of 0.1% SLS to about 50:1. Then this diluted emulsion was put into a quartz cuvette and the droplet diameter, distribution and standard deviations were recorded in five minutes. The latex particle size was measured in the same way but the dilution with the 0.1% SLS solution was 100:1.

Shelf-life Stability

Emulsion and latex shelf-life were measured by placing approximately 30 mL of sample in a capped glass vial and observing the time necessary for a visible creaming line to appear. Two drops of a water-soluble red pigment solution were added to each sample to increase the contrast between phases.

Double Bond Content Analysis

The double bond content in the resin-monomer mixtures and in the graft copolymers were measured by ^{13}C -NMR. Chloroform was used as an internal standard for all NMR spectra.

Degree of Grafting and Degree of Crosslinking

Solvent extraction experiments were performed in a Soxhlet extractor with approximately 0.5 g dried latex. Ethyl ether was applied for 24 hours. All resin and grafted copolymer were assumed to be dissolved completely. Grafting efficiency was calculated from the quantity of polymer extracted. Chloroform, toluene, tetrahydrofuran (THF) and 1,4-dioxane were used sequentially in an exhaustive extraction to determine the percentage of the polymer which was crosslinked. Each solvent was applied for 12 hours. Material which remained after extraction with the four solvents was considered to be crosslinked.

Film Hardness and Adhesion

Film hardness testing was determined by the Pencil Test (ASTM D 3363-74), and film adhesion was measured by the Tape Test (ASTM D 3359-78). These films were cast from latex with 1-5% hydroxyethyl cellulose added as a thickener. The films were dried at room temperature.

Results and Discussion

Droplet and Particle Size

For both systems (alkyd and OMPU), droplet sizes ranged from 90 to 260 nm. Droplet size was influenced by duration and intensity of shear, level of cosurfactant (PMMA), and level of resin (alkyd or OMPU). Increased length and intensity of shear developed smaller particles, as did the inclusion of polymethyl methacrylate (PMMA) as a cosurfactant. The inclusion of PMMA was not entirely necessary, as both resins act as cosurfactants. Droplet size decreased with increasing level of resin.

Polymerized polymer particles size correlated well with monomer droplet size, implying predominant droplet nucleation. Particle size ranged from 110 to 240 nm.

Shelf-Life Stability

Shelf life stability varied with resin level. With adequate sonication and 60 to 100% (based on total acrylate) resin, shelf lives ranged from one to greater than five months. Shelf life is determined by two factors. The first is Stokes law creaming; small droplets will cream much more slowly, and droplets of approximately 1 to 200 nm diameters will be prevented by Brownian motion from creaming at all. The second is Ostwald ripening. If significant ripening takes place, droplets will grow into the range where Stokes law creaming is significant, and visible creaming will occur. The long shelf lives exhibited by these materials indicate small initial droplet size and effective retardation of Ostwald ripening, allowing the monomer droplets to remain small enough so that droplet nucleation predominates.

Polymerization

Figures 1 and 2 show the conversion-time curves for the hybrid miniemulsion polymerization of alkyd and OMPU, respectively. Some features are common to both systems. First, complete conversion is not achieved, even at 80 °C. Second, the rate of polymerization goes down as the level of resin is increased. This suggests that the resin might be retarding the polymerization. Both the alkyd and OMPU contain unsaturated vegetable oils containing linolenic, linoleic and oleic fatty acids. During polymerization, grafting can occur by chain transfer from the propagating free radical to double bonds on the fatty acid portion of the resin (6). The resulting fatty acid radical may be substantially less reactive than the acrylic radical, resulting in a reduction in polymerization rate. This resin inhibition can be overcome to some extent by using a high polymerization temperature (80 °C) and mixed (KPS and BPO) initiator.

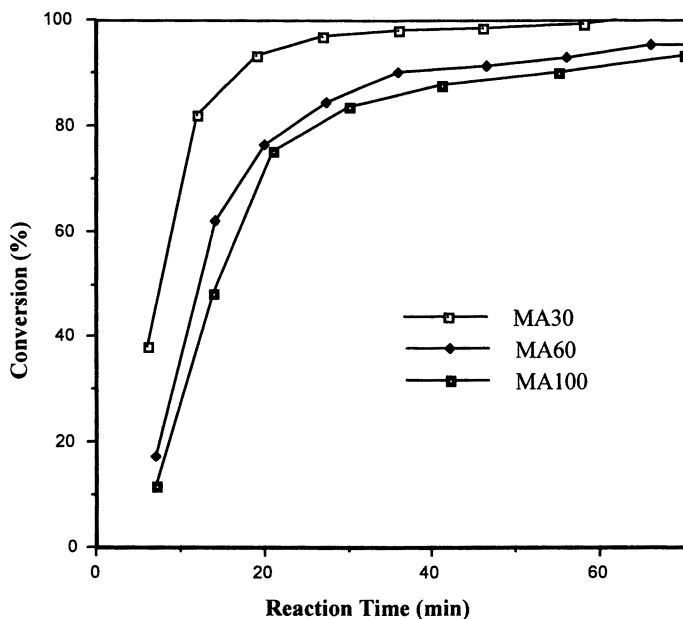


Figure 1. Conversion-Time Profiles for Alkyd/Acrylate Hybrid Miniemulsion Polymerization at 80 °C

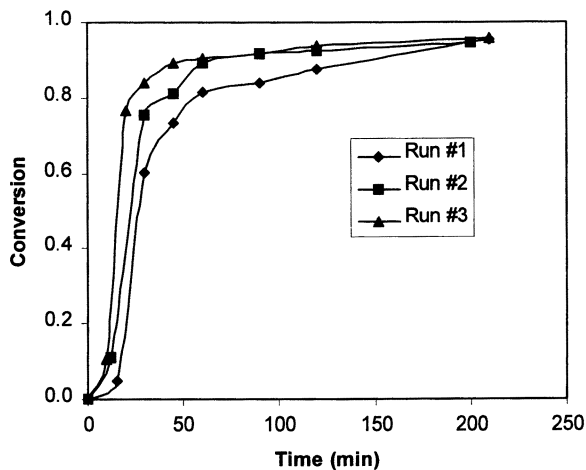


Figure 2. Conversion-Time Profiles for OMPU/Acrylate Hybrid Miniemulsion Polymerization at 80 °C

Residual Double Bond Content Analysis

The residual double bond content was determined for both hybrid materials. For the alkyd/acrylate hybrid, the residual double bond content was 70 to 80%. For the OMPU hybrid, the residual double bond content was 60 to 70%. This means that in both materials, between 60 and 80% of the original double bonds in the fatty acid components remained after polymerization. This is critical, since these residual double bond are necessary to participate in the film "drying" reactions. In these reactions, residual double bonds in the fatty acid components react with atmospheric oxygen to form crosslinks. It is these crosslinks that give alkyd or oil-based coatings their desirable hardness.

Degree of Grafting and Degree of Crosslinking

For both materials, the degree of grafting was determined by selective extraction. Degree of grafting is defined as the percent of the polyacrylate which is grafted to alkyd or OMPU. For the alkyd/acrylate hybrid, the degree of grafting ranged from 20 to 70%, with materials containing higher levels of alkyd having higher levels of grafting. For the OMPU/acrylate hybrid, the degree of grafting ranged from 30 to 60%, again with materials containing higher levels of resin having a higher levels of grafting. In all cases, the level of grafting was significant. This is important, since the acrylate and resin may be incompatible. Significant levels of grafting will prevent phase separation into acrylate-rich and resin-rich phases.

Degree of crosslinking is defined as the percentage of total polymer which is insoluble after exhaustive extraction. For both the alkyd/acrylate and OMPU/acrylate hybrid materials, degree of crosslinking was below 5%. This is significant, since a high level of crosslinking during polymerization will result in poor film formation, and poor film properties.

Film Hardness and Adhesion

The alkyd/acrylate materials, when cast into films, were found to be of approximately "B" hardness. Addition of standard metal drying catalysts ("dryers") increased film hardness to "H" or even "2H". The OMPU/acrylate materials also had a "B" hardness. Addition of dryers increased film hardness to "HB." These hardnesses are not particularly high, but represent a starting point for developing the higher hardnesses desired for commercial coatings. Film hardness may be increased by changing the fatty acid component of the resin, adding different levels and types of dryers, and by increasing the glass transition temperature of the acrylate component. Adhesion was good (4-5 on a 1-5 scale) for all materials.

Conclusions

The hybrid miniemulsion polymerization process has been shown to have a promising role in converting solvent-based coatings into environmentally-friendly water-based coatings. Alkyd/acrylate coatings are targeted as a replacement for solvent-based architectural coatings, and OMPU/acrylate coatings may provide a low VOC alternative to solvent-based clear coats. A wide range of coatings resins might be used in this way, providing they are highly water-insoluble and highly monomer-soluble in order to act as good hydrophobes. There are a number of advantages associated with hybrid miniemulsion polymerization. First, it is a very stable process without coagulation and flocculation. Second, the robust droplet nucleation makes it easier to control the particle number and particle size during the production process. It also enhances the likelihood that the composition of each particle is the same as formulated. Due to the extremely low water solubility of the resin, and its resultant extremely retarded transport across the aqueous phase, hybrid miniemulsion polymerization provides a means of incorporating resins which could not be incorporated by conventional emulsion polymerization. Finally, by employing resin as both reactant and hydrophobe, higher purity of product can be achieved, since no additional hydrophobe is required.

Films obtained from the acrylic/OMPU latexes show good adhesion and fair hardness. Mixed metal drying agents can enhance the drying rate substantially. Problems remaining to be solved include increasing rate of polymerization and reducing residual monomer content in spite of the inhibitory nature of the alkyd or OMPU resin, and increasing film hardness.

Acknowledgments

The financial support of the Environmental Protection Agency (Grant No. 825326010), the Hoechst Celanese Corporation and the Georgia Tech Foundation are gratefully acknowledged.

Literature Cited

1. P. L. Tang, E. D. Sudol, M. E. Adams, C. A. Silebi, and M. S. El-Aasser, *Polymer Latexes*, American Chemical Society, Washington, D.C., 1992, p. 74.
2. B. J. Chamberlain, D. H. Napper, and R. G. Gilbert, *J. Chem. Soc. Faraday Trans. I*, 78, 591 (1982).

3. Y. T. Choi, M. S. El-Aasser, E. D. Sudol, and J. W. Vanderhoff, *J. Polym. Sci.(Polymer Chem.)* 23, 2973 (1985).
4. S. T. Wang, F. J. Schork, G. W. Poehlein, and J. W. Gooch, *J. Appl. Polym. Sci.*, 60, 2069 (1996).
5. Dong, H. Gooch, J. W. and F. J. Schork: "Water-Borne Oil-Modified Polyurethane Coatings via Hybrid Miniemulsion Polymerization," *J. Appl. Polym. Sci.*, (in press).
6. G. Odian, *Principles of Polymerization*, Wiley, New York, 1991, p. 716.

Chapter 3

Pollution Prevention in the Magnetic Tape Industry: Solventless Coating Formulations for Magnetic Tape Manufacture

David E. Nikles, Matthew M. Ellison, Jin Young Huh, James P. Parakka, and Adam Power

Department of Chemistry and Center for Materials for Information Technology, The University of Alabama, Tuscaloosa, AL 35487-0209

Significant progress has been made toward identifying a binder materials package that enables solventless magnetic tape manufacturing and subsequently eliminate the possibility of air pollution. Mixtures of commercial acrylate monomers and acrylate-terminated urethane oligomers were cured by electron beam irradiation, resulting in films with good tensile properties and adequate adhesion to the polyester base film. The binder polymers suffered no significant decrease in tensile strength after accelerated aging at 60°C and 90% relative humidity. Commercial magnetic particles were treated with a methacrylate-functionalized silane coupling agent, which enabled the preparation of dispersions with rheological properties that approach those of conventional solvent-based formulations. A comparison of the economics of the solventless process with a conventional solvent-based process, showed the solventless process could be slightly lower in cost.

Introduction

Magnetic tape consists of a magnetic coating on a polyester base. The coating contains magnetic particles held to the base with a polymeric binder and other additives, such as lubricants, carbon black and alumina (*1*). Magnetic tape is

manufactured by a continuous web coating process. Polyester base film is coated with a fluid that contains a dispersion of the magnetic particles in a mixture of organic solvents. The fluid also contains dissolved binder polymers, cross-linking agents, lubricants, and other additives. The coating is applied by either reverse roll coating, gravure, or slot die techniques. Immediately after coating, the wet film passes through a magnetic field that orients the pigment particles. The film then enters a drying oven, where it is dried under a stream of hot air. The web leaves the oven and is either wound onto a reel, or calendered on-line to compact the magnetic coating and smooth the surface. The cured, calendered web is then slit to the required width and wound onto a reel for packaging.

The organic solvents used in magnetic tape coating formulations include 2-butanone (MEK), 4-methyl-2-pentanone (MIBK), tetrahydrofuran (THF), toluene, and cyclohexanone. These solvents present an occupational hazard to the workers and emissions hazard to the environment. MEK, MIBK, and toluene are on the list of 189 hazardous air pollutants and on the list of 18 for the EPA's 33/50 voluntary pollution reduction program (2). In modern tape manufacturing plants the solvent vapors from the drier are recovered by use of a carbon bed adsorber, which is stripped by steam. The steam is condensed or is put through a distillation column. This allows recovery and reuse of the individual components. However, the water has trace levels of organics and must be properly disposed. The coating operations meet EPA air emission standards. Considerable capital equipment is required to contain and recycle the organic solvents. Furthermore, maintaining the emission prevention equipment adds complexity to the tape manufacturing process. We have estimated that a modern tape coating line uses more than 650 kg of solvent per hour (3,4). Industry sources tell us that in modern tape coating operations 93 to 95% of the solvents are captured, which means that 5 to 7% are released to the environment. Assuming two, eight-hour shifts per day and 250 work days per year, a coating operation may release 130 to 180 metric tons of solvents per year. With more stringent federal regulations on emission controls, tape manufacturers may be forced to install even more capital equipment to comply with the regulations. Alternatively, they may be forced to shut down their operations and move offshore. The U. S. can not afford to lose manufacturing jobs, particularly in a high technology industry that plays an important role in the information superhighway. If there were alternative magnetic tape coating processes that avoid using organic solvents, the considerable capital expense, required in capturing the organic solvents, would be eliminated. The industry would be in a better position to maintain compliance to any present or future emissions regulations. The concept of pollution prevention, instead of pollution control, would be realized.

The objective of our research program is to lead the magnetic tape industry into the 21st century by providing new tape manufacturing processes that prevent air pollution. Our approach has been two-fold: waterborne coating formulations and solventless, electron beam-cured formulations. In the waterborne tape coating process, the organic solvents are replaced with water, thereby preventing pollution. We have demonstrated a waterborne video tape formulation, prepared tape in a pilot tape-coating trial at a commercial tape manufacturer, and demonstrated an economic

incentive to adopt the waterborne coating process (3,4). Here we report research directed at a solventless magnetic tape manufacturing process, where the organic solvents are replaced with a mixture of liquid acrylate monomers. The monomers serve as a solvent to disperse the magnetic pigment and dissolve any oligomers, rendering fluidity and coatability to the formulation. After coating and electron beam, irradiation the acrylates polymerize to give the binder.

To realize a solventless, electron beam-cured magnetic tape manufacturing process a number of materials problems must be solved. First, a mixture of acrylate monomers and oligomers must be identified that will undergo free radical polymerization upon electron beam irradiation to give a binder polymer with the requisite mechanical properties. The tensile properties of commercial tape are trade secrets and each tape manufacturer has its own specification. For our purposes, we have measured the tensile properties of a unpigmented, commercial, organic solvent-based binder system and found a tensile strength of 18 MPa, a Young's modulus of 710 MPa, and an elongation at break of 60%. These will be used as a guide for identifying electron-beam cured binders. The binders must provide good adhesion between the magnetic coating and the polyester base film. The International Standards Organization has set a specification of a peel force of 0.96 N for 8 mm helical scan tape in a 180° peel test (5). In modern magnetic tape, the particle loading exceeds 30 volume percent and this limits the amount of liquid monomer that can be used in the coating fluid. In turn this limits our ability to dilute the coating formulation to the desired viscosity and leads us to expect that there will be a rheology problem with the coating fluid. Another problem is cupping, which is a curling of the tape about an axis parallel to the longitudinal direction. Cupping arises from the stresses developed in the tape due to excessive shrinkage in the coating during curing. Cupping can lead to edge wear, generating debris that spreads throughout the tape system. After the tape has been coated and cured, the next process step is calendaring to compact the coating and impart a smooth surface finish. The binder must be designed so that the electron beam-cured films can be calendared. An additional consideration is the toxicity of the monomers. We do not want to solve an air pollution problem, but create a worker exposure hazard problem.

Here we report progress toward a solventless magnetic tape manufacturing process. We have prepared a series of electron beam cured acrylate binders, developed a procedure for attaching acrylate-functionalized silane coupling agents to commercial iron particles, prepared solventless dispersions, characterized their rheological properties and prepared electron beam cured magnetic tape coatings. We also report a comparison of the potential costs for a solventless, electron beam cured coating process and the costs for a conventional solvent-based process.

Experimental

The acrylate monomers and oligomers used in this study are listed in Table I. These were commercially available and donated from either Sartomer or UCB Radcure. Unpigmented binder films were prepared by mixing the acrylates and

casting films on glass substrates using a Gardner blade. The films were cured using an Energy Science, model CB-150 Electrocurtain, electron beam processor. The acceleration voltage was 150 keV, while the dose was 3 Mrad. The cured films were lifted from the glass, cut into dog-bone shaped test pieces and their tensile properties were measured on an Instron Universal Tensile Tester using an ASTM procedure (6). Adhesion was measured by a 180° peel test on the Instron Universal Tensile Tester, using the procedure described in the ISO standard (5). Binder films were exposed to 60°C and 90% relative humidity in a Tenney model Th Jr temperature-humidity chamber.

Table I. Acrylate Monomers and Oligomers

<i>Acrylate</i>	<i>Description</i>	<i>Vendor</i>
SR 395	isodecyl acrylate	Sartomer
SR 506A	isobornyl acrylate	Sartomer
SR 306	tripropylene glycol diacrylate	Sartomer
SR 9003	propoxylated neopentyl glycol diacrylate	Sartomer
OTA 480	Triacrylated monomeric glycerol derivative	UCB Radcure
SR 9035	highly ethoxylated trimethylolpropane triacrylate	Sartomer
CN965A80	aliphatic urethane diacrylate with 20% SR 306	Sartomer
Ebacryl 8402	aliphatic urethane diacrylate	UCB Radcure

The magnetic particles were a commercial grade of iron particles for high performance metal particle tape. These particles came with an amorphous aluminum oxide coating that protected them against corrosion. The average particle size was 200 nm, the coercivity was 1500 Oe and the saturation magnetization was 122 emu/g. These particles were surface treated with a methacrylate-functionalized silane coupling agent, Z-6030 from Dow Corning. A mixture of 1.00 g particles, 10 g of toluene and 0.05 g Disperbyk-111 (Byk-Chemie) were sonicated in a glass vial for 30 seconds. Then 0.5 g of 6 N ammonium hydroxide and 0.2 g Z-6030 were added, the vial was closed and agitated on a wrist-action shaker for three days. After three days the particles were allowed to settle and the supernatant liquid decanted away. The particles were washed four times with ethanol and then four times with acetone. They were then dried at 60°C for 24 hr.

Magnetic dispersions were prepared by ball milling 27 g of the surface treated particles with 0.1 g DisperByk-111 and 26 g of the acrylate Formulation 1 in Table II. Stainless steel beads, 2 mm diameter were used for the grinding medium and the milling was continued for 24 hr. Magnetic coatings were cast onto polyester base film by hand draw-down and the films were cured by a 3 Mrad, 150 keV electron beam dose.

The rheological properties of the magnetic dispersions were characterized by oscillating shear rheometry using a Haake RS-100 oscillating shear rheometer. Elastic (G') and viscous (G'') moduli were measured as a function of frequency. TGA curves were obtained under nitrogen with a heating rate of 20°C/min on a TA Instruments model 2850 thermogravimetric analyzer. Magnetic hysteresis curves

were obtained on a digital measurement systems model 880 vibrating sample magnetometer. The magnetometer was calibrated using a high purity nickel standard.

Results and Discussion

In the 1980's the tape industry examined the use of electron beam curing for either magnetic tape or floppy disk manufacture. These were solvent-cast formulations featuring acrylate-terminated urethane oligomers (7-10). The object was to improve the durability of the tape. There was a discussion of the possibility of 100% solids formulations, however at the time this was not thought to be a priority (11).

Table II. Acrylate Formulations

<i>Formulation</i>	<i>Oligomer</i>	<i>Diacrylate</i>	<i>Triacrylate</i>	<i>Monoacrylate</i>
1	CN 965 A80 (31%)	SR 9003 (62%)	SR 9035 (3.5%)	SR 506 A (3.5%)
2	Ebacryl 8402 (30%)	SR 9003 (60%)	SR 9035 (5%)	SR 395 (5%)
3	Ebacryl 8402 (30%)	SR 9003 (60%)	SR 9035 (3%)	SR 395 (7%)
4	Ebacryl 8402 (40%)	SR 9003 (50%)	SR 9035 (5%)	SR 395 (5%)
5	Ebacryl 8402 (20%)	SR 9003 (70%)	SR 9035 (5%)	SR 395 (5%)
6	CN 965 A 80 (30%)	SR 9003 (60%)	OTA 480 (5%)	SR 506A (5%)
7	CN 965 A 80 (40%)	SR 9003 (50%)	OTA 480 (3%)	SR 506A (7%)
8	CN 965 A 80 (25%)	SR 9003 (65%)	OTA 480 (7%)	SR 506A (3%)
9	CN 965 A 80 (20%)	SR 9003 (70%)	OTA 480 (3%)	SR 506A (7%)
10	CN 965 A 80 (35%)	SR 9003 (55%)	OTA 480 (7%)	SR 506A (3%)
11	Ebacryl 8402 (35%)	SR 9003 (50%)	OTA 480 (8%)	SR 395 (7%)
12	CN 965 A 80 (35%)	SR 9003 (55%)	OTA 480 (8.75%)	SR 395 (1.25%)

Table III. Tensile Properties of the Cured Acrylate Formulations

<i>Formulation</i>	<i>Tensile Strength (MPa)</i>	<i>Young's Modulus (MPa)</i>	<i>Elongation at Break (%)</i>
1	12±1	100±3	12±3
2	21±2	227±44	48+10
3	28±3	276±78	40±6
4	29±6	374±115	34±8
5	22±1	311±46	36±17
6	28±4	158±38	28±4
7	29±3	133±37	28±4
8	21±4	167±32	21±1
9	20±2	100±24	32±6
10	35±11	226±65	17±1
11	23±2	80±20	33±4
12	29±1	967±571	12±2

Acrylate Formulations

We have used the earlier work as a starting point and have identified some promising formulations. Table II lists commercial acrylate monomers and oligomers, including mixtures of monoacrylates, diacrylates, triacrylates and acrylate-terminated urethane oligomers (12,13). The aliphatic urethane diacrylate oligomers include Ebacryl 8402, from UCB Radcure, and CN 965A80, from Sartomer, and are used to add strength to the cured coatings. The acrylate monomers were chosen to minimize viscosity, allow fast curing, with low shrinkage and low toxicity. The diacrylates and triacrylates increase the curing speed. The monoacrylates are used as reactive diluents to lower the viscosity. The tensile properties of the cured films produced from the formulations in Table II are listed in Table III. The tensile strength for all formulations, except Formulation 1, exceeded our target of 19 MPa. Only Formulation 12 had a Young's modulus that exceeded our target of 710 MPa. We realize that each media manufacturer has proprietary specifications. Therefore we provide a menu of different formulations with tensile and thermal properties. Interested manufacturers could use that menu as a starting point for designing their own formulations.

We chose Formulation 1 to begin particle dispersion experiments. First we carried out a preliminary accelerated aging study of this formulation. Exposure to 60°C and 90% relative humidity revealed no significant degradation in tensile strength as indicated in Figure 1. We conclude that this class of binders does not present an undue environmental stability problem at this time. We will revisit this issue later in the project when we have further defined the binder materials package.

Solventless Dispersions

Our first attempts to prepare pigmented, solventless formulations demonstrated the severity of the rheology problem. In magnetic tape the signal comes from the

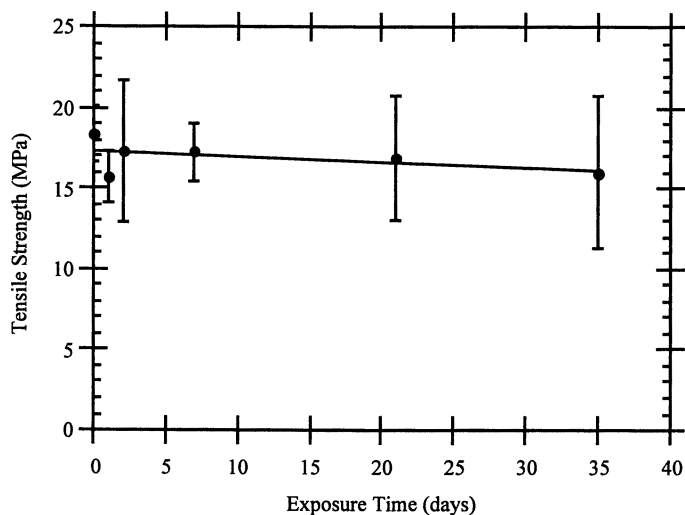


Figure 1. Plot of tensile strength for an electron beam cured films of formulation 1 as a function of time exposed to 60°C and 90% relative humidity.

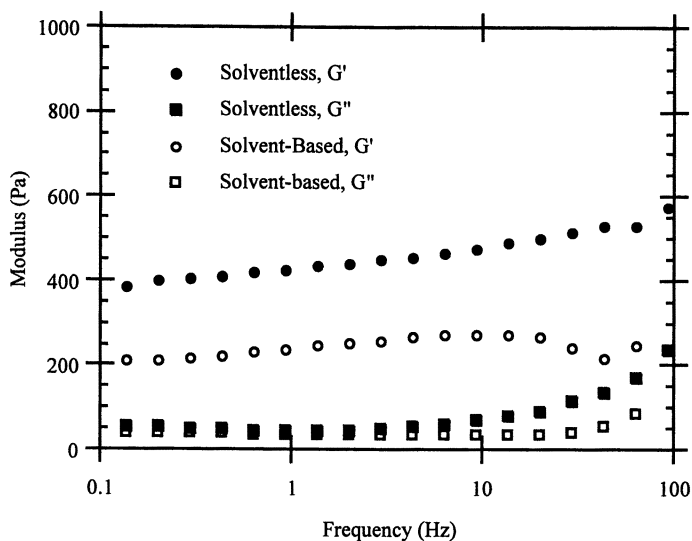


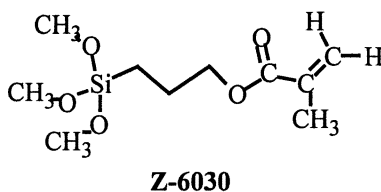
Figure 2. Plot of elastic modulus (G') and viscous modulus (G'') as a function of frequency for the conventional solvent-based formulation and the solventless formulation, containing 50 weight percent treated particles.

magnetic particles and in order to maximize the signal, the particle fraction must be as large as possible. A typical magnetic tape had 30 volume percent particles, which means the coating fluid must contain 30 volume percent particles, or about 80 weight percent. The iron particles, with a specific surface area of 54 m²/g, adsorbed all the liquid in our first formulation after predispersing for 1.5 hr in a double planetary mixer. The dispersion had the consistency of brick dust, not at all satisfactory for coating.

The commercial acrylate-functionalized silane coupling agent, Z-6030, was covalently bonded to the surface of the iron particles. The original purpose was to use the magnetic particles to mechanically reinforce the binder by linking the binder to the particles. The commercial iron particles had a protective coating containing amorphous aluminum oxide.

We assumed that the surface contains hydroxyl groups that can react with silanol groups from the coupling agent. This is standard silane coupling agent chemistry, with an important difference. The coupling agent chemistry worked out for fiberglass surfaces uses an acid catalyst, usually acetic acid. When the iron particles were exposed to these acid conditions they rapidly corroded. The key step in the reaction between the coupling agent and the particle surface was the hydrolysis of the methoxy groups. After hydrolysis the silanol groups condensed to form a silicone polymer. The polymer adsorbed onto the particle surface and condensed with surface hydroxyls, thereby anchoring the coupling agent to the particle surface. The hydrolysis reaction can be catalyzed by acid or by base. Without particles, the reaction was followed by ¹H NMR spectroscopy and required five to six hours, regardless of the choice of solvent (cyclohexanone, 95% ethanol, tetrahydrofuran or toluene) or choice of catalyst (acetic acid, boric acid, or ammonium hydroxide). Since the particles were sensitive to acid, we pursued reactions catalyzed by ammonium hydroxide. After treatment the particles had a saturation magnetization of 110 emu/g, a loss of 17%. A TGA curve showed a 12% weight loss upon heating. We attribute the loss in magnetization to the increase in mass due to the surface coating, not degradation in the particles.

When dispersions were prepared using the particles treated with Z-6030 at 80 weight percent, a viscous paste was obtained. The paste had a viscosity too high to be measured with our rheometer and clearly too high for coating. The viscosity of a typical solvent-based coating fluid is in the range of 10³ cps, with significant shear thinning. When the surface-treated magnetic particles were used at 50 weight percent, we obtained a coating fluid with rheological properties comparable to a conventional, solvent-based coating fluid (Figure 2). The rheological properties of magnetic coating fluids are dominated by the magnetic attraction forces between the particles, which increase the elasticity (*G'*) of the coating fluid. The surface treatment occupied surface sites on the particles that would otherwise adsorb acrylate monomers. The surface coating also provided a steric barrier against particles approaching each other, which decreased the strength of the magnetic attraction between particles, thus decreasing the elasticity of the fluid. Although we have yet



not prepared a fully loaded (30 volume percent) coating formulation, this was an important discovery, as it provided an approach to solving the dispersion and coating fluid rheology problem. Ongoing work is directed at identifying new silane coupling agents that will allow us to achieve 80 weight percent particle loadings.

Economic Analysis

We have estimated the costs of our solventless, electron beam cured magnetic tape manufacturing process. The motivation was to determine whether the operating cost of the solventless process would preclude its adoption by the industry. Earlier we had compared the hourly operating costs of a conventional solvent-based process with our waterborne process and determined that the waterborne process had a 15% lower operating cost (3,4). The model was a video tape coating line running at 600 m/min, a 48" wide web, with a coating thickness of 2.00 μm . Here we use that analysis as a basis for comparing our solventless process with a conventional solvent-based process. The loading of magnetic particles, carbon black, alumina, and lubricant were the same for both cases. In table IV is the hourly consumption of materials and the costs for the solventless process, using the acrylate formulation 1 from table II. The cost was dominated by the magnetic particles, as expected, since they comprise the highest weight percent in the coating. The acrylates also are a significant contributor to the materials cost. In table V is a comparison of the hourly operating costs for the conventional solvent-based and our solventless process. In all cases the costs are dominated by the materials costs. For the solvent-based process we considered the case of no recycle and the case where the solvents were captured, purified and recycled. The details of this analysis was published earlier (3,4). Clearly for the solvent-based process, recycling pays, as it lowered the materials cost to \$1570 per hour while only adding \$13.56 per hour. Most modern tape manufacturing operations recycle their solvents. For the solventless process the hourly materials costs were lower, largely because the solvents were eliminated. Energy Sciences provided information on the cost of operating a commercial electron beam processor. They estimated the energy consumption of running a 1800 Mrad-m/min processor at 125 keV to be 130 kW. If electricity costs 6¢/kW-hr, then the energy cost would be \$7.80 per hour. Oxygen inhibits free radical polymerization and generates ozone when irradiated with high energy electron beams. Therefore the web must be blanketed with an inert gas and we estimated the processor would use \$30 per hour worth of nitrogen. By our preliminary analysis the operating cost of the solventless process is comparable to that for the conventional process. Clearly economics does not preclude adoption of the solventless process. A problem with this analysis is that we assumed that the cost of the particles was the same for all cases. However, our research has indicated the need to surface treat the particles. This will add to their price and increase the cost of the solventless process. If the surface treatment increased the particle price by 10%, then the overall cost of the solventless process would be \$1616 per hour, higher than the cost of the solvent-based process with recycle. However, our analysis for the solvent-based process does not include the cost of curing the tape. The tape cured in a thermal process by sitting

in a curing room over night. It is difficult to get information about the cost of this process step and so we have not included this cost in our analysis. In the solventless process the electron beam processor cures the tape on-line, a cost savings, which also increases productivity. The tape can be further processed immediately, without the need to sit in the curing room overnight. Another cost that is hard to measure is the cost of complying with air emissions regulations. The solvents used in conventional magnetic tape coating operations are regulated under the Clean Act Amendments, RCRA and TSCA. In addition to the engineering controls required to safeguard the workers and the environment, these regulations require compliance monitoring and reporting. We assume that an operation that uses our solventless process would be relieved of the reporting requirements, which would lower costs. We expect that in addition to eliminating the possibility of air pollution, our solventless magnetic tape manufacturing process could also provide better tape at a lower cost. The focus of our research project is to systematically demonstrate feasibility and substantiate the assumptions in our analysis. As the project proceeds we will continuously refine the economic analysis.

Table IV. Hourly Materials Consumption and Costs for the Solventless Process.

<i>Material</i>	<i>Consumption (kg/hr)</i>	<i>Cost (\$/kg)</i>	<i>Cost (\$)</i>
Magnetic Particles	200.8	4.85	974
Carbon Black	4.01	3.40	14
Alumina	12.1	5.69	69
Butyl Stearate	2.51	1.30	3
Stearic Acid	2.51	1.01	3
CN 965 A80	17	9.36	159
SR 9003	34	6.54	222
SR 9035	1.9	10.04	19
SR 506 A	1.9	9.67	18
Total			1481

Table V. Comparison of the Hourly Cost of Operation.

	<i>Solvent-based, no recycle</i>	<i>Solvent-based, with recycle</i>	<i>Solventless</i>
Materials	2022	1570	1481
Dryer Energy	7.69	7.69	
E-Beam Curing			7.80
Nitrogen			30
Solvent Recovery		13.56	
Thermal Curing	?	?	
Compliance	?	?	
Total	2030	1591	1519

Acknowledgments

This project was funded in part by The University of Alabama, Federal funds under the cooperative agreement CR822961-01-0 with the Risk Reduction Engineering Laboratory, U. S. Environmental Protection Agency, and Federal funds as part of the program of the Gulf Coast Hazardous Substances Research Center, supported under cooperative agreement R815197 with the EPA. The project used shared instrumentation purchased through the NSF Materials Research Science and Engineering Center award DMR-9400399. The contents do not necessarily reflect the views and policies of the U. S. EPA nor does the mention of trade names or commercial product constitute endorsement or recommendation for use.

Literature Cited

1. Koster, E. and Arnoldussen, T. C. In "Magnetic Recording" Mee, C. D.; Daniel, E. D. Eds.; Vol I: Technology; McGraw-Hill: New York, 1987, 98-243.
2. Thayer, A. M. *Chemical & Engineering News* 71(30): 8-25 (1993).
3. Cheng, S.; Fan, H.; Gogineni, N.; Jacobs, B.; Jefcoat, I. A.; Lane, A. M.; Nikles, D. E. *CHEMTECH* 1995, 25 (October), 35-41.
4. Cheng, S.; Fan, H.; Gogineni, N.; Jacobs, B.; Jefcoat, I. A.; Lane, A. M.; Nikles, D. E. *Waste Management* 1995, 15(4), 257-264.
5. ISO/IEC DIS 10779 - 8 mm Wide Magnetic Tape Cartridge for Information Interchange - Helical Scan Recording
6. ASTM Designation D 882-91 "Standard Test Methods for Tensile Properties of Thin Plastic Sheeting"
7. Santosusso, T. M. *Radiat. Phys. Chem.* 1985, 25(4-6), 557-566.
8. Seto, J.; Nagai, T.; Noguchi, T.; Arakawa, S.; Shibata, A.; Ishimoto, C.; Miyashita, M. *Radiat. Phys. Chem.* 1985, 24(4-6), 567-579.
9. Laskin, L.; Ansel, R. E.; Murray, K. P.; Schmid, S. R. *Radiat Phys. Chem.* 1985, 24(4-6), 587-598.
10. Ukachi, T.; Haga, K.; Matsumura, Y. *Radiat. Phys. Chem.* 1989, 33(5), 437-442.
11. Lueck, L. *Radiat. Phys. Chem.* 1985, 25(4-6), 581-596.
12. Parakka, J. P.; Nikles, D. E. *Proc. Div. Polym. Mat.: Sci. Eng.* 1996, 75, 297-298.
13. Ellison, M. M.; Huh, J. Y.; Power, A.; Purse J. B.; Nikles, D. E. *Proc. Div. Polym. Mat.: Sci. Eng.* 1997, 76, 115-116

Chapter 4

Eliminating Solvents and Acids in Wafer Processing

Richard L. Bersin

ULVAC Technologies, Inc., 401 Griffin Brook Drive,
Methuen, MA 01844

A new dry plasma ENVIRO™ process methodology has been developed for solubilizing photoresist-ashing residues after plasma etching or ion implantation. RIE and microwave downstream plasma treatment with NF_3 , O_2 and other gases are employed. 100% solubilization in dI water has been attained with no use of solvent or acids.

Computer chip manufacturing consumes large quantities of liquid solvents and acids for cleaning dry-plasma-stripped photoresist residues from silicon wafers. Described here is a new technology that eliminates these chemicals by enhancing the solubility of the residues and thereby enabling their removal with simple dI water rinses. For understanding this new technology, a brief description of the key manufacturing steps in the production of silicon wafers is provided.

Also described are Dry Plasma Ashing and Etching, the continuing need for usage of these wet chemicals in cleaning operations, and how the shrinking of device dimensions has had a major influence on the dry plasma processes in particular, requiring greater consumption of hazardous and polluting wet chemicals. Finally, we then describe the principles of the new process, the present program for introducing the technology to industry, and the potential reductions in manufacturing costs and pollution burden that can be achieved as the industry changes to this new process. Environmental and monetary concerns are also discussed, followed by a discussion of important safety considerations relative to this work.

Fundamentals of Device Manufacturing

A silicon wafer is first sliced from an ingot, polished, and cleaned in preparation for chip manufacturing. Dopant impurities are added to selected regions of the chip to modify their electrical properties. Defining these regions is done through lithographic procedures. Photoresist is applied to the wafers, patterned, and the

dopants are introduced into the silicon by ion implantation, or diffused in a furnace through an oxide mask that has been patterned. In addition, thin films of materials are deposited onto the wafer and patterned in like manner through etching processes. Each of these steps requires the application, and the subsequent removal of a photoresist mask.

It is essential that all components of the resist mask be totally removed from the wafer before the next process step can proceed. Impurities left behind will degrade the electrical performance of the finished chip. Because the resist is designed to withstand harsh ion implantation or etching environments it becomes difficult to remove after the processes are completed. Hence, the initial adoption of strong solvents and acids by the industry to assure total removal of any residuals from the resist.

Figure 1 is a cross-sectional view of a typical CMOS device illustrating the important fabrication-processing steps from the beginning to the point of slicing up the die at completion. Starting from the bottom P-Well in the silicon up to the bottom of the BPSG layer lay all of the electrically active portions of the device, which are imbedded in the silicon or are directly on its surface. The processing done up to this point is called "front-end" processing because it comprises all of the work necessary to create the basic devices in the silicon. From here on the processes relate to the necessary steps needed to make electrical contact with the devices on the silicon. The latter processing is called "back-end" processing.

The third plug from the left through the BPSG layer is a contact hole filled with tungsten. BPSG, a thick film of insulating oxide, surrounds this metal plug. The covering of the wafer with this oxide layer now physically separates the bare silicon structure from subsequent "back-end" processing. Before the metal can be deposited into this plug, however, this insulating oxide which completely covers the entire wafer must be patterned with photoresist, with a pattern showing holes where the plugs will go. The insulating oxide is then plasma etched through the oxide down to the contact point on the silicon. The photoresist is ashed from the wafers, the contact holes are cleaned of any polymeric residue or other contaminants from the etching process using solvents as required, and the metal tungsten is deposited into the contact holes. Once the contact holes are filled with tungsten, the bare silicon substrate is never further exposed to processing. All process steps hereafter fall into the category of "back-end" processing.

After filling the contact holes, the wafer surface is planarized to leave a clean smooth surface and a layer of aluminum is deposited over the wafer. A photoresist mask is put on the aluminum surface defining the lines of contact between the various tungsten plugs; the aluminum is then plasma etched from other areas of the wafer leaving the metal lines in place. The resist mask is ashed again and the residue polymers from the aluminum etching are removed with solvents. At this point electrical tests can be performed to assure that all contacts are good and that electrical performance at this layer is acceptable. This aluminum pattern is "metal 1" (not noted on the figure). Additional insulating layers are deposited, via holes etched as were the contact holes (i.e., the contact holes made between insulating layers), and metal layers are added until "metal 6" layer on this device. Metal 6 is the thick aluminum layer to which outside electrical contacts are made.

Each patterned layer is followed by a resist ash and a solvent-clean step. This requires 12 separate solvent steps to reach metal 6 level. The elimination of these

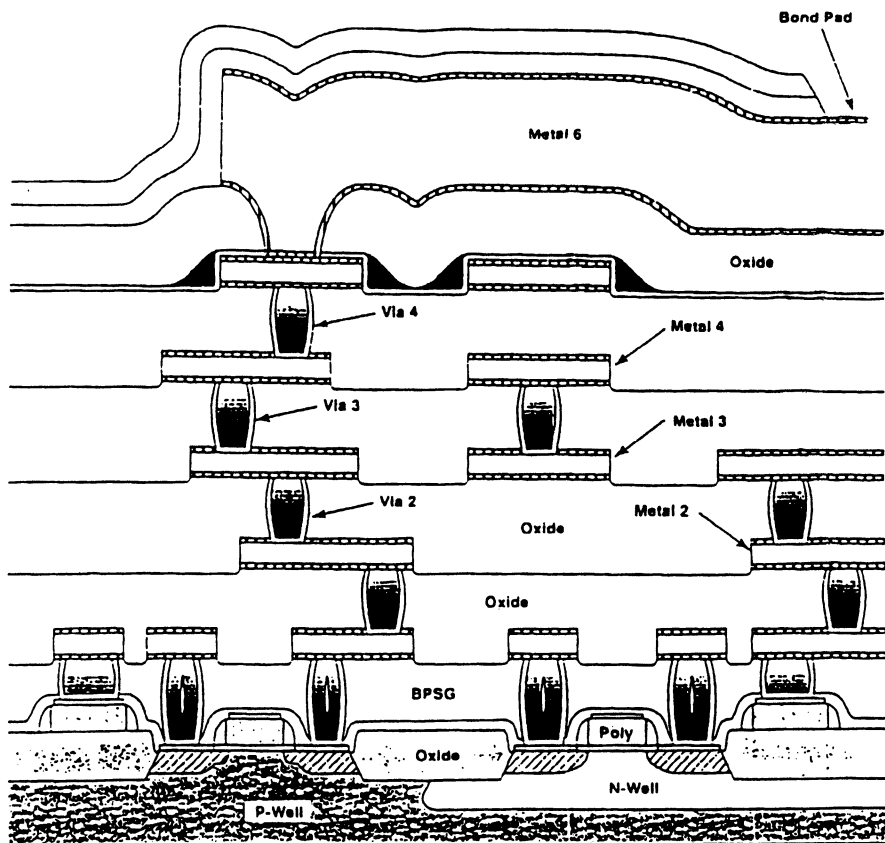


Figure 1. CMOS Process Flow

solvent-clean steps is the key subject matter of this paper. It is important to realize that at this stage of the fabrication process a very large investment has been made in the device manufacturing and failures at these levels and further ones are very costly.

Dry Ashing and Isotropic Dry Etching

In late 1968, dry plasma ashing was introduced to the industry. This dry plasma process utilizes oxygen gas, under a vacuum of a few torr, to ash off the photoresist material at temperatures around 250° to 300°C, thus utilizing the reactivity of atomic oxygen and ions made in the plasma. Conventional furnaces using air or oxygen must be heated to 600°C or higher, a temperature that would destroy devices. This new plasma process offers the opportunity to remove the bulk of the photoresist mask in a dry process at an acceptable temperature using no wet chemicals, and was quickly adopted by the industry because of the major cost savings. However, this process does not leave a totally clean resulting wafer. Residues from the process-damaged resist remain on the wafer and still require exposure to strong acids or solvents to assure their total removal. Thus the process of dry plasma ashing is associated with follow-on wet processing steps and to this day remains the conventional procedure for resist removal throughout the entire industry.

In the early 1970s, dry plasma etching was introduced to the industry. In this process, gases such as CF₄ or SF₆ are used in the plasma to create free F atoms. The atomic fluorine reacts with silicon compounds to form the gas SiF₄ which etches away thin films of polysilicon, silicon nitride, and silicon dioxide, thereby further replacing the use of acids which were the common etchants at that time. The etching, both dry plasma and wet chemical, is isotropic in nature. This means that there is always a pattern undercut on the photoresist equal to the depth of the film being etched. For the device geometries of the 1970s, this was quite adequate, and plasma dry etching along with plasma ashing became well ensconced in the industry.

Shrinking Devices and Anisotropy in Etching

The dramatic pace of device shrinking which started in the 1980s fueled the need for anisotropic plasma etching to define patterns with finer degrees of dimensional control. This is illustrated in Figure 2. Note that for the anisotropic case the etched pattern precisely follows the pattern of the photoresist mask. This kind of etching is essential when the lateral dimensions of the features of the devices become comparable to the vertical dimensions of the feature being defined.

The etcher manufacturers successfully developed these processes. However, anisotropic etching requires the deposition of heavy polymeric etch residues on the pattern sidewalls to protect the patterns from lateral etching. The polymers on the vertical sidewalls remain intact because there is low-energetic ion bombardment in the lateral direction. Any polymers that tend to form on the base material being etched, however, are removed by energetic bombardment by vertically directed ions in the plasma. Materials that are typically etched are indicated in Figure 3. These

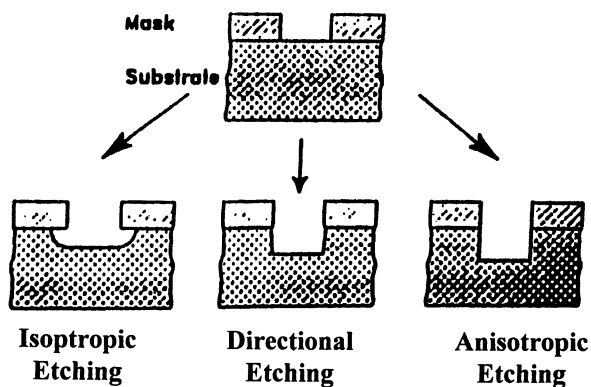


Figure 2. Isotropic, Directional, and Anisotropic Etching

- Metals Which are Dry Etched, Giving Volatile Products:
 - * Al, AlSi, AlSiCu, Ti, TiW, TiN, W, WSi, Ta, TaSi, and all Substrates Listed Below
- Substrates Which Also Become Etched and Volatized:
 - * SiO₂, polysilicon (Doped/Undoped), BPSG, TEOS, Si₃N₄, Si, PSG, and Above-Referenced Metals in Vias
- Implanted Ions:
 - * B, BF₂, As, P, H, O, Si

Figure 3. Photoresist Contaminants Contained in Residues

materials are removed as volatile chlorides, fluorides, or bromides. Depending upon the etch chemistry, as the polymers are deposited, they incorporate volatilized etch products within their structure. When the time comes to remove the resist mask, the polymers containing metals and complex organic structures are not removed by conventional ashing which has been an important reason for increased usage of solvents and acids following the ashing operation. Illustrations of these deposited polymers are shown in Figure 4.

Evolution of Conventional Ashing to 1998

Conventional ashing, introduced in 1968, was based primarily on ashing an oxygen plasma. This technology saw no change until the middle 1980s, when the idea was introduced to move the wafers outside of the plasma (now generated at microwave as well as radio frequencies) and provide external sources of heat to activate the chemistry. This change totally isolates the wafers from the possibility of electrical charge damage from the plasma. However, while the hardware configurations were changed, the basic oxygen chemistry of the process remained the same until the late 1980s when research began on the process methodology discussed here.

Introduction of ENVIRO™ Processing

The materials removed from the wafer surface typically comprise bulk photoresist that are primarily organic in nature, and plasma-formed organic polymers containing inorganic entrapped constituents such as metal chlorides, fluorides, or bromides. These contaminants can comprise up to 50 atom-percent of the polymer material (*J*). Many of these contaminants are water soluble, such as metal chlorides and often fluorides. Table 1 lists the boiling points of the most common etch products. The organic structures are typically reacted to form CO, CO₂, and water products. Conventional ashing processes, which employ oxygen chemistry and operate at 250-300°C, result in oxidation of the metal constituents, thereby converting the original compounds to insoluble and refractory oxides trapped in the organic matrices.

In the ENVIRO™ process, a microwave plasma is employed, remote from the wafer to avoid any heating, but rich in atomic oxygen with addition of NF₃ or CF₄ to release fluorine. This process very rapidly attacks hydrocarbon organic materials through abstraction of the hydrogen, leaving activated sites where reaction with atomic oxygen is initiated. The effect is low-temperature dry removal of the organic matrix leaving a residual, water-soluble ash of chlorides, fluorides, etc. The removal of organics without oxidation of contaminating metals is, therefore, one important feature of the ENVIRO™ process. In addition to microwave plasma, the chamber is equipped with RIE process capability. It is common for the complex polymer structures formed during the etch process to be incompletely ashed by remote microwave plasma processing. By combining microwave processing with RIE treatment, the polymer can be adequately ashed and solubilized, without oxidizing the

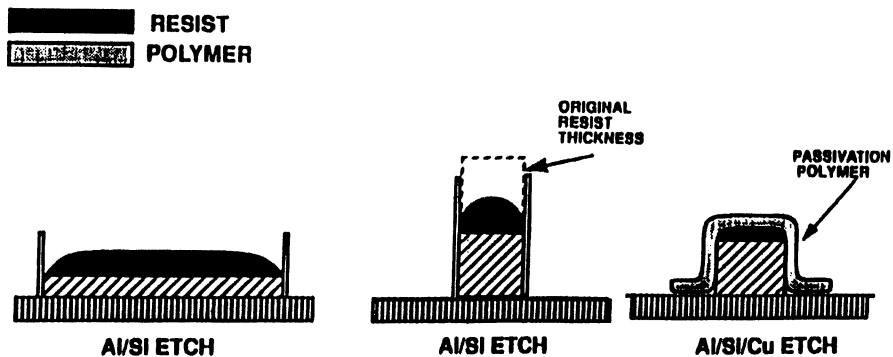


Figure 4. Sample Configurations after Aluminum Etching

Table I

Fluoride	Units Deg C	Chloride	Units Deg C
WF ₆	20	WCl ₆	345
WOF ₄	190	WOCl ₄	230
MoF ₆	35	MoCl ₅	270
MoOF ₄	180	MoOCl ₄	180
TiF ₄	285 s	TiCl ₄	35
TaF ₅	230	TaCl ₅	240
SiF ₄	-85	SiCl ₄	60
AlF ₃	1290 s	AlCl ₃	180 s

entrained metal chlorides to insoluble oxides. Numerous examples of this appear in the literature and are not extensively reviewed here (2,3,4,5,6).

The processing is done in a plasma reactor as shown in Figure 5. The microwave plasma is generated as indicated, and the active radicals flow through the chamber inlet into the plasma reactor. There is no external heating. The active radicals flow over the wafer and remove the organic matrix materials. In situ RIE processing is used either as a separate step or simultaneously with the microwave processing, depending upon the exact nature of the sample.

Every stripping process, including the ENVIRO™ process, consists of a series of steps. Generally, after etching or ion implantation, the resist patterns will have a fluorinated or chlorinated surface film deposited, or a hard carbonized crust layer on the surface. There may also be sidewall polymers that have been deposited on the resist as well as on the features that have been etched. If the etched film is layered, then the composition of these polymers will change as the various layers are etched away. Therefore prior knowledge of the etching process is essential before planning a stripping scheme. This is particularly true if some post-etch treatment has been done within the etcher, e.g. to avoid corrosion.

Details of the ENVIRO™ stripping process depend very much on the structure of the etched metal or via or on the type of etch process employed. Figure 6 illustrates an example of the etching of a TiN/Al/TiW sandwich metal film. Note that three layers of polymer are indicated. The inner layer is heavily contaminated with Ti (the first etched film), the middle layer with aluminum, and the outer layer with TiW. The solubilization process must work in reverse order, which in some instances requires the use of multi-step processes to achieve total solubilization.

Fluorine plasmas have a very strong tendency to etch films like TiN, TiW, or SiO₂. If such plasma is used for solubilization, then care must be taken to avoid damaging etching of exposed layers of these materials. This is of particular concern, for example, in the case above where an aluminum metal layer is sandwiched between TiN and TiW. It is essential that the TiN on top remains intact and that the TiW underneath does not become undercut. This can be accomplished with appropriate control of gas composition, plasma intensity, and wafer temperature during the solubilization process.

We are working with several semiconductor manufacturers to evaluate these new processes in their manufacturing lines. Such evaluations are costly and time consuming. "Lots" of wafers must be split at each process step where the new process is used. Half of the lot passes through the conventional process and the other half passes through the new process. The lots are then combined and processed jointly until the next new process step when the lot is split again and recombined as before. At each step along the way, standard device inspections and tests are performed to search for possible problems initiated by the new process.

Each process step using the new process is evaluated as a single step, and effects are determined through multiple steps until the entire manufacturing scheme has been evaluated. Completed devices must be tested electrically for initial performance; they must also be life tested to ensure that no long-term reliability problems are initiated by the new process. Many months are consumed to do these studies. Finally, when the processes has been proven to be successful to the manufacturer, its

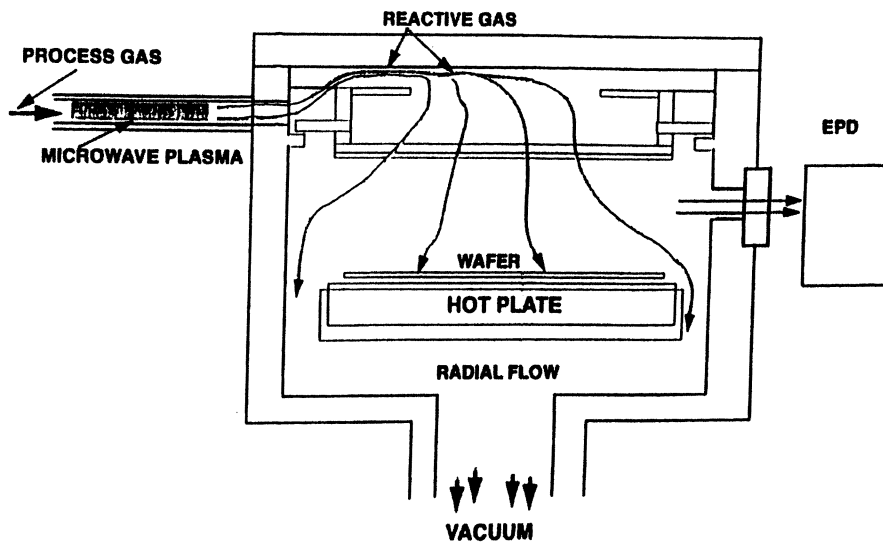


Figure 5. Microwave Downstream Stripping Chamber

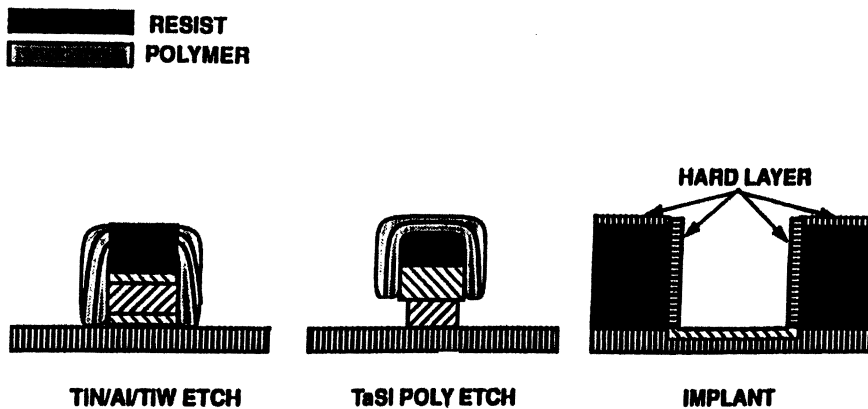


Figure 6. Sample Configurations after Complex Multi-Level Etching and Ion Implantation

implementation must be cleared with key customers. Before any dramatic change in device manufacturing processes is put into effect, it is always subject to review by key customers who must be convinced based on performance and test data that the reliability and performance of the chips they purchase will not be compromised.

Results to date have been very encouraging. Several manufacturers¹ have placed solventless processes into full production for some products, for both front-end and back-end applications. In some instances improved yields, reduced scrap, and better device electrical performance have been realized as additional benefits. Work will continue towards qualifying additional products dedicated to solventless processing as time permits, as well as expanding the number of manufacturers using this technology..

Acceptance of a new semiconductor manufacturing process is a very slow and careful procedure that must pass many checkpoints before it receives industry-wide acceptance. This is primarily a reflection of the complexity of these manufacturing process and the severe consequences that can arise from chip failures in the field. It is also the reason why chip buyers always have a back-up source manufacturer.

Environmental and Monetary Concerns

In 1997, the U.S. computer-chip industry alone used over 250 million pounds (approximately 35 million gallons) of a variety of acids, bases, and solvents (Figure 7). A large percentage of these chemicals were used for stripping of photoresist and/or removal of residues from dry ashing. Many of these chemicals are hazardous, toxic, and environmentally destructive.

With the current emphasis on 'green' chemistry, a major effort has been underway by suppliers to develop chemical processes that use less hazardous, toxic, and environmentally damaging components. At the same time, however, the movement of the industry to finer geometry devices and newer materials for processing has introduced new problems to the stripping and cleaning community. Heavier polymer deposition, along with new materials like copper, exacerbates the problem of developing adequately effective benign solvents.

The ENVIRO™ process technology discussed in this paper supports these efforts by facilitating the use of more benign chemicals to meet industry needs through chemical modification of the residues. In many cases it offers the ultimate in benign processing by rendering simple dI water perfectly suited to stripping and residue removal applications. At the present time the fore-mentioned companies are using these processes in their production, in which no wet chemicals other than dI water are employed for resist stripping and residue removal on selected products.. Based on the reported results it is estimated that a 10,000 8" wafers/week fab manufacturing a TLM product (Triple Level Metal) could eliminate 40,000 gallons of solvent annual use [with an annual cost savings of ~\$2,000,000] by adopting the process to only via-veil removal. Expansion to the post-metal step could approximately double these figures.

¹ Included are Motorola, Conexant Systems, Inc., LSI Logic

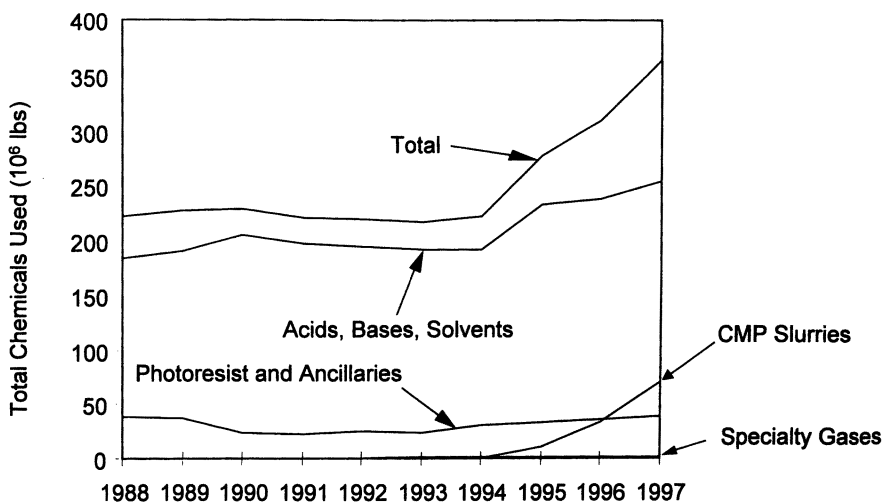


Figure 2, Submitted for Publication,
 Chapter: Environment, Safety and Health
 Authors: Scott Elrod and Walter Worth
 "Handbook of Semiconductor Manufacturing Technology",
 edited by Dr. Yoshio Nishi and Dr. Robert Doering, Marcel Dekker Publishers

Figure 7. Total U.S. Chemical Usage

The total costs of using hazardous, toxic, and damaging chemicals typically runs up to 2-3 times the initial chemical cost (typically \$30-\$50 per gallon) because of waste-handling and waste-disposal requirements, necessary safety measures, and out-of-compliance costs for exceeding levels of disposal set by government regulations. Substantial potential manufacturing cost savings are therefore envisaged with the ENVIRO™ process. However, because the industry has a major investment in equipment designed for the use of these chemicals, the move to more benign processing is mostly anticipated to come as capacity expansion develops. In general, the same wet-process equipment can be used or adapted for use with the more benign chemicals now becoming available. Thus one can envision ENVIRO™ technology as fostering wider adoption of these more benign chemicals as they become available.

Both front-end and back-end manufacturing can benefit from ENVIRO™ technology. For example, a major percentage of the sulfuric acid/hydrogen peroxide consumed is used for resist stripping and residue removal after ion implantation (a front-end process). Enviro™ processes using dI water rinsing have been developed to accomplish the same steps, and have been placed into manufacturing by several of the aforementioned manufacturers. It is important to note that one might think that consumption of dI water would rise by conversion to the Enviro™ process. However, a very large percentage of dI water usage is used for rinsing off solvents and acids in the conventional processes that are being replaced. In this instance sulfuric acid requires more water for rinsing than any other chemical. With the Enviro™ process, however, a simple spin rinser-dryer (SRD) provides adequate rinsing capacity. Indeed, the switch to dI water-rinsing with Enviro™ processing may substantially reduce the total dI water consumed.

Safety Considerations

The equipment needed to perform the processes described here is very similar to that of a dry plasma etching system. The gases used, including NF_3 , Cl_2 , and CF_4 , are the same gases employed in etching. These gases are compatible with standard fab operation. A scrubber is normally used to remove the products from the exhaust line in the conventional manner as is done with all fab equipment handling the same gases. The same safety considerations apply with respect to equipment and chemistries for the Enviro™ process as for conventional plasma etching processes.

From the standpoint of safety, however, far more important than the choice of equipment is the *elimination of toxic and hazardous acids and solvents* to which the manufacturing personnel are constantly exposed. Where there are hazardous chemicals, there is the potential for accidental spills, acid burns, and the like. In the situations where sulfuric acid/hydrogen peroxide resist stripping after ion implantation has been replaced with these new processes using dI rinses, the response of the manufacturing personnel has been very positive. Elimination of solvents also reduces hazard from TOC's (Toxic Organic Compounds); another important safety consideration.

Conclusion

Adoption by the industry of the processing methodology discussed in this paper can move the industry significantly closer to elimination of the many hazardous and toxic materials conventionally used for wafer manufacturing.

Literature Cited

1. Kay, E, A. Dilks and U. Hetzler, *Incorporation of metals into Fluoropolymer Films Synthesized by Plasma Techniques*, J. Macromol. Sci.-Chem., A12(9), pp. 1393-1398 (1978).
2. *Application-Specific Resist Stripping with Integrated Processing in a Single Multilevel-Process Chamber*, by Richard L. Bersin, presented at SPIE Symposium on Microelectronics Processing September 20, 1992, San Jose, California.
3. *Reduction of Via Resistance Using an H₂O+CF₄ Ashing Process*, presented at NCAVS PEUG Meeting on June 12, 1998. Authors: Randy Solis, Iam Harvey and Calvin Gabriel VLSI Technology, Inc.
4. Boumerzoug, M., H. Xu, R.L. Bersin, Mat. Res. Soc. Symp. Proc. **495**, 345 (1998).
5. Bersin, R.L., M. Boumerzoug, Q. Geng, I. Nakayama, H. Xu, *Semiconductor Fabtech*, **6**, 341 (1996).
6. Xu, H., M. Boumerzoug, R.L. Bersin, SEMI Symposium on Contamination-Free Manufacturing for Semiconductor Processing, F-1 (1998).

Chapter 5

Qualitative and Quantitative Analysis for Environmentally Benign Electroplating Operations

H. H. Lou and Y. L. Huang¹

Department of Chemical Engineering and Materials Science,
Wayne State University, Detroit, MI 48202

Source reduction has the highest priority in Pollution Prevention Act's waste minimization (WM) hierarchy, since it aims at solving environmental problems at the roots. Effective source reduction relies on a comprehensive and deep analysis of process operations. In an electroplating plant, however, process information is always incomplete, imprecise, and uncertain, and process dynamics pertaining to source reduction are always unknown. This has made process analysis very difficult, superficial, narrow, and less valuable. In this chapter, we introduce a novel approach for qualitative and quantitative analyses of clean electroplating operations. By resorting to fundamental engineering principles and practical industrial experience, a computer-aided tool was developed that greatly facilitates effective process analysis for waste reduction.

In electroplating plants, various chemicals and a large amount of water are consumed daily to finish and plate parts with a variety of metallic coatings (1). These plants are generating huge amounts of waste that contains over 100 hazardous or toxic chemicals, metals, and other regulated contaminants. Certainly, significant waste reduction is an urgent need for the metal finishing industry. According to Pollution Prevention Act's waste minimization (WM) hierarchy, source reduction is of the highest priority since it aims at minimizing wastes from the first place (2).

¹Corresponding author.

During the past decade, a variety of source reduction strategies have been developed (3). These strategies are helpful for minimizing chemical and water consumption as well as reducing waste solutions and sludge. Unfortunately, most of them have not fully permeated the industry (4). Even for those adopted in plants, the success in real applications is limited. One of the major reasons is that the strategies are basically heuristic, qualitative, and general. An implementation of those strategies requires extensive knowledge in diverse fields and sufficient experience in production and WM. Most electroplating plants are medium or small. Their operators usually do not have sufficient expertise to achieve optimal production and source reduction. On the other hand, heuristic, qualitative, and general strategies do not ensure the most effective solutions.

It is very important for the academia, industry and government to collaborate for the green engineering in the manufacturing industry. The opportunities for pollution prevention need to be fully identified at the first place. To reduce pollution at the source is the core of environmentally benign processing (5). In this chapter, we introduce a hybrid approach by resorting to both fundamental and heuristic knowledge for source reduction. By using mass balance principles, process kinetics, and process systems theory, a set of process dynamic models were developed for all major operations. By utilizing artificial intelligence and fuzzy logic techniques, numerous fuzzy rules were developed for systematic representation and manipulation of heuristic knowledge. A computer-aided tool for process environmental analysis is briefly described with two application examples.

Process Waste and Source Reduction

An electroplating process is a typical chemical batch process in which barrels of parts are processed in three types of units: cleaning tanks (e.g., alkaline cleaning, electrocleaning, and acid cleaning), rinsing tanks (with different configurations and stages), and plating tanks (involving different plating metals) (Figure 1). Process wastes can be generated in all these operations. In cleaning tanks, most of the dirt on parts (e.g., oil, soil, and oxides) is removed by solvents and electrical energy; sludge accumulates at the bottom of the tanks. Barrels of parts with loose dirt remaining on the surface after cleaning also carry a certain amount of the cleaning solutions to succeeding rinsing tanks. The drag-out from one tank equals the drag-in to the succeeding tank. This becomes a major source of pollutants in wastewater from rinsing systems. Similarly, parts from plating tanks also contribute large amounts of pollutants to final rinsing operations. On the other hand, bath solutions have to be replaced after their useful lives; These spent solutions contain high levels of metals and compounds that are difficult to separate. The solutions can be bled into on-site waste treatment facilities for treatment and recovery, or otherwise be encapsulated for off-site disposal.

The current source reduction strategies have been classified as those for: (i) minimizing drag-out, (ii) extending bath life, (iii) reusing rinse water, (iv) using cyanide-free solutions, (v) adopting alternative plating metals, and (vi) improving process operations (6). Their implementation involves technology change, process

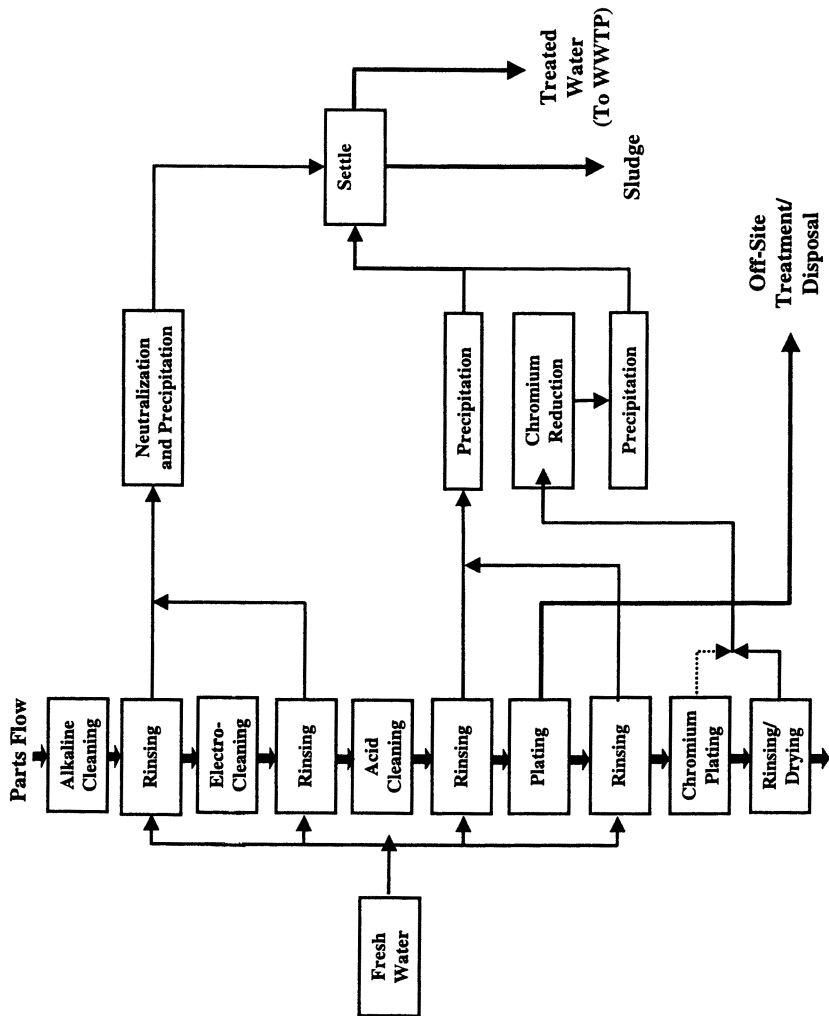


Figure 1. Process flowsheet of an electroplating plant. (Reproduced from reference 11. Copyright 1997 Elsevier Science Ltd)

and equipment modification, operational procedure change, and chemical and material substitution.

Process Modeling for Quantitative Analysis

A thorough process analysis of waste generation must rely on a deep understanding of process operational principles and system dynamics. This can be accomplished by developing process dynamic models, which should reveal the cause-effect relationships between process operation and waste generation. More specifically, the models should characterize parts cleaning, rinsing, and plating quality, chemical and water consumption, and waste stream compositions. In this section, general models for the major operations are described. More detailed modeling for cleaning and rinsing can be found elsewhere (7).

Cleaning Model

In a cleaning tank, dirt (oil, soil, and solid particles) on the surface of parts is removed by applying certain types of energy, such as mechanical, chemical, thermal, electrical, and/or radiation energy. The loose dirt on parts sinks to the bottom of the tank as sludge; the dirt remaining on the surface is carried to succeeding tanks together with the drag-out solution. The model characterizing dirt removal and chemical consumption is as follows:

$$A_p \frac{dw_{p_c}(t)}{dt} = -r_{p_c}(t) \quad (1)$$

$$r_{p_c}(t) = \gamma_c(t) C_a(t) w_{p_c}(t) \quad (2)$$

$$\gamma_c(t) = \gamma_0 \left(1 - e^{-\alpha(t-t_0)} \right) \quad (3)$$

$$V_c \frac{dC_a(t)}{dt} = -\frac{r_{p_c}(t)}{\mu} + w_c(t) \quad (4)$$

where A_p is the total surface area of parts (cm^2);
 $r_{p_c}(t)$ is the dirt removal rate (g/min);
 $\gamma_c(t)$ is the looseness coefficient ($\text{cm}^2 \cdot \text{gal}/\text{gal} \cdot \text{min}$);
 γ_0 is the kinetic constant ($\text{cm}^2 \cdot \text{gal}/\text{gal} \cdot \text{min}$);
 $w_{p_c}(t)$ is the amount of dirt on parts (g/cm^2);
 $C_a(t)$ is the chemical concentration (gal/gal);
 V_c is the capacity of the cleaning tank (gal);
 α , μ are model parameters;
 $w_c(t)$ is the rate of chemical addition (gal/min).

Rinsing Model

After cleaning, the loose dirt on the parts and drag-in should be washed out in the rinsing step. The efficiency of the dirt removal is largely dependent on the gradient between the cleanness of the rinse water, the dirtiness of the parts, and the uniformity of the rinse water in the tanks. On the other hand, the configuration of a rinsing process and the water flow rates are directly related to the wastewater minimization and parts rinsing quality. To derive an optimal configuration and water flow rates, we need to know the cleanness of barrels of parts after rinsing. This requires the models for parts and water of each rinsing tank.

$$A_p \frac{dw_{pr}(t)}{dt} = -r_{pr}(t) \quad (5)$$

$$r_{pr}(t) = k_r \gamma_c(t_e) (\theta (w_{pr}(t) - w_{pc}(t_e)) - x_r(t)) \quad (6)$$

$$V_r \frac{dx_r(t)}{dt} = r_{pr}(t) + F_r(t)(x_r(t_{in}) - x_r(t)) \quad (7)$$

where $w_{pr}(t)$ is the dirt on parts (g/cm^2);
 $w_{pc}(t_e)$ is the dirt on parts when leaving the cleaning tank (g/cm^2);
 $r_{pr}(t)$ is the dirt removal rate (g/min);
 $x_r(t)$ is the pollutant composition (g/gal -water);
 $\gamma_r(t_e)$ is the looseness of dirt when leaving the cleaning tank ($cm^2 \cdot gal/gal \cdot min$);
 θ, k_r are model parameters;
 $F_r(t)$ is the rinse water flowrate (gal/min);
 V_r is the rinsing tank capacity (gal);
 $x_r(t_{in})$ is the pollutant concentration in influent rinse at time t (g/gal -water).

The parameters of these models are determined according to the chemicals used, process equipment, and experimental data under specific operating conditions.

When a barrel of parts is withdrawn from a rising tank, rinse water still flows through the tank. The contaminant concentration in the tank is reduced; it can be derived by the following equation:

$$V_r \frac{dx_r(t)}{dt} = F_r(t)(x_r(t_{in}) - x_r(t)) \quad (8)$$

Plating Model

Electroplating is the key step for plating quality. It is of both environmental and economic importance to determine optimal operating conditions and plating processing time. In a plating tank, it is always expected that metal and chemical

concentrations are reduced while the plating quality and production rate are guaranteed. This results in the following model:

$$\frac{dm_p(t)}{dt} = r_p \quad (9)$$

$$r_p = f_p(C_s, \mu_p) g_p(h_p, \gamma_p) \quad (10)$$

$$\rho V \frac{dC_s(t)}{dt} = -r_p \alpha_p \quad (11)$$

$$\alpha_p = \psi_p(C_s, \mu_p) \quad (12)$$

where m_p is the amount of metal plated on parts (g);
 C_s is the concentration of solution in the plating tank (g/gal-water);
 r_p is the reaction rate of plating process (g/min);
 μ_p is the efficiency of the solution;
 γ_p is the factor of effective of the shape of parts;
 h_p is the thickness of the plating metal on parts (cm);
 V is the volume of plating tank (gal);
 ρ is the density of the solution (g/gal);
 α_p is the model coefficient.

Note that the three models above are general for those operations. Once they are applied to a process, specific cleaning, plating, and rinsing configurations should be differentiated. Thus, the model parameters should be adjusted.

Fuzzy Rules for Qualitative Analysis

Effective WM also needs certain experiences that cannot be expressed mathematically, since they are usually expressed linguistically. More importantly, the available information pertaining to WM is frequently uncertain, imprecise, and incomplete. This hinders the use of conventional mathematical approaches (8). Artificial intelligence and fuzzy logic, however, are appropriate techniques for representing and manipulating linguistic knowledge (9)(10). The available source reduction strategies can be expressed as IF-THEN fuzzy rules. For instance, a rule for drag-out minimization says (11):

IF the surface tension of a solution is very low, AND
 the temperature of the solution is much lower than the
 optimal setting, AND
 no wetter is added,
 THEN excessive drag-out will be generated.

It is nearly impossible to define the boundary between the linguistic concepts of very low, low, and high surface tension, lower and much lower than optimal temperature setting, as well as less excessive and excessive drag-out. Thus, fuzzy logic is employed to bound these linguistic terms.

**American Chemical Society
Library**

1155 16th St., N.W.

Washington, D.C. 20036

In Green Engineering, Anastas, P., et al.;

ACS Symposium Series 825, American Chemical Society, Washington, DC, 2000.

In this rule, the variable, surface tension, in the first antecedent, can only be estimated based on experience due to the lack of a measurement device in most electroplating plants. A set of fuzzy numbers needs to be defined empirically. The variable, temperature, in the second antecedent of the rule, can be precisely measured. However, how much a very low temperature, together with other factors, can affect source reduction is extremely difficult to determine. This is especially true when the bath temperature is not very stable. Industrial practice suggests to define three fuzzy membership functions. One is for the temperature, the other is for the surface tension. The last antecedent in the rule, the addition of wetter, can be either true or false, but not both. This allows the introduction of a crisp membership function with no fuzziness. Note that the fuzzy set theory is a generalization of the ordinary set theory, and a crisp set is a special case of a fuzzy set. With the definitions of linguistic terms, the above rule can also be mathematically expressed by fuzzy logic as follows:

$$A_L \wedge B_{ML} \wedge C_N \rightarrow D_M \quad (13)$$

where A_L , B_{ML} , C_N , and D_M are the fuzzy sets for the linguistic terms of LOW surface tension, MUCH LOWER temperature, NO addition of wetter, and EXCESSIVE drag-out, respectively.

As stated above, there are six categories of strategies available for source reduction: drag-out minimization, rinse water reduction, batch life extension, etc. The heuristics strategies lead to the development of over 200 fuzzy IF-THEN rules. These rules are activated by the following fuzzy MIN-MAX algorithm (12).

$$\mu_j(x) = \max_{i=1} \left\{ \min_{i=k} \{ \mu_{ik}(x_k) \mid k = 1, 2, \dots, K \} \right\} \quad (14)$$

where $\mu_j(x)$ and $\mu_{ik}(x_k)$ are the fuzzy membership functions of variables x_k ; subscript i denotes the rule number; and subscript j denotes the layer of the rule i is in. The selected rules provide a variety of decisions on source reduction. These decisions are ranked in a prioritized order. Figure 2a, 2b illustrates an example of rule evaluation by fuzzy logic.

OP2EP — Environmental Decision Support System

An environmental decision support system can integrate different fields of knowledge in an interdisciplinary manner. It can help decision makers who utilize the information in a smart way to solve poorly or insufficiently structured problems, as are often the case in environmental situations. It cannot, however, replace decision makers. A system can provide a combination of several tools necessary to support the process of structuring WM problems, to gain new insights into them, to look for examples of problems that have already been solved, or otherwise to derive

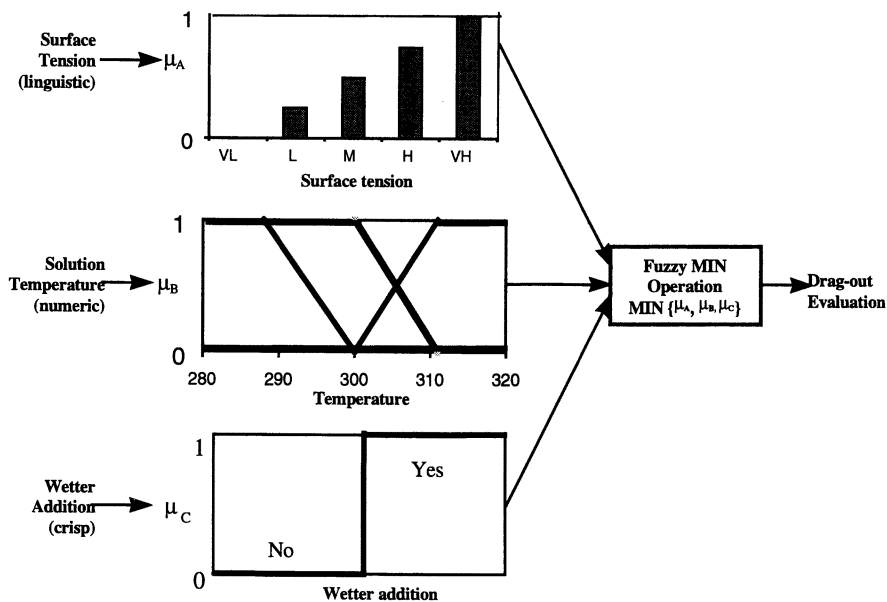


Figure 2. Decision making process using the fuzzy MIN-MAX algorithm.
 (a) MIN operation on a rule. (Reproduced from reference 11. Copyright 1997 Elsevier Science Ltd)

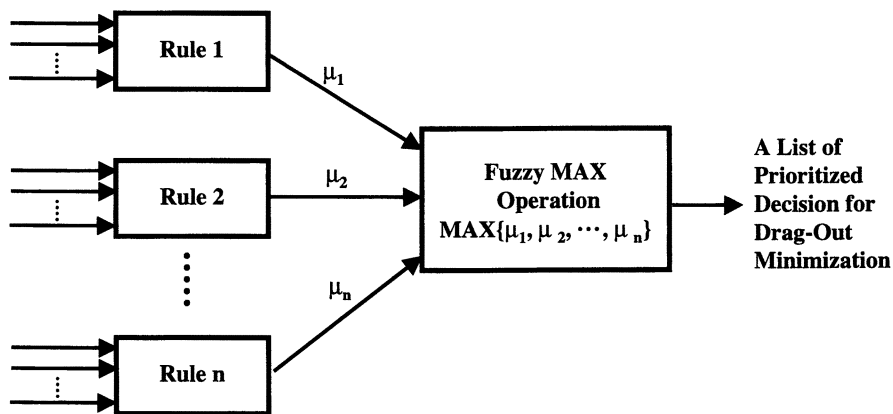


Figure 2. Decision making process using the fuzzy MIN-MAX algorithm.
 (b) MAX operation on a set of rules. (Reproduced from reference 11. Copyright 1997 Elsevier Science Ltd)

alternative solutions. Figure 3 shows the structure of the tool, OP2EP, which is specifically developed for optimal pollution prevention in electroplating plants. The system consists of a knowledge base, a database, and an inference engine. The system integrates the models and heuristic rules we developed into its knowledge base for both quantitative and qualitative analyses. The expertise elucidated is a collection of problem definitions, process variables and their relations, specialized facts, algorithms, strategies, and heuristics about the process and WM re-enforcement. The system is particularly good for conducting comprehensive and deep process analysis based on numerical and symbolic data, precise or imprecise information, and fundamental and heuristic knowledge.

To derive optimal source reduction solutions, an optimization problem is defined that is to minimize the consumption of freshwater (which means the minimization of wastewater), chemicals (which means the minimization of pollutants in wastewater), and energy used for heating and plating. This optimization must be constrained by quality requirements for cleaning, rinsing, and plating upper and lower limits, scheduling of parts processing, etc. On the other hand, process equipment, operational sequence, and procedure must also be followed. All these concerns can be mathematically formulated as equality and inequality constraints, and logical relationships. This gives rise to the following :

$$\min J = \sum_{i=1}^I W_i + \sum_{j=1}^J M_{c_j} + \sum_{l=1}^L E_l \quad (15)$$

$$\text{sub.to:} \begin{cases} f_1(x) = 0 \\ f_2(x) \geq 0 \\ g_1(y_a) \rightarrow g_2(y_c) \\ h_1(z_a) \rightarrow h_2(z_c) \end{cases}$$

where W_i is the water consumption in rinsing tank I;
 M_{c_j} is the chemical usage in cleaning tank c_j ;
 E_l is the energy consumption in electroplating tank l;
 $f_1(X)$ is a set of equality constraints;
 $f_2(X)$ is a set of inequality constraints;
 $g_1(Y_a)$ and $g_2(Y_c)$ are the sets of crisp logic expressions;
 $h_1(Z_a)$ and $h_2(Z_c)$ are sets of fuzzy logic expressions;
 X is a vector of variables x_i ;
 Y_a and Y_c are the vectors of crisp logic variables in antecedent and consequent parts of a logic expression, respectively;
 Z_a and Z_c are the vectors of fuzzy logic variables in antecedent and consequent parts of a logic expression, respectively.

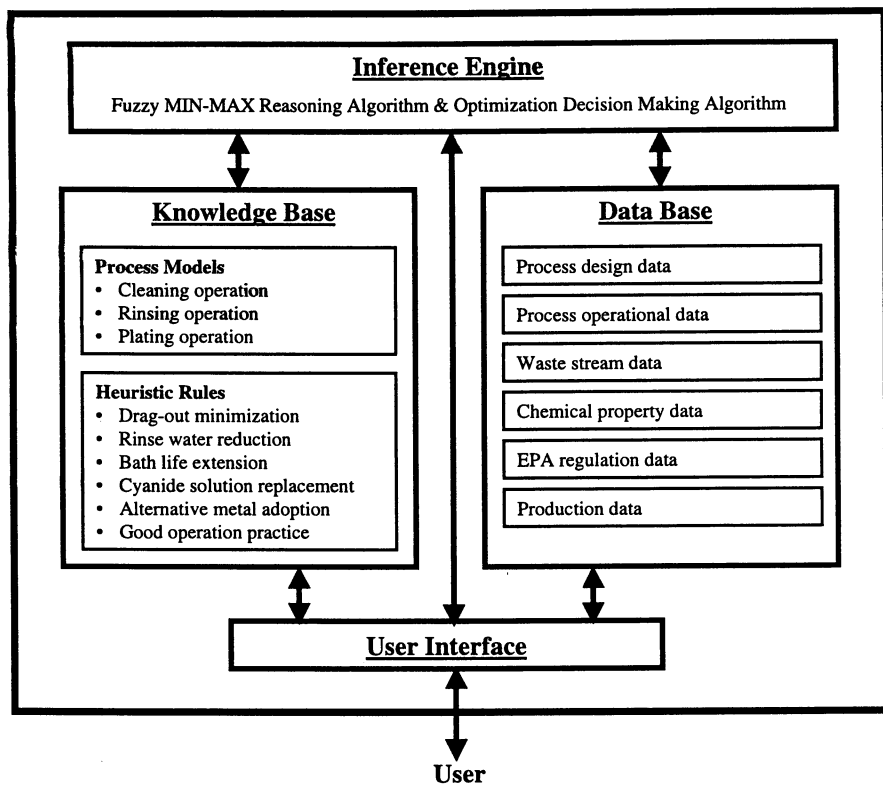


Figure 3. System structure of the environmental decision.

Applications

The OP2EP tool has been used to analyze a variety of electroplating processes for the reduction of chemicals and wastewater. Figure 4 shows the first window of the system, where a user can click the pushbutton of either “*Qualitative*” or “*Quantitative*” to activate a model-based or a knowledge-based source reduction sub-system.

Qualitative Analysis

If the knowledge-based source reduction sub-system is activated, it can perform process analysis for source reduction, recycling/reuse, and wastewater pretreatment using a variety of heuristics. If the source reduction function is activated, the system will ask the user to select one of the six WM categories for deep analysis.

Figure 5 shows an example for drag-out minimization during zinc-acid plating. A barrel of cup-shaped parts is cleaned in a presoak tank of 440-gallon capacity. The solution in the tank has a solvent concentration of 20% at 80°F. The viscosity is measured as 3 cp, while the surface tension is estimated as medium, due to the lack of a sensor, as is very common in plants. The part size is 1 inch each, and the drainage time is about 3 seconds. In this case, the system analysis concludes that the WM practice to this tank is “*Poor*”, as shown in Figure 6. The user can then click the pushbutton, “*Why?*”, in the menu bar on the top part of the window to find why the rating is low. In fact, the system provides the following reasons: (i) the cup-shaped parts are without up-rotation in the process, (ii) the chemical concentration is too high, and (iii) there is insufficient drainage time for the barrel with holes of 0.5 inch. The user can also click the pushbutton, “*Decision*”, to find out how to deal with this situation. For this case, the system suggests to install an up-rotation device, to lower the chemical concentration in the process bath, and to add a wetter. The total cost will be in the range of \$2,500 and \$10,000, depending on the type of up-rotation device used. These suggestions help the user to make final decisions.

Quantitative Analysis

The pushbutton, “*Quantitative*”, shown in Figure 4 activates the model-based process analysis sub-system. A simulation window then pops up which the user can use to construct a process flowsheet. Figure 7 gives an example that consists of a number of cleaning and rinsing steps, and a plating unit. The user can then click the icon of any unit in the process or the barrel of parts hanging on the top of the process to input process data.

Figure 8 illustrates the data input window for parts. The information necessary for process analysis includes the total weight of parts with total surface area, the initial dirtiness of parts and the dirt stickiness, and the number of barrels of parts to be simulated. In addition, the user needs to input data for each unit. Figure 8 shows the parts information needed by the system. Figure 9 gives an example for Soak



Figure 4. First window of the environmental decision support system, OP2EP.

Source Reduction

Plating Metal:

WM option:

Pick up a tank for investigation:

Basic Information of the Tank

Capacity: Gallons
Chemical ID:
Source:

Specification for the tank

Temperature (F):

Concentration of Chemical (Vol.%):

Viscosity (cp):

Size of the part (in):

Hole Size of the barrel (in):

Drainage Time (sec.):

Shape of the parts

Cup Tube Straight

Surface Tension of Solution:

Addition of Wetter

Install an up-rotation device

Figure 5. Data input window for drag-out minimization in the qualitative decision support sub-system in the OP2EP.

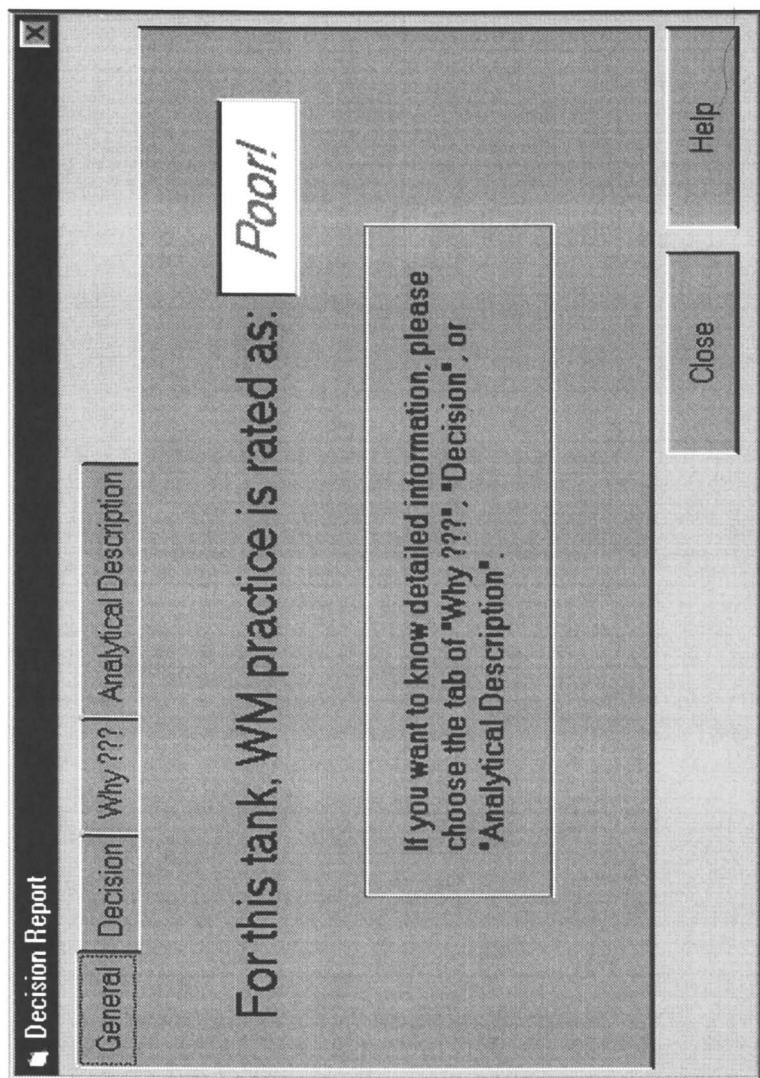


Figure 6. Waste minimization rating window of the qualitative decision support subsystem of the OP2EP tool.

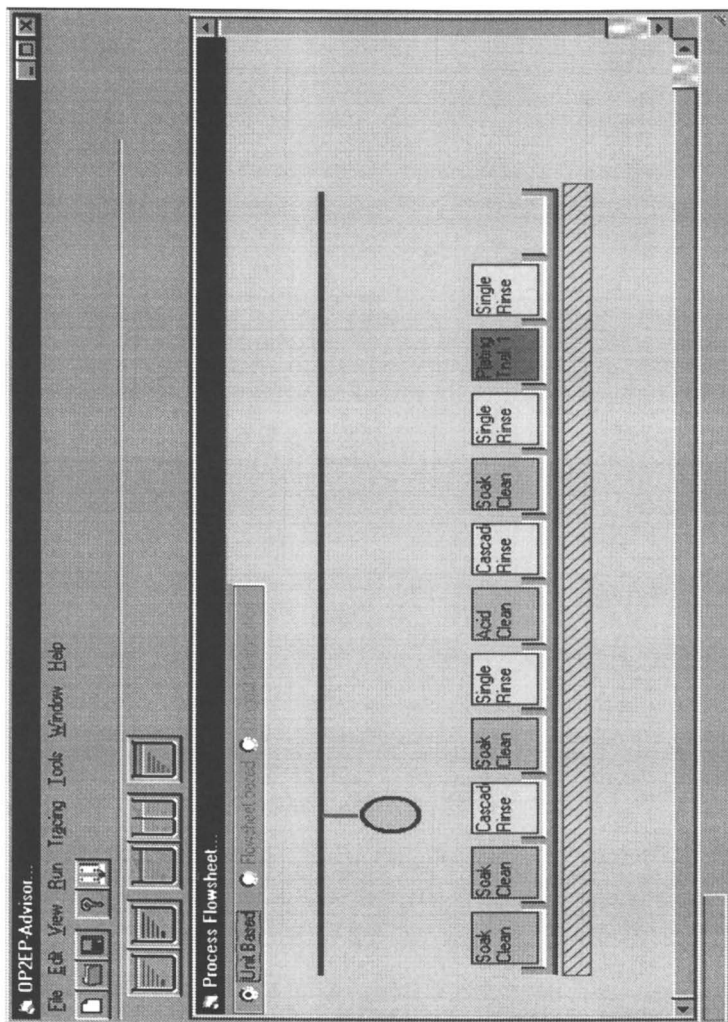


Figure 7. Process dynamic simulation window of the quantitative decision support sub-system of the OP2EP tool.

Parts Specification

Name of parts:

Specification for parts

Total Weight per Barrel:	<input type="text" value="200"/>	(Lb)
Surface Area:	<input type="text" value="0.103"/>	(Squ. Ft/Lb)
Initial Dirt:	<input type="text" value="26.6"/>	(g/Sq.Ft)
Stickness of:	<input type="text" value="0.0161"/>	
Number of barrel(s) to be processed:	<input type="text" value="20"/>	

Figure 8. Data input window for parts in the quantitative decision support subsystem of the OP2EP tool.

Unit-based Simulation

Name of Unit:

Operating condition

Volumn of Tank: Gallons

Concentration of Chemical:

Processing time: Seconds

Control option

Automatic control

Manual Operation

Chemical parameters

Efficiency of Chemical (u):

Capacity (B):

Figure 9. Data input window for process units in the quantitative decision support sub-system of the OP2EP tool.

Cleaning Tank 1 where the volume of the tank, chemical concentration, current parts processing time, and chemical solvent parameters are required. The system can then perform dynamic simulation and analysis at an either unit-based or flowsheet-based level. In Figure 10, a complete dynamic simulation of 20 barrels of parts cleaning in Soak Cleaning Tank 1 is given. Each “vertical” curve represents the dirt removal from the beginning to the end of cleaning. For instance, the first “vertical” curve starts from 26.6 g/ft², (which means 16.6 g dirt per ft² barrel) to 2.5 g/ft²; this indicates that the barrel is too clean at the end (the permissible dirt residue on parts is 5.32 g/ft², or 80% of dirt removal). On the other hand, the chemical concentration is reduced from 6.5% to 6.38% due to the cleaning of the first barrel. As the cleaning process proceeds, the chemical concentration is gradually reduced, as shown by the concentration curve in the figure. As shown, the cleanness of each barrel of parts at the end of cleaning gradually deteriorates. The last barrel has 5.74 g/ft², which is equivalent to a dirt residue of 22% (exceeding the requirement). This information has been summarized by the tool at the bottom part of the figure. Moreover, the system indicates that the chemical consumption of processing 20 barrels of parts is 5.54 gallons. This dynamic simulation clearly describes what is going on in a processing unit. This will greatly help plants identify the opportunities for reducing chemical and water consumption, or equivalently, for reducing wastewater and its pollutants.

Conclusion

Effective waste minimization in electroplating plants requires a comprehensive and deep analysis of process operations. Traditionally, process analysis for clean operation has been performed at the qualitative level; the effectiveness of the analysis is largely dependent on the engineer’s experience. This has limited severely the completeness of source reduction. This chapter has introduced a hybrid process analysis approach utilizing fundamental as well as heuristic knowledge. The process dynamic models and model-based optimization strategy, a large number of fuzzy rules, and the adoption of a fuzzy MIN-MAX reasoning mechanism help to conduct deep analysis for the identification of waste problems and solutions. The computer-aided tool, namely OP2EP, has demonstrated its capability for both quantitative and qualitative analyses. It can provide the most desirable information to help electroplating plants operators reduce the quantity and toxicity of the waste streams.

Acknowledgement

The authors gratefully acknowledge financial support from National Science Foundation, United States Environmental Protection Agency, The American Electroplaters and Surface Finishers Society, and the Institute of Manufacturing Research at Wayne State University.

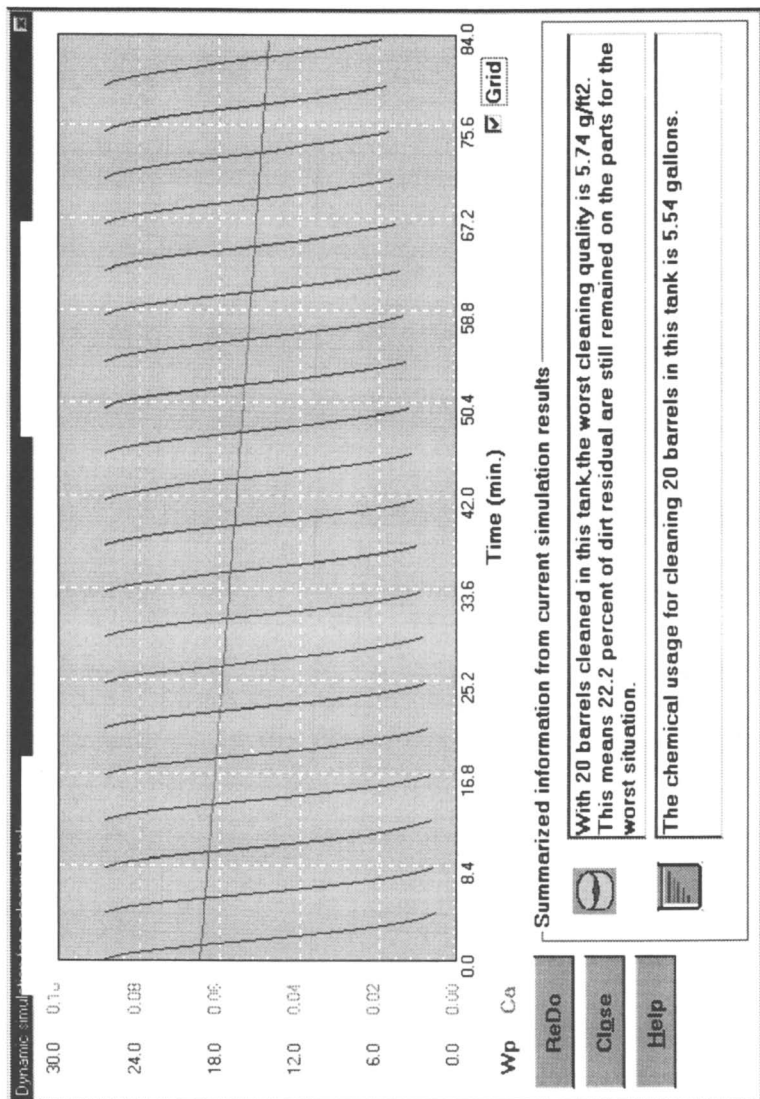


Figure 10. Dynamic simulation window of process unit in the quantitative decision support sub-system of the OP2EP tool.

Literature Cited

1. Noyes, R. *Pollution Prevention Technology Handbook*; Noyes Publ.: Park Ridge, NJ, 1993; Chpt. 28; pp534-543.
2. *Pollution Prevention Act of 1990*; 42 U.S.C.; 1990; §§13101-13109.
3. Melter, M.; Callahan, M.; Jensen, T. *Metal-Bearing Waste Streams: Minimizing, Recycling, and Treatment*; Noyes Data Corporation: Park Ridge, NJ, 1990; pp207-216.
4. Duke, L. D. *Waste Management*. **1994** *14*, 49-58.
5. Hancock, K.G.; Cavanaugh M.A. in *Benign by Design Chemistry*; Anastas, P.T.; Farris, C.A., Ed.; American Chemical Society Symposium Series, No. 577; American Chemical Society: Washington, DC 1994; pp23-30.
6. PRC Environmental Management Inc. *Hazardous Waste Reduction in the Metal Finishing Industry*; Noyes Data Corporation: Park Ridge, NJ, 1989; pp17-36.
7. Gong, J. P.; Luo, K. Q.; Huang, Y. L. *J. of Plating and Surface Finishing* **1997**, *84(11)*, 63-70.
8. Zadeh, L. A. *Information and Control*, **1965**, *8*, 338-353.
9. Huang, Y. L.; Sundar, G.; Fan, L. T. *Envir. Prog.* **1991**, *10*, 89-95.
10. Huang, Y. L.; Fan, L. T. *Comp. Chem. Eng.* **1993**, *17*, 181-192.
11. Luo, K. Q.; Huang, Y. L. *Engng Applic. Artif. Intell* **1997**, *10(4)*, 321-334.
12. Zimmermann, H. J.; *Fuzzy Set Theory and Its Application*; Kluwer-Nijhoff Publishing: Hingham, MA, 1985; Chpt. 10, pp. 250-286.

Chapter 6

Emission Reduction of Perfluorocompounds in Semiconductor Manufacturers via Capture and Recycle

Y. E. David Li¹, Joseph E. Paganessi¹, and Denis Rufin²

¹American Air Liquide, 5230 S. East Avenue, Countryside, IL 60525

²Air Liquide Electronics Europe, B.P. 248–F 71106 Chalon-Sur-Saone Cedex, France

Perfluorocompounds (PFCs), including SF₆, C₂F₆, CF₄, NF₃, CHF₃, and C₃F₈, are essential to many manufacturing processes in semiconductor industry. However, these gases raise environmental concerns because they are classified as greenhouse gases. They are much more potent than carbon dioxide due to their extremely long lifetime and strong absorption of infrared radiation. Environmental scientists believe these gases may persist for as long as 50,000 years in the atmosphere. Over 1.6 million pounds of PFCs were used in 1995 in the US semiconductor industry, at an estimated cost of over 45 million dollars. This amount could be doubled by year 2000. The US government has responded to its international commitment (RIO Earth Summit '92 and Kyoto Protocol '97) by promoting reduction in PFC emissions in various industries.

The semiconductor industry has four strategies currently available for addressing emission reduction: 1) change the process chemistry by eliminating the use of PFCs, 2) improve the process efficiency where these gases are used, 3) destroy these gases at considerable financial and environmental cost, and 4) capture and recycle of PFCs from the exhaust lines.

Air Liquide has recently developed a patented membrane-based recycle system that can capture more than 95% of PFC gases from the process exhausts. Among the PFCs, the capture efficiency for SF₆, CF₄ and C₂F₆ exceed 98%. At the same time, the system can concentrate the gases from a few ppm to more than 99%. This paper reviews the options for emission reduction and discusses in detail the technology behind the Air Liquide's recycle system.

The sun's radiation, much of it in the visible region of the spectrum, warms our planet. On average, earth radiates back to space the same amount of energy, which it gets from the sun. Being cooler than the sun, earth radiates in the infrared. The wavelengths at which the sun and the earth emit are, for energetic purposes, almost completely distinct. Greenhouse gases in earth's atmosphere, while largely transparent to incoming solar radiation, absorb most of the infrared emitted by earth's surface retaining heat somewhat like the glass panels of a greenhouse.

Without this natural "greenhouse effect," temperatures would be much lower than they are now, and life as known today would not be possible. Since the industrial revolution, human activity has increased global warming gas concentrations. As a consequence of the building-up of these heat trapping gases, it is anticipated that changes in regional and local climate conditions, including temperature, precipitation, and sea level, will occur.

Gases with global warming potential are chemicals that are capable of trapping infrared radiation in the earth's atmosphere. They include both naturally occurring gases like carbon dioxide, methane, etc, and anthropogenic compounds like PFCs. These gases are ranked by their global warming potential (GWP) which is related to their estimated atmospheric lifetimes and their capacity for absorption of infrared radiation relative to the most abundant greenhouse gas, carbon dioxide (Table I). The concept of GWP allows one to compare the ability of each global warming gas to trap heat in the atmosphere. Table I summarizes the global warming potentials of CO₂ and some of the most commonly used PFCs. Of all the greenhouse gases, PFCs including CF₄, C₂F₆ and SF₆ are identified as having the greatest global warming potential due to their stability in atmosphere and strong absorption capacity for infrared radiation. For example, SF₆ is about 23,900 times more potent than CO₂.

Table I. Global Warming Potentials (GWP)

<i>GAS</i>	<i>Lifetime (year)</i>	<i>GWP₁₀₀</i>
SF ₆	3,200	23,900
NF ₃	740	13,100
CHF ₃	250	11,700
C ₂ F ₆	10,000	9,200
C ₃ F ₈	2,400	7,000
CF ₄	50,000	6,500
CO ₂	200	1

Many environmental scientists believe that the buildup of greenhouse gases in atmosphere will drastically alter the climate: causing more severe storms, droughts, floods, and melting more polar ice, thus raising sea levels with potentially disastrous

results. All of the PFC gases emitted will exist in the atmosphere for several hundreds of human generations, so actions must be taken to address the emission reduction.

The United States is actively pursuing a course to limit the emission of these very potent global warming gases. In the 1997 Kyoto Protocol, the U.S., the European Union, and Japan committed to reducing the global warming gas emissions by 7%, 8% and 6%, respectively, based upon 1990 emission levels.

Semiconductor manufacturers use large quantities of PFCs for etching and reactor cleaning processes. These processes, however, are inefficient and as much as 80% of the PFCs are not reacted/decomposed inside reactors and escape the process. Since early 1994, the industry has been proactively researching various options to address emission reduction of PFCs from the manufacturing process. Air Liquide, as an industrial gas supplier, has been actively working with the industry to develop various technologies, addressing both the needs of the industry and the environment.

Emission Reduction Options for Semiconductor Industry

The semiconductor industry has been working on several emission reduction options. These strategies can be classified into four groups: 1) change of process chemistry so that it eliminates the usage of PFCs; 2) optimization of process efficiency so that fewer PFCs are emitted; 3) abatement of PFCs from the process exhaust lines; and 4) capture and recycle. The last approaches are “end-of-pipe” solutions that require only minimal process changes.

Process Chemistry Alteration

An obvious solution is to substitute PFCs with more environmentally benign chemicals. PFCs are known to have very desirable properties from both a process standpoint and a handling standpoint. Among the first challenges is the selection of a chemical compound which is different enough to result in a good characteristic in chamber cleaning and wafer surface etching that emits less or no global warming gases, yet similar enough to retain desirable process and handling characteristics. From a handling point of view, PFCs are very stable, pose little health or safety risks and it tends to have a long atmospheric lifetime. More reactive species (e.g., ClF_3) tend not to have long-term environmental impacts due to their short lifetime in the atmosphere; however, they also tend to possess potentially unacceptable health and safety risks. The selection criteria for PFCs replacement should include personal health, safety, economic, process, facilities and environmental risk factors. Assuming that new chemicals are identified which meets the above stated criteria, manufacturers must change their processes, which includes re-qualification of products and product yields.

In the semiconductor industry, various other chemistries are proposed to replace C_2F_6 for etching and cleaning application. Some research groups attempts to replace the high GWP C_2F_6 with a lower GWP gas, e.g., C_3F_8 , with a non-global warming gas, e.g., ClF_3 , which is a very toxic and reactive chemical compound. Any new chemical candidates must also address the environmental, safety and hazardous considerations. It is a complex problem in that the very stable, low-toxicity, and low reactivity of PFCs, which leads to their ease of use, is also the basis for global warming. Short-lived, more reactive chemical compounds could reduce the environmental concerns, but tend to pose new health and safety issues. It will take some years before PFCs can be phased out.

Process Improvement

The second option is to adjust the process parameters so that it reduces the PFC emission. In some case, it involves the reduction of PFC byproduct formation, while in other cases, it entails the improvement of process efficiency of PFC utilization. This approach not only reduces the PFC emission, but also is very economically attractive. It lowers the production cost by reducing energy and/or raw material consumption.

The utilization rate of C_2F_6 during the cleaning/etching process is typically about 20 - 40%. By adjusting various process parameters, the rate could be improved, so that the emission of unreacted C_2F_6 can be reduced. In some instances, some modifications on existing processes have produced savings of 50 - 70% in C_2F_6 usage.

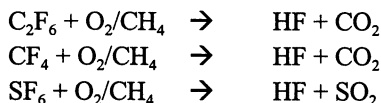
Destructive Abatement

Destructive abatement decomposes PFCs into their corresponding simple molecular form. It requires an energy source in the form of fuel, electricity or plasma. There are basically three types of abatement technologies: 1) combustion abatement; 2) thermal-chemical abatement; and 3) plasma abatement.

Combustion Abatement

Combustion based abatement was the first commercially available technology for PFC emission reduction. Various burners already existed in the semiconductor manufacturer's sites for the abatement of toxic gases, like SiH_4 , WF_6 , BCl_3 , etc.

Engineering-wise, the combustion process involves a flame to supply both the thermal energy and the reactants for the decomposition. PFCs are typically mixed with an oxygen source and decomposed or oxidized in a high temperature reaction chamber. The high temperature reaction transforms PFC into hydrogen fluoride and carbon dioxide or sulfur dioxide as follows:



The effluent gases and particulates from the chamber are normally scrubbed out by a wet caustic solution before venting into atmosphere. The combustion based abatement system consists two sections: combustion followed by caustic scrubbing. The footprint of the whole system is very compact, which is crucial in semiconductor industry where the floor space is very expensive.

There are several different commercial systems in the market based upon the combustion abatement. Basically, they can be categorized into two groups based upon the combustion temperatures: 1) direct-flame combustion, and 2) catalytic combustion.

In the direct-flame combustion, PFC containing gases are guided through the flame in a fuel-fired refractory-lined chamber to the auto-ignition temperature. Oxidation of the PFCs occurs with or without a visible flame to yield HF and other by-products. In electrically heated systems, fuel has to be added to the exhaust stream to provide a hydrogen source.

Besides HF, other possible by-products are CO_2 and CO from fluorocarbons; SO_x from SF_6 , and NO_x from NF_3 . Combustion systems can be fine tuned to an optimum working point, where the PFC destruction efficiency is high, and the formation of unwanted byproducts is suppressed. The reactive effluents from the combustion process have to be removed in a subsequent cleaning process. All commercial systems use water or closed-loop caustic scrubbers to remove HF and particulates.

The foremost challenge to effective thermal decomposition of PFCs is the inherently high thermal stability of these compounds. With some modifications, burners have demonstrated destruction efficiency exceeding 90% for C_2F_6 . However, in order to achieve the same destruction efficiency for CF_4 , the use of hydrogen fuel in burners is required because of its high combustion temperature. Although high temperature combustion achieves the high destruction efficiency of PFCs, byproducts of combustion included significant concentration of NO_x . Various manufacturers are redesigning their processes to minimize the generation of NO_x , reducing hydrogen usage, and maximizing the destruction efficiency of PFCs.

Catalytic combustion has recently emerged that offers both low NO_x generation and high destruction efficiency of PFCs. The catalytic process is similar to the direct-flame combustion with the exception that a catalyst is used to facilitate the reaction. Use of a catalyst significantly lowers the operating temperature relative to the thermal process. It lowers both fuel cost and NO_x emissions.

The major obstacle with this technology is the development of new catalysts. A good catalyst must be able to achieve high destruction efficiency, possess the thermal stability, and be resistant to decomposition byproducts. Preliminary results indicated that destruction efficiency greater than 95% for C_2F_6 and CF_4 can be reached at temperature about 700 C

Thermal-Chemical Abatement

It is a technology based upon the reactive adsorption with suitable materials at elevated temperatures. The adsorbents provide a large surface area with active sites to promote extracting the first fluorine atom from the PFC molecule, which is typically, the rate limiting step.

This technology is very similar to catalytic combustion, except that the decomposed byproducts from PFCs remain on the adsorbent surface. Typically, the gas stream containing PFC passes through a heated packed bed. The packing material contains proprietary inorganic materials. PFC is then decomposed on these inorganic materials at elevated temperatures. The spent inorganic material containing fluorine is then routinely removed from the bed and sent for either further treatment or landfill. The advantage of this type of system is that it is very compact in size, but the cost of packing material could be an issue.

Plasma Abatement

There are two types of plasma systems for this application. One is based upon the gas-phase plasma reaction. Typically, radio-frequency or microwave generated plasma is used to decompose PFC into fluorine containing gas, which is then scrubbed before being released to atmosphere. The other type is based upon plasma enhanced chemical vapor deposition techniques to extract PFC as film deposits on electrode surfaces. The spent electrode material is then routinely exchanged with new ones.

Capture and Recycle

The fourth option for PFC emission reduction is to capture and recycle unreacted PFCs from process exhaust lines. This relatively new technology was developed for this industry in 1995. In 1997, the membrane-based PFC capture and recycle technology was selected by the R&D Magazine as One of the 100 Most Technologically Significant New Products of the Year (i.e., R&D 100 Award). The rest of the paper will be devoted to the membrane-based PFC capture and recycle technology. Table II summaries the strengths and weaknesses of each emission reduction strategy.

PFC Recycle System: Membrane Technology

Polymeric membranes have been used successfully in the refining and petrochemical sectors for many years to separate hydrogen from various hydrocarbon streams, and to separate carbon dioxide from natural gas wells. More recently, membrane systems have opened a new spectrum of applications for industrial gas

Table II. Comparison of Different PFC Emission Reduction Technologies

<i>Technology</i>	<i>Strength</i>	<i>Weakness</i>
Combustion based abatement	<ul style="list-style-type: none"> • Commercially available • Currently in use 	<ul style="list-style-type: none"> • By-product management (e.g., HF, etc.) • High cost/safety issues for hardware & consumable (fuel) • Limited efficiency for CF₄ destruction
Plasma based abatement	<ul style="list-style-type: none"> • Incorporated on pure process stream • Commercially available • No external chemical/fuel 	<ul style="list-style-type: none"> • By-product management (e.g., HF, etc.) • Gas back-diffusion to process tool • Limited efficiency for CF₄ destruction
Chemical-Thermal based abatement	<ul style="list-style-type: none"> • No external chemicals/fuel • Commercially available 	<ul style="list-style-type: none"> • By-product management (spent solid disposal) • Plugging, breakthrough of packed bed • Limited efficiency for CF₄
Process optimization	<ul style="list-style-type: none"> • Less expensive than abatement • No feedstock changes to process 	<ul style="list-style-type: none"> • PFC emission still present but at lesser degree. • Not a long term viable solution • Qualification at manufacturing site
Alternative process chemistry	<ul style="list-style-type: none"> • Lower emissions with new precursors 	<ul style="list-style-type: none"> • PFC emissions still present in some cases • Not commercially available • New process qualification at manufacturing site
Capture & recycle	<ul style="list-style-type: none"> • No external chemicals/fuel • No hazardous chemicals generation • Value for the recovered products 	<ul style="list-style-type: none"> • Operating cost for the total management system for situations where PFC emissions are still allowed

companies by on-site generation of low-cost nitrogen. Its applications include purging for flammable or oxygen sensitive materials, inerting, and sparging in various industries: chemical, metals, mining, foods, printing, aerospace, analytical equipment, and electronics, among others.

The transport of gas through a polymeric membrane is governed by a solution/diffusion mechanism. In this model, a gas at the high partial pressure side of the membrane dissolves in the membrane polymer, diffuse through it, and then is released on the lower partial pressure side via an imparted pressure gradient. It is assumed that the gas phase on either side of the membrane are in thermodynamic equilibrium with their respective polymeric interfaces, and that the interfacial sorption and desorption processes are rapid compared to the rate of diffusion through the membrane. The transport rate is governed by the partial pressure differential across the membrane and thickness of the active layer of the membrane. A thin membrane film is very desirable, because the gas transport rate is inversely proportional to the thickness of the membrane active layer.

The gas permeability (P) is a material property of the membrane and for a given penetrate molecule:

$$P = DS$$

where P is the gas permeability, D is the diffusivity and S is the solubility. Selectivity (or sometimes called separation factor) of a membrane is the ratio of the individual permeability for a pair of gases:

$$\alpha = P_i/P_j = (D_i/D_j) \times (S_i/S_j)$$

Another parameter for the characterization of a membrane is flux (J). The flux is a measure of the amount of gas transported through a given area of membrane film per unit of time under a given partial pressure differential, where p_H is the pressure at high-pressure side, p_L is the pressure at low-pressure side, and A is the membrane surface area.

$$J = P (p_H - p_L)/A$$

Membranes are characterized by two parameters: selectivity and flux. Large values of flux (J) lead to higher productivity, smaller membrane areas, and lower capital costs whereas higher selectivity (α) lead to more efficient separation, higher recoveries, and lower power costs. It is evident that membranes that simultaneously possess high selectivity and flux would lead to the most economical processes. Unfortunately, for any given separation, flux and selectivity are inversely proportional, so an appropriate balance of properties must be considered in forming a compromise between flux and selectivity.

In air separation applications, nitrogen is the “slow” non-permeable gas and oxygen is the “fast” permeable gas. However, for PFC capture applications, both nitrogen and oxygen (i.e., air) are fast permeating species. This is due to the fact that

both nitrogen and oxygen have a much smaller kinetic diameter than the PFCs (Table III). Furthermore, since PFCs are found in the exhaust streams at very low concentrations, its partial pressure driving force through the membrane is minimal, and conversely, its recovery in the non-permeate stream of the membrane is very high. Another system advantage is that air is recovered in the permeate stream at nearly atmospheric pressure and can be vented without waste of compression energy. PFCs are maintained at pressure in the non-permeate stream, which in turn facilitates downstream processing.

Table III. Kinetic Diameter of Different Gas Molecules

Name	Formula	Kinetic Diameter (Å)
Oxygen	O ₂	3.5
Nitrogen	N ₂	3.7
Sulfur hexafluoride	SF ₆	4.9
Carbon tetrafluoride	CF ₄	4.4
Ethane hexafluoride	C ₂ F ₆	5.1

Technology advances now allow production of extremely efficient hollow fiber separation systems. Hollow fibers lend themselves to high packing densities and can be operated at elevated pressures. High pressure can be fed either to the bore or to the shell side of the fiber, depending upon the application. Permeable gases migrate across the fiber wall as the gas travels through the permeator vessel. The fibers are assembled in pressure vessel housing or “module” which contains a multitude of hollow fibers (e.g., 1 million) as shown in Figure I.

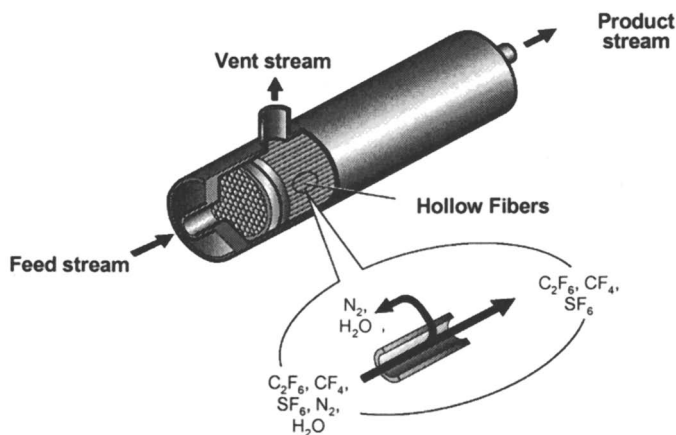


Figure I. PFC-containing exhaust gas is fed to the bore side of the fiber. Air permeates through the fiber wall and is vented at atmospheric pressure, while PFC remains under pressure inside the fiber bore.

In order to concentrate a highly diluted stream of PFCs from ppm level to greater than 50%, a membrane system must have the following basic design parameters: a base polymer material with good selectivity, flux and extremely lower defect rates. Additionally, a multistage of membrane system design will enable the system to achieve both high capture rate and high purity level of the captured product in an economical way. Figure II shows a cascade system in which high PFC concentrations and recovery efficiency may be achieved. The first stage acts as bulk gas removal in which the permeate is exhausted to atmosphere. The PFC-rich stream from the first permeator is fed to second membrane. To maintain high PFC recovery rates, the permeate stream from the second permeator is then recycled back to the 1st stage membrane module. Typically, recovery efficiencies as high as 98% can be reached, with PFC concentrations in the product stream as high as 99%. A complete system also requires removal of hazardous air pollutants prior to the PFC recovery section. This is usually accomplished by conventional dry or wet scrubbing systems.

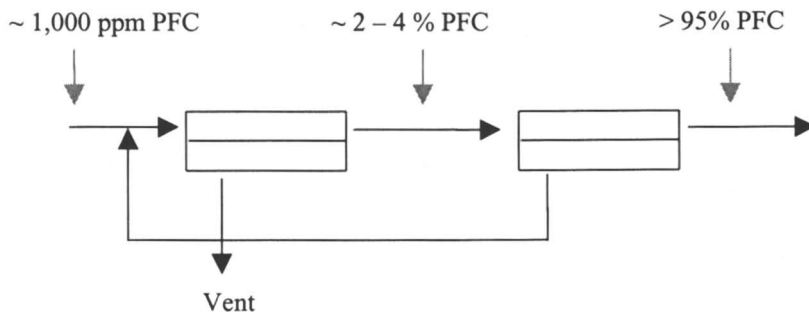


Figure II. In a cascaded membrane system, the first membrane stage removes the bulk of the nitrogen and the second membrane stage concentrates PFCs. The permeating stream from the second stage is recycled to maintain high capture rates.

Performance of Air Liquide PFC Recycle System

The PFC recycle system consists of three segments: pretreatment, capture and packaging/purification. The choice of the pretreatment process depends upon the individual process conditions. Generally, it involves the removal of solid particulates and corrosive gases from the PFC-containing exhaust stream. This is achieved by using conventional scrubbing and filtration operations. The outlet of the pretreatment process is then compressed to pressure in the range of 10 bar. This pressure is sufficient to reach good PFC capture efficiency thus allowing the use commonly available air compression equipment. The compressed stream is then fed into the

bore side of the membrane module. Gases, such as oxygen, nitrogen, carbon dioxide, argon, etc., permeate through the membrane to the shell side and exit at low pressure, while the PFCs are retained at high pressure on the bore side.

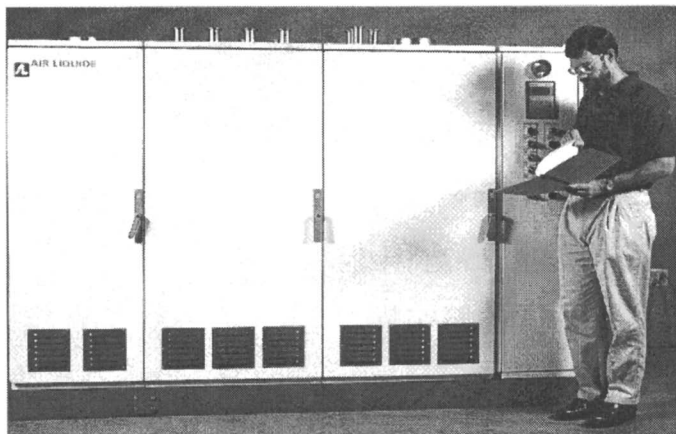


Figure III. The PFC capture unit is equipped with a completely analytical package and was tested at a semiconductor-manufacturing site for more than 2,000 hours.

Depending upon specific situations, the recovered PFCs can either be reused directly on-site or sent off-site for use as a feedstock in PFC production. The selection of pretreatment technology is process exhaust dependent, while the membrane recovery system is more generic.

Air Liquide developed this PFC recovery system and tested the system at several major semiconductor-manufacturing sites. Figure III shows such a unit containing pretreatment, compression and membrane modules. The system has the capacity to treat a waste stream of 30 Nm³/hr or more and was successfully tested for over 2,000 hours at a semiconductor-manufacturing site. The performance was quantitatively measured with actual exhaust from the Applied Material 5000 processes (Table IV)

Table IV. Applied Material 5000 Processes

Process Name	Chemicals Involved
Tungsten deposition	SiH ₄ , WF ₆ , NF ₃
Tungsten etch-back	SF ₆ , Cl ₂
Plasma-enhanced nitride	SiH ₄ , NH ₃ , NF ₃
Plasma-enhanced TEOS	TEOS, C ₂ F ₆

Figure IV indicates the various chemical species present in the process exhaust as a function of time. The unreacted process gas, here C₂F₆, and its byproducts, CF₄, COF₂ and HF were quantified by quadruple mass spectrometer.

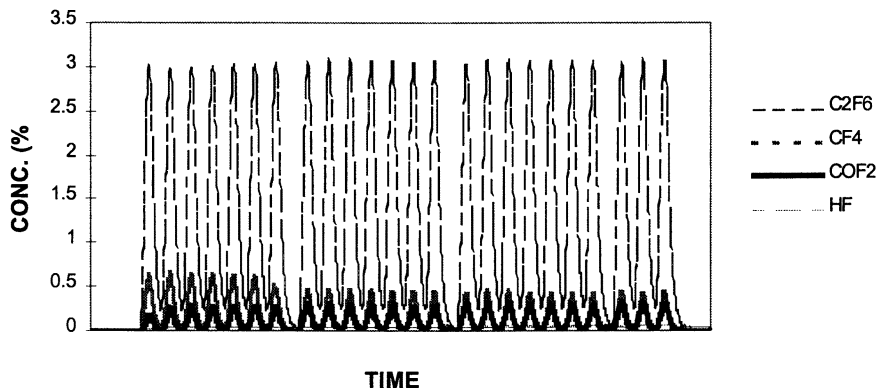


Figure IV. The unreacted process gas, C_2F_6 , and its byproducts, CF_4 , COF_2 , and HF were quantified by QMS techniques. Efficient elimination of these components was also confirmed by quadrupole mass spectrometry measures.

Figure V shows the concentrations of CF_4 and C_2F_6 at the inlet and outlet of the membrane unit and demonstrates that a membrane system responds well to wide fluctuations in PFC concentrations by releasing only ppm levels of PFCs to the vent.

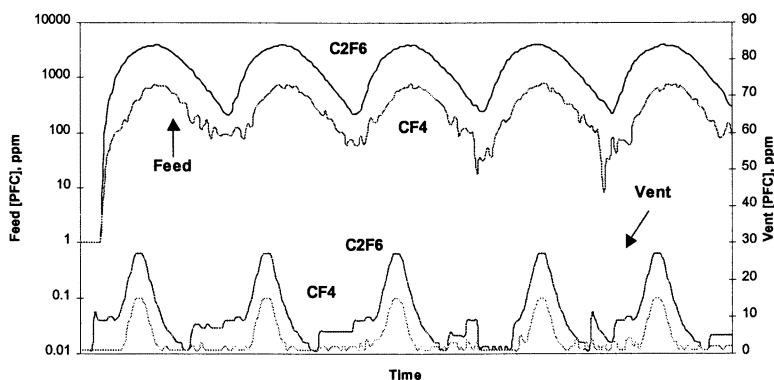


Figure V. The system adapts well to the cycling of PFC concentrations in the process exhaust; concentrations of C_2F_6 and CF_4 in the vent stream remain below 30 ppmv at all times.

This PFC recovery system went through rigorous quantification test under the umbrella of SEMATECH, a research consortium for semiconductor manufacturers.

Test results demonstrated that a membrane-based system offers PFC capture efficiency in excess of 95% with captured PFC concentration above 99%. Membrane technology has shown stable performance under widely variable feed conditions. The advantages of the membrane system are as follows:

- it does not need a drying process, the moisture in the exhaust line will permeates with air through the membranes;
- it can handle a large range of flow rates, from a few standard liters per minute to more than thousand liters per minute due to its modular nature;
- it is very compact, therefore, it can be placed in areas where space is limited, e.g., semiconductor chip manufacturers; and
- it does not have moving parts in the system, which reduces the operational cost.

Summary

Although uncertainty exists about exactly how the earth's climate responds to increased concentration of gases with global warming potential, global temperatures are rising. All of the global warming gases emitted will persist in the atmosphere for several human generations. As such, action should be taken to address emission reductions when ever feasible. Although there is no magic bullet for complete reduction, there are several strategies for the emission reduction of the most potent global warming gases, namely, PFCs. This includes process chemistry alteration, process improvement, recycling and abatement.

Process chemistry alteration is a long-term option and it can not address the immediate goal of emission reduction. Treatment and abatement technology is commercially mature, but it does not address the roots of the pollution problem. It transforms a global warming issue into a hazardous waste management problem, and is expensive to operate because it requires external energy input in the form of fuel and/or electricity. Both process improvement and PFC recycling lead to an increased rate of the raw PFCs material utilization. They are valuable strategies because they benefit both industry and society by overall reduction in PFC emissions.

Membrane-based PFC capture/recycle systems are well suited for capturing and concentrating highly diluted PFCs from manufacturing exhaust lines. Among the PFCs, the capture efficiency for SF₆, CF₄ and C₂F₆ exceeds 98%, and at the same time, the system can concentrate these gases from a few ppm to more than 99%.

Literature Cited

1. Mocella, M. (1994). PFC Reduction Strategy/Options. In *Greenhouse Gases Issues in the Semiconductor Industry*. Proceedings of 1994 Global Warming Symposium.

2. Rufin, D. and et al. (1996). Preliminary Test Results of Air Liquide's PFC Recovery System. *The 1996 Semiconductor PFC Workshop*.
3. Li, Y. and et al. (1996). Performance of Air Liquide PFC Recycle System at Semiconductor Facilities. 1996 ACS Symposium On Emerging Technologies.
4. Cummins, W. and et al (1997). Evaluation of Air Liquide's Perfluorocompound (PFC) Capture Technology (ESH002). SEMATECH Doc ID#970132291-TR.
5. Dupuis, G. and et al (1997). Permeation Technology Use in PFC Capture, Cryogenic Technology Use in PFC Recycling. Proceedings of 1997 SIA/SSA/SEMATECH PFC Technical Update.
6. Li, Y. and et al (1998). Process And System For Selective Abatement Of Reactive Gases And Recovery Of Perfluorocompound Gases. US Patent 5,759,237.
7. Li, Y. and et al (1998). Process and System For Separation And Recovery of Perfluorocompound Gases. US Patent 5,785,741.

Chapter 7

Combined Reaction–Separation Processes in CO₂

D. Hâncu, C. Powell, and E. J. Beckman¹

Chemical Engineering Department, University of Pittsburgh,
1249 Benedum Hall, Pittsburgh, PA 15261

Production of hydrogen peroxide and recovery of platinum group metals (PGM's) represent good application targets for the CO₂-technology. Hydrogen peroxide is currently produced via the sequential hydrogenation and oxidation of a 2-alkyl anthraquinone. Recovery of PGM's include leaching of the metals from the crushed ore using HCl / Cl₂ biphasic mixture at elevated pressure, followed by selective extraction of the metal chloride species, recovery and reduction of the zero-valent metal. In each of these processes, the use of CO₂ as the sole process solvent ameliorates several environmental and engineering problems including (a) eliminating the contamination of the product during its recovery by liquid-liquid extraction into water, (b) optimizing throughput via elimination of mass transport limitations, which also reduces energy input. We have generated functionalized anthraquinones (FAQ's) and CO₂-philic chelating agents that are miscible with carbon dioxide, thus making it possible to run the processes in liquid CO₂. Not only is the use of CO₂ as a solvent a green route to hydrogen peroxide manufacture or recovery of PGM's, but it is also economically feasible owing to the ability to recover the product without employing a large pressure drop, ready recycling of the functionalized anthraquinones or the chelating agents, and operation at relatively low absolute pressure due to special characteristics of the phase behavior of the CO₂-philic compound.

Introduction

Carbon dioxide is generally considered to be an environmentally benign solvent, given that it is naturally abundant, relatively non-toxic, and non-flammable. Although CO₂ itself is inexpensive, the capital and operating costs for a CO₂-based process can be prohibitively high if the technology is misapplied or if a process design is not optimized. A simple set of heuristics can be applied to a proposed CO₂-based process to aid in deciding whether in-depth economic analysis and ultimately scale-up are warranted. These heuristics are based on previous experience in the

¹Corresponding author.

design of high-pressure processes as well as knowledge of those characteristics of CO₂ which make it desirable as a solvent. Process characteristics that may be amenable to the use of CO₂ as solvent include:

- (a) *Food/pharmaceutical processing* (Use of CO₂ can ease regulatory hurdles and liability concerns).
- (b) *Where gaseous reactants are used in liquids* (Elimination of the gas-liquid interface can eliminate transport limitations to reaction).
- (c) *Generation of "unavoidable" emissions* (Applications such as polymer foaming, dry cleaning, enhanced oil recovery, and solvent-based coating operations, where it is difficult to avoid emitting solvent to the environment).
- (d) *Contact between hydrophilic and hydrophobic phases* (In liquid-liquid extraction or inverse emulsion polymerization, contact between aqueous and organic phases leads to cross-contamination).
- (e) *CO₂ as raw material* (If CO₂ can be properly activated, it is a relatively inexpensive source for carbonyl groups in materials).
- (f) *Plasticization of polymers* (CO₂-plasticization of polymers is benign and reversible, and thus has been used to process thermally labile systems).

It must be remembered that the presence of one or more of these characteristics in a process does not guarantee that use of CO₂ as solvent will be both environmentally-benign and economically feasible. Consequently, we also include a set of process constraints whose consideration will aid in minimizing both energy use and capital cost:

- (1) *Minimize the operating pressure using CO₂-philic substrates where possible* (Design of materials that can be employed in CO₂ at moderate-to-low operating pressures can greatly reduce capital cost).
- (2) *Recover products from CO₂ solution without using large pressure drops* (Operating costs increase significantly if one must continually flash and then recompress CO₂).
- (3) *If CO₂-philic materials are employed in a process, they should be recycled* (Custom CO₂-philic materials are typically more expensive than their conventional analogs and thus should be recycled to reduce process cost and waste).
- (4) *Employ continuous processing where possible* (Typically, continuous processing minimizes equipment size).
- (5) *Minimize CO₂ flow rate* (Assuming that CO₂ is used as the solvent, operation in concentrated solution minimizes reactor and pump size).

The highly successful CO₂ coffee decaffeination process, for example, exhibits characteristics (a) and (d). The caffeine is retrieved from CO₂ using water and consequently process constraint (2) is obeyed. This chapter presents two additional examples of processes which exhibit one or more of characteristics (a) - (f), and that can include most or all of the process constraints listed as (1) - (5).

Example 1: Hydrogen Peroxide

The anthraquinone / hydroquinone process (Figure 1) to produce hydrogen peroxide appears to be a good application target for CO₂ technology. In the conventional process, an alkyl anthraquinone (AQ) dissolved in a solvent (usually a mixture of an aromatic with an alcohol) is hydrogenated over a Pd catalyst in a three phase reactor to produce anthrahydroquinone (AQH₂). AQH₂ is then transferred to the second reactor where it is oxidized back to the initial AQ while forming one mole of hydrogen peroxide; the latter is stripped into water via liquid-liquid extraction. The hydrogenation-oxidation cycle is completed by transferring the AQ back to the hydrogenation reactor (1).

Although the anthraquinone/anthrahydroquinone process has been used to produce hydrogen peroxide for over 50 years, it exhibits a number of innate disadvantages (2). For example, both the hydrogenation and oxidation reactions are limited by the transport of H₂ and O₂ across gas-liquid (g-l) or liquid-solid (l-s) interfaces; larger reactors and higher temperatures than optimum are required to compensate for these limitations. Further, the aqueous hydrogen peroxide is contaminated with traces of organics during the extraction stage and further purification is required. During the purification and concentration (normally by distillation), hydrogen peroxide can be thermally decomposed or can form explosive mixtures. Finally, anthraquinone is degraded during the hydrogenation-oxidation cycles due to the hydrogenation of the aromatic rings or due to hydrogenolysis of the C=O bonds (3). The side products have to be continuously removed, increasing the consumption of the raw materials. To minimize the formation of the side products, the conversion of the hydrogenation reaction is kept between 40-50%.

The use of a CO₂-based process for production of hydrogen peroxide can provide both environmental and economic advantages. Elimination of the organic solvent via replacement by CO₂ eliminates the contamination of the aqueous product. This solves both the economic and environmental problems associated with the extraction and purification stages of the process. Waste generated in the process is reduced due to the minimization of the side reactions. Due to the high miscibility of hydrogen and oxygen in CO₂ at elevated pressures, the mass transfer limitations during hydrogenation/oxidation are eliminated and the reactions can be conducted under kinetically controlled regimes. Hence, one could move to plug-flow operation in the hydrogenation reactor, minimizing the backmixing and the side reactions.

The high capital and operating costs often times associated with the use of CO₂ at elevated pressure can be lowered owing to the special features of the AQ/AQH₂ process. First, the CO₂ travels in a loop (where pressure is relatively constant), and the H₂O₂ can be recovered without a large pressure drop via stripping into water. Operating costs are minimized because there is no need to recompress the gas after each reaction cycle. Further, the use of kinetically controlled regimes will increase the amount of hydrogen peroxide produced per cycle while reducing the equipment size and lowering the reaction temperature. Also, anthraquinone degradation is diminished, lowering raw material consumption. Continuous processing is clearly feasible, helping to minimize the equipment size.

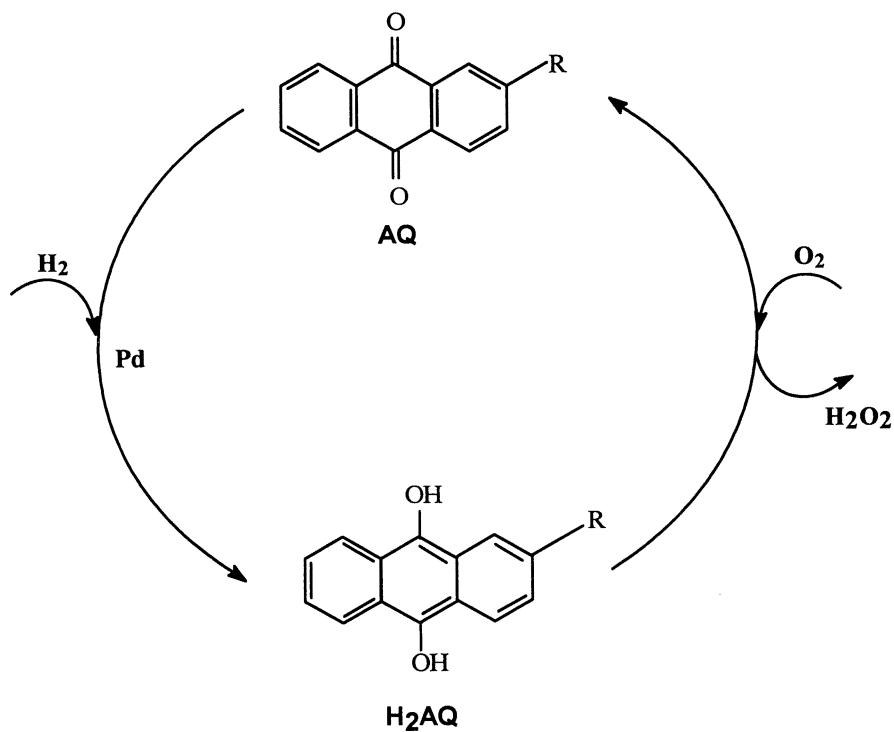


Figure 1. Anthraquinone-anthrahydroquinone process of generation of hydrogen peroxide.

The primary obstacle to the use of CO₂ as the working fluid in hydrogen peroxide (HP) production from the AQ-AQH₂ system is that conventional 2-alkylAQ's exhibit poor to negligible solubility in carbon dioxide at pressures up to 200 bar (4). Thus, the initial focus of our research has been to design and generate CO₂-philic analogs of 2-ethylAQ that would support the production of HP via sequential hydrogenation and oxidation. A family of functionalized anthraquinones (FAQ) has been designed and synthesized by attaching perfluoroether tails to either amino or hydroxy anthraquinones. In a typical FAQ, a CO₂ philic tail (perfluoroether polymer), is attached through an amidic or ester linker and a spacer to different positions of the anthraquinone rings (Figure 2). Both the phase behavior of FAQ's in CO₂ and the reactivity of these materials in the hydrogenation process were studied. The use of CO₂-philic AQ's allows one to run the H₂O₂ process in CO₂ at moderate pressures, thus minimizing capital cost. Further, the impact of the redesigned AQ on the economics of the process is minimized because the anthraquinone is recycled after each hydrogenation-oxidation cycle.

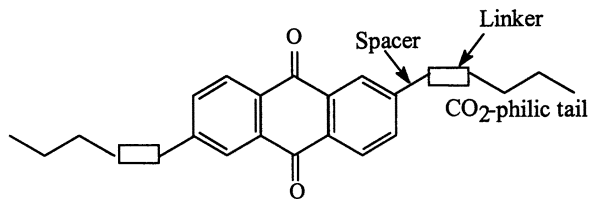
Experimental

Fluoroether-functional anthraquinones (FAQ's) were synthesized via formation of a fluoroether acid chloride from the analogous acid, followed by reaction with either amino- or hydroxy-functional anthraquinones obtained from Aldrich (5). Phase behavior of FAQ's in CO₂ was measured in a high pressure, variable volume view cell (D. B. Robinson and Associates) as described previously (6).

Both the hydrogenation of FAQ and the oxidation of FAQH₂ were conducted in high-pressure batch reactors at room temperature and P = 235 bar (7). In a typical experiment, known amounts of Pd/Al₂O₃ catalyst (Aldrich) and FAQ were charged to the hydrogenation reactor and the system was then evacuated to eliminate traces of oxygen that might interfere with the hydrogenation reaction. The solution of FAQ in CO₂ was prepared in the hydrogenation reactor and the CO₂-H₂ and CO₂-O₂ mixtures in high-pressure syringe pumps (High Pressure Equip Co.). After injection (via Rheodyne HPLC Valve) of H₂ to the hydrogenation reactor, the reaction mixture was recirculated through the UV spectrometer (Linear Systems), and the kinetics of hydrogenation reaction were followed by measuring the disappearance of the FAQ peak in the UV spectrum. After completion of the hydrogenation, the solution of FAQH₂ was transferred to the oxidation reactor, oxygen was injected, and oxidation was followed by measuring the rate of appearance of FAQ peak (310-330 nm⁻¹ region) in the UV spectrum.

Results and Discussion

The FAQ's produced for this study are either liquids at room temperature or amorphous materials that liquify upon contact with CO₂. The phase diagrams determined experimentally represent only a portion of the generalized liquid-liquid phase envelope shown in Figure 3. Above the minimum miscibility pressure (P_{min}),



Linker - OCO or NHCO

Spacer - $(\text{CH}_2)_m$; $m = 0, 1$

Position - (1,2), (1,4), (2,6)

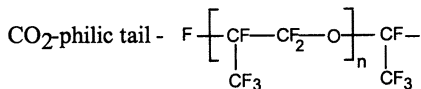


Figure 2. General formula of functionalized anthraquinone (FAQ) (General formula for the amide FAQ is $x\text{-(Kr-CONH)AQ}$ and for the ester FAQ is $x\text{-(Kr-COO-CH}_2\text{)AQ}$, where: Kr – poly(perfluoropropylene oxide) polymer).

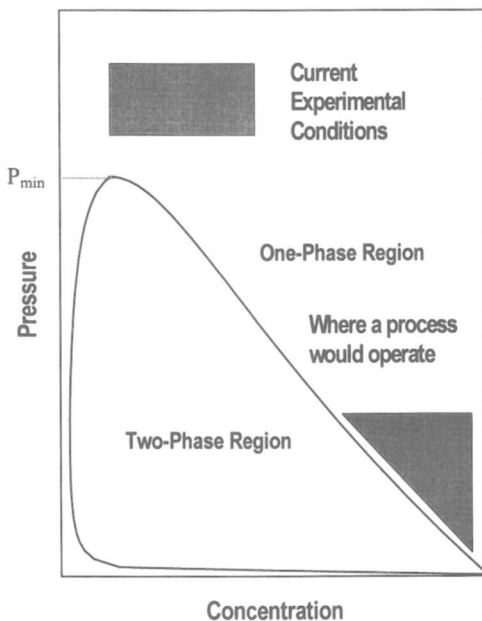


Figure 3. Generalized liquid-liquid phase diagram.

CO₂ and FAQ are miscible in any proportion and the process can be conducted either in dilute solution (to accommodate concentration constraints of the UV detector) or in the concentrated regime where CO₂ acts more as a viscosity reducing agent than a solvent. Phase behavior studies revealed that all FAQ's investigated exhibit liquid-liquid phase behavior which is influenced by (1) the length of the CO₂-philic tail; (2) the nature of the linker and spacer; (3) the topology of the tails on the anthraquinone rings.

The dependence of the cloud point curves on the molecular weight of the CO₂-philic tail shows that there is an optimum chain length (for AQ-ester-fluoroethers, at 5000 molecular weight) for which the cloud point pressures are minimized, a characteristic we have observed previously for the phase behavior of fluoroether-functional amphiphiles in CO₂ (8).

We also studied the influence of the linker on the phase of behavior of FAQ in CO₂ for a family of FAQ's having the same length CO₂-philic tail (Figure 4). As expected, the capability of the linker to form intermolecular H-bonds produces cloud point curves at higher pressures, as seen for 1 and 2-amido-FAQ's. Between the tertiary amide and the ester, the ester-FAQ has the lower cloud point pressures, revealing a thermodynamic preference by CO₂ for the less polar linker and reduced strength of solute-solute interactions.

Di-amido functionalized AQ's were synthesized by attaching two 2500 FW CO₂-philic tails in three different configurations on the anthraquinone rings: (1,2), (1,4) and (2,6); their cloud point curves are shown in Figure 5. The high cloud point pressures exhibited by the 2,6-Twin(2500) isomer can be the result of both high molecular symmetry and intermolecular H-bonding of the secondary amidic linker.

These results suggest that a strategy to lower the minimum miscibility pressure of FAQ in CO₂ would be to attach a number of small to medium CO₂-philic tails in an asymmetric configuration through non-H bond donating linking groups such as esters or ethers.

Hydrogenation of Functionalized Anthraquinone in CO₂

For a given FAQ, we ran a series of hydrogenations while varying catalyst particle size and loading to identify the controlling regimes in the process and determine the true kinetic constant (k_c), diffusion coefficients (D_e 's) of FAQ's in bulk CO₂ and the effective diffusivities (D_{eff} 's) of FAQ's inside the catalyst pores. The model assumes that (a) the only transport limitations considered are due to l-s (liquid-solid) mass transfer of FAQ and intraparticle diffusion of FAQ inside the catalyst pores, due to the total miscibility of hydrogen and CO₂ at elevated pressures (9), and (b) due to use of a 10-fold excess of hydrogen, FAQ is the limiting reactant inside the pores of the catalyst, and the reaction can be treated as pseudo-first order in FAQ. The global rate constant k_g can then be written as (10):

$$\frac{1}{k_g} = \frac{1}{w} \cdot \frac{1}{k_{eff}} \quad (1)$$

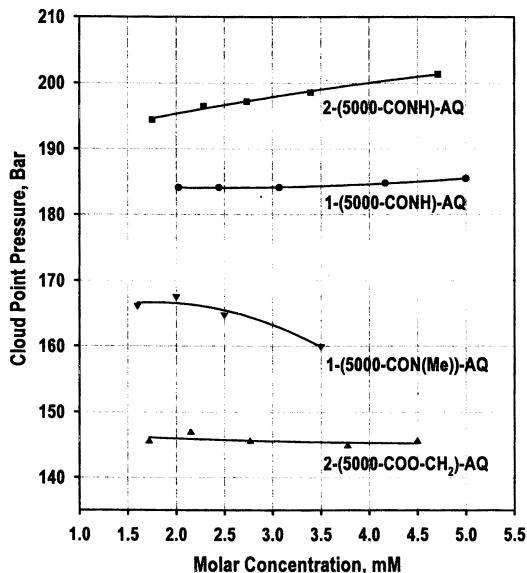


Figure 4. Effect of linking group on phase behavior FAQ's in CO₂ (data measured at T = 25 °C; Number in chemical formula shows the molecular weight of the CO₂-philic tail): (▲) 2-(5000-COO-CH₂)-AQ; (▼) 1-(5000-CON(Me))-AQ; (●) 1-(5000-CONH)-AQ; (■) 2-(5000-CONH)-AQ.

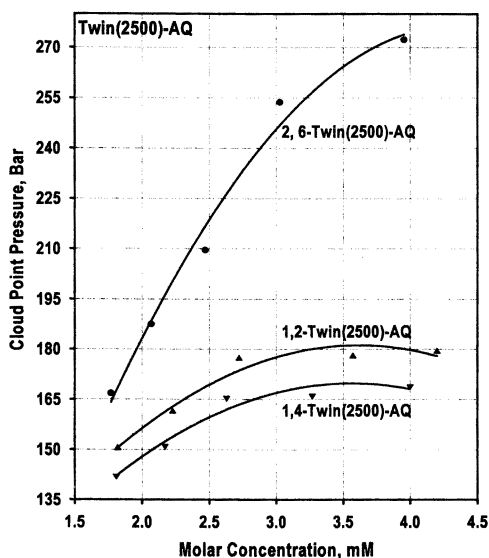


Figure 5. Effect of topology on phase behavior of Twin (2500)-AQ's in CO₂ (data measured at T = 25 °C; Number in chemical formula shows the molecular weight of the CO₂-philic tail): (▼) 1,4-Twin (2500)-AQ; (▲) 1,2-Twin (2500)-AQ; (●) 2,6-Twin (2500)-AQ.

where w is the catalyst loading and k_{eff} is given by:

$$\frac{1}{k_{\text{eff}}} = \frac{\rho_p}{6 \cdot F_c \cdot \omega(D_e, d_p)} + \frac{\phi(D_{\text{eff}}, d_p)}{k_c} \cdot \frac{1}{\left(\coth(3\phi) - \frac{1}{3\phi} \right)} \quad (2)$$

The first term in equation (2) accounts for the transport resistance from the bulk liquid to the solid catalyst, while the second term is the true rate constant modified by the efficiency factor, which accounts for transport resistance inside the catalyst particle. Further, ϕ is the Thiele modulus written for a first order reaction while F_c is the shape factor as defined in (10). To determine k_c and D_e 's and D_{eff} 's for a group of functionalized anthraquinones having the same AQ block, spacer, and linker, but different CO₂-philic tail lengths, we would:

- (1) Determine global rate constant (k_g) while varying the catalyst particle size and loading by fitting the experimental data ($C_{\text{FAQ}} = f(t)$) with an exponential 1st order function.
- (2) Determine k_{eff} by plotting k_g as a function of catalyst loading (w) for different particle size catalysts (eq. 1).
- (3) Determine k_c , D_e 's, and D_{eff} 's by fitting experimental data $1/k_{\text{eff}} = f(d_p)$ with the function given in eq. 2. The simultaneous regression was run considering that for all FAQ's in the group the intrinsic rate constant (k_c) is the same, while D_e and D_{eff} depend on the length of the CO₂-philic tail.

Mass Transfer Effects

Figure 6 shows the experimental and regressed effective rate constant for the group of amide-FAQ's with different length CO₂-philic tails. For all three FAQ's, k_{eff} is dependent on d_p indicating that the reaction is under a mixed "diffusional-kinetic" regime. To quantify the diffusional effects, the regressed value of k_c was used to calculate the overall effectiveness factor β ($\beta = k_{\text{eff}}/k_c$, see Table I). For small CO₂-philic tails and small particle size catalysts, β is close to 1 and the reaction is kinetically controlled. By increasing either the particle size of the catalyst or the size of the CO₂-philic tail, β drops to values of 0.1-0.3 indicating that in this case the diffusion of FAQ within the catalyst pores is the controlling step in the process.

The resulting diffusion coefficients are in the range of 10^{-3} – 10^{-4} cm²/s, in good agreement with values reported in the literature for diffusion coefficients of organic substances in CO₂ (Table II) (11). For small CO₂-philic tails, diffusion is fast, and the reaction is kinetically controlled. By increasing the length of the CO₂-philic tail, the diffusion coefficients decrease and diffusion becomes the rate-determining step of the process.

In Table II, the true kinetic constants (k_c 's) for the amide- and ester-FAQ's are compared to the corresponding value calculated for 2-ethyl AQ in organic solvents. Ester-FAQ's are twice as reactive as the amide variants while the amide FAQ's in

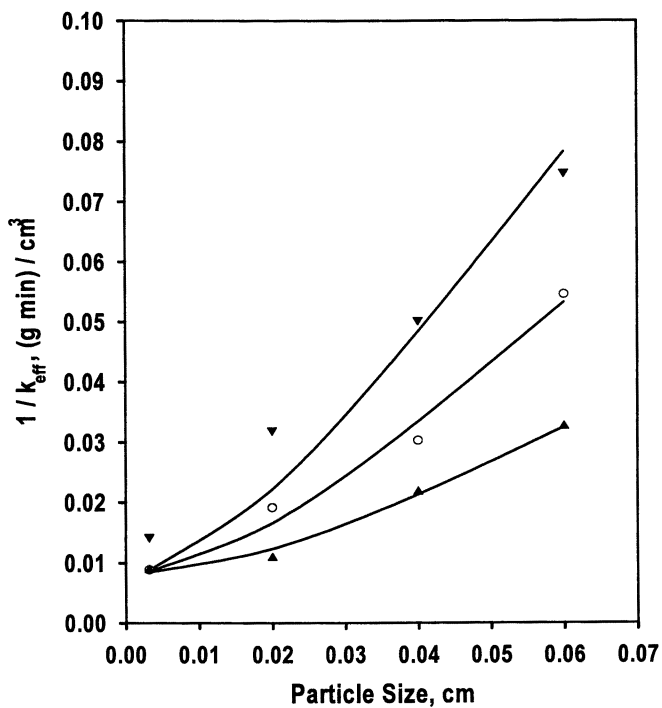


Figure 6. Effect of d_p on $1/k_{eff}$ for: (▲) 2-(2500-CONH)AQ; (○) 2-(5000-CONH)AQ; (▼) 2-(7500-CONH)AQ ($P=235$ bar. Number in the chemical formula indicates the molecular weight of the CO_2 -philic tail).

Table I. Overall effectiveness factors (β) for hydrogenation of FAQ's in CO₂ (P = 235 bar, T=25 °C)

$d_p^{(a)}$ C_m	$\beta = k_{eff}/k_c^{(b)}$			$\beta = k_{eff}/k_c$		
	2-(Kr-COO-CH ₂)-AQ ^(c)			2-(Kr-CONH)-AQ		
	700 ^(d)	2500	5000	2500	5000	7500
0.0032	~1	0.92	0.55	0.9	0.9	0.65
0.02	0.71	0.84	0.37	0.75	0.4	0.3
0.04	0.55	0.42	0.26	0.35	0.25	0.15
0.06	0.32	0.21	0.11	0.25	0.15	0.1

(a) d_p - Average catalyst particle diameter. (b) k_{eff} - effective rate constant calculated from eq. (1); k_c - "true" kinetic constant regressed from eq. (2). (c) Kr - perfluoroether polymer. (d) Molecular weight of the perfluoroether polymer attached to AQ block.

Table II. Kinetic and mass transfer parameters determined by regression (P = 235 bar, T = 25 °C)

2-(Kr-NHCO)AQ ^(a)			2-(Kr-COO-CH ₂)AQ ^(a)		
FW	$k_c^{(b)}$	$D_e^{(c)}$	FW	$k_c^{(b)}$	$D_e^{(c)}$
700	-	-	700	3.8	13.5
2500	2.0	4.8	2500	3.8	7.0
5000	2.0	2.1	5000	3.8	2.5
7500	2.0	1.13	7500	-	-
2-etAQ	0.47 ^(d)				

(a) Chemical formula defined as in Figure 2. (b) [cm³ / (g s)]. (c) [cm²/s 10⁴]. (d) Reference 12.

CO₂ are 4 times more reactive than 2-*et*AQ in organic solvents. We suspect that the electronic effect of the group attached to the AQ's block plays an important role. The acyl-amino group (NHCO) is a mildly electron donating group, stabilizing the quinone in the redox equilibrium quinone-hydroquinone. The ester group separated by the methylene spacer from the aromatic rings has an opposite effect, stabilizing the anthrahydroquinone by its electron withdrawing effect.

Oxidation of Functionalized Anthrahydroquinone (FAQH₂) in CO₂

Oxidation of functionalized anthrahydroquinone (FAQH₂) was followed by measuring the rate of appearance of the FAQ peak in the UV spectrum. Preliminary oxidation experiments performed using 2-(7500-CONH)AQ show that the initial FAQ is fully recovered after one hydrogenation–oxidation cycle, based on the initial and final values of the UV absorbance of FAQ (Figure 7). We are currently investigating the reactivity of FAQH₂ as a function of the nature of the linker – spacer and the length of the CO₂-philic tail.

Example 2: Refining of Metals

Currently, the most widely used route for purification of platinum group metals (PGM's, i.e., platinum, palladium, rhodium, gold, etc.) consists of mining and crushing PGM-bearing ore, then leaching the metals using an HCl/Cl₂ biphasic mixture at elevated pressure. The resulting aqueous solution is a mixture of AuCl₄⁻², PtCl₆⁻², PdCl₄⁻², and the analogous rhodium, iridium, and ruthenium species. In addition, small amounts of less-valuable metals are also extracted from the ore. Consequently, the next step in the purification train is the solvent extraction of the PGM chloride species, followed by recovery and reduction to the zero-valent metal (13).

Although H₂AuCl₄ is soluble in oxygenated solvents (ethers, ketones, esters, etc. (14)), neither the platinum nor palladium species are soluble in organic solvents, and thus a mixture of solvent and phase transfer ligands (PTL's) is used to remove these materials in additional steps. For example, tri-octyl amine is commonly employed to extract platinum, while either a disulfide or beta-hydroxy oxime is employed to subsequently strip the palladium chloride from the mix. The organic solvent used is typically an aliphatic or aromatic petroleum distillate. The metal chloride-ligand complexes are eventually reduced to zero-valent metal using a variety of compounds, such as oxalic acid for gold. In addition to primary refining, the recycling of PGM's from spent catalytic converters also employs dissolution in an aqueous HCl/Cl₂ mixture followed by solvent extraction to separate and purify the metals (15). Solvent extraction is also used heavily in copper and lanthanide refining.

As in the case of hydrogen peroxide production, the current process for PGM refining employs a liquid-liquid extraction between an organic and aqueous phase to retrieve valuable products. Thus, replacement of the organic phase with CO₂ eliminates the need to remediate the water from the organic contamination. As in the

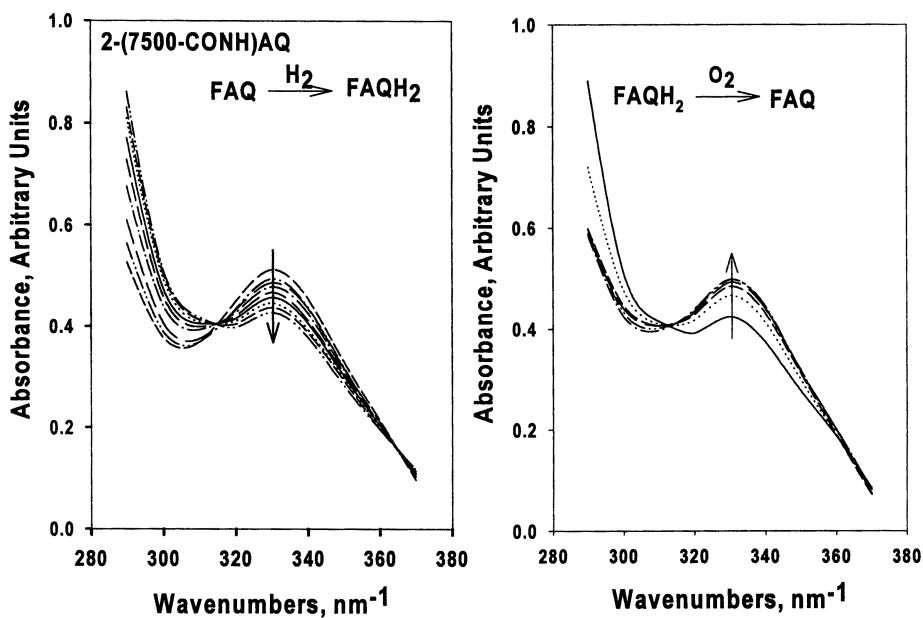


Figure 7. Hydrogenation and oxidation of 2-(7500-CONH)-AQ in liquid CO₂ followed by UV spectroscopy.

case of the anthraquinone process, we have found that the solubility of conventional PGM extractants and/or the solubility of the PTL-metal chloride complexes in CO₂ is poor, necessitating design of CO₂-philic ligands to achieve extractions at moderate pressures. The other criteria described in the introduction do not apply to the current version of the PGM refining process, yet if we substitute hydrogen for currently employed reducing agents, then the other benefits are realized. If hydrogen were used in *conventional* PGM refining, a two-phase gas-liquid system would result, representing a potential safety hazard as compared to, for example, use of oxalic acid to reduce Au⁺² (as AuCl₄⁻²) to Au⁰. However, it is known that hydrogen can be employed to reduce the PGM chloride-ligand complexes (16), and dilution of the hydrogen in a CO₂ solution will allow reduction while maintaining safe concentrations. In addition, because hydrogen's molecular weight is much lower than conventional reducing agents, hydrogen is a more atom-efficient reducing agent. Use of hydrogen in a CO₂-based PGM recovery scheme thus allows recovery of the metals without depressurization, recycle of the CO₂-philic ligands, and the use of gaseous hydrogen in a CO₂-based solution renders this means for reducing the metals much more efficient than in an analogous gas-liquid version.

Experimental

Highly CO₂-soluble PTL's for the extraction of Pt and Au into CO₂ were generated via the reaction of amino-functional tertiary amines with the acid chloride of either fluoroalkyl or fluoroether carboxylic acids. Single, twin- and triple-tailed tertiary amines were generated. Not surprisingly, all of these materials exhibited complete miscibility with liquid CO₂ (22 °C) at moderate pressures. Complexes of PTL's with metal chlorides were prepared by contacting an aqueous solution of either H₂AuCl₄ or H₂PtCl₆ with a solution of the ligand in a fluorinated solvent (here 1,1,2 trichlorotrifluoroethane), where the metal is present in large excess. Separation of the phases followed by removal of the solvent left the metal-ligand complex.

Phase behavior in CO₂ was observed as described above; extractions of either platinum or gold into CO₂ were conducted as described by Yazdi and Beckman (6), where a glass liner was inserted into the extraction vessel to prevent premature reduction of the metal by Fe ions stripped by the aqueous HCl from the vessel walls. Metal concentrations in the aqueous phase before and after extraction were measured using ICP-MS.

Results

We have found previously that triethyl amine (TEA), a ligand used in conventional PGM refining, is miscible with CO₂, yet complexes of TEA with either gold or platinum are not. Hence, fluorinated phase transfer ligands were required to allow extraction of either Pt or Au into CO₂. Phase behavior results of two complexes using identical ligands (Figure 8) show that the extraction is feasible and that, because

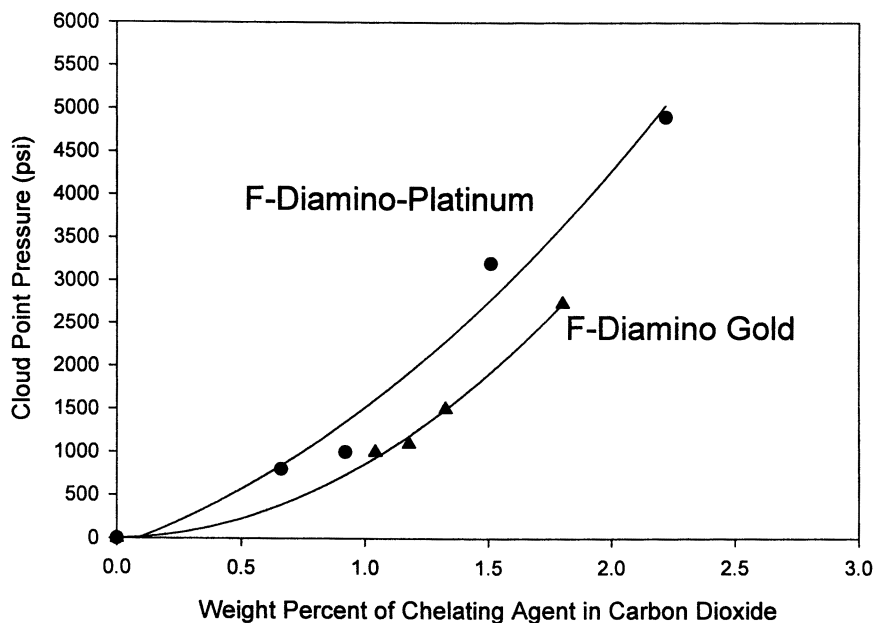


Figure 8. Cloud-point curves ($T = 22\text{ }^{\circ}\text{C}$) of complexes formed between a bis(fluoroalkyl)tertiary amine and either gold or platinum in carbon dioxide.

the phase boundary curves of the two complexes differ appreciably, one might be able to separate metals using pressure as the control variable in CO₂.

In addition, an extraction from aqueous HCl (1M) into liquid CO₂ (22C, 1500 psi) was performed for platinum (PtCl₆) using a twin-tailed, fluoroalkyl-functional tertiary amine. Using 50% excess PTL, 88% of the platinum was extracted in a single equilibrium stage.

Summary

A simple set of heuristics can be used to identify processes where use of carbon dioxide provides environmental benefits, while an analogous set of process constraints aids in the optimization of such processes. Based on the constraints imposed by the use of CO₂ as a process solvent, both production of hydrogen peroxide and precious metal refining are ideal application targets for CO₂ technology. In both applications, CO₂ travels in a loop, where pressure is relatively constant, and the products can be recovered without a large pressure drop. Design of the CO₂-philic substrates is feasible allowing lowering the operating pressure. Finally, both functionalized anthraquinones and CO₂-philic chelating agents can be recycled thus the added cost owing to redesign of the substrate for use in CO₂ is minimized.

Using the examples of hydrogen peroxide production and precious metal refining, we have shown that carbon dioxide can provide green solutions to various chemical processing problems. First, in each process we are proposing to replace organic solvents with CO₂ and thus eliminate a process step where water is remediated. In hydrogen peroxide production, operation in CO₂ will allow process intensification, in that the distillation train can likely be eliminated and therefore energy consumption is reduced. Finally, the unique characteristics of CO₂ allow us to design smaller and more efficient plants because the reactions can be conducted under kinetically controlled regimes.

Thus, although CO₂ is often promoted as a green solvent, for the case of H₂O₂ generation or precious metal refining the use of CO₂ allows for a more efficient and thus less expensive process as well.

Literature Cited

1. Powell, R. *Hydrogen Peroxide Production*; Noyes Develop. Corp.: Park Ridge, 1968.
2. (a) Hess, W. T. Hydrogen Peroxide. In *Kirk-Othmer Encyclopedia of Chemical Technology*, 4th edition; Kroschwitz, I., Howe-Grant, M., Eds., John Wiley & Sons, Inc.: New York, 1995; Vol. 13, 961. (b) Guenter, T. E. Hydrogen Peroxide. In *Encyclopedia of Chemical Processing and Design*; McKetta, J. J., Cunningham, W. A., Eds., Marcel Dekker, Inc.: 1988; Vol. 27, 27.
3. (a) Drelinkiewicz, A. Deep Hydrogenation of 2-Ethylanthraquinone over Pd/SiO₂ Catalyst in the Liquid Phase. *J. Mol. Catal.* **1992**, *75*, 321. (b) Drelinkiewicz, A.

- Kinetic Aspects in the Selectivity of Deep Hydrogenation of 2-Ethylanthraquinone over Pd/SiO₂. *J. Mol. Catal. A: Chem.* **1995**, *101*, 61. (c) Santacesaria, E.; Di Serio, M.; Velloti, R.; Leone, U. Hydrogenation of the Aromatic Rings of 2-Ethylanthraquinone on Palladium Catalyst. *J. Mol. Catal.* **1994**, *94*, 37.
- (a) Swidersky, P.; Tuma, D.; Schneider, G. M. High Pressure Investigations on the Solubility of Anthraquinone Dyes in Supercritical Gases by VIS-Spectroscopy. Part II - 1,4-Bis-(*n*-alkylamino)-9,10-anthraquinones and Disperse Red 11 in CO₂, N₂O, and CHF₃ up to 180 MPa. *J. Supercrit. Fluids* **1996**, *9*, 12. (b) Joung, S. N.; Yoo, K. P. Solubility of Disperse Anthraquinone and Azo Dyes in Supercritical Carbon Dioxide at 313.15 to 393.15 K and from 10 to 25 MPa. *J. Chem. Eng. Data* **1998**, *43*, 9.
 - Hancu, D.; Beckman, E.J. Production of Hydrogen Peroxide in Liquid CO₂. 1. Design, Synthesis and Phase Behavior of CO₂-Miscible Anthraquinones. *Ind. Eng. Chem. Res.* **1999**, *38*, 2824.
 - Yazdi, A. V.; Beckman, E. J. Design, Synthesis, and Evaluation of Novel, Highly CO₂-Soluble Chelating Agents for Removal of Metals. *Ind. Eng. Chem. Res.* **1996**, *35*, 3644.
 - Hancu, D., Beckman, E. J. Production of Hydrogen Peroxide in Liquid CO₂. 2. Catalytic Hydrogenation of CO₂-Phylic Anthraquinones. *Ind. Eng. Chem. Res.* **1999**, *38*, 2833.
 - Lepilleur, C.; Beckman, E. J.; Schonemann, H.; Krukons, V. J. Effect of Molecular Architecture on the Phase Behavior of Fluoroether-Functional Graft Copolymers in Supercritical CO₂. *Fluid Phase Equilib.* **1997**, *134*, 285.
 - Tsang, C. Y.; Streett, W. B. Phase Equilibria in the H₂/CO₂ Systems at Temperatures from 220 to 290 K and Pressures to 172 MPa. *Chem. Eng. Sci.* **1981**, *36*, 993.
 - Ramachandran, P. A.; Chaudhari, R.V. *Three-Phase Catalytic Reactors*; Gordon and Breach, Science Publishers, Inc.: New York, 1983.
 - (a) Akgerman, A.; Erkey, C.; Orejuela, M. Limiting Diffusion Coefficients of Heavy Molecular Weight Organic Contaminants in Supercritical Carbon Dioxide. *Ind. Eng. Chem. Res.* **1996**, *35*, 911. (b) Silva, C. M.; Macedo, E. A. Diffusion Coefficients of Ethers in Supercritical Carbon Dioxide. *Ind. Eng. Chem. Res.* **1998**, *37*, 1490.
 - Santacesaria, E.; Di Serio, M.; Velloti, R.; Leone, U. Kinetics, Mass Transfer, and Palladium Catalyst Deactivation in the Hydrogenation Step of the Hydrogen Peroxide Synthesis via Anthraquinone. *Ind. Eng. Chem. Res.* **1994**, *33*, 277.
 - (a) *Precious Metals: Science and Technology*; Benner, L. S.; Suzuki, T.; Meguro, K.; Tanaka, S., Eds.; Internat. Prec. Met. Inst.: Allentown, PA, 1991. (b) Harris, G.B. *14 Precious Metals*, R.K. Mishra, ed., Pergamon Press, Toronto, CAN, 1993, pg 351.
 - Fink, R.; Beckman, E. J. *High Pressure Reaction Equipment: Design and Safety in Chemical Synthesis Using Supercritical Fluids*, Jessop, P.G., Leitner, W.; Eds; Wiley-VCH, in press.

15. Mishra, R.K. *A Review of Platinum Metals Recovery from Automobile Catalytic Convertors*. *Precious Metals* 1993, Proc. of 17th Int. Prec. Met. Conf.; 1993, p 449.
16. (a) Findlay, M. The Use of Hydrogen to Recover Precious Metals in *Precious Metals 1982*; El Guindy M.I., Ed., Pergamon Press: Toronto, Can, 1983, p 477. (b) Toshima, N.; Harada, M.; Yamazaki, Y.; Asakura, K. Catalytic Activity and Structural-Analysis of Polymer-Protected Au-Pd Bimetallic Clusters Prepared by The Simultaneous Reduction of H₂AuCl₄ And PdCl₂. *J. Phys. Chem.* **1992**, *96*, 9927. (c) Santacesaria, E.; Galli, C.; Carra, S. *React. Kinet. Catal. Lett.* **1977**, *7*, 361.

Chapter 8

Green Process Concepts for the Pharmaceutical Industry

Bala Subramaniam¹, Said Saim^{2,3}, Roger Rajewski², and Valentino J. Stella²

¹Department of Chemical and Petroleum Engineering, University of Kansas, Lawrence, KS 66045–2223

²Center for Drug Delivery Research, Higuchi Biosciences Center, University of Kansas, Lawrence, KS 66047–2535

Process concepts for producing drug particles using supercritical carbon dioxide (*scCO*₂) as an antisolvent and for substrate coating employing *scCO*₂ as the fluidizing medium and antisolvent are described. Particle micronization with *scCO*₂ allows for reproducible crystal formation with the potential for increased surface area and dissolution rates. Coating with *scCO*₂ allows the use of traditional organic-soluble coatings with complete solvent recovery and virtually no atmospheric emissions. For formation of drug nanoparticles, an ultrasonic nozzle that employs *scCO*₂ as the energizing medium is used to form droplets of the drug-laden solution. The *scCO*₂ also selectively extracts the solvent from the droplets, precipitating the drug. Submicron particles of hydrocortisone and ibuprofen (600 nanometers or less) formed in this manner are presented. Advantages include the production of virtually solvent-free drug particles in a narrow size range. For particle coating, *scCO*₂ is used to fluidize the core substrate particles. The *scCO*₂ also removes the solvent from the coating solution sprayed on the substrates, thereby precipitating the coating. This coating process expands the range of substrate/coating combinations possible with the conventional air-suspension Wurster coater, making it feasible to coat water-soluble substrates with solutes sprayed from organic solutions.

³Current address: Boehringer Ingelheim Pharmaceuticals, Inc., 900 Ridgebury Road, Ridgefield, CT 06877–0368.

Introduction

Conventional pharmaceutical processing involves extensive use of organic solvents as antisolvents for recrystallizing drugs from solutions, as reaction media in the synthesis of drugs or as extracting agents for selectively isolating drugs from solid matrices. This may lead to environmental emissions of toxic solvents (such as methylene chloride) or trace solvent residues in the product. Concerns about solvents have propelled research efforts aimed at developing environmentally-benign chemical processing techniques that either eliminate or significantly mitigate pollution at the source (*J*). A major research focus in pharmaceutical processing has been the replacement of traditional solvents with *scCO*₂. In this paper, we discuss two applications developed in our laboratory: the formation of nanoparticles of sparingly soluble drugs, and the coating of drugs. Research and scaleup challenges facing successful implementation of these promising technologies in practice are also discussed.

Nanoparticles in Pharmaceutical Applications

For drugs that show poor intrinsic water-solubility, decreasing the particle size enhances the dissolution rate in the human system, and therefore, the drug bioavailability. Creating nanoparticles of such drugs is therefore desirable. In addition, it has been reported that nanoparticles smaller than 500 nanometers (nm) can cross Peyer's patches and the mesentery on the surface of gastrointestinal mucosa to directly deliver a drug to the systemic circulation (2, 3). For parenteral application, drugs that are 500 nm or less are also suitable for intravenous injection in a suspension form, further enhancing their drug-delivery potential. The development of environmentally-benign methods for production of solvent-free nanoparticles of poorly water-soluble pure drugs is thus highly desirable. For instance, Cyclosporin A (CyA) is a highly lipophilic cyclic peptide that is poorly soluble in water. It is the immunosuppressant of choice for the prevention of allograft rejection of transplanted bone marrow, kidney, heart, liver, lung, pancreas, and skin and appears to be efficacious in the treatment of autoimmune diseases, such as diabetes mellitus and rheumatoid arthritis (4, 5). At present, dosage forms of CyA (intravenous and oral solution) are not very effective therapeutically due to slow and highly variable absorption. The low aqueous solubility of CyA has prevented the development of alternative dosage forms. Other dosage forms such as liposomes and lipophilic carriers have limited *in vitro* and *in vivo* stability. Other poorly-soluble drugs whose bioavailability depends on particle size include camptothecin (a potential anti-cancer agent), pposulfam, steroid A, and indomethacin.

Particle Formation Using *scCO*₂

Conventional techniques for particle size reduction include mechanical comminution (crushing, grinding and milling), recrystallization of the solute

particles from solution using liquid antisolvents, freeze drying and spray drying. Among the limitations associated with these processes are excessive solvent use and disposal, thermal and chemical degradation of products, trace residues, and interbatch particle size variability. Two CO₂-based particle formation processes have received increased attention in recent years. In the first process, termed rapid expansion of supercritical solutions (RESS) (6), the solute is solubilized in scCO₂. The solution is then expanded across a nozzle or capillary at supersonic velocities. The rapid expansion leads to supersaturation of the solute and precipitation of virtually contaminant-free particles. The RESS process has been shown to produce contaminant-free drug particles ranging from a few microns to several hundred microns (7). A major limitation of the RESS process is that at moderate temperatures and pressures (<60°C and 300 bar), the solubilities of pharmaceutical compounds in scCO₂ are on the order of 0.01 wt% or less. The addition of co-solvents, such as methanol, to CO₂ is often necessary to enhance solubilities. However, these added solvents affect the environmentally-benign nature of the RESS process. Other challenges are the operational and scale-up issues associated with nozzle design to avoid particle accumulation and freezing caused by the rapid expansion.

The relatively low solubilities of pharmaceutical compounds in unmodified CO₂ are exploited in the second CO₂-based process wherein the solute of interest (typically a drug, polymer, or both) is dissolved in a conventional solvent to form a solution. The preferred ternary phase behavior is such that the solute is virtually insoluble in dense CO₂ while the solvent is completely miscible with dense CO₂ at the recrystallization temperature and pressure. The solute is recrystallized from solution in one of two ways. In the first way, a batch of the solution is expanded several-fold by mixing with dense CO₂ in a vessel. Because the CO₂-expanded solvent has a lower solvent strength than the pure solvent, the mixture becomes supersaturated forcing the solute to precipitate or crystallize as microparticles. This process was termed Gas Antisolvent (GAS) recrystallization (8). The second way involves spraying the solution through a nozzle into compressed CO₂ as fine droplets. This process has been termed in general as Precipitation with Compressed Antisolvents (PCA) (9) and employs either liquid or scCO₂ as the antisolvent. When using a supercritical antisolvent, the spray process has been termed Supercritical Antisolvent (SAS) Process (10) or Aerosol Spray Extraction System (ASES) (11).

The GAS or PCA process is thus complementary to RESS. Advantages of GAS/PCA include higher solute throughput and the flexibility of solvent choice. As reviewed elsewhere (12), the PCA and GAS techniques have been used to micronize a wide variety of pharmaceutical compounds such as polymers used in controlled-release formulations, protein powders and anti-inflammatory agents. These size ranges encompass those suitable either for pulmonary delivery (1-3 μm) or in implantable devices (<100 μm). Because the spray-processes (PCA, SAS, and ASES) permit faster depletion of the solvent (and hence greater production rate of particles) relative to the GAS process, they have received increased attention in recent years.

Use of Ultrasonic Nozzles for Spray Atomization

In the spray processes reported to date, standard capillary nozzles, electrically actuated ultrasonic atomizer (13) and coaxial nozzles (14, 15) have been employed to spray the solution. Regardless of the type of nozzle used (capillary, ultrasonic or coaxial nozzles), the average particle size of the precipitated materials is generally around 1 μm or more in previously reported spray processes. In the spray processes, the particle size and morphology are dependent on several factors such as the operating pressure, temperature, jet breakup and the mass transfer rates between the droplet and antisolvent phases. Jet breakup and the droplet sizes depend on the relative magnitudes of the droplet deforming (inertial, external) and reforming (viscous, interfacial tension) forces. These forces in turn are dictated by the nozzle configuration, the spray velocity and the physical properties of the droplet and antisolvent phases. While some useful attempts have been made to interpret the effects of process variables on particle size and morphology in terms of the dimensionless groups (Reynolds, Weber and Ohnesorge groups) that characterize the spray dynamics and jet breakup (16-18), a better understanding of the spray process based on the underlying rate processes (spray dynamics, mass transfer and nucleation processes) remains a challenge.

Some mechanistic clues emerge when one considers the schematic of the SAS process (Figure 1). When the solution is sprayed through conventional nozzles, primary droplets form which then undergo secondary atomization into finer droplets. For supersaturation and crystallization to occur, the solvent has to be transported from the droplets to the CO_2 phase. When the antisolvent medium is relatively stagnant, this interphase mass transfer step can be slower than the rate of droplet coalescence, resulting in larger particles. Clearly, the interphase mass transfer rate is a key determinant of particle size.

In our studies, we employ an ultrasonic nozzle (energized by compressed CO_2) to atomize the spray into droplets. High frequency sound waves can be generated via various types of transducers, such as piezoelectric, magnetostrictive, electromagnetic, pneumatic devices (so-called whistles similar to the common whistle based on the organ-pipe effect), and other mechanical transducers. The use of sound waves produced by one or more of these devices to generate droplets from liquid surfaces or to atomize liquid spray jets has been known for more than half a century (19). One of the earliest 'pneumatic devices' used to generate sound waves employed a jet of air impinging on a cavity to generate sound waves -- the so-called Hartmann whistle (20). Focusing the generated sound waves on spray jets has been employed to atomize liquid spray-jets. Because the smallest practical focal region of a wave is a sphere one wavelength in diameter, the focal region of a focused sound wave is relatively large compared to a focused light wave. Whistle-type devices have been used to generate high-intensity sound waves in both air and liquids. A practical upper frequency for applications using air is approximately 30 kHz. Using helium or hydrogen, such whistles are capable of generating ultrasonic energy up to 500 kHz.

In the device we used (Figure 2), a gas such as helium (He), or a supercritical fluid like CO_2 , or combinations of both is used as the energizing gas. A hollow

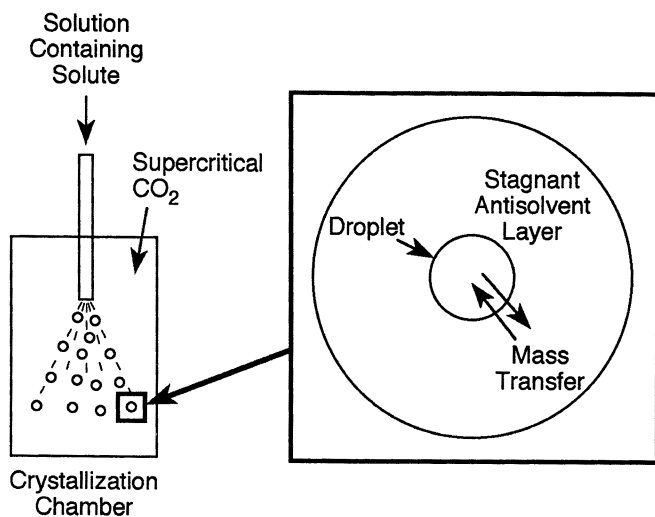


Figure 1. Schematic of conventional SAS process.

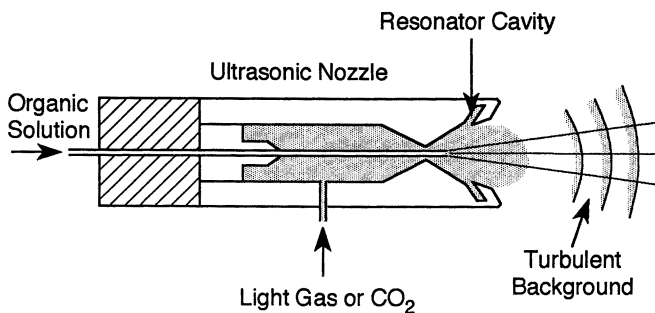


Figure 2. Schematic of the ultrasonic nozzle used for nanoparticle formation.

resonator cavity is radially disposed such that the generated sound waves are focused on the spray jet in order to facilitate enhanced atomization of the spray. For precipitation to occur, the solvent from the droplets must be transferred to the antisolvent phase surrounding the droplets. It is well known in the field of ultrasonics that sound waves are beneficial for enhancing heat and mass transfer rates. Thus, in addition to enhancing atomization, the concomitant increase in the mass transfer surface area produced by the sound waves will also enhance the mass transfer rate between the droplets formed and the surrounding fluid medium, thereby increasing the rate of solid precipitation.

The generation of sound waves in a supercritical medium has not been widely investigated. However, since supercritical fluids display gas-like compressibilities, the speed of sound should become smaller relative to the ideal gases in the vicinity of the critical point. The speed of sound in ambient air is roughly 1000 km/h. Based on correlations (21), the velocity of sound is estimated to reach nearly 700 km/h in *scCO*₂ at 37 °C and 80 bar -- conditions similar to those employed in the SAS process. Therefore, the wavelength of the propagated sound is expected to decrease proportionately, aiding droplet breakup and increasing mass transfer rates.

In the device shown in Figure 2, the solution is sprayed from a capillary tube fitted inside the device in a direction concurrent with the energizing gas. It should be clear that the spray jet could also originate external to the device as long as the generated sound waves from the ultrasonic nozzle are focused on the jet to achieve atomization. For example, the capillary tube used to spray the drug-laden solution can be positioned at the exit of the ultrasonic nozzle either perpendicular or diametrically opposite to the ultrasonic nozzle. In the latter case, the drug solution will be sprayed countercurrent to the energizing gas.

Figure 3 shows a schematic diagram of the apparatus employed to form drug nanoparticles. The apparatus consists of an isothermal and isobaric recrystallization chamber (a 450-ml stainless steel chamber), an ultrasonic spray nozzle (as shown in Figure 2), a source of *scCO*₂, a drug and excipient solution, a solvent collection vessel, and a CO₂ vent. The crystallizer is housed in an isothermal water bath. The experimental unit allows experiments to be conducted at pressures up to 340 bar and temperatures up to 70 °C. When the bath temperature is stable at a desired value, CO₂ is pumped through the top side port of the cell with an ISCO (Lincoln, NE) 260D syringe pump at a constant rate (typically 5 ml/min as liquid) to pressurize the chamber. When used as the energizing gas for the nozzle, *scCO*₂ was also added to the outer converging-diverging section of the nozzle (see Figure 2). When the temperature and pressure in the cell are stabilized, the organic solution of the drug is metered through the central port of the nozzle. Both fluids are preheated to operating temperature by passing them through heat exchangers housed together with the cell in the water bath. Particles are collected on SEM (Scanning Electron Microscope) stubs placed inside the cell. The solute-depleted mixture of CO₂ and organic solution then flows through a step-motor controlled, computer-actuated micrometering valve. Upon expansion to a subcritical pressure in a flash drum, the mixture separates into an organic liquid phase and a CO₂ gas phase. The liquid phase consisting mostly of the solvent flows through a micrometering

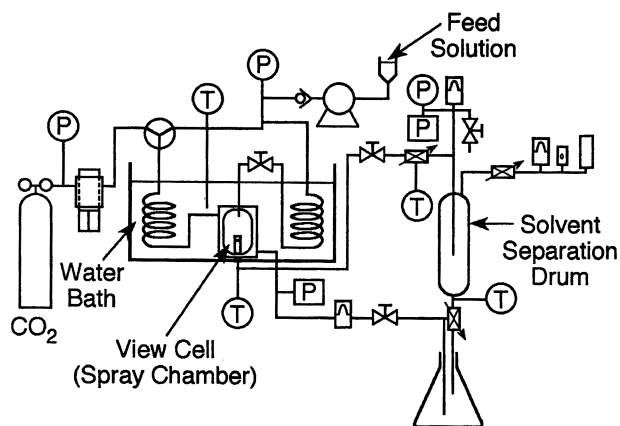


Figure 3. Schematic of SAS crystallizer.

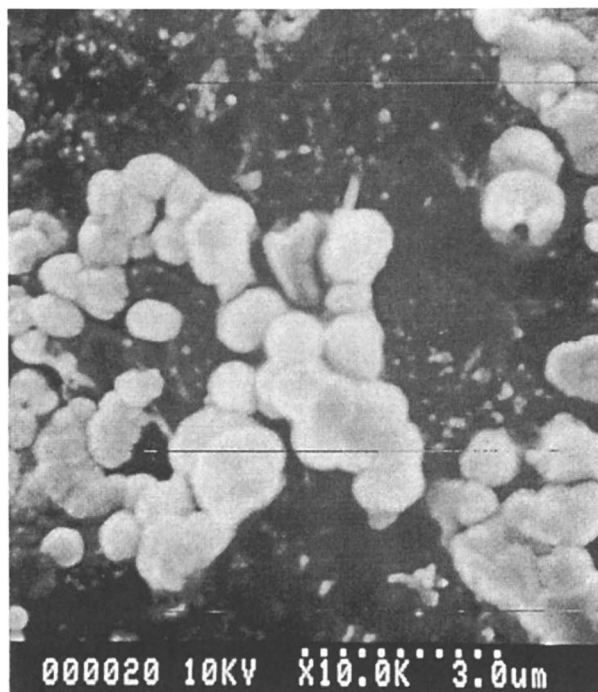


Figure 4. SEM micrograph of hydrocortisone micronized by recrystallization from a 5 mg/ml DMSO solution using the conventional SAS process with a 100 μm capillary nozzle.

valve and is collected. The CO₂ is vented through a step-motor controlled micrometering valve, a rotameter and an electronic mass flowmeter. Pressure control in the cell, along with monitoring of pressure, temperature and flow rate, are accomplished using a Camile® (Midland, MI) 2500 Data Acquisition and Control system. More details of the equipment may be found elsewhere (22)

Figure 4 shows an SEM micrograph of hydrocortisone particles recrystallized from a 5 mg/ml dimethyl sulfoxide (DMSO) solution using the 100 μm capillary nozzle (P = 103 bar; T = 35 °C; CO₂ flow rate = 5 ml/min.; solution flow rate = 2.5 ml/min.). Particles are agglomerated, nearly spherical, and range in size from 0.5-1 μm. Recrystallization of hydrocortisone from a 30 mg/ml DMSO solution yielded long (up to 1 mm), 1 μm thick, whisker-shaped particles as shown in Figure 5 (P = 103 bar; T = 35 °C; CO₂ flow rate = 5 ml/min.; solution flow rate = 2.5 ml/min.; capillary I.D. = 100 μm). It appears that the increase in viscosity at the higher solute concentrations resists spray-jet breakup, resulting in the formation of elongated, whisker-like particles. The increase in particle size with an increase in solute concentration was observed for all solutes recrystallized using the conventional SAS process.

Figure 6 shows an SEM micrograph of hydrocortisone particles recrystallized from a 30 mg/ml DMSO solution using the ultrasonic nozzle in Figure 2 and CO₂ as the energizing gas. In the recrystallization chamber: P = 85.6 bar; T = 35 °C; and the solution flow rate is 2.5 ml/min. The resulting particles are discrete, and appear to be narrowly distributed around 500 nm. Nearly all particles are smaller than 600 nm. These results are in contrast to the 1 μm wide and nearly 1 mm long fibers obtained when using the 100 μm capillary nozzle. Hence, a significant decrease in the average particle size is observed with the use of the ultrasonic nozzle.

Figure 7 shows a SEM micrograph of ibuprofen particles recrystallized from a 30 mg/ml DMSO solution under the same nozzle and identical operating conditions as for hydrocortisone (Figure 6). Again, the recrystallized nanoparticles are discrete, with most particles being in the range of 600 nm or less.

DMSO is not a preferred solvent because of concerns about residual solvent traces on the drug. In addition, its high viscosity compared to other common organic solvents (such as ethyl acetate and acetone) hinders jet breakup. However, the drug particles produced by our method had a residual DMSO concentration below the detection limit of the flame ionization detector (~10 ppm). By demonstrating that virtually solvent-free drug micro- and nanoparticles can be produced using DMSO as solvent, our results suggest that it should be easier to produce nanoparticles with other less viscous and more acceptable solvents such as ethanol, ethyl acetate and acetone. The main advantages of the scCO₂-powered ultrasonic nozzle over conventional capillary spray nozzles reported in the literature are as follows: (a) the ultrasonic nozzle-based process is capable of producing discrete nanoparticles in a narrow size range; and (b) the sound waves aid jet breakup into small droplets, increasing the interfacial area. In addition, the turbulence created by the focused sound waves also enhances the mass transfer rate between the droplets and the CO₂. Since near-critical CO₂ is highly compressible, it should be possible to vary the frequency (or wavelength)

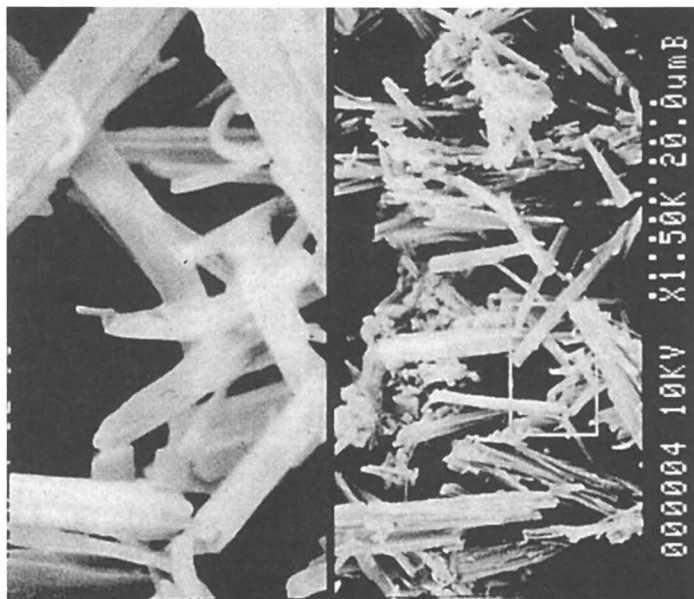


Figure 5. SEM micrograph of hydrocortisone micronized by recrystallization from a 30 mg/ml DMSO solution using the conventional SAS process with a 100 μm capillary nozzle.

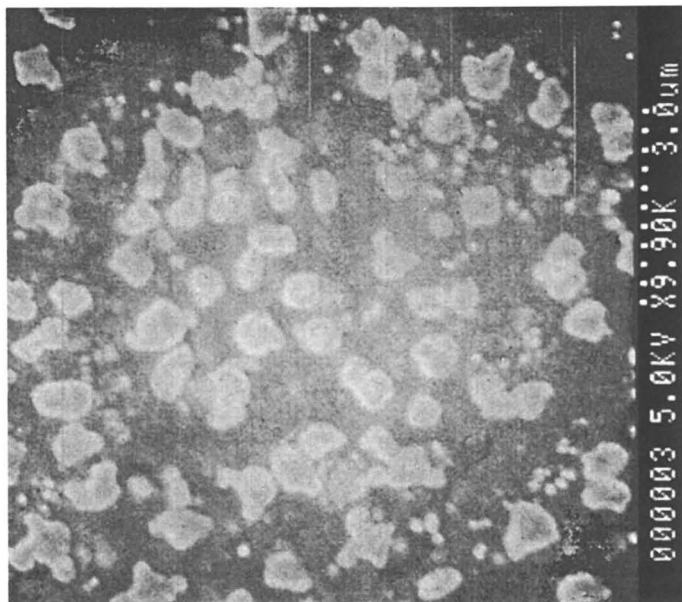


Figure 6. SEM micrograph of hydrocortisone nanonized by recrystallization from a 30 mg/ml DMSO solution using the ultrasonic nozzle (compressed CO_2 is used as energizing gas and as antisolvent).

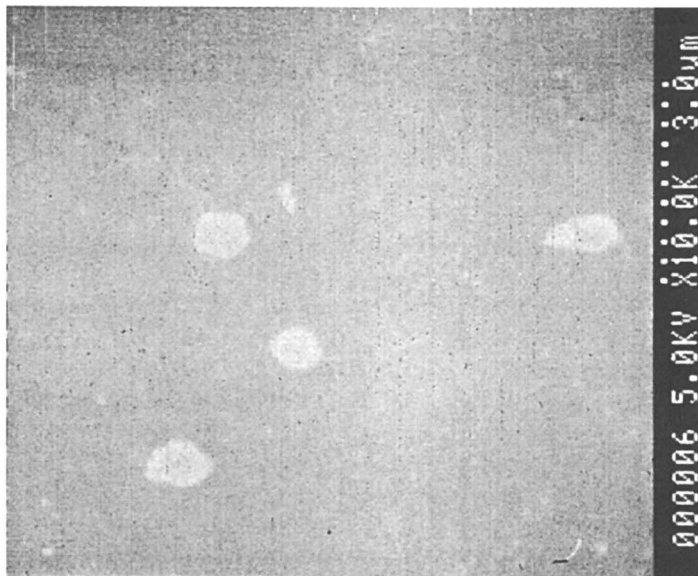


Figure 7. SEM micrographs of ibuprofen nanonized by recrystallization from a 30 mg/ml DMSO solution using the ultrasonic nozzle (compressed CO₂ is used as energizing gas and as antisolvent).

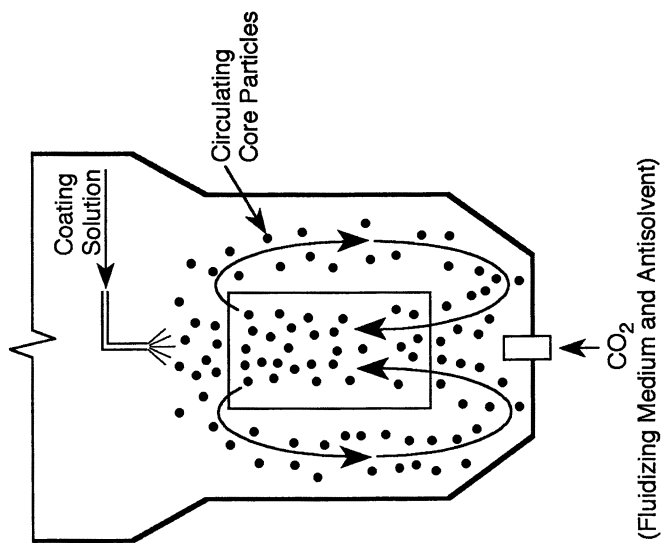


Figure 8. Schematic diagram of CO₂-based coating process.

of the generated sound waves by simple pressure-tuning. This ability to control the frequency of the generated sound waves could potentially be employed to control particle size.

Suspension Coating Using $scCO_2$

In the pharmaceutical industry, it is desired to coat drug particles either for aesthetic/handling purposes or for delayed release applications such as taste masking. Generally, such coating has been carried out using techniques such as electrolysis, vapor deposition, and fluidized bed suspension. However, these methods all suffer from drawbacks, including difficulty maintaining aseptic conditions, inability to generate extremely fine particles for coating purposes, and difficulty controlling solvent emissions.

The CO_2 -based coating technology is an extension of the SAS recrystallization process. The SAS process may be viewed as a spray-drying process in which hot air is replaced with thermally-mild (31-45 °C), environmentally-benign CO_2 . In the coating process demonstrated by us (Figure 8), the beads or tablets to be coated are kept suspended in $scCO_2$. The solution containing the drug(s) is then sprayed into the suspension. The drug particles that result upon contact with $scCO_2$ are then deposited as a coating on the substrate particles.

The CO_2 -based coating process described above is an enabling technology for coating water-soluble substrates from organic solutions. The coating process is similar to conventional air suspension coating using a Wurster coater (23), with additional advantages as follows: (1) Operation at lower temperatures, and hence with thermally labile core and coating materials; (2) The ability to process active ingredients from organic solutions with no risk of ignition; (3) The ability for forming finer coatings; and (4) Easy recovery of the organic solvent, leading to decreased emissions. Thus, our technology complements the conventional Wurster coater by expanding the range of substrate-solvent possibilities.

For the coating experiments, we employed a 65 ml Jurgeson gage (view-cell) fitted internally with a 16 cm long, 8 ml glass tube (similar to that shown in Figure 3). The glass tube was initially charged with the substrate (nonpareil sugar beads or glass beads) to be coated, and then fitted at the bottom of the view cell. When the bath temperature is stabilized at a desired value, CO_2 is pumped at a constant rate (typically 5 ml/min. as liquid) until pressure in the cell reaches a desired level (103 bar). When temperature and pressure in the cell are stabilized, the organic solution (DMSO or ethyl acetate solution of drug and/or polymer) is metered through capillary nozzle tubing.

In order to establish countercurrent flow and fluidize (i.e., suspend) the beads, the CO_2 was introduced at the bottom of the tube while the organic solution of the coating material was sprayed from roughly two inches above the suspended bed. Fresh CO_2 and the organic solution streams thus mixed within the glass tube. The resulting particles descended down the tube and either adhered to the glass tube walls or were deposited on the beads. Any particles not

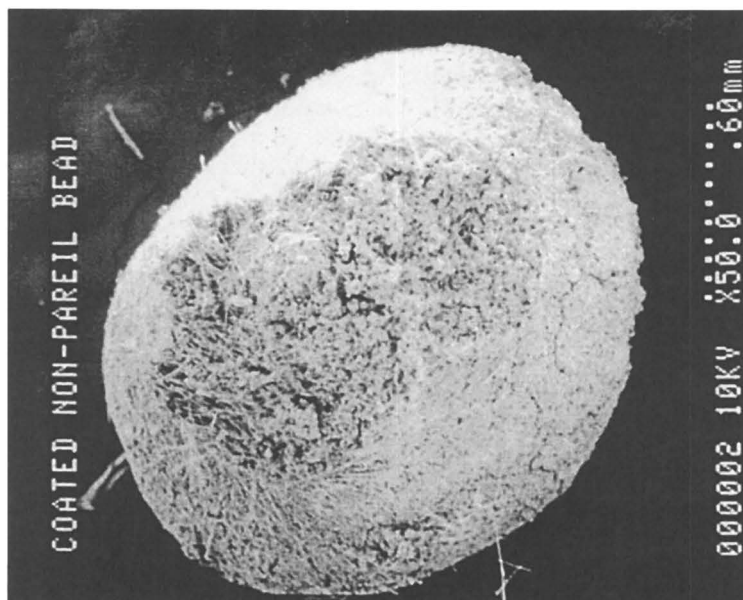


Figure 9. SEM micrograph of a non-pareil bead coated with RG503H microparticles.

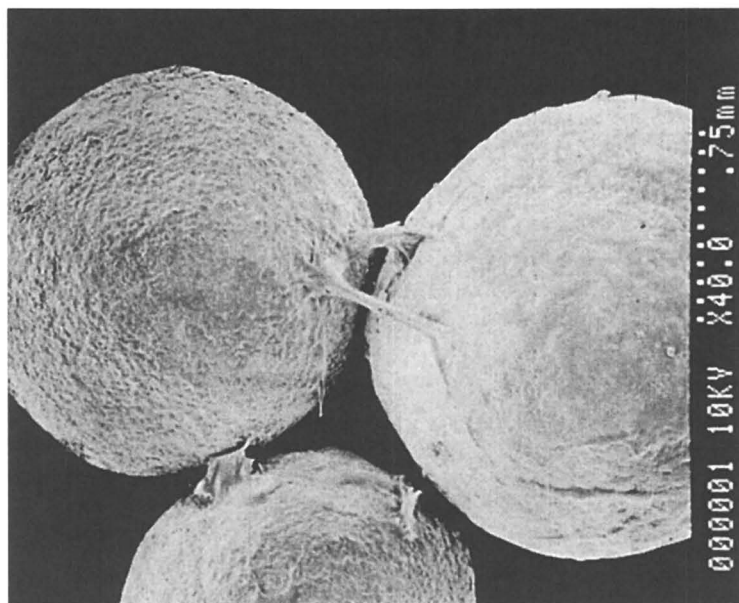


Figure 10. SEM micrograph of nonpareil sugar beads coated with a continuous film of RG503H.

retained within the view cell chamber were retained on the steel frit housed in the exit line. Pressure control in the cell and solvent recovery was achieved as explained in the previous section. For coating nonpareil sugar beads (1.5 mm) with RG503H (lactide-glycolide copolymer), a 10 mg/ml ethyl acetate solution of RG503H was sprayed into the glass tube for 5 minutes. Capillary nozzle I.D., temperature, pressure, solution flow rate and liquid CO₂ rate were 100 μm, 35 °C, 103 bar, 2.5 cc/min, and 5 mL/min, respectively.

Figure 9 is a SEM micrograph of a coated nonpareil sugar bead. The bead is nearly uniformly coated with a layer of RG503H microparticles. The recrystallized microspheres are of similar size (roughly 10 μm) to those obtained in runs at identical conditions with the same solution in the absence of the beads. Figure 10 is an SEM micrograph of nonpareil sugar beads coated with RG503H recrystallized under the same conditions as in Figure 9 except that the view cell temperature was held at 40 °C in the former case. At the increased temperature of 40 °C, the polymer deposits on the sugar beads as a continuous film, likely due to the lowering of the glass transition temperature by *sc*CO₂. Thus, either particle or film coating may be achieved depending upon the process temperature.

The foregoing CO₂-based coating process offers the following advantages compared to conventional fluidized air based coating processes:

- Significant reduction in the risk of fire and explosion (when using organic solvents) because of operation at lower temperatures (31-45 °C) with dense CO₂;
- The process offers enormous flexibility for controlling the size and morphology of particulate coatings. Using an ultrasonic nozzle with *sc*CO₂ as the energizing gas, nanoparticle coatings should be possible;
- The organic solvent and the CO₂ can be easily separated and recycled;
- Precipitation occurs when the solvent from the droplets is extracted (i.e., solubilized) by CO₂, which can be faster when compared to drying by solvent evaporation into air. In other words, virtually solvent-free coating may be obtained in a relatively short time.

Concluding Remarks

With *sc*CO₂, we have demonstrated two attractive technologies for pharmaceutical processing that could result in significantly reduced use of conventional liquid solvents and the production of relatively contaminant-free products. Supercritical CO₂ energized ultrasonic nozzle offers an attractive means of producing micron and sub-micron particles of sparingly water soluble drugs with controlled particle size and purity. Challenges facing successful implementation of the technology include scaleup, demonstrating continuous production and harvesting of nanoparticles with desired and reproducible product quality.

The CO₂-based coating process complements the conventional Wurster coater, expanding the range of substrate-solvent combinations to include water-soluble substrates and organic solvents. The extensive knowledge-base that exists in the design and operation of the conventional Wurster coater can be conveniently exploited in the design, scaleup, and operation of the coater. The main challenge lies in the internal design of the coater such that a circulating fluidization pattern for the substrate particles and core particle wetting are obtained. These attributes are essential for obtaining uniformly coated particles. Our research group is currently addressing the aforementioned challenges.

In addition to being environmentally safer, the CO₂-based processes presented here are enabling technologies for forming nanoparticles of sparingly water-soluble drugs and in coating water-soluble substrates from organic solvent-based sprays.

Acknowledgment

This work was supported in part by the Kansas Technology Enterprise Corporation (KTEC) through the Centers of Excellence program.

References

1. Anastas, P.T. and Williamson, T.C., *Green Chemistry: Frontiers in Benign Chemical Syntheses and Processes*, Oxford University Press, Oxford (1998).
2. Tomlinson, E., *Int. J. Pharm.*, **1983**, *4*, 49-57.
3. Kreuter, J., *J. Controlled Release*, **1989**, *16*, 169-176
4. Borel, J.F and Gunn, H.C. *Ann. N.Y. Acad. Sci.*, **1985**, *475*, 307-319.
5. Sanchez, A., Vila-Jato, J.L. and Alonso, M.J., *Int. J. Pharm.*, **1993**, *99*, 263-273.
6. Matson, D. W.; Fulton, J. L.; Peterson, R. C.; Smith, R. D. *Ind. Eng. Chem. Res.* **1987**, *26*, 2298-2306.
7. Tom, J. W.; Debenedetti, P. G. *Biotechnol. Prog.* **1991**, *7*, 403-411.
8. Gallagher, P.M.; Coffey, M.P.; Krukonis, V.J.; Klasutis, N. In *Supercritical Science and Technology*; ACS Symposium Series 406; Johnston, K.P.; Penninger, J.M.L., Eds., American Chemical Society: Washington, D.C., 1989; pp 334-354.
9. Dixon, D.J.; Johnston, K.P.; Bodmeier, R.A. *AIChE J.* **1993**, *39*, 127-139.
10. Yeo, S.-D.; Lim, G.-B.; Debenedetti, P. G.; Bemstein, H. *Biotech. Bioeng.* **1993**, *41*, 341-346.
11. Müller, B. W.; Fischer, W.; German Patent Appl. No. DE 3744329 A1 1989.
12. Subramaniam, B.; Rajewski, R. A.; Snavely, W. K. 1997, *J. Pharm. Sci.*, **1997**, *86*, 885-890.
13. Randolph, T. W.; Randolph, A. D.; Mebes, M.; Yeung, S. *Biotechnol. Prog.* **1993**, *9*, 429-435.

14. York, P.; Hanna, M. In *Respiratory Drug Delivery V: Program and Proceedings*; Dalby, R.N., Ed.; Interpharm Press: Buffalo Grove, IL, 1996; pp 231-239.
15. Mawson, S; Kanakia, S.; Johnston, K.P. *J. Appl. Polym. Sci.* **1997**, *64*, 2105-2118.
16. Dixon, D.J.; Johnston, K.P.; Bodmeier, R.A. *AIChE J.* **1993**, *39*, 127-139.
17. Saim, S.; Subramaniam, B.; Rajewski, R. A.; Stella, V. J. *Pharm. Res.* **1996**, *13*, S-273.
18. Eggers, R.; Wagner, H.; Jaeger, P. In *High Pressure Chemical Engineering; Process Technology Proceedings*, 12; von Rohr, P. R.; Trepp, C., Eds.; Elsevier: Amsterdam, 1996; pp. 247-252.
19. Ensminger, D. *Ultrasonics: Fundamentals, Technology, Applications*, 2nd ed., Marcel Dekker, 1988.
20. Hartmann, J. *Journal of Scientific Instruments*, **1939**, *16*, 140-149.
21. Span, R.; Wagner, W. *J. Phys. Chem. Ref. Data*, **1996**, *25*, 1509-1596.
22. Subramaniam, B; Saim, S.; Rajewski, R.A.; Stella, V.J. U. S. Patent, 5,833,891, 1998.
23. Wurster, D.E. *J. Amer. Pharm. Assoc. Sci. Ed.*, **1959**, *48*, 451-454.

Chapter 9

Two-Stage Drawing of Poly(ethylene terephthalate) Fibers Using CO₂

Terry Hobbs and Alan J. Lesser

Polymer Science and Engineering Department, University of Massachusetts, Amherst, MA 01003

Fibers of poly(ethylene terephthalate) were drawn by a two stage drawing technique: drawing at 23°C in liquid CO₂ followed by hot drawing $\geq 200^\circ\text{C}$ at a constant strain rate. CO₂ pressure dramatically affected the drawing behavior during the first stage. At 200°C, the maximum achievable draw ratios (TDRs) for the CO₂ treated and untreated fibers were 12.2 and 8.2 respectively. The highest modulus and strength values for the treated fibers were about 10% higher compared to untreated fibers. When the drawing temperature was increased in the second stage, the fibers had high crystallinity values (>60%) and a much lower amorphous orientation.

Introduction

The drawing behavior of poly(ethylene terephthalate) (PET) for the production of high modulus and high strength fibers has been studied intensely for the past several years. Although fairly high modulus values of 35 GPa have been reported, it is still difficult to produce high strength fibers. Because of its high performance, low cost, and recyclability, it is one of the most attractive candidates for high strength fibers. The final strength of a given PET sample is dependent on several factors including sample geometry, entanglement density, load applied during drawing, and molecular weight (1-3).

Generally, ultrahigh molecular weight PET has a high melt viscosity and melt spinning is difficult. In addition, the entanglement density for melt spun fibers is high which can limit drawability. Commercial fibers produced by melt spinning have low molecular weight thus making it difficult to achieve tenacity and modulus values above a well-established level (4).

For the production of high strength fibers, researchers have focussed on solution spinning utilizing various organic solvents (5,6). From a processing point of view, these solvents are undesirable since they are expensive, toxic, and must be removed which can further complicate the fiber morphology. As an alternative, it has been shown that melt spun fibers (i.v. = 0.9 dL/g) can be treated with acetone or DMF/water solutions. These organic solvents plasticize the fiber along with creating an imperfect crystal structure which enhances drawability (7). The resultant fibers can be drawn to higher draw ratios using a two-stage draw technique resulting in 20% higher strength values. The initial superstructure or morphology created in the first stage draw is extremely important with regard to properties achieved after the second stage draw.

A large number of other experimental techniques have been investigated for improving PET including solid state coextrusion, zone drawing, and vibrational hot drawing (8-10). Compared to other processing methods, tensile drawing in CO₂ is unique because CO₂ is both a plasticizer and a pressure transmitting media. Upon depressurization, CO₂ escapes from the polymer substrate. Hence, it acts as a *reversible plasticizer*. The concept of reversible plasticization was originally developed by Zachariades and Porter using NH₃ during the solid state extrusion of nylon 6 and nylon 6,6 (11).

Compared to traditional or uniaxial drawing, drawing in CO₂ can place the polymer fiber in a multi-axial stress state under certain process conditions, i.e. no permeation of the polymer. Under non-permeable conditions, our process mimics solid state extrusion or drawing in pressurized silicone oil. Under conditions of good permeability and sorption, the process is similar to Ito's solvent treatment. These conditions and transport properties can readily be tuned by changing pressure and/or temperature. It is widely accepted that CO₂ cannot permeate the crystalline component of polymers, hence the crystalline component is under hydrostatic stress. Upon drawing, permeability of the CO₂ in the amorphous phase can change as the chains orient into a more densely packed state. This is a known phenomenon for other polymer systems (12). Overall, drawing in CO₂ is a unique process pressurizing the crystalline phase

The development of CO₂ processing for fibers has several environmental benefits. It reduces energy consumption and eliminates waste. CO₂ is environmentally benign and escapes a polymer as a gas, a natural component of air. Replacement of traditional organic solvents with CO₂ has the potential to prevent the formation of large amounts of wastewater in coagulation and post treatment processes. In addition, the use of CO₂ as a plasticizer can reduce processing temperatures and save energy. These concepts have been proven by the replacement of methylene chloride in dry cleaning and dyeing operations. Hence, one can see the large potential of CO₂ processing in the fiber industry in the realm of green chemistry and engineering. In addition, CO₂ processing offers opportunities to create fibers and films with unique engineered properties not available by other means.

In this paper, we investigate the use of subcritical and supercritical CO₂ (SC CO₂) as a drawing media for initially amorphous PET fibers produced by melt spinning. Subcritical CO₂ refers to CO₂ below its critical point (72.8 atm, 31.1°C). The use of

CO₂ for fiber treatment parallels the use of solvent treatment. Both penetrate and remain in the fiber during the drawing process. The use of subcritical and SC CO₂ in a drawing process have many potential advantages including solvent tunability, suppression of brittle failure due to imposed hydrostatic pressure, environmental friendliness as a benign solvent, and plasticization of the amorphous phase. Unlike conventional plasticizers, CO₂ is easily removed simply by depressurization.

The critical point for CO₂ is at 31.1° C and 72.8 atm where it enters the supercritical state displaying transport properties between a gas and a liquid and solvent-like properties of a liquid. For most polymers including PET, CO₂ is a non-solvent. However, it does penetrate the fiber acting as a diluent or plasticizer. As pressure is further increased above the critical point, the density of CO₂ increases rapidly along with the solubility parameter (13) Hence, one would expect the entropic interaction of a given polymer with CO₂ to change as density changes, as predicted by various theories such as the one by Flory (14).

The interaction of amorphous PET with traditional organic solvents has been studied extensively, but the studies with SC CO₂ are essentially nonexistent. Limited studies with subcritical CO₂ have shown that CO₂ slowly crystallizes PET resulting in a small crystallite/imperfect crystal structure where WAXD scattering peaks are rather broad (15). In addition, the crystallization rate is highly pressure dependent (16). We will discuss the drawing behavior in CO₂ and morphological developments of the PET fibers using a two-stage process. Comparisons will be made to cold drawn and solvent treated fibers. We will also discuss the tensile properties of the fibers produced in this unique process.

Experimental

Sample Preparation

High molecular weight PET with a reported inherent viscosity of 2.01 dL/g was used for all fiber preparations. The intrinsic viscosity of the PET measured in our laboratory was 1.18 dL/g using a 50/50 (v/v) mixture of trifluoroacetic acid and methylene chloride at 30°C. The polymer was ground to fine powder and passed through a sieve ensuring that the particles were less than 1000 µm in diameter. The powder was dried for 20 hours at 140° C in a vacuum oven. Fibers were melt spun under a nitrogen blanket in a Randcastle microextruder with a die temperature of 295° C. Fiber mechanical properties were very sensitive to heating, melting, and die zone temperatures. As-spun fibers were taken up on a spool a rate of approximately 250 m/min resulting in a final diameter of 67 µm. The fibers had a birefringence of 1.5×10^{-3} while DSC and flat plate WAXD patterns showed that the fibers were primarily amorphous (< 5% crystallinity).

Measurements

The first stage drawing of the fibers was performed in air or a custom high pressure drawing apparatus as shown in Figure 1. The apparatus is mounted on an Instron model 1333 tensile testing machine. Coleman grade CO₂ is supplied through a Hydro-pac, Inc. high-pressure carbon dioxide pump and filtered through activated carbon and a drying agent. The high-pressure apparatus is constructed primarily of standard high-pressure components and fittings. The mechanical grips are positioned in a high-pressure cylindrical vessel and connected to a cantilever beam and a movable piston. The piston forms a seal against the vessel wall with two standard nitrile rubber O-

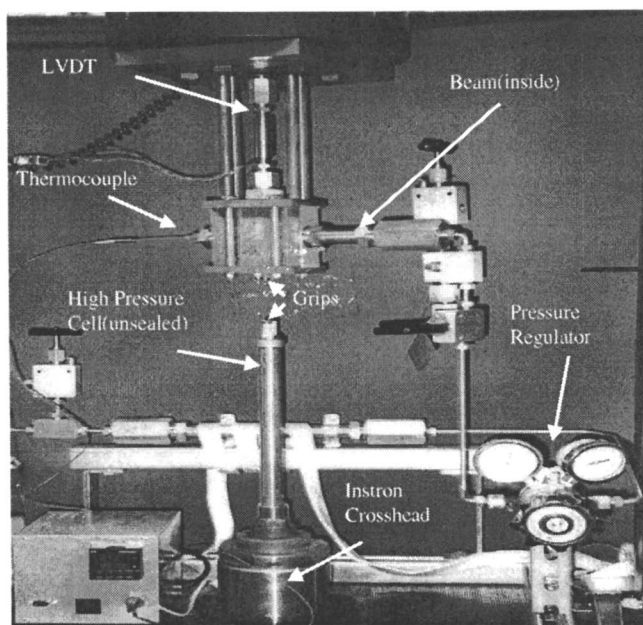


Figure 1. Picture of stainless steel high pressure drawing apparatus.

rings. The apparatus is capable of making in situ force measurements using a calibrated stainless steel cantilever beam inside the pressure environment and a linear variable displacement transducer (LVDT) with electronics outside of the CO₂ media. The electronic signals and crosshead displacement are monitored using a personal

computer using MTS Teststar II software. Stress values were calculated from force measurements normalized by the fiber cross sectional area. The initial cross sectional area was determined from the linear density of the bundles and the amorphous fiber density of 1.325 g/cm^3 . Fiber bundles typically contained 50 filaments. Strain was calculated from the relative displacement between the crosshead and beam normalized by the fiber gage length. Draw ratios were directly calculated from the strain measurements. All fiber bundles unless otherwise specified were drawn at a strain rate of 1 min^{-1} .

Single filament tests were performed on an Instron 5564 using a 10 N load cell at a strain rate of 0.1 min^{-1} and a gauge length of 25 mm. Tensile strength, modulus, and elongation to failure results were based on 5 specimens. Specimens were tabbed onto a cardboard template using a 5-minute epoxy gel adhesive. The fiber diameter was measured using a high magnification microscope calibrated with a micrometer scale. Birefringence measurements were made using an Olympus polarizing microscope equipped with a $1\text{-}20\lambda$ Berek compensator. The retardation was measured using the thick Berek compensator with individual filaments being mounted on a glass slide.

Crystallinity measurements were made based on a two-phase model using a density column prepared from n-heptane and CCl_4 . Differential Scanning Calorimetry (DSC) was performed using a TA Instruments thermal analyst 2100 with a heating rate of 10° C/min . Wide angle X-ray measurements (WAXD) were made on a Siemens D500 diffractometer with a Ni filtered Cu-K α source at 40 kV and 30 mA. Scanning electron microscope (SEM) images were obtained using a JEOL SC-35 with a filament voltage of 20 kV. Flat plate X-ray diffraction patterns were obtained using a Statton camera (40 kV, 30 mA) under vacuum conditions.

The second draw stage was conducted in a high temperature convection air oven chamber on an Instron 1233. The second stage draw unless otherwise specified was conducted at 200° C . For higher temperatures, the fibers were dried for 30 hours at 50° C to prevent hydrolysis. Fibers were drawn under constant strain rate until individual filaments began failing as the load reached a plateau. The crosshead was stopped and the fibers were held under a high load during cooling in order to preserve or maximize amorphous orientation. During cooling, the load would decrease when the crosshead was stopped and then increased upon further cooling near 130° C .

Results and Discussion

Crystallization

The initial morphology and degree of crystallinity are extremely important factors, which effect drawability and structural development in PET fibers. PET can be crystallized very slowly at lower temperatures above its glass transition temperature, T_g . It has been recently shown that CO_2 at 50 atm and 50° C crystallizes amorphous PET slowly over 3 days (17). The resulting PET displays broad peaks indicating small/imperfect crystallites. At the same pressure and 85° C , the half-life of

the crystallization is 10 minutes by infrared spectroscopy measurements (18). It is difficult to determine how much crystallization actually occurs in the high-pressure environment as the removal of CO₂ upon depressurization may drive the crystallization process further. When amorphous PET is treated with acetone, removal of the acetone by vacuum results in a distinct sharpening of the diffraction pattern indicating further crystallization and/or an increase in perfection of the crystallites (19).

The morphology prior to acetone removal has been identified with a more drawable structure. Treatment with CO₂ gas and organic solvents seem to produce similar morphologies with regard to the crystalline regions. We have found that the use of CO₂ over a wide pressure range results in a similar morphology in a treatment time of 15 minutes as shown by WAXD scan in Figure 2. The diffraction peaks are rather broad especially compared to a melt crystallized sample indicating the presence of small and/or imperfect crystallites. Pressure has an insignificant effect on breadth of the peaks. Therefore, the change in crystallite size is negligible. The angular position of the peak intensities in the 2 θ scans (Figure 2) for CO₂ fibers and a melt crystallized sample are nearly identical indicating similar unit cell dimensions. This indicates that the CO₂ treatment process did not alter the triclinic crystal structure.

Fundamental crystallization differences do occur when using CO₂ compared to acetone. CO₂ diffuses as a gas or supercritical fluid into the sample at rate, which is

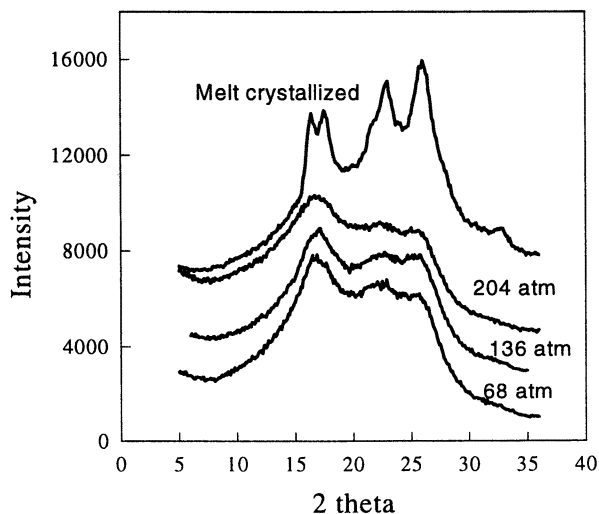


Figure 2. WAXD results for fibers treated at various pressures

two orders of magnitude faster. When the samples were simply treated with either subcritical or SC CO₂, the entire fiber bundle relaxed resulting in a shrinkage of 20%.

When we treated fibers with acetone, they whitened but the dimensions of the sample did not change.

The morphology for CO₂ treated fibers is believed to be less complex because of the extremely fast diffusion of the CO₂ and slow crystallization. The crystallization of PET occurs in two distinct limiting modes (20). In the first, the solvent penetrates the polymer inducing crystallization creating a barrier that slows further diffusion of the solvent. An advancing front can be detected separating the amorphous unpenetrated core and crystallized outer layers. The crystallization process is kinetically faster than the diffusion and sorption process. This process occurs for PET upon treatment with traditional solvents such as acetone and aromatic hydrocarbons.

In the second mode, PET is completely saturated by the solvent followed by crystallization where the kinetic rate of crystallization is usually slow. The second mode describes the crystallization of PET with CO₂ gas. We believe that the same mode occurs at higher pressures as well. This contention for complete plasticization is supported by high diffusion constants for CO₂ at elevated pressures and the observed gross macroscopic shrinkage of fiber bundles observed after CO₂ treatment (40-204 atm) (21). If the fiber bundles crystallized prior to complete penetration, macroscopic shrinkage would not be observed. The initial morphology of the acetone treated fibers is extremely complex because of the slow diffusion and fast crystallization processes. The outer shell of the fiber crystallizes under different conditions compared to the core of the fiber. In contrast, one would expect the CO₂ treated fibers to be nearly homogenous in the radial direction as a result of high diffusion rates and slow crystallization. The resultant morphology is inherently less complex.

Because crystallization occurs, we know that PET in CO₂ is above its glass transition temperature (T_g) at pressures above 68.0 atm and temperatures of 25° C. In situ mechanical measurements support this notion as fibers are completely plasticized and show no resistance to drawing. Previous research using DSC indicates that the T_g of PET is depressed to 35° C when exposed to CO₂ at 35 atm (22). The T_g decreased as the treatment pressure increased with the highest pressure being 35 atm. In summary, high pressure CO₂ completely plasticizes and crystallizes amorphous PET fibers creating a unique morphology that is similar yet distinguishable from solvent treated fibers.

Ductility and One-Stage Drawing

We have observed that the drawability of PET fibers is increased by 30% when using CO₂ as a drawing media. Fibers can be drawn in CO₂ to 650% strain compared to 500% for untreated fibers, a comparable increase in drawability to DMF/H₂O mixtures. Our studies on the drawing behavior of PET in CO₂ indicate profound pressure effects on the drawability as shown in Figure 3. A cold drawn PET sample was included in Figure 3 for comparison of drawing behavior. The drawing behavior is clearly due to the CO₂ as hydrostatic pressure itself would increase the yield stress and T_g of a cold drawn sample. High pressure CO₂ clearly decreases the yield point along with the T_g.

The 68.0 atm curve does not display a yield response so the increase in drawability is due to an appreciable amount of CO₂ in the polymer. If crystallization had occurred to a significant extent, a yielding behavior would be observed as seen in acetone and DMF treated fibers. It should be noted that the experiment at 68.0 atm was stopped due to instrumental limitations, i.e. limited stroke in the servohydraulic machine. The fibers could have potentially been drawn further. The 68.0 atm curve is very smooth showing that the experimental apparatus is quite sensitive to slippage or individual filament failures. For the 68.0 atm curve, the slope in the strain induced crystallization regime is much lower. This is the most crucial effect as noted when drawing PET fibers treated with DMF/water mixtures (23). We have performed similar experiments in the pressure region near 68 atm. The maximum drawability for these fibers (660% strain) occurred slightly above the critical pressure between 80-95 atm.

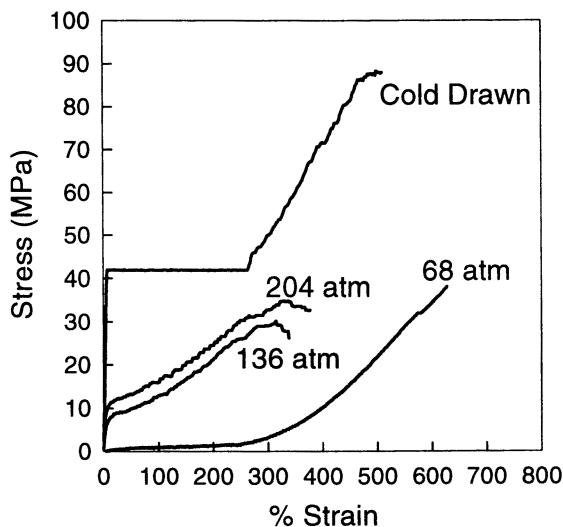


Figure 3. Stress-strain behavior as a function of CO₂ Pressure

The fiber bundles drawn in SC CO₂ corresponding to pressures of 136.1 atm and 204.1 atm show similar drawing behavior to each other. Their drawing behavior characterized by the absence of a plateau in the stress/strain curve is very different compared to subcritical (68.0 atm) and cold drawn samples. In addition, increasing pressure to this range severely limits the drawability of the fibers to 320% strain. The SC CO₂ samples show a definite yield behavior which is not observed at lower

pressures. We believe the yield behavior is due to crystal formation. Note that the yield stress at 204.1 atm is slightly higher compared to 136.1 atm possibly due to a larger extent of crystallization. Near 320% strain, individual fibers begin failing as the experiments were stopped before all of the fibers failed. At this point, the crystallinity in the polymer network may contribute to fiber failure. Crystallites generally act as crosslinks in the molecular network limiting deformation.

We believe that the improved drawability is due to the plasticization effect of CO₂ in the amorphous phase allowing for chain slippage and disentanglement. Strain-induced entanglements may be reduced as well. The role of small/imperfect crystallites is of less importance because they are a minor phase particularly at lower pressures. Our experiments show that drawability can be enhanced by plasticization alone. The simpler morphology of the CO₂ fibers compared to solvent treated fibers give greater insight toward the mechanism of improved drawability.

The structure of the one-stage drawn fibers is quite distinct. CO₂ clearly enhances the development of the crystalline phase. At a draw ratio of 4, X-ray patterns display diffuse yet well separated arcs. These patterns have been published previously (24). The crystallinity of the CO₂ treated fibers is 10-13% higher. However, the crystallinity of these fiber is still low (<30%). The subcritical CO₂ fibers show significantly lower birefringence values compared to cold drawn fibers, 0.15 versus 0.19. Birefringence indicates that the total orientation is significantly less for fibers drawn in CO₂. This can be accounted for by the fact that the CO₂ treated fibers are drawn above T_g. The mechanical properties of these fibers are fairly low probably due to the low orientation and crystallinity. To increase the mechanical properties further, second-stage drawing was carried out at 200° C or higher.

Two-Stage Drawing

The morphology of the fibers after the first stage draw significantly effects the structure and properties achieved after the second stage. CO₂ treated fibers could be drawn to significantly higher total draw ratios, 12.2 versus 8.2, compared to untreated fibers at 200°C. The improvement in drawability occurred in both stages. The drawability was further enhanced by using higher draw temperatures in the second stage. At 230° C, the TDR was increased to 14.4 compared to TDRs~9 for untreated fibers. Clearly, the use of CO₂ is a very effective means for improving drawability.

The two stage drawn PET fibers were physically characterized by various methods to further investigate their structure at smaller length scales. WAXD, birefringence, and crystallinity measurements were used to calculate orientation functions for the amorphous and crystalline phases, f_a and f_c , respectively. In general, the CO₂ treated PET fibers have slightly higher crystallinity values compared to untreated fibers and achieved the same level of orientation.

The volume percent crystallinity increases slightly with TDR. At a treatment temperature of 200° C, the CO₂ treated fibers have a crystallinity of 55.5% compared to 53.1% for the untreated fibers. The crystallinity of the treated fibers at higher draw ratios is increased substantially to 65.4 % at a drawing temperature of 230° C. To

attain 65% crystallinity, untreated fibers have to be annealed under tension for 2-3 hours. This annealing process is accompanied by an undesirable decrease in molecular weight resulting in poor tensile strength (25).

The birefringence was measured for all fibers drawn under constant strain rate at 200⁰ C. Birefringence is a direct measurement of total or global orientation of the polymer chains. The maximum birefringence (0.228) obtained for the treated fibers is just slightly higher compared to untreated fibers (0.226) indicating only a slightly higher orientation. It should be noted that these fibers were drawn in the first stage above the critical pressure for CO₂. The combined effect of the heat treatment and further drawing in the second stage has a profound effect. The birefringence

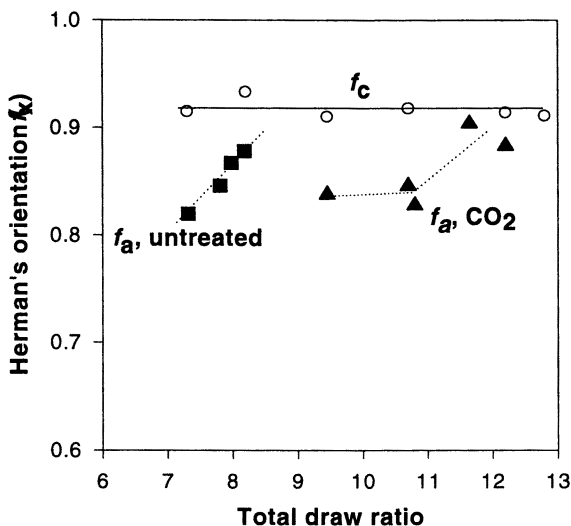


Figure 4. Development of orientation in the amorphous and crystalline phases.

increases substantially and the crystallinity values nearly double. The development of the total orientation occurs much more rapidly for untreated fibers. For CO₂ treated fibers, the birefringence increases more slowly and attains only a slightly higher mean value.

Figure 4 shows the TDR dependence on the chain orientation factors for the crystalline and amorphous regions for the two stage drawn fibers at 200⁰C. The f_c was measured by a well known X-ray diffraction method (26). The amorphous orientation, f_a was calculated by combining the optical birefringence data with f_c and sample crystallinity (27). The intrinsic birefringences of the crystal and amorphous phases were taken to be 0.220 and 0.275 respectively (28). The f_c values of the samples are

very similar and stay an almost constant value of 0.915. This behavior has been reported previously for different two stage drawn PET systems (29,30). It is a general behavior for many polymer systems. The f_a values increase with draw ratio for both the treated and untreated fibers. High f_a values are not obtained in the CO₂ treated fibers until the highest draw ratios are achieved where the TDR>11. The development of the amorphous orientation is much slower for the CO₂ treated fibers. This is a direct consequence of the low orientation produced during the first stage draw. Although the amorphous orientation develops relatively slowly, the CO₂ treated fibers have slightly higher f_a values compared to the CO₂ treated fibers at DR_{max} values. Overall, the amorphous orientation for both fibers is quite high.

The amorphous orientation is probably not optimum due to the use of a constant strain drawing technique. Ito et al. has shown that load upon drawing is a critical factor which affects the orientation in the non-crystalline regions and the final tensile properties as well (31). Constant strain drawing can reach fairly high stress levels in the fibers as the maximum achievable draw ratio is approached. However, the load after constant strain drawing can decrease upon cooling allowing for relaxation and sub-optimum conditions.

Comparison of Structure and Mechanical Properties

Table 1 shows the structural and mechanical properties of CO₂ treated fibers at various temperatures in comparison to untreated fibers and solvent treated fibers (32,33). In comparison to untreated fibers, CO₂ treated fibers have 10% higher strength and modulus at 200°C. With increasing temperature, the tensile strength decreases and the modulus increases. The loss of tensile strength can be attributed to degradation and loss of molecular weight at higher temperatures. The increased modulus is the direct result of the high crystallinity. At 230°C, the amorphous orientation ($f_a \sim 0.6$) is much lower compared to fibers drawn at 200°C.

Compared to solvent treated fibers, CO₂ fibers show slightly lower strength values. This can be attributed to the loss of molecular weight because of the lengthy heat treatment time (~ 35 minutes) (34). The CO₂ fibers show much lower moduli compared to Ito's values. These are samples 3,4, and 5 in Table 1. We are not certain why such a large discrepancy exists. Our values are quite close to the values reported for commercial fibers. Ito et. al. does use a constant load technique which may effect the mechanical response at low strains. The CO₂ and solvent treated fibers are very similar from a structural point of view. Both have relatively low amorphous orientation ($f_a \sim 0.6$) and high crystalline orientation ($f_c \sim 0.9$). In addition, these fibers have similar crystallinity values ~ 65% which are significantly higher compared to untreated fibers (< 53%). These results indicated that the CO₂ and solvent drawing processes are very similar in nature.

Table 1: Comparison of CO₂ treated, solvent treated, and untreated PET fibers.

<i>Sample</i>	<i>Temp.</i> (°C)	<i>TDR</i>	<i>X_c</i>	<i>f_c</i>	<i>f_a</i>	<i>Modulus</i> (GPa)	<i>Strength</i> (GPa)
1.Untreated	200	8.2	53	0.933	0.88	13	1.0
2. CO ₂	200	12.2	56	0.914	0.90	15	1.1
3.Untreated	230	8.5	50	0.887	0.98	24	1.0
4.Acetone	230	10.0	68	0.896	0.58	27	1.2
5.DMF/H ₂ O	230	11.5	----	----	----	28	1.2
6.CO ₂	220	12.5	62	0.911	0.66	17	1.0
7.CO ₂	230	14	65	0.925	0.62	16	1.0

Conclusions

When amorphous PET fibers were treated with high pressure CO₂ at 23°C, plasticization and crystallization occurred. CO₂ exposure resulted in the formation of small/imperfect crystallites. Crystallite size/perfection was not significantly effected by pressure. The morphology created by CO₂ is simpler compared to acetone treated fibers. The diffusion of CO₂ into the fiber is much faster than the crystallization process.

A two-stage drawing technique was utilized for drawing. The drawing of PET in CO₂ can be dramatically effected by pressure. The CO₂ morphology enhances the drawability of the PET fibers in both stages of the drawing process. After a second stage draw (230° C), fibers with very high crystallinity values (65%) could be obtained. These fibers had very similar structural characteristics to acetone or DMF/H₂O treated fibers. Both had high crystalline orientation ($f_c \sim 0.9$) and low amorphous orientation ($f_a \sim 0.6$). Drawing in CO₂ can be used as an effective, environmentally friendly process for producing high performance PET fibers.

Acknowledgements

The authors wish to acknowledge the financial support from the National Science Foundation Materials Research Science and Engineering Center at the University of Massachusetts and from the University of Massachusetts. The authors would also like to thank Professor Masayoshi Ito for discussion. The authors especially thank the late Roger Porter for his great insight and many useful discussions.

Literature Cited

1. Ito, M., Takahashi, K., Kanamoto, T., *Polymer*, **1990**, 31, 58.

2. Huang, B., Ito, M., Kanamoto, T., *Polymer*, **1994**, 35, 1214.
3. Ito, M., Takahashi, K., Kanamoto, T., *J. Appl. Polym. Sci.*, **1990**, 40, 1257.
4. G. Wu and J. Cuculo, *J. Appl. Polym. Sci.*, **1995**, 56, 869.
5. G. Wu and J. Cuculo, *J. Appl. Polym. Sci.*, **1995**, 56, 870.
6. Ito, M., Takahashi, K., Kanamoto, T., *J. Appl. Polym. Sci.*, **1990**, 40, 1258.
7. Ito, M., Hosoi, H., and Kanamoto, T., *Polymer*, **1992**, 35, 2575.
8. Pereira, J. R. C., Porter, R. S., *J. Polym. Sci., Polym. Phys. Ed.*, **1983**, 21, 1133.
9. Kunugi, T., Suzuki, A., Hashimoto, M., *J. Appl. Polym. Sci.*, **1981**, 26, 1951.
10. Amano, M., Nakagawa, K., *Polymer*, **1986**, 27, 429.
11. Zachariades, A. E., Porter, R. S., *J. Appl. Polym. Sci.*, **1979**, 24, 1371.
12. Wang, L. H., Porter, R. S., *J. Polym. Sci., Polym. Phys. Ed.*, **1984**, 22, 1645.
13. Eckert, C., Knutson, B., and Debenedetti, P. *Nature*, **1986**, 383, 313.
14. Flory, P. J., *Disc. Faraday Soc.*, **1970**, 49, 7.
15. Mensitieri, G., Del Nobile, M. A., Guerra, G., Apicella, A., Al Ghatta, H., *Polym. Eng. Sci.*, **1995**, 35, 510.
16. Mizoguchi, K., Terada, K., Hirose, T., Kamiya, Y., *Polym. Comm.*, **1990**, 31, 146-47.
17. Mensitieri, G., Del Nobile, M. A., Guerra, G., Apicella, A., Al Ghatta, H., *Polym. Eng. Sci.*, **1995**, 35, 509-511.
18. Mizoguchi, K., Terada, K., Hirose, T., Kamiya, Y., *Polym. Comm.*, **1990**, 31, 146-47.
19. Ito, M., Miya, H., Watanabe, M., and Kanamoto, T., *J. Appl. Polym. Sci.*, **1990**, 40, 546.
20. Mesitieri, G., Del Nobile, M. A., Guerra, G., Apicella, A. and Al Ghatta, H., *Polym. Eng. Sci.*, **1995**, 35, 506-507.
21. Hobbs, T. and Lesser, A. J., *J. Polym. Sci., Part B: Polym. Phys.*, **1999**, 37, in print.
22. Chiou, J., Barlow, J., Paul, D., *J. Appl. Polym. Sci.*, **1985**, 30, 3921.
23. Ito, M., Hosoi, H., Kanamoto, T., *Polymer*, **1992**, 33, 2577-78.
24. Hobbs, T. and Lesser, A. J., *J. Polym. Sci., Part B: Polym. Phys.*, **1999**, 37, in print.
25. Ito, M., Miya, H., Wanatobe, M., and Kanamoto, T., *J. Appl. Polym. Sci.*, **1990**, 40, 551-552.
26. Huang, B., Tucker, P., Cuculo, J., *Polymer*, **1997**, 38, 1103.
27. Huang, B., Tucker, P., Cuculo, J., *Polymer*, **1997**, 38, 1103.
28. Sun, T., Desper, R., Porter, R. S., *J. Mat. Sci.*, **1986**, 21, 803.
29. Ito, M., Hosoi, H., Kanamoto, T., *Polymer*, **1992**, 33, 2575.
30. Ito, M., Takahashi, K., Kanamoto, T., *J. Appl. Polym. Sci.*, **1990**, 40, 1257.
31. Ito, M., Takahashi, K., Kanamoto, T., *J. Appl. Polym. Sci.*, **1990**, 40, 1262-63.
32. Ito, M., Hosoi, H., Kanamoto, T., *Polymer*, **1992**, 33, 2575.
33. Ito, M., Miya, H., Wanatobe, M., Kanamoto, T., *J. Appl. Polym. Sci.*, **1990**, 40, 543.
34. Ito, M., Miya, H., Wanatobe, M., Kanamoto, T., *J. Appl. Polym. Sci.*, **1990**, 40, 552.

Chapter 10

Supercritical CO₂ Carbonation of Cement and Cement–Fiber Composites: The Supramics Process

Roger Jones

Materials Technology Limited, 14525 Rim Rock Road, Reno, NV 89511

Carbon dioxide was recovered from flue gas, made supercritical, and used to treat pastes derived from fly ash and other dusty wastes to produce several valuable products. Examples of these products include a lightweight roofing tile that resembles a cedar shake and fiberglass-reinforced ceramic wallboard. These products were made by combining conventional technologies in new ways, avoiding the need for and cost of custom technological innovation. The Supramics® process described in this manuscript eliminates numerous intermediate manufacturing steps, lowers capital costs, and greatly reduces direct and associated energy requirements as compared to similar products produced via conventional technologies. The process both sequesters CO₂ and replaces products whose manufacture creates CO₂ and other wastes at the same time it offers improved profit margins. It is hoped that implementing this process will help lead to a cleaner planet.

Imagine awakening tomorrow morning to hear on a news report that scientists had determined that the world was flat. Or that the sun revolved around the earth. Surely you would not accept this. Yet every day people are asked to believe that despite the evidence of a significant rise in atmospheric CO₂, there is no way, short of destroying national economies, to do anything about our polluting, energy-wasting manufacturing methods. Well, the good news is that solutions are available and they are being further developed today. It is possible to transform our CO₂-producing, waste-generating industries and electric power plants into suppliers of important feedstocks and to situate them as the primary resource hubs of eco-industrial parks.

As described in this chapter, CO₂ can be used to make valuable products. The feasibility of this concept is demonstrated by the manufacture of two products, typical of building materials used extensively in the United States. One is a lightweight

roofing tile that resembles a cedar shake, and the other is fiberglass-reinforced ceramic wallboard. The materials system described for their production can be applied to produce a lower-cost, quality alternative to virtually any product made of metal, wood, paper, glass, thermoplastic, ceramic, or composites.

Green Business/ Green Manufacturing

While it is ethical and responsible to develop products in a way that minimizes or eliminates negative environmental impacts, it is important to recognize that if a product cannot be justified by economics, it cannot be sustained. As such, green chemistry and engineering are driven as much by economics as by molecular dynamics. This project demonstrated that a manufacturer can make money, sequester CO₂, and offset CO₂ production, using what had formerly been considered a waste stream. Furthermore, development and manufacture of these products was accomplished without capital investment by government or by industry.

Building products were selected for initial development because they could be manufactured fairly quickly and sold at good profit. It was expected that these new building materials would displace current products without compromising quality or increasing price; further, our new products would not cause a net increase in CO₂ or exacerbate other waste disposal problems. In order to keep costs down, low-cost feedstocks were selected with the additional advantage that the use of these feedstocks allowed formation of products that could be easily altered to improve quality.

In 1993, we discovered a way to strip CO₂ from flue gas and to subsequently elevate its pressure and temperature to make it supercritical. In this state CO₂ becomes an aggressive reagent (for manufacturing purposes) that reacts with and alters the micro-structure and chemistry of substances such as fly ash and hydraulic cement pastes. Coal ash, one of the world's largest waste streams, was selected as a feedstock material along with supercritical CO₂ to produce ceramic composites that perform like plastic resin-based composites (*1*). We will refer to that reinforcement made from resin-based composites generally as fiberglass. Products created from coal ash and supercritical CO₂ were named Supramics® products, much as we refer to those made of fired clay generally as ceramics. In the Supramics® process, the feedstocks of portland cement, quicklime, and fly ash paste are substituted for resins. Yet, the paste is shaped using conventional process equipment, in the same way that plastic products are shaped.

Strategic Considerations

Before implementing the Supramics® process technology, several ground rules for manufacturing were formulated. First, we chose to stick with tried-and-true technology for manufacturing. Because commonly used equipment is generally cheaper than specialty equipment, it made more sense to combine existing equipment

and process methods in new ways, rather than to invent new technology. That way, off-the-shelf equipment could be purchased rather than custom engineered and built.

Second, we chose a technology with low capital intensity. Going directly from garbage to goods with few intermediate refinements allows one to reduce the amount of hardware in the first place. While this seems obvious, it is an important consideration for a manufacturer. Fewer intermediate steps with less attendant equipment also means less process energy consumption, which is important to the final customers who end up paying indirectly for energy used to make the product. Amortization of capital and energy costs, along with costs of labor and raw materials are included in the cost of goods. Using the Supramics® process, the bulk of raw materials are not only free, but have a negative price.

Finally, it was considered important to have a good profit margin for the product, over and above basic costs of materials, labor, amortization, and selling expense. This would allow enough economic room to serve a wide market from a remote location. Instead of shipping a low-value product like fly ash to distant markets where it would sell for barely enough money to cover the transportation costs, we chose to create goods on site from materials that, for the most part, originated on site. High-value products are shipped to markets that pay more than enough to cover the costs. With higher profits, investment can be paid off more rapidly, allowing further investment into expansion or other product areas, or return to shareholders as dividends. At a cost of no more than eleven million dollars, the plant is expected to be fully amortized in only three years.

The Project

The test site was Arizona Public Service's Four Corners Power Plant, located near Farmington, New Mexico. The Four Corners plant burns about 8 million tons of coal a year and produces about 1.8 million tons of ash. Of that, about 1.5 million tons are fly ash and about 370,000 tons are bottom ash. The Four Corners plant also produces about 35,000 tons of CO₂ per day, or about 12.8 million tons, annually. This is roughly ten tons of carbon dioxide per residential customer.

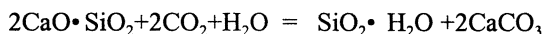
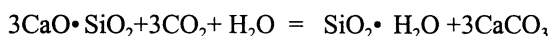
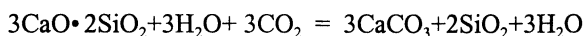
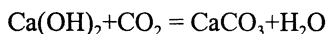
The Product

The products manufactured and described in this manuscript are fully carbonated, fiberglass-reinforced hydraulic cement/fiber composites. Fiber and textile are traditional reinforcing materials used in fiber-reinforced cementitious products (2). Fiber-reinforced cement has been around for at least fifty years without benefit of carbonation. Products made from glass fiber-reinforced cement have never been as popular as fiberglass-reinforced plastics. The main reason is that ordinary fiberglass (generally referred to as 'E-glass') is severely degraded in the highly alkaline environment of portland cement (3, 4). Special glasses, in the form of textiles or

chopped fiber, are used as reinforcement in the place of ordinary fiberglass in order to prevent degradation. In order to accommodate these special glasses in the product, the manufacturing practices must be adjusted. As a result, costs go up. In addition, prices of products made of fiberglass-reinforced portland or sorrel (magnesite) cement, most notably the fiberglass-reinforced cement board known as “wet area tile backer board”, are constrained by intense competition and profit margins are held to precariously low levels. Even plants operating at full capacity barely recoup the cost of manufacture, depreciation, and amortization of these products.

To add to these difficulties (special glass, special manufacturing techniques, low profit margins, relatively high price to consumers), fiberglass-reinforced cement building products have had problems with quality. They are heavy, brittle, and difficult to cut, shape, and apply. Up to now, employment of special glass has been the only commercially exploited way to inhibit the alkali-silica reaction between E-glass and portland cement. The alkali-silica reaction forms expansive gels, particularly in wet environments, which damage cement materials. The special glasses, either alkali-resistant glass (which is brittle) or plastic-coated glass (which is expensive and does not bond well with the portland cement) end up contributing as much as ninety percent to the materials cost.

The use of supercritical CO₂ treatment permits manufacturers to use a different strategy. Supercritical CO₂ infusion lowers the alkalinity of cement products to about neutral (pH 7). Thus it is possible to use standard, i.e., continuous or chopped E-glass fiber or textile. The use of E-glass is as much as 90% cheaper and is much more readily available than plastic-coated or alkali-resistant-glass (ARG). In the Supramics® carbonation process, the metal hydrates that are present in portland and pozzolan cements are rapidly (minutes) converted into carbonates, a process that takes years to complete under atmospheric conditions. The common calcium carbonation reactions in portland cements are represented as follows:



The use of cement is not restricted to portland cement. Supercritical CO₂ can be made to fully carbonate a range of mixtures that contain calcium, magnesium, aluminum, or other reactive metal oxides and silica expressed as hydrates. Four distinct products are made by first forming a paste out of the substances listed in Table I.

Table I. Sample Mix Designs for Supramics® Precursors

<i>Product 1</i>	<i>Product 2</i>
Portland cement Water Fly ash Pre-formed aqueous foam Reinforcing fiber or textile Calcium/magnesium quick lime	Calcium quick lime Kiln dust Water
<i>Product 3</i>	<i>Product 4</i>
Calcium/magnesium quick lime Kiln dust Quarry fines Water	Basic oxygen furnace slag Calcium quick lime Calcium silicate Water

The Process

The key step in the formation of Supramics® products is the reaction of supercritical CO₂ with the metal hydrates in hardened (cured) cement products to form carbonates. Alkalinity is lowered and physical properties can be broadly manipulated. Finite process control is derived from the characteristics of supercritical fluids; this includes control over solubility, miscibility, rheology, viscosity, molecular density and reactivity. Such control is the driving reason for the use of supercritical conditions for CO₂ (5). The Supramics® process uses supercritical CO₂ in order to turn a process that is ordinarily completed on the order of hundreds of years into one that is done on the order of minutes or less. Carbonation is 'Mother Nature's' favorite reaction. The Supramics® process simply speeds it up and puts it under process control. Over millennia, all cements carbonate, but the greater their density, the longer it takes for carbonation to be completed. Supercritical CO₂, in contrast, rapidly penetrates through and alters even the most dense cements.

To industrialize this reaction, existing equipment and technology was modified to move from laboratory-based batch reactors to factory-based processes in continuous lines (6). Figure 1 illustrates schematically the Supramics® process. First, a paste is formed out of one of the sets of substances listed in Table I. The two initially developed products contain continuous E-glass yarn for reinforcement, as well as chopped E-glass and other materials to make them nailable. The paste is shaped into the desired product, e.g., roofing shingles or wallboard, using conventional cement product forming equipment. The paste can be molded, cast, extruded, or even rolled

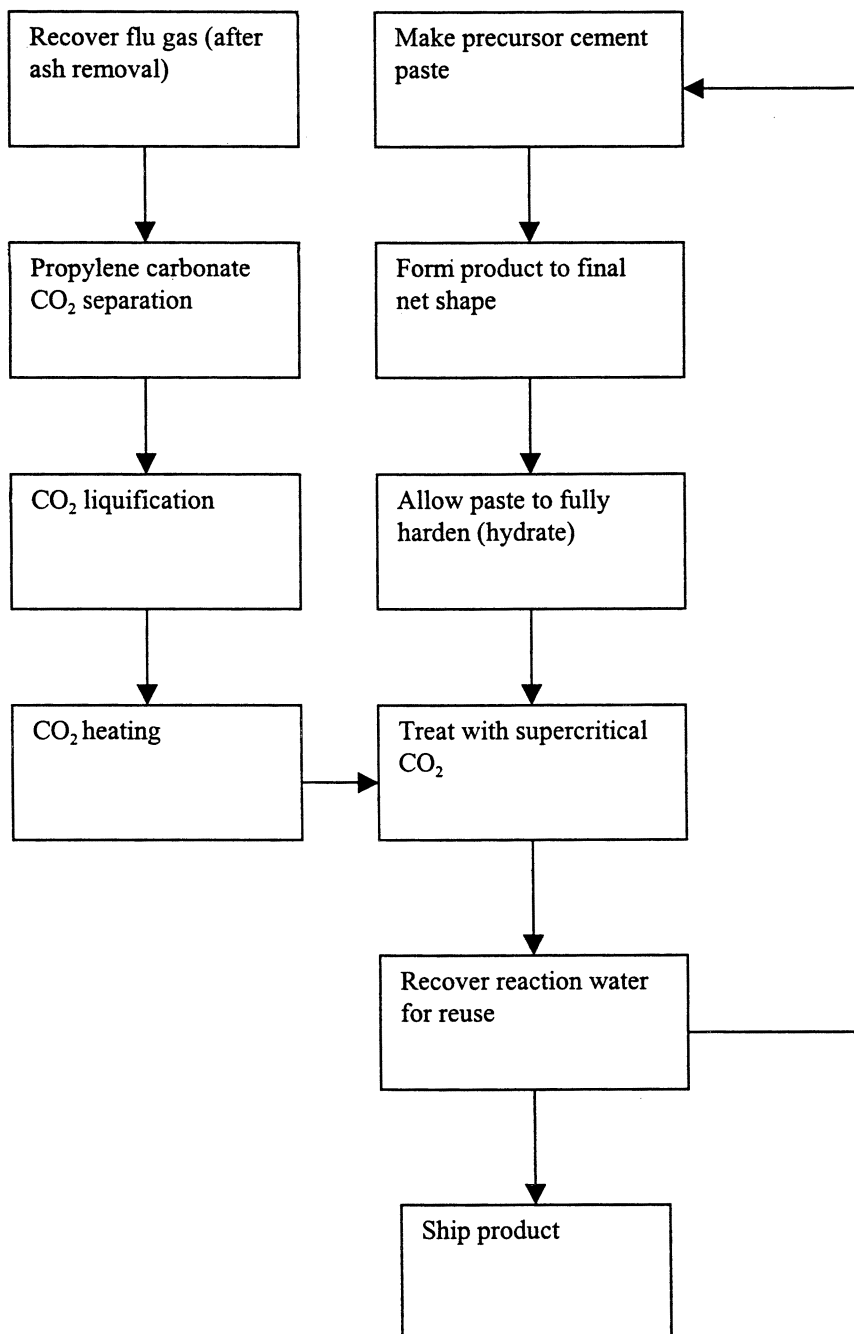


Figure 1. Supramics® process flow

out like pie dough using conventional shaping equipment manufactured by companies such as Wehrhahn GmbH, Kvaerner Panel Systems, Vortex-Hydra and Siemelkamp GmbH to name only a few.

After the product has been formed and cut into individual pieces, it is allowed to cure (hydrate). During curing, metal hydrates and some zeolites are formed. The curing takes place on a continuous line and can be greatly accelerated by any combination of chemical, thermal, or steam curing.

Meanwhile, post-scrubber gas stripping facilitates the process of separating CO₂ for use in the manufacturing process. The method employed is a modified stripping column similar to those used in the natural gas industry. There are four tried-and-true methods commonly used for CO₂ stripping. However, the propylene carbonate absorption path commonly used at industrial scale for stripping CO₂ from natural gas (methane), was selected as a simple and low cost CO₂ recovery method. The other viable options considered were membrane separation followed by absorption, membrane absorption, and pressure-swing absorption.

Propylene carbonate is thermally activated to release CO₂ absorbed from the scrubbed flue gases. CO₂ compression is also thermally driven, much like heat is recovered from a household refrigerator and used to compress the coolant, reducing energy requirements and conserving heat energy both from the power plant and from the compression process itself.

The hydrated or cured product is then brought together with CO₂ that has been heated and compressed to 40 °C and 4,000 psi in a continuous process on a conveyor. The metal hydrates are converted into carbonates. Additional changes can be made to the product by dissolving and infusing materials previously doped onto the product's surface. This treatment facilitates chemical control over the final properties of the composite, which is called a "chemically bonded ceramic." By using CO₂ instead of heat to create the final properties, the product is made stronger, tougher, more ductile, and more durable than conventional molded products. As described earlier, supercritical CO₂ treatment neutralizes the ceramic matrix, preventing the alkali-silica reaction with E-glass and strengthening the material. Because one can control the final chemical and physical properties of such products, they can be made to replace a variety of materials that actually create CO₂ in their production e.g., steel, aluminum, thermoplastics, or conventional, fired ceramics (7).

The flagship Supramics® product is a lightweight cedar shake look-alike which can also be made to look like a premium slate. It can be applied to a roof deck with a standard nail gun or a roofer's hammer and nails. It splits along the long axis, just like a wood shingle. But that is where the similarities end. Unlike a shake, it does not discolor over time. It is not degraded by moisture, rot, or thermal and humidity fluctuations. Not only is it waterproof, but it floats. And for all practical purposes, it is hail-proof. This shingle can withstand the weight of a person walking on it, making it easy to install and maintain. This product could last a hundred years, in contrast to the status quo of ten or twenty years. Since it is a chemically bonded ceramic, it does not support combustion. It can be made highly insulating and reflective in the infrared range, reducing a home's heating and cooling costs. And best of all, it can be

effectively priced to cost no more than the cheapest three-tab composition shingle on today's market.

The second product, made on the same production line, is a fiberglass-reinforced ceramic wallboard that weighs one-third less than conventional fiberglass-reinforced cement board. A four-by-eight-foot sheet of conventional cement board weighs approximately ninety-eight pounds. The Supramics® board weighs 63 pounds. At this reduced weight, it can be installed by a single worker, rather than by two or three as is the current practice. This wallboard is also insulating. Like the shingle, it can be applied with nails or it can be screwed directly to the framing or to optional plywood sheathing. Because it has a higher shear strength than conventional cement board, the plywood is not really necessary. And since it is a ceramic and not cement, it is far more durable. Like the shingles, it is fireproof and waterproof. It can be applied with conventional tools and fasteners and can be fabricated with a simple knife. And also like the shingle, it costs less than conventional fiberglass-reinforced cement board.

Both of these products employ the same materials system and both are produced by means of foaming. The use of a foaming process results in a product of which much of the volume is made up of air bubbles, further reducing material costs. The total costs of materials and energy needed to make these products are less than half those of ordinary cementitious shingles and wallboard. Research and development of additional Supramics® products are currently underway.

Economics

The Supramics® process relies heavily upon use of the waste energy from the power plant to do most of the work. Currently waste heat is discharged into cooling ponds and cooling towers. The processes can also take energy from steam. However, power generators cannot afford to experience significant parasitic energy losses even if there are indirect environmental benefits. Incorporation of the Supramics® process into manufacturing operations are designed to accomplish manufacturing objectives without draining away the very commodity that the plant sells. The supercritical CO₂ processes are isobaric in that the CO₂ is pumped as a liquid to approximately 4,000 psi and maintained at that pressure. Only the addition and removal of heat is required to change the CO₂ from sub-critical to critical and back again. Because the heat is obtained from the power plant's cooling system, the use of energy is minimal.

The Supramics® process is energy efficient in part because it proceeds directly from waste to product, with essentially no intermediate manufacturing steps. Most other systems have several intermediate levels of manufacturing. Steel, for example, undergoes approximately sixteen clearly discrete intermediate manufacturing levels by the time a final building product is made. There are also associated reductions in transportation-associated energy (fuel, vehicles, etc.). With the elimination of the intermediate steps in other systems, transportation associated energy use is eliminated as well.

In short, there is great efficiency in the Supramics® process because "industrial garbage" (in this case fly ash and CO₂) is converted directly into goods. Ordinarily,

most coal-fired powerplant waste is landfilled or ponded. While expensive, this has traditionally been the only practical choice. On average, the current cost to landfill or pond powerplant ash waste in the U.S. is about \$12.50 per ton of ash. At a plant like the Four Corners Plant, which produces about 1.5 million tons of fly ash each year, the annual cost to dispose of waste ash can run up to about \$18.4 million. These costs are comprised of many factors that are not necessarily manifested up front. They are most visible as primary cost components which include construction, maintenance, transportation, de-watering, pond or landfill closure, re-vegetation, and long-term monitoring.

To ameliorate some of these costs, some ash can be sold. As much as forty percent of all fly ash is suitable for use in concrete. However, ash tends to retard the set of portland cement, and as a result, only the very fine ash particles really work well. Processes that separate the very fine ash also increase costs. The remainder of the forty percent could be used for things like geo-fills, but most of it is not. It is simply dumped. In contrast, the Supramics® process works well with just about any kind of ash. Even wood ash and ash from burning rice and almond hulls has been used successfully. As a result, it is possible to use waste ash that is unmarketable under normal circumstances.

Other composite products that can be produced by this material system include aircraft and automotive products. Friction products such as brake shoes and discs are also likely candidates for manufacture, but there is nothing to preclude making entire automobile bodies. Other options include electronics packaging, materials for printed circuit boards and other electronic parts, and even vehicle and personnel armor. All of these concepts are currently under development as prototypes.

Given how well this process works, it seems surprising that fly ash has not been used in more products. Several possible reasons for this are noted. First, fly ash is produced in power plants that are, for the most part, remote from centers of manufacturing and population where finished goods are made and used. Even for concrete, one must transport the ash to the batch plant. Since ash is of low value, transportation adds costs which can rapidly offset any margin. Second, the use of CO₂ is faced with another problem. There is simply more of it than can be consumed by conventional manufacturing processes. In fact, one can buy CO₂ in industrial or food quantities at about two cents a pound in almost any major population center that has an oil refinery, a brewery, or an ammonia plant. Because it is abundant, the principal contribution to its cost are the logistics of “moving the metal”, as the saying goes in industrial gas industry.

Finally, it is possible that the use of ash and CO₂ is hindered because they are generally not looked upon as feedstocks. There is a tautological paradigm that “waste is waste.” To make significant inroads into utilizing these waste streams, one must consider ash and CO₂ to be by-products, with the key word being “products”. Ash is not quite a feedstock, but certainly the potential is there. A shift in perception transmutes the coal-burning boiler (also the electric arc furnace and the blast furnace) into a different kind of machine – a mineral-matter transformer. With such a change in perception, it is more likely that industry will use these by-products as feedstocks. Finally, past research has focused on fly ash and similar dusty wastes as constituents

in low-value concrete, not as a primary ingredients used to make high-value goods like building products or electronic components. As a result both research and product development opportunities were blinded to such innovative use.

The Global Perspective

The Supramics® process uses dusty wastes and carbon dioxide to replace other materials systems. But there is some question as to whether this is likely to happen quickly in developed countries. Because of the capital investment already sunk into materials systems like plastics, synthetic-resin-based composites, metals and forest products, it is expected that this technology will catch on much more quickly in developing economies. Going directly from garbage to goods is cheaper and more efficient than following the many-tiered manufacturing approach typical of the 19th-century rooted practices of Western economies. If history provides example, then adoption of the Supramics® process may be analogous to 19th-century Britain where, despite inventions like those of Bessemer, the entrenched iron industry slowed implementation of new steel technology and relied mainly on improvement of existing plants and equipment. It was in the developing 19th-century United States that implementation and improvement could rapidly take place. Such development in the U.S. was not held back by entrenched investment, fated to become sunk investment, if the technology became outmoded. In developed economies, sunk capital already invested into mature technologies creates enormous resistance to change. Therefore it is expected that Supramics® process offers the greatest opportunity to developing economies, resulting in maximum immediate return for precious capital. Investment in newer technologies seems more likely when the total capital requirement across the economy as a whole is less with greater production capacity and higher profit margins.

Conclusions

Supercritical CO₂ can be recovered from flue gas and used to treat pastes made from fly ash or other dusty wastes to produce valuable cement or cement/fiber products. Such products are made by combining conventional technologies in new ways and by minimizing the need for and cost of custom engineering. This and the elimination of numerous intermediate manufacturing steps result in lower cost and improved profit margins. It is important to remember that beyond the favorable economics are other reasons for the significance of the Supramics® process. CO₂ is sequestered and products are replaced whose manufacture generates CO₂ and other wastes. The Supramics® process has the potential to reduce the negative environmental impact of multiple manufactured products and thus contribute to a cleaner planet.

Literature Cited

1. Jones, Jr., R. "Cement Treated With High Pressure CO₂." United States Patent 5,518,540 issued May 21 1996
2. Perez-Pena, M. and Mobasher, B., "Mechanical Properties of Fiber-Reinforced Lightweight Concrete Composites," *Cement and Concrete Research*, Vol. 24., No. 6 (1994) pp. 1121-1132
3. Takaji, J., "Some Properties of Glass Fiber-Reinforced Concrete," American Concrete Institute (ACI) Special Publication SP-44, (1974) pp. 93-111
4. Majumdar, A. and Tallentire, A., "Glass Fiber Reinforced Cement Base Materials," *ibid.*, pp. 350-362
5. Li, F. Li, M., Lee, L., Starling, K. and Chung, F., "An Accurate Equation of State for Carbon Dioxide," *J. Chem., Eng. Japan*, Vol. 18 (1995) p. 490
6. Jones, Jr., R., "New Process Converts Ordinary Portland Cements Into Low Cost Advanced Composites," *Materials Technology*, Vol. 13, No. 3 (1998) pp. 104-106
7. Loud, S., "Low Cost Processing – Fillers," *Composites News International: Infrastructure #54*, (1996) pp. 5-6

Chapter 11

Low-Pressure Oxidative Carbonylation of Aniline with Pd/C and Ag-Pd/C

Steven S. C. Chuang¹, Pisanu Toochinda, and Mahesh V. Konduru

Department of Chemical Engineering, The University of Akron,
Akron OH 44325-3906

Extensive carbonylation catalyst screening studies show that oxidative carbonylation provides a low-pressure pathway for isocyanate synthesis without the use of highly toxic phosgene. Formation of diphenyl urea takes place even at low pressures of 0.101 MPa and at 373 K; formation of methyl N-phenyl carbamate can also occur at 0.101 MPa and 438 K from methanol, aniline, CO, and O₂ over Pd/C and Ag-Pd/C with NaI as a promoter. Diphenyl urea formation at 373 K and methyl N-phenyl carbamate formation at 438 K suggest that aniline dehydrogenation occurs at a lower temperature compared to alcohol dehydrogenation. Absence of Pd in the reactant/product solution suggests that the carbonylation reaction occurs on the surface of the Pd catalyst. High yields of carbamate (82%) obtained during low-pressure reaction studies demonstrate that the Pd-catalyzed oxidative carbonylation is economically viable.

INTRODUCTION

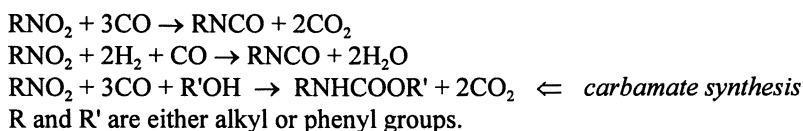
The growing concern for the environment, increasingly stringent standards for the release of chemicals into the environment, and economic competitiveness have promoted extensive efforts to improve chemical synthesis and manufacturing methods, as well as the development of new synthetic methodologies that minimize

¹Corresponding author (email: schuang@uakron.edu).

or completely eliminate pollutants (1,2). Approaches to developing novel synthetic methodologies include feedstock substitutions, alternative synthetic and separation processes, and product reformulation. One reaction that is being developed from the concept of feedstock substitution is the carbonylation of nitro-compounds, aimed at the replacement of phosgene as a feedstock for isocyanate synthesis (1-3).

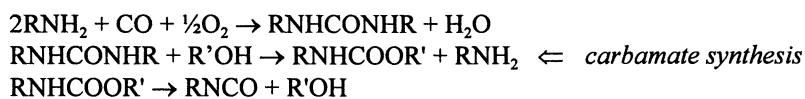
The reaction of phosgene with a primary amine is currently the most important process for the synthesis of isocyanates (1). The environmental impact of the process stems from not only the highly toxic and corrosive nature of phosgene but also the use of chlorinated hydrocarbons as a solvent for the reaction. To reduce the risk of pollution and improve process safety, it is highly desirable to use feedstock with low toxicity and to eliminate solvent use. The catalytic carbonylation of aniline/amines and nitrocompounds provides a direct route to isocyanate without the use of phosgene. This reaction process is currently considered to be the most promising environmentally benign process to replace the conventional method of isocyanate synthesis (1). Depending on catalysts and types of reactants used, the process can lead to either isocyanate or carbamate in a single step by either reductive or oxidative carbonylation.

Reductive carbonylation involves the use of nitrobenzene, alcohol, CO, and H₂ at a high-pressure reaction condition of 10.13 MPa. The overall reductive carbonylation steps are listed in scheme 1.



Scheme 1

Oxidative carbonylation utilized aniline, alcohol, CO, and O₂. The overall reaction can be written as seen in scheme 2.



Scheme 2

Among these reactions, the carbamate synthesis has been the most attractive for its high selectivity, high stability of the carbamate products, and selective conversion of carbamate to isocyanates. In contrast, the direct isocyanate synthesis from carbonylation of nitro-compounds suffers from the polymerization side reaction (1).

The major differences between oxidative and reductive carbonylation are the use of O₂ and H₂, aniline and nitrobenzene, and reaction conditions. Reductive carbonylation has been carried out at 4.83 MPa and 413-473 K; most of the reported

oxidative carbonylation processes have been carried out at 3.79 MPa and 373–443 K (1–4). Oxidative carbonylation may take place at mild conditions due to the formation of H₂O from the reaction of oxygen with hydrogen from the hydroxyl group of alcohol and from the NH₂ functional group of aniline. This step should provide sufficient thermodynamic driving force to move the oxidative carbonylation forward without the use of high pressures. In fact, oxidative carbonylation has been attempted at room temperature and 0.1 MPa with a homogeneous PdCl₂/HCl/CuCl₂ catalyst in methanol and aniline solution with CO and O₂ (4). The major challenges for the development of a low-temperature and low-pressure process are low catalyst activity, separation of carbamate from the reactant mixture, and the use of a corrosive reactant/catalyst solution mixture.

The problems associated with the removal of corrosive solution can be solved if the reaction is carried out over an effective heterogeneous catalyst. NaI-Pd/C catalyst has exhibited activity for oxidative carbonylation at 3.79 MPa (6,7). Prior to mechanistic investigation and heterogeneous catalyst development, two technical issues must be addressed: whether or not this reaction takes place [1] on the truly heterogeneous catalyst surface and [2] at sufficiently mild conditions to allow economic operation of the reaction process. The objectives of this study are to investigate [a] the ability of Pd catalyst to catalyze the oxidative carbonylation of aniline to produce diphenyl urea and methyl N-phenyl carbamate at low-pressures (0.101 MPa) and [b] the effect of Ag addition to Pd/C on the carbamate synthesis activity.

EXPERIMENTAL

Catalyst Preparation

5 wt% Pd/C was prepared by incipient wetness impregnation of PdCl₂/HCl (Sigma Chemicals Co.) solution onto activated carbon Ambersorb-563 (Rohm and Haas Co.). The impregnated sample was air-dried at 298 K for 24 h and calcined at 573 K for 10 h. Ag promoted Pd/C catalyst (Ag-Pd/C) was prepared by sequential impregnation of AgNO₃ (Alfa Chemicals) on to the prepared Pd/C catalyst. The sample was air-dried at 298 K for 24 h and calcined at 673 K for 4 h. The ratio of the volume of the salt solution to the weight of support was 1 cm³ to 1 g in the impregnation step during the preparation of both catalysts.

Reaction studies

The oxidative carbonylation reaction was carried out using methanol (CH_3OH), aniline ($\text{C}_6\text{H}_5\text{NH}_2$), CO , and O_2 with NaI-Pd/C catalyst in a 300 cm^3 autoclave (Pressure Products Inc.). Experimental details including the reaction conditions are listed in Table I. The autoclave reactor was pressurized to the desired pressure and subsequently heated to the desired temperature.

Reactant and product analysis

The reactant/product samples, consisting of a solid and liquid mixture, were obtained periodically from the reactor and bottled. The solid product was allowed to settle and separate from the liquid in the bottle. The solid, dried and diluted with KBr ($\text{KBr/solid} : 9/1$), was analyzed by diffuse reflectance infrared Fourier transform spectroscopy (DRIFTS). The liquid was analyzed by transmission infrared (IR) spectroscopy, gas chromatography (GC) with a $6' \times 1/8''$ 12% SE-30 packed column (Supelco Inc.), and a ^{13}C nuclear magnetic resonance (NMR) spectrometer.

Safety

The present study involved the use of aniline, methanol, CO , O_2 , and NaI-Pd/C catalysts. Due to the varying toxicity of these species the reaction was carried out under a safety hood with all the components handled using neoprene gloves and safety goggles. Development of alternative reaction pathways and new catalysts for this reaction always presents a potential for the formation of species containing toxic $-\text{NCO}$ and $-\text{CN}$ functional groups as the reaction involves C, N, and O species. A careful and detailed product analysis is needed to insure that highly toxic compounds are not produced.

RESULTS AND DISCUSSION

Figure 1(a) shows the IR spectra of the reactant/product mixture obtained at conditions listed for step 1 in run 1 (Table I). The reactant solution spectrum showed the presence of methanol at 1450 cm^{-1} and aniline at 1500 cm^{-1} and 1601 cm^{-1} (5). Increasing the reaction temperature to 373 K produced a solid product whose spectra indicated diphenyl urea ($\text{C}_6\text{H}_5\text{NHCONHC}_6\text{H}_5$) at 1546 and 1640 cm^{-1} (5). The formation of the solid diphenyl urea in the reactant solution does not allow the use of GC to characterize the product distribution. The IR spectra of the sample taken at 60

Table I. Reaction conditions during the Oxidative Carbonylation of Aniline on Pd/C and Pd-Ag/C

	<i>Catalyst</i>	<i>T (K)</i>	<i>P (MPa)</i>	<i>Aniline (cm³)/g of catalyst</i>	<i>Reactant ratio (moles/moles)</i>	
				<i>Aniline/MeOH</i>	<i>CO/O₂</i>	
Run 1	5-wt% Pd/C 0.5 g NaI 0.13 g	Step 1: 373 Step 2: 438	3.79 3.79	190	1/42.7	10/1
Run 2	5-wt% Pd/C 0.5 g NaI 0.13 g	Step 1: 373 Step 2: 438	0.101 0.101	190	1/42.7	10/1
Run 3	5-wt% Pd/C 0.5 g NaI 0.13 g	373	0.506	190	1/42.7	10/1
Run 4	2-wt% Pd-Ag/C 1.25 g NaI 0.13 g	438	3.79	76	1/42.7	10/1
Run 5	2-wt% Pd-Ag/C 0.625 g NaI 0.13 g	438	3.79	152	1/42.7	10/1

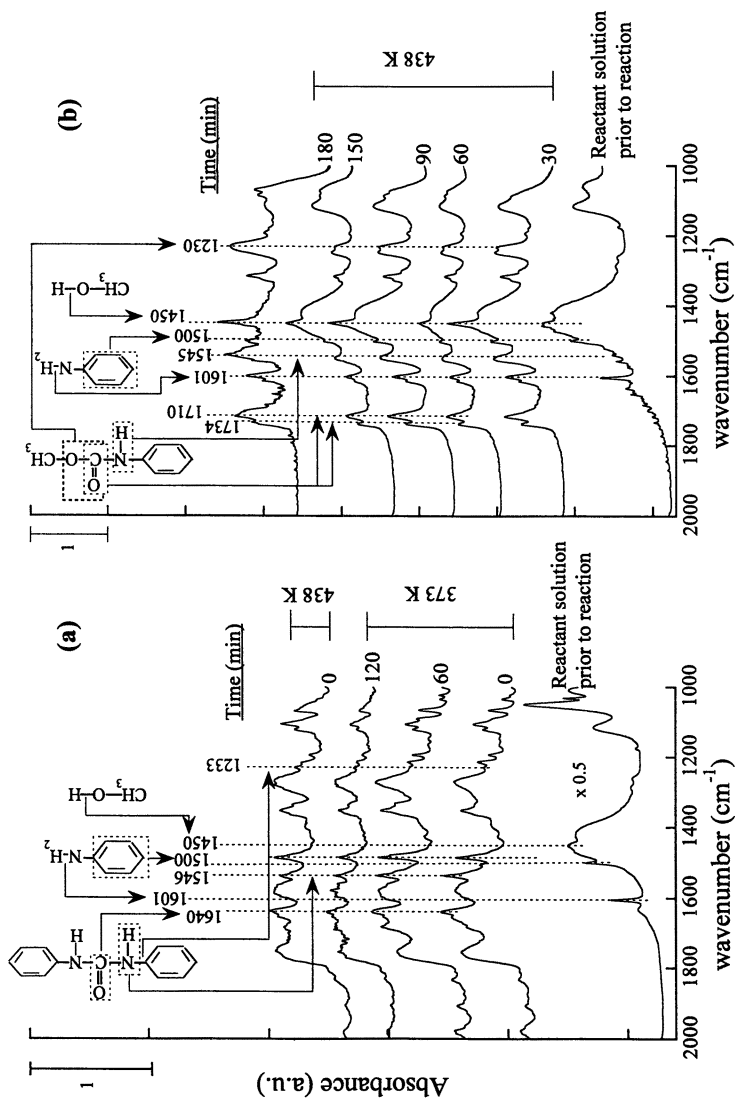


Figure 1. (a) DRIFTS Spectra of the reactant/product mixture at 373 K and (b) transmission IR spectra of the liquid products at 438 K during the oxidative carbonylation of aniline on Pd/C at 3.79 MPa (run 1).

and 120 min did not vary suggesting that the composition of the product remained the same, even at prolonged reaction times.

The IR spectrum of the solid collected instantly after increasing the reaction temperature to 438 K showed strong diphenyl urea bands (Figure 1(a)). Samples obtained after 0.5 h of reaction at 438 K consisted of reactants/products only in the liquid phase. DRIFTS analysis of this liquid sample produced weak IR signals. Transmission IR spectra of the liquid sample, displayed in Figure 1(b), however, showed the formation of methyl N-phenyl carbamate ($C_6H_5NHCOOCH_3$) at 1545, 1710, and 1734 cm^{-1} (5) along with methanol and aniline at 438 K. IR analyses of the samples provided qualitative information about product formation. However, GC analyses provided accurate measurements of aniline concentrations in the reaction before and after reaction. GC results showed a 96 % aniline conversion for the entire reaction process. This level of aniline conversion corresponded to a 98% yield of carbamate, using aniline as a base. The rest of the product formed was nitrobenzene.

Results in Figure 1 demonstrate that NaI-Pd/C is active for the oxidative carbonylation of aniline at 373 K and 438 K at a pressure of 3.79 MPa, consistent with the literature (6,7). To determine the feasibility of carrying out this reaction at low pressures, the reaction was repeated at pressures of 0.101 MPa and 0.506 MPa.

Figure 2(a) shows the transmission IR spectra of the liquid samples obtained for conditions described in step 1, run 2, (Table I). Aniline intensity at 1605 cm^{-1} decreased with reaction time; GC analyses further confirmed the decrease in aniline concentration. The aniline concentration before and during the reaction was used to obtain the conversion (Figure 2(b)). Surprisingly, no reaction products were observed from the IR and GC analysis of the liquid samples taken from the reactor at 373 K. Upon opening the autoclave, a solid layer of diphenyl urea was found deposited on the reactor wall. This solid layer was confirmed to be diphenyl urea as shown from the IR spectra of the dried solid displayed in Figure 3. Repeating the reaction at 0.506 MPa (run 3) led to the formation of similar products shown also in Figure 3. Continuing the reaction at 438 K and 0.101 MPa for 120 min with the liquid solution present in the reactor and solid deposited on the reactor wall produced liquid products. IR spectra of the liquid, displayed in Figure 2(a), showed the formation of methyl N-phenyl carbamate at 1710 and 1734 cm^{-1} . ^{13}C NMR analysis of the liquid, displayed in Figure 4, confirmed the formation of the carbamate species with the C atom in the C=O bond of the carbamate exhibiting a chemical shift of 150.26 (5). GC analysis of the liquid product obtained after 120 min of reaction time at 438 K showed a carbamate yield of 82 %.

Atomic adsorption (AA) analysis did not show any traces of Pd in the product solution obtained from run 2 indicating that Pd did not dissolve from Pd/C into the reactant/product solution during the reaction. This observation confirms that the reaction occurred on the surface of the Pd catalyst and that no Pd complex was formed in the solution obtained during the reaction at 0.101 MPa and 373-438 K.

CO is known to adsorb on the Pd surface to form linear and bridged CO (8). Ag has been known to block the site on which the bridged CO adsorbs (9) and may play a role in the carbonylation reaction. Oxidative carbonylation was conducted over Ag-Pd/C to reveal the potential effect of Ag addition on the reaction.

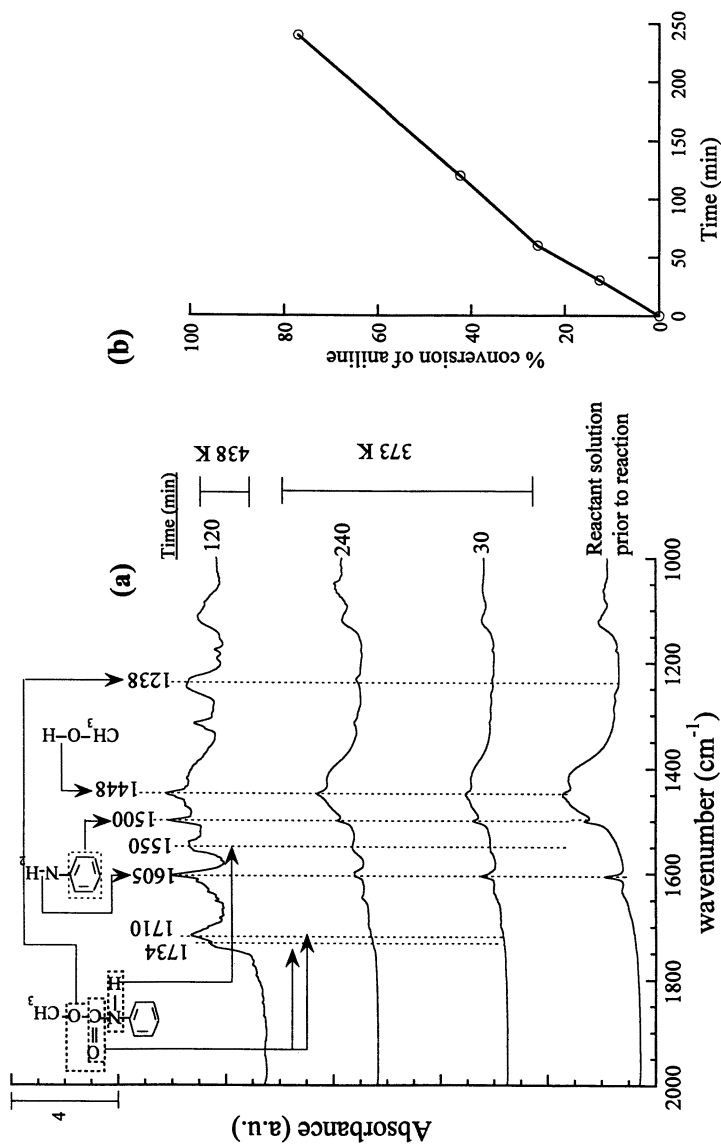


Figure 2. (a) transmission IR spectra of the liquid sample at 373 K and 438 K and (b) variation of aniline conversion with time at 373 K during the oxidative carbonylation of aniline at 0.101 MPa (run 2).

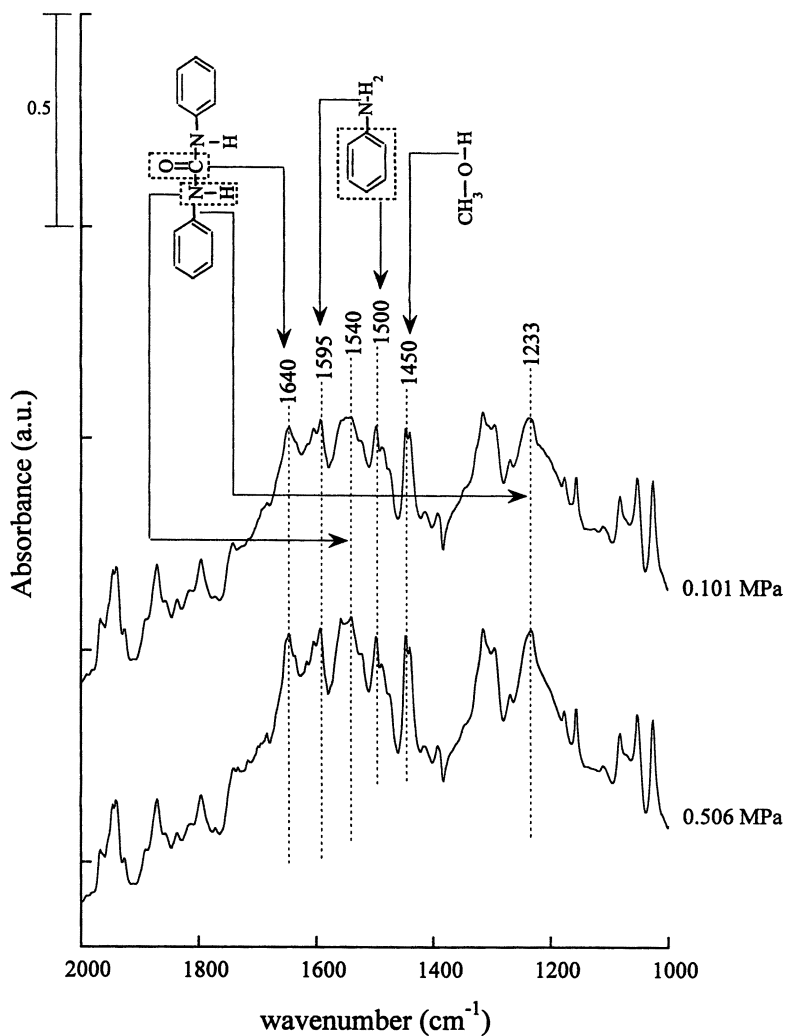
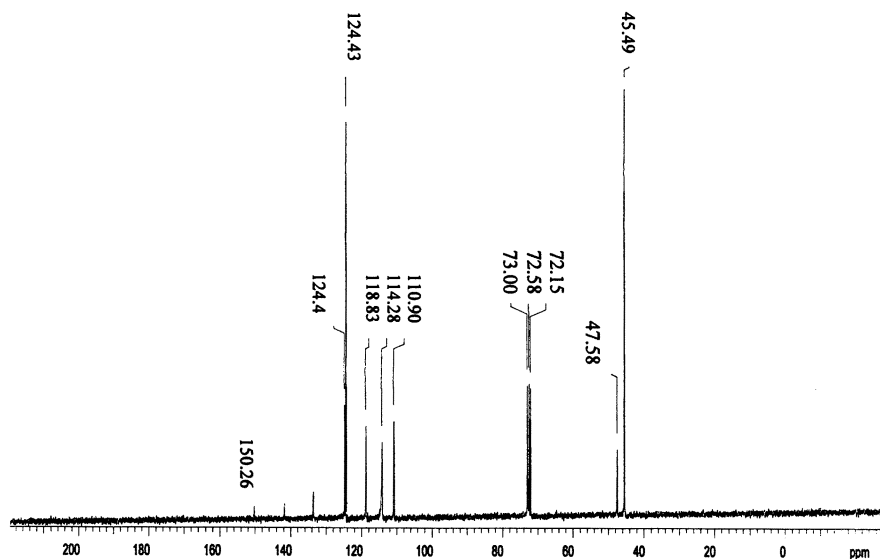


Figure 3. DRIFTS spectra of the solid layer obtained from the reactor wall during the oxidative carbonylation of aniline on Pd/C at 0.101/0.495 MPa, and 373 K (run 2/3).



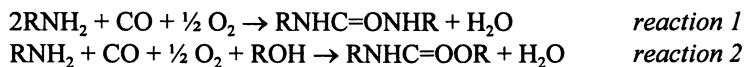
Functional group	Chemical Shift (δ)
Methoxy group from MeOH	45.50
Methoxy group from methyl-N-phenyl carbamate	47.58
CDCl_3	72.15~73.00
Aromatic carbons from aniline and methyl-N-phenyl carbamate	110.9~141.72
Carbonyl group from methyl-N-phenyl carbamate	150.26

Figure 4. ^{13}C NMR spectrum of the liquid product obtained during the oxidative carbonylation of aniline on Pd/C at 0.101 MPa and 438 K (run 2).

Figure 5(a) shows that Ag-Pd/C exhibited activity for the carbonylation of aniline to form methyl N-phenyl carbamate at conditions detailed for run 4 (Table I). Longer reaction time was needed for carbamate formation when lesser amount of catalyst was used (run 5) as observed from Figure 5(b). Comparison of the IR intensity peaks of the carbamate species from run 1 and run 4 show that addition of Ag did not improve carbamate synthesis activity.

Neither diphenyl urea nor methyl N-phenyl carbamate was formed during the oxidative carbonylation reaction carried out with Pd catalysts in the absence of NaI. NaI is, therefore, an essential component in the catalyst used for the oxidative carbonylation of aniline. In addition, these Pd catalysts were inactive for reductive carbonylation of aniline. Reductive carbonylation, carried out over a series of Pd catalysts, produced only trace amounts of carbamate.

Examination of the reactants and products from the oxidative carbonylation at 373 K (*reaction 1*) and at 438 K (*reaction 2*) shows that the major function of O₂ is to dehydrogenate RNH₂ to RNH- species and ROH to RO- species. Formation of diphenyl urea at 373 K and carbamate at 438 K indicates that dehydrogenation of aniline can take place at a lower temperature than that for alcohol. In addition diphenyl urea is able to react with methanol to produce the carbamate species at 438 K. The high yield of carbamate (82%) obtained from the oxidative carbonylation of aniline at 438 K and 0.101 MPa indicates that this reaction process is more economically viable than those requiring high pressure conditions. Although, the carbamate process development will face the challenge of separation of product from the catalyst and reactant mixture, the use of low-pressure and low-temperature conditions will minimize the operating costs for this reaction.



CONCLUSIONS

Extensive catalyst screening studies showed that oxidative carbonylation occurs at mild conditions while reductive carbonylation requires pressures above 4.8 MPa and temperatures of 438-453 K. Oxidative carbonylation involved the use of oxygen to produce H₂O/CO₂, providing the required thermodynamic driving force for the reaction to occur at mild conditions. The present study showed that Pd/C catalyzed the oxidative carbonylation of aniline to produce diphenyl urea at 373 K and methyl N-phenyl carbamate at 438 K, even at a low-pressure of 0.101 MPa. The carbamate synthesis at 0.101 MPa occurred on the surface of Pd catalyst. No Pd metal species is dissolved in the reactant/product solution during the reaction. Oxidative

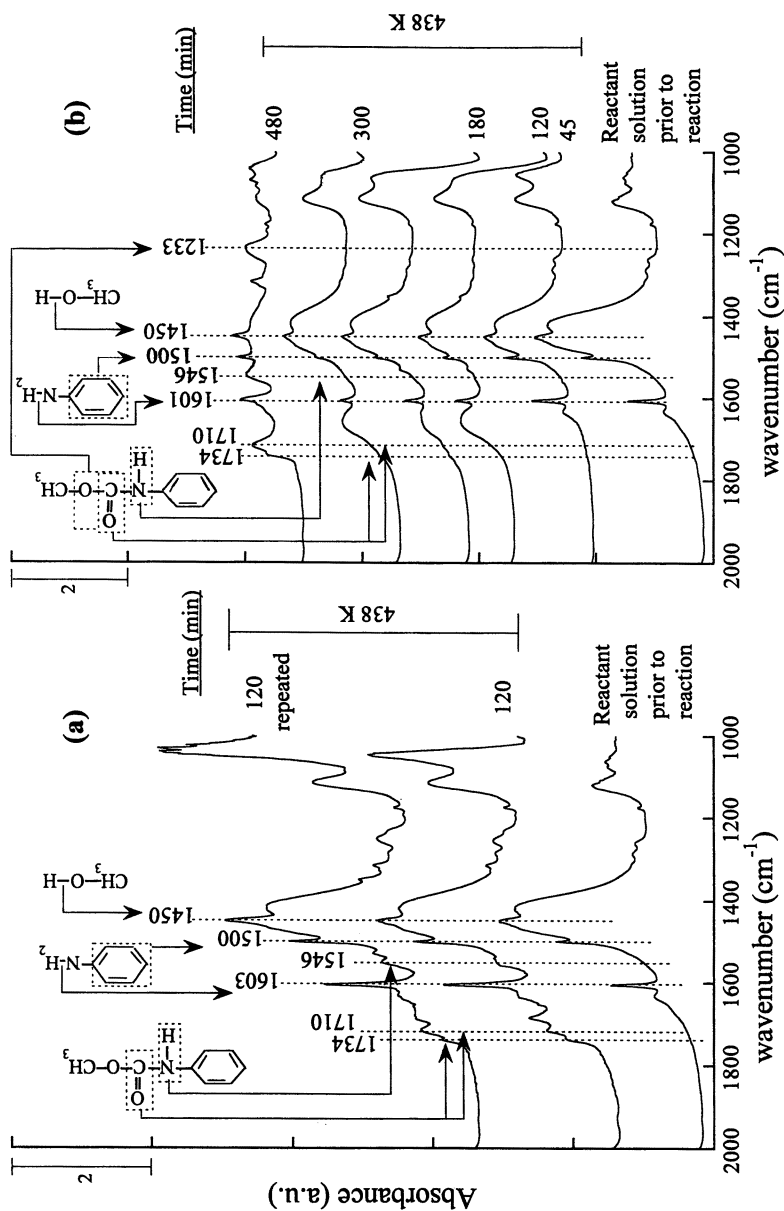


Figure 5. Transmission IR spectra of the liquid products obtained during the oxidative carbonylation of aniline at 3.79 MPa and 438 K over (a) 1.25 g Ag-Pd/C (run 4) and (b) 0.625 g Ag-Pd/C (run 5).

carbonylation of aniline was not promoted upon Ag addition to Pd/C. High carbamate yields at 0.101 MPa show that the Pd-catalyzed oxidative carbonylation reaction may provide an economically viable route for replacing the existing highly toxic amine-phosgene route for the synthesis of isocyanate. This study demonstrates that the potential for the development of an alternative benign route relies on the design of a highly active and selective heterogeneous catalyst.

ACKNOWLEDGEMENT

This work has been supported by the National Science Foundation (NSF) Grant CTS 9816954.

REFERENCES

1. Cenini, S., Pizzotti, M., and Crotti, C., In *Aspect of Homogeneous Catalysis: A Series of Advances*, Ugo, R., Ed.; D. Reidel Publishing, Holland, 1988; vol. 6, pp 97-198.
2. Anastas, P. T. and Williamson, T. C., *Green Chemistry: Frontiers in Benign Chemical Syntheses and Processes*, Oxford University Press, Oxford, 1998.
3. Parshall, G. W., and Ittel, S. D., *Homogeneous Catalysis, The Applications and Chemistry of Catalysis by Soluble Transition Metal Complexes*, 2nd ed., John Wiley and Sons, New York, 1992.
4. Alper, H., and Hartstock, F. W., *J. Chem. Soc., Chem. Commun.* **1985**, 1141.
5. Silverstein, R. M., and Webster, F. X., *Spectrometric Identification of Organic Compounds*, John Wiley and Sons, Inc., New York, 1998.
6. Fukuoka, S., and Chono, M., *J. Chem. Soc., Chem. Commun.* **1984**, 399.
7. Gupte, S. P., and Chaudhari, R. V., *J. Catal.* **1988**, 114, 246.
8. Grill, C. M., and Gonzalez, R. D., *J. Phys. Chem.* **1980**, 84, 878.
9. Chuang, S. S. C., Pien, S-I., and Narayanan, R., *Appl. Catal.* **1990**, 57, 241.

Chapter 12

Clean Combustion: Catalyst Challenges

Robert J. Farrauto

Engelhard Corporation, 101 Wood Avenue, Iselin, NJ 08830-0770

Three technologies for generating power for vehicular and stationary applications with improved fuel efficiency and decreased emissions are discussed. The lean burn gasoline and diesel internal combustion engines are fuel efficient but will require new catalytic technology to lower emissions of nitric oxides. The proton exchange membrane fuel cell promises to provide higher energy efficiency with lower emissions than the internal combustion engine but a number of catalyst improvements must be made for commercial success. Stationary power generation using catalytic assisted thermal combustion is an example of a technology that does not generate pollutants during combustion. These three technologies will be discussed in the present paper.

Introduction

There is much discussion within the chemical and transportation industries about ways to conserve energy while simultaneously cleaning emissions. However, in the quest for meeting goals for Vision 2020, it is important to remember that transportation, i.e., automobiles, trucks, buses, as well as stationary power sources, are enormous consumers of energy and generators of pollutants. To date, most of the technology developed for both mobile and stationary sources has been directly related to what is called post-treatment. The catalyst is fixed into the exhaust system or vent and emissions are abated. The obvious challenge is how to make a vehicle or a power plant more fuel efficient, without sacrificing emissions standards.

Lean Burn Engines

Most people are familiar with the three-way catalyst (TWC), used in gasoline fueled vehicles since 1980, that converts carbon monoxide (CO) and hydrocarbon (HC) to carbon dioxide (CO₂) and water (H₂O) and nitric oxides (NO_x) to nitrogen (N₂). It operates with the precise quantity of oxygen necessary to completely react with all the hydrocarbon. For gasoline the stoichiometric air-to-fuel weight ratio is about 14.6 (stoichiometric $\lambda = 1$ is defined as the actual air to fuel ratio in the exhaust divided by the stoichiometric air to fuel ratio). At $\lambda = 1$, shown in Figure 1, the catalyst simultaneously converts all three pollutants (1). Anything to the left is a fuel rich environment ($\lambda < 1$), in which there is an insufficient amount of O₂ to oxidize all the HC. Unreacted HC and/or CO can then reduce the NO_x. Once lean of stoichiometric ($\lambda > 1$), the effectiveness of the catalyst towards NO_x reduction is lost since the reducing agents (HC and/or CO) are preferentially oxidized by the excess air (i.e. oxygen). To significantly improve fuel economy one can operate the engine very lean of the stoichiometric point ($\lambda \gg 1$). Therefore, a highly selective catalyst is needed that will either decompose or enhance the rate of reduction of NO_x in the presence of large excesses of air. A family of catalysts can be used when ammonia or urea is the reducing agent, a practice common in the power generation industry (1), but for mobile source applications, on-board derived fuel is preferred. Such a catalyst would allow fuel efficient lean burn engines to be widely produced while meeting NO_x emission standards. It would increase fuel efficiency by perhaps 20 to 25 percent and subsequently green house gas CO₂ emission by the same amount.

There are a number of companies that are currently developing lean burn gasoline engines. Diesel engines are lean burn engines. Many commercial trucks and passenger cars use diesel engines because they are very fuel-efficient. Abatement of the liquid particulate or soluble organic fraction (SOF), CO and HC (2) are abated using catalytic after treatment however, NO_x is not adequately treated for the reasons given above. The absence of a suitable NO_x reduction catalyst with on-board fuel has led engine manufacturers to use various control strategies such as exhaust gas recirculation (EGR) to reduce NO_x. This approach does not reduce NO_x to the low levels required and decreases fuel economy. If a NO_x abatement catalyst were developed it would impact both lean burn gasoline and diesel engines.

There has been little progress made in the last 10 or 15 years in the development of suitable catalysts for reducing NO_x with hydrocarbons in a lean environment although studies have been numerous (3,4). Figure 2 summarizes the status of the current platinum (Pt) and copper/zeolite (Cu-ZSM-5) catalyst technologies using propylene as the HC. The conversion of NO_x is plotted against temperature. The conversion plot using a platinum catalyst shows a "leading edge" at about 175 °C with a maximum at around 225°C. The hydrocarbon is reacting with the NO_x according to reaction (1).

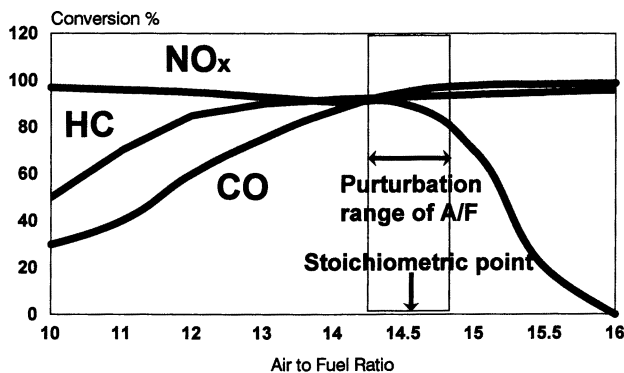
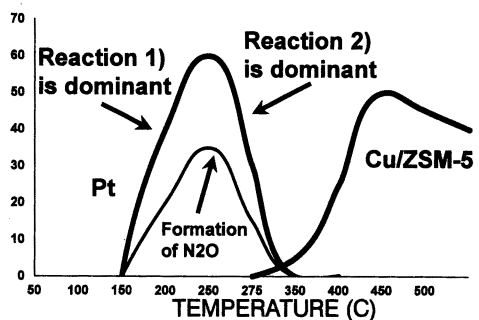


Figure 1. The conversion profile for CO, HC and NO_x as a function of the air to fuel ratio for the three way gasoline automobile catalyst

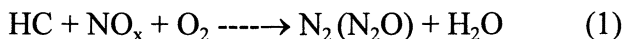


- 1) $-\text{CH}_2- + \text{NO}_x + \text{O}_2 \longrightarrow \text{N}_2 + \text{CO}_2 + \text{H}_2\text{O}$
- 2) $-\text{CH}_2- + \text{O}_2 \longrightarrow \text{CO}_2 + \text{H}_2\text{O}$

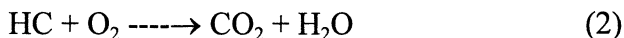
Technical Issues:

1. Selectivity of HC is poor/N₂O formation for Pt
2. Temperature ranges of activity are too narrow
3. Thermal stability and SO_x poisoning of Cu/ZSM-5 are not adequate

Figure 2. The typical conversion of NO_x versus temperature profile using propylene as the hydrocarbon reductant for Pt and Cu/ZSM-5 catalysts.



Above 225°C the conversion precipitously decreases because the hydrocarbon is now preferentially reacting with the O₂ as shown in reaction (2).



Because of this lack of selectivity the temperature range in which Pt is functional is too narrow relative to the operating ranges of the vehicle. Below about 275 °C about 50% of the NO_x is partially reduced to N₂O, a powerful greenhouse gas.

There have been many studies performed over the past 10 years using Cu supported on a pentasil zeolite called ZSM-5, as a catalyst for HC-NO_x reduction in lean environments. The problem with this catalyst is that it is not hydrothermally stable above 550 - 600°C; a condition expected in a vehicle. A small amount of sulfur, just 20-30 vppm in the exhaust, has a significant damaging affect on the overall performance (5). Therefore, in terms of lean NO_x technology for mobile sources, the goal is to develop a catalyst that is very selective for reaction (1) and not for reaction (2). It is important to note that the focus on reducing NO_x with hydrocarbon is due to the lack of success in finding a catalyst that can decompose NO_x. Thermodynamically, one could decompose NO_x to N₂ and O₂ but the reaction is very slow and is poisoned by water and sulfur oxides present in the exhaust. Therefore, catalysis research will continue to address lean NO_x decomposition or selective reduction with hydrocarbon fuels well into the next century.

The Fuel Cell

Fuel cells hold promise as an alternative to combustion for power generation for stationary and/or mobile source applications in the near future. They are about twice as fuel efficient as the internal combustion engine and effectively produce no CO, HC or NO_x. They operate on the basic principal of direct conversion of chemical energy into electrical energy, avoiding the mechanical steps and thermodynamic limitations of traditional combustion energy cycles. Hydrogen gas is electrochemically oxidized to hydrogen ions at the anode, Figure 3, which pass through a proton conductive membrane to the cathode where they combine with electrochemically reduced O₂ (from the air) producing H₂O. The electrons flow through the external circuit and do work.

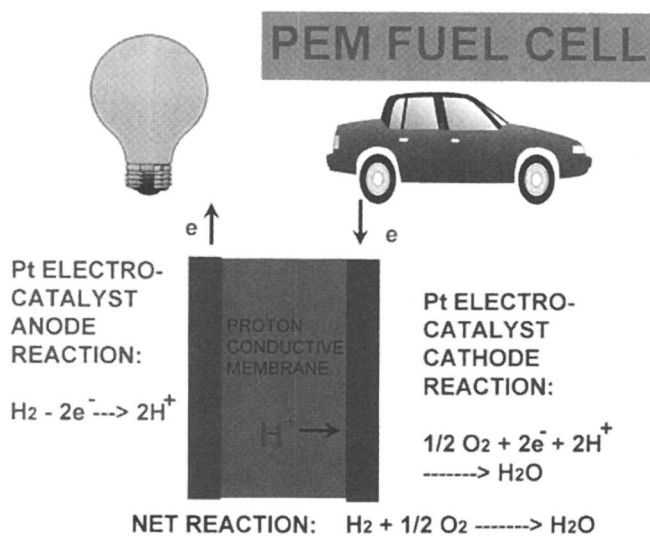


Figure 3. A cartoon sketch of the PEM fuel cell using H_2 and O_2 as fuels

The Proton Exchange Membrane (PEM) fuel cell, which operates at about 80°C, is the most promising of all the fuel cell systems (6). The proton selective membrane is a fluorocarbon polymer of sulfonic acid. The anode and cathode are primarily Pt containing materials.

At the present time H₂ is the only fuel that can be electrocatalytically oxidized at the anode. There is considerable research in the direct electrochemical conversion of methanol but success is not imminent. In contrast to gasoline or natural gas, there is no infrastructure for obtaining hydrogen at the local gas station or in the home. A number of automobile companies (i.e., Daimler-Benz Ballard, General Motors, Toyota, Honda,) have targeted methanol as an on-board source of H₂ as the first generation fuel but the fuel of the future is to be determined. The US initiative called the Partnership for a New Generation Vehicles (PNGV) is a partnership between US industry, universities, and government with the goal of developing technologies that can be used to create cost effective full size sedans capable of obtaining 80 miles/gallon of fuel. The fuel cell is the predominant technology under consideration.

For stationary applications natural gas is the most preferred fuel by companies such as Plug Power and Ballard Generating Systems. Producing H₂ from sulfur containing hydrocarbons is currently practiced in the chemical industry (7) for production of ammonia and alcohol under steady state conditions with carefully controlled catalytic unit operations. The first step in the production of H₂ using sulfur containing hydrocarbons is catalytic (Co, Mo) desulfurization as seen in reaction (3).



The H₂S produced is removed by adsorption on ZnO (4). Sulfur removal is

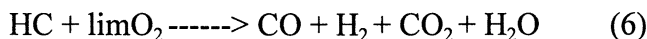


necessary due to the sensitivity of downstream catalysts to deactivation. This step is not necessary for sulfur free methanol.

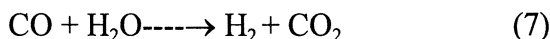
The next step is nickel (Ni) catalyzed steam reforming (5) which is highly endothermic and requires high energy input (inlet temperatures exceed 800°C) depending on the fuel. Equilibrium limits conversion so a partial oxidation reaction



or secondary reformer (6), also using a Ni containing catalyst, is used to generate more heat and more H₂ according to reaction (6).

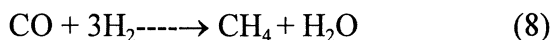


The exit from the secondary reformer contains about 10-12% CO which is fed to a high temperature water gas shift (WGS) reactor, reaction (7), using an Fe, Cr containing catalyst at about 350°C. This further increases the H₂ content and



decreases the CO to about 2% as governed by the thermodynamics of the exothermic reaction.

The product gas is fed to a low temperature Cu, ZnO, Al₂O₃ WGS catalyst at about 200°C. The CO is decreased to less than about 0.5 %. The remaining CO, which poisons down stream ammonia or methanol synthesis catalysts, is removed by pressure swing absorption or in some case methanation (8) over a Ni or Ru based catalyst at about 250°C.



Weight, size, and transit operations are not critical for H₂ plants but are important for fuel cell systems. Therefore, this technology will have to be modified significantly to meet the demands of the fuel cell. This will entail new catalysts and process conditions along with considerable catalytic engineering.

Catalytic Assisted Thermal Combustion in a Gas Turbine

Conventional combustion for utility power generation consumes a large amount of energy and produces large quantities of CO, HC, NO_x and CO₂. Although the pollutants can be treated with end of pipe or post-technology (1), this strategy is often less than ideal. It is more beneficial to simply avoid their generation at the source. A gas turbine technology referred to as catalytically assisted thermal combustion utilizes a catalyst deposited on the walls of a parallel channel monolithic structure to initiate air oxidation

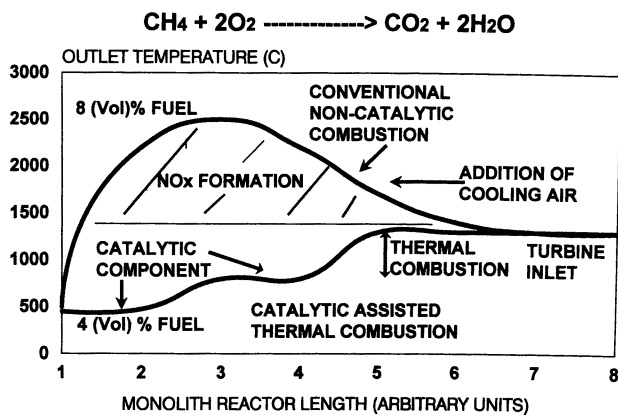
of the fuel i.e., natural gas, which then supports and stabilizes homogeneous reaction. Because the mixture combusted is lean the adiabatic temperature rise is below 1500°C avoiding the temperature range where NO_x is readily formed by reaction of N₂ and O₂. With the proper reactor design the emissions of CO, HC and NO_x are less than about 2 ppm. The catalyst initiates conversion of the gaseous hydrocarbon fuel and raises the temperature to a point where thermal reaction completes the combustion process. The product gases are at 1,300°C and drive a turbine to generate electricity, Figure 4. In a conventional combustor the natural gas-air mixture is close to eight volume percent because it is necessary to be in the flammable range to ignite the fuel. Once ignited, temperatures can reach as high as 2,500°C which is well above the NO_x formation regime. This temperature is too high for the blades of the turbine so it is necessary to add air to cool it to 1300 °C. Instead of starting with 8 percent fuel and then adding the air downstream it makes more sense to add the air to the feed gas diluting it to about 4 volume percent and to allow a catalyst to initiate oxidation around 450 to 500°C. After the catalytic reaction is initiated the gas composition coupled with the temperature brings the mixture into the flammable regime where homogeneous combustion is stable and complete. The fuel is burned efficiently and the temperature where NO_x forms is never reached. Therefore, this technology would permit efficient combustion without forming NO_x at the same temperature needed for the gas turbine inlet.

Applications are primarily targeted for stationary power generation using natural gas fuel but one could envision a small power generation station on a gasoline-electric hybrid vehicle which recharges the battery.

While this technology was patented in 1975 (8) it has not been commercialized. Catalysts need to be improved because the exposure temperatures are higher than what traditional catalysts can withstand. There is also a need for improved monolithic substrates that can withstand the thermal stresses experienced in a gas turbine. There has been progress in both of these areas (1) but more is needed. Finally, there is a need for engineering demonstration of system reliability (9).

Conclusions

Catalysis research must continue to improve emissions from existing power stations or preferably to develop cleaner technologies. Improved catalysts for decomposing or reducing NO_x from lean burn internal combustion engines is an enabling technology for improved fuel economy and decreased carbon dioxide emissions. Clean and efficient energy provided by fuel cells requires cost effective and reliable catalysts and systems to be developed. Catalysts with stable activity and durability after continuous operation

**Technical Issues:**

1. Improved catalysts and substrates
2. Engineering demonstration

Figure 4. catalytic assisted thermal combustion profiles compared to traditional non catalytic combustion

at 1300 °C will enable pollution free catalytic assisted thermal combustion to revolutionize power generation.

Literature Cited

1. *Catalytic Air Pollution Control: Commercial Technology*, R.M. Heck and R. Farrauto, Van Nostrand Reinhold (now Wiley and Sons), New York, New York, 1995, Chapter 6
2. R. J. Farrauto and Kenneth E. Voss, *Applied Catalysis B: Environmental* 1996, 10, 29
3. M. Misono, *CATTECH* 1998, 4, 183
4. M. Amiridis, T. Zhang and R. J. Farrauto, *Applied Catalysis B: Environmental* 1996, 10, 203
5. J. Feeley, M. Deeba and R. J. Farrauto, *SAE 950747* 1995
6. R. Singh, *Chemical Engineering Progress* 1999, 95(3), 59
7. *Fundamentals of Industrial Catalytic Processes*, R. Farrauto and C. Bartholomew, Kluwer Academic Publishers, 1997, Chapter 7
8. W. Pfefferle, *US Patent 3,928, 961*, 1976
9. J. McCarty, *Industrial Catalysis News* 1998, 11, 98

Chapter 13

Zeolite Technologies for a Greener Environment

B. K. Marcus and W. E. Cormier

Zeolyst International (<http://www.zeolyst.com>) Research and Development, Conshohocken, PA 19428

Applications using zeolites of aluminosilicate and other compositions are undergoing intensive development and commercialization in diverse areas due to their process advantages. Because of their wide-range of properties, these materials are also finding applicability in industrial processes that are environmentally sensitive. A review of some of the properties of zeolites, how these properties are useful for extension into environmental areas, and some of the diverse “green” application areas where zeolites are being used are covered in this paper.

Introduction

Chemical processes involving catalysis and adsorption are increasingly being designed to minimize risk to humans and the environment through the use of “greener” materials. The drivers for cleaner technologies are numerous and interwoven, and they include regulatory pressures, economic considerations, and social concerns. The regulations and laws of many countries are becoming increasingly more stringent requiring a marked decrease in effluents, wastes, and by-products; fines and possible plant closures are among the penalties for non-compliance. Increased legislative pressures often results in increased costs, and these economic considerations are driving companies to devise new, cheaper methods to produce materials in order to compete with third world countries that do not face similar legislative pressures. Social issues centering on the desire for a clean environment are driving consumers to demand that materials be produced in a socially and environmentally conscious manner. There are many materials being studied for use in the applications being developed to meet these requirements; one of

the main classes of inorganic materials being investigated is zeolites. Applications using aluminosilicate and other composition zeolites are undergoing intensive development and commercialization due to their process and environmental advantages. Zeolites have diverse properties that allow them to be used in a variety of applications and chemical environments. In order to understand how zeolites are able to function as catalysts, adsorbents, ion exchangers, desiccants and carriers, it is necessary to explain the unique and diverse properties that zeolites possess.

Zeolite Properties

Molecular sieve zeolites are a class of stable mineral and synthetic crystalline inorganic compounds characterized by the presence of an open three-dimensional oxide framework structure. This framework is composed of SiO_4^{4-} and AlO_4^{5-} tetrahedral atoms linked at the corners of the tetrahedra via shared oxygen atoms. This leads to a net negative charge on the aluminum that is balanced by a cation. Depending on how the tetrahedral atoms are connected, different zeolites structures are formed. There are more than 40 natural zeolites, but when synthetic materials are included, more than 100 structure types have been reported since the first synthetic zeolites were produced in the 1940's.

The open repeating framework of a zeolite forms a regular network of uniform, microporous openings leading to channels, cages, or cavities and results in a large internal surface area. Figure 1 shows the faujasite structure (synthetic zeolites X and Y). The pore opening of approximately 7 angstroms leads into a supercage that is approximately 12 angstroms wide; the entire internal volume is accessible through the system of repeating, three dimensionally interconnected pores and cages. The sieving characteristics of zeolites are largely determined by the size of the pore opening, while the size, shape, and dimensionality of the internal structure can lead to shape and product selectivity.

In addition to the uniform pore openings and large surface areas, other zeolite properties include (Table I): thermal stability, allowing their regeneration by heat; large ion exchange capacity of the mobile charge balancing cations, leading to their use as ion exchangers and leading to the inclusion of active metals; water capacities ranging from extremely hydrophilic to hydrophobic, allowing their use as adsorbents in a variety of environments; acidity that ranges from very strong to negligible; and the ability to replace the framework silicon and aluminum atoms with other atoms leading to diverse applications. These properties of zeolites have led to their use in a variety of application areas such as water softeners in detergents, sequesters of radioactive nucleotides, desiccants, odor removers, acid and shape selective catalysts, and in many "green" areas.

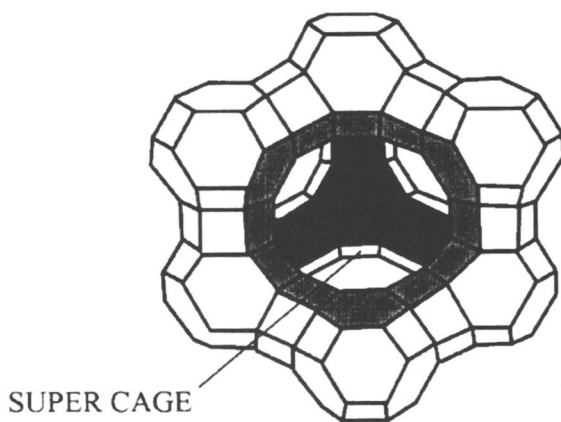


Figure 1. Zeolite Faujasite Structure – Synthetic Zeolite X and Y.

Table I. Zeolite Properties

<i>Property</i>	<i>Value</i>
Channels	2.2 - 8 Angstroms
Cavities/Cages	6.6 - 11.8 Angstroms
Thermal Stability	500 to 1000°C
Ion Exchange Capacity	Up to 700 meq/100g
Surface Area	Up to 900 m ² /g
Water Capacity	≤ 1 to ~ 25 wt.%
Properties	Hydrophilic to Hydrophobic Shape Selectivity Strong to No Acidity

Zeolites and Green Technologies

It is recognized that most of the obvious and inexpensive solutions to pollution problems have been investigated and that more creative materials and technologies will be needed in the future to meet the increasing regulatory push for cleaner technologies. Zeolite researchers and manufacturers know that there is a continuing need to develop new cost-effective materials with characteristics and properties that will be useful in emerging technologies. Some of the emerging technology areas where zeolites have been studied for use are 1) air cleanup (VOC removal, stationary and mobile deNO_x and deSO_x, automotive cold start), 2) land and wastewater cleanup, and 3) fine chemical process improvement (waste minimization, higher efficiency, cheaper feedstocks). Several of these areas are used as examples of the potential for using zeolites in green technologies.

Volatile Organic Chemicals (VOCs)

Historically, zeolites have been used as desiccants because they are hydrophilic and have excellent water capacities. They are capable of maintaining a very low water concentration in closed systems even at low partial pressures. One application area where this is useful is in insulated glass windows, where zeolites are used to entrap the moisture left between the panes during manufacture. However, through the years, there has been an increase in the number of zeolites available with high silica to alumina (Si/Al₂) ratios. These materials are either directly synthesized, as in the case of silicalite (very high silica ZSM-5), or materials that have been dealuminated using hydrothermal or chemical means. These siliceous materials are thermally stable to temperatures in excess of 900°C and are more hydrophobic in

nature. This hydrophobic property has led to their use in applications where organic vapors must be removed from air streams and into areas where carbon has been the traditional adsorbent. Zeolites, unlike carbon, are especially effective where the stream is dilute, where the contact time is short or when water is present; they are also non-combustible and can be regenerated on site. The use of mixtures combining different zeolites and/or carbon is being investigated, and there are several companies marketing systems containing zeolites for the removal of VOCs.

Nitrogen Oxides (NO_x)

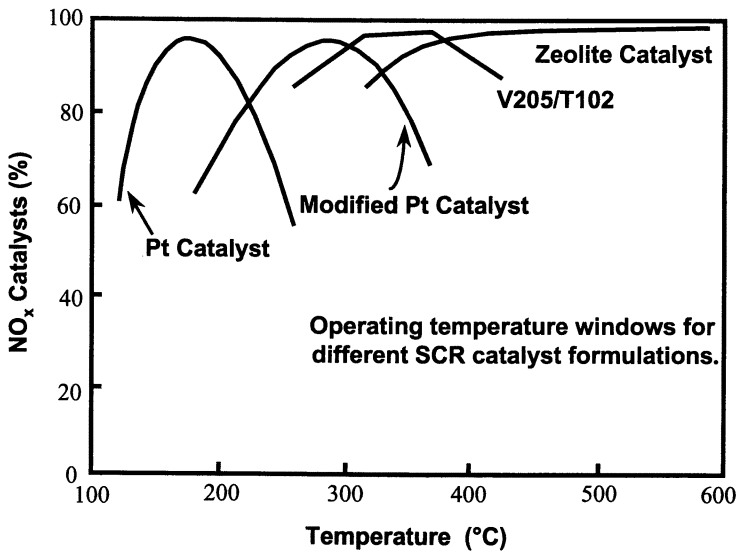
One important area of environmental research is the reduction of atmospheric nitrogen oxide gases that cause photochemical smog. Stationary sources of NO_x include power plants and chemical operations, and the reduction technology that has been used in these sources is selective catalytic reduction (SCR). SCR uses ammonia as the reductant but is temperature limited. NO_x conversions are increased at higher temperatures, and therefore, higher temperature catalysts and new process methods are being developed to further decrease NO_x.

As regulations have tightened on the amount of NO_x that can be emitted and the types of streams that have to be treated, the temperature limits for various catalysts have improved, and new materials to meet the regulations have been introduced. Figure 2 (1) shows the operating temperature windows for SCR catalyst formulations. In the temperature range below 400°C, precious metal catalysts are effective. Vanadia/titania catalysts are effective to approximately 425°C but are poisoned when sulfur is present in the gas stream. At higher temperatures, zeolite catalysts such as metal containing ZSM-5 and mordenite are effective. In these materials, the zeolite ion exchange property has been utilized to exchange copper into the zeolitic structure, where it is available for the reaction.

The use of zeolites has extended the range over which it is possible to have effective deNO_x systems and offers several advantages. These advantages include: dust resistance, allowing their use in coal fired boiler applications; temperature resistance, allowing their use in higher temperature streams that could not be treated previously; increased selectivity at higher temperatures since they do not oxidize ammonia to NO_x, and they are less expensive than precious metals.

An emerging extension technology is NO_x conversion under lean burn (oxidizing) conditions in which hydrocarbons are used as the reductant in place of ammonia. The hydrocarbons used include methane and ethane that come from the fuel source. This results in a system that is cheaper and requires no special handling of the reductant. The materials of choice in this application are copper or cobalt ion exchanged ZSM-5 and cobalt exchanged beta zeolite (2,3).

By removing the need for ammonia in the deNO_x system, it is possible to extend the application to mobile emission sources such as diesel automobiles, and much research has been done in the area (4,5). Diesel engines are lean burn and are oxygen rich. They produce less CO₂ than a gasoline car and are more efficient. However, the traditional precious metal three-way catalyst is not effective in removing the NO_x



Heck, R.M. and Farrauto, R.J., "Catalytic Air Pollution Control: Commercial Technology", Van Nostrand Reinhold, 1995.

Figure 2. Operating Temperature Windows for NO_x Conversion Catalysts. (Reproduced from Reference 1. Copyright 1995 VanNostrand Reinhold.)

formed. The zeolites being researched for this application include copper and cobalt ion exchanged ZSM-5 and beta.

Nitrous Oxide (N₂O)

Nitrous oxide is a powerful greenhouse gas because it absorbs in the infrared region. It is produced in large quantities in nitric acid plants and in adipic acid plants; adipic acid being used in the production of nylon. At higher temperatures, a variety of metal exchanged zeolites will decompose N₂O (6), and this process has been licensed for commercial use.

Automobile Cold Start

Increasingly strict regulation of automobile exhaust is occurring in order to approach the ZLEV (Zero Level Emission Vehicle) requirement. The majority of emissions (70–90%) produced by automobiles today are emitted during the first one to two minutes of use known as the cold start time. During this time, the three-way catalyst has not heated up sufficiently to burn the hydrocarbons produced and those hydrocarbons are emitted into the atmosphere. In 1992, it was reported (7) that a 35% reduction in cold start emissions could be achieved using a high silica ZSM-5 zeolite as a trap to hold the hydrocarbons until the catalyst reached light off temperature. The adsorbed hydrocarbons are gradually released during the heat up time. Four years later, the amount that could be removed, using a mixture of zeolites, doubled to more than 70% (8,9,10). Work continues on improving the zeolite trap so that the hydrocarbons are released at, temperatures equal to or higher than, the light off temperature. The challenge is to find a zeolite that has the maximum high temperature adsorption capacity at the same time that it is hydrothermally stable in the exhaust stream.

Fine Chemical and Chemical Applications

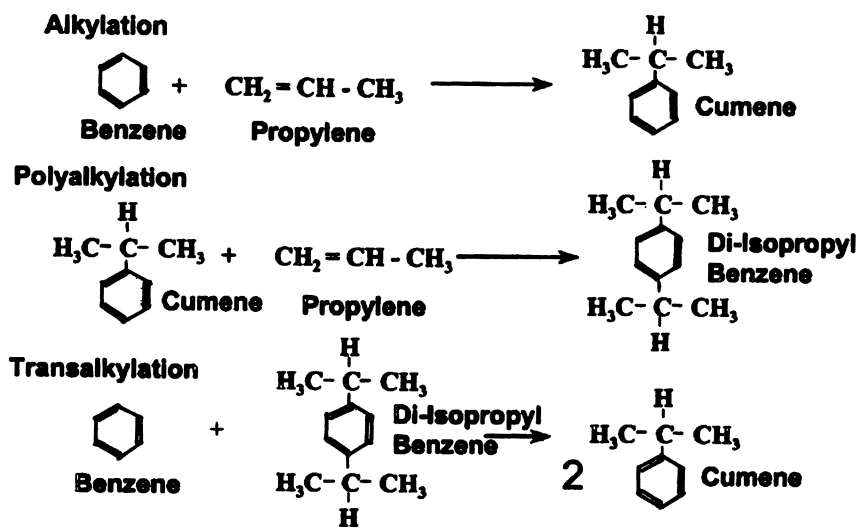
During the first twenty years that zeolites were used commercially as catalysts, their main applicability was in the areas of refinery and petrochemical catalysis. Since then, applications using zeolites have grown to include fine chemical areas such as flavors and fragrances, agricultural products, food, and pharmaceuticals. In the chemical industry, zeolites are used in the production of fibers, resins and composites. Traditionally, these areas have used homogeneous liquid catalysts that generate large quantities of waste including water streams, salts and heavy metals, the disposal of which can lead to many environmental problems. The use of zeolites as

heterogeneous catalysts results in many process advantages such as: easier recovery of the catalyst, thermal regeneration, and decreased corrosion.

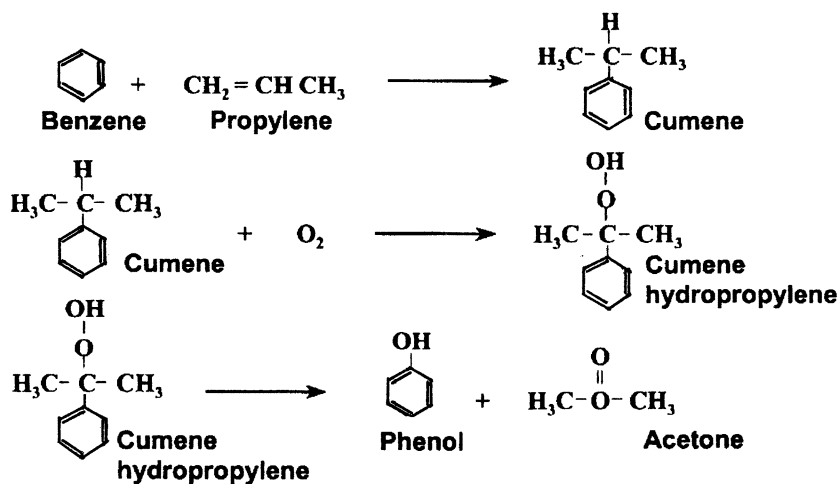
One such example is the synthesis of cumene, production of which involves three separate reactions (Scheme 1). There are several commercial processes for making cumene (Table II) with the predominant one licensed by UOP using solid phosphoric acid (SPA). This process generates a lot of waste since the catalyst is non-regenerable. Monsanto has licensed an aluminum chloride process that has greater unit efficiency. Recently, zeolite-based processes have been announced by several companies (Table III) using a variety of zeolites. Users of these zeolite processes claim that they have greater unit efficiency and better selectivity. In addition, the catalyst is regenerable, non-hazardous and non-corrosive; this is a much more environmentally friendly process. Environmental benefits are indicated in italic text in Table II below.

Table II. Cumene Synthesis Catalysts

<i>Solid Phosphoric Acid (SPA)</i>	<i>AlCl₃</i>	<i>Zeolite Catalyzed</i>
Predominant process	At least five licensees	A number of recently announced projects
High formation of polyalkylates High impurities, lower yield	Lower impurities	Lower impurities
No transalkylation function	Transalkylation function <i>Lower B/P ratio allows higher capacity, greater unit efficiency</i>	Transalkylation function <i>Lower B/P ratio allows higher capacity, greater unit efficiency</i>
High benzene to propylene (B/P) ratio required to maximize yield Some propylene oligomerization Olefin impurities, lower yield May require treatment	Greater tendency to form n-propylbenzene impurity	<i>Excellent selectivities claimed</i>
Non-regenerable Catalyst disposal issues	Hazardous waste disposal issues with spent AlCl ₃	<i>Regenerable, non-hazardous catalyst</i>
Small flow of aqueous phosphoric acid effluent corrosion and/or environmental issues	Corrosive catalyst requires special, higher cost capital equipment	<i>Non-corrosive</i>



Scheme 1. Cumene Synthesis Reactions.



Scheme 2 Phenol Production by Cumene Peroxidation.

Table III. Zeolite Based Cumene Synthesis Catalysts

<i>Company</i>	<i>Zeolite Type</i>
Dow-Kellogg	Dealuminated Mordenite
Mobil-Badger	MCM-22 (?)
EniChem	Zeolite Beta
CD Tech	Zeolites Y, Beta, or Omega
UOP Q-Max	Zeolite not identified

Cumene is not generally produced as an endproduct. Except for a small amount of cumene used in a bisphenol resin, it is currently made for only one reason – as the precursor used for the synthesis of phenol (Scheme 2). Since cumene is a hazardous chemical, it would be desirable to eliminate it oxidizing benzene to phenol directly with as few intermediate steps as possible. This would be an environmentally important improvement in chemical processing, and numerous attempts have been reported. In the 1960's, Schenectady Chemicals commercially practiced the direct vapor phase oxidation of benzene to phenol using oxygen, but there were numerous impurities produced in the process. In the 1970's, UOP reported a process using hydrogen peroxide and HF (11).

In 1997, there was a major breakthrough with exciting environmental ramifications (12,13). Solutia (previously Monsanto) and the Boreskov Institute announced a process using the previously discussed greenhouse gas, N₂O, as the oxidant in the direct oxidation of benzene to phenol over a modified ZSM-5 zeolite catalyst. This process utilizes a greenhouse gas to produce phenol directly with good yields and selectivity and eliminates the need to produce cumene.

The phenol produced can be used to produce cyclohexanone that is used to make caprolactam, another constituent of synthetic fibers. The traditional Raschig process (Scheme 3) is a complicated scheme, with many hazardous raw materials and waste streams, that produces a product that is approximately 83% pure. In 1983, Snamprogetti S.P.A./Enichem patented TS-1 (14), a very high silica ZSM-5 containing small amounts of titanium. In this material, the titanium is neither ionic nor present as the oxide, but replaces some of the silicon atoms in the framework. Enichem developed an ammoximation process (Scheme 3) using hydrogen peroxide as the oxidant and ammonia. As can be seen from the schemes, the number of processing steps is dramatically reduced resulting in much less waste. Recently there have been reports that the last step, which is a Beckmann rearrangement, can be done using another zeolite, eliminating the oleum (fuming sulfuric acid) and the ammonia resulting in even less waste.

In the fine chemical area, one example of using zeolites in new applications is in the production of flavors and fragrances. Many of the traditional synthetic routes involve multiple steps that produce low yields and much waste. Zeolites have been studied, but have been plagued by one main drawback: the need to use batch reactors. Recently (15), the group of Wolfgang Hölderich at the University of Aachen, Germany, developed a process using beta zeolite in a continuous reactor to

heterogeneously catalyze the hydroalkoxylation of limonene and alpha-pinene with $C_1 - C_5$ alcohols to the 1-methyl-4- [alpha-alkoxy-isopropyl]-1-cyclohexenes. They got excellent yields and were able to regenerate the catalyst in the same reactor resulting in an industrially viable process. Strong acids such as HCl, H_2SO_4 , p-toluenesulfonic acid, and $AlCl_3$ have been used commercially, but due to environmental and corrosion problems, they are no longer suitable for industrial applications.

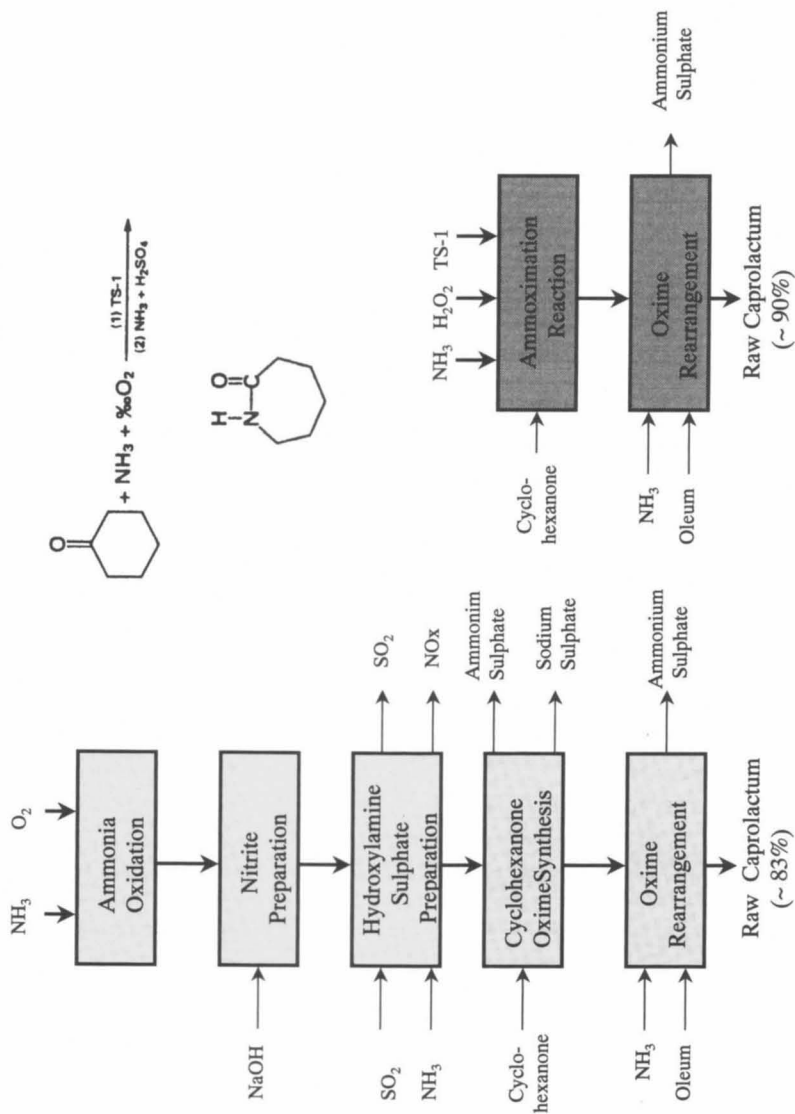
Zeolites are increasingly replacing homogeneous catalysts in fine chemical and chemical applications due to their high activity and yields and their improved selectivity with fewer competing consecutive or parallel reactions. Zeolite catalysts are easier to separate from the products, and produce less complex reaction mixtures, resulting in easier separation of the product stream. In addition, they do not cause corrosion of the reaction vessels, and can be regenerated using a variety of techniques including thermal and pressure swings and heat and solvent stripping. The regeneration step can frequently be done *in situ*.

Conclusions

Since zeolites were introduced commercially, they have made major contributions in the field of chemistry especially in the areas of ion exchange, separations, drying and petroleum catalysis. These areas have been extensively studied and are, in many ways, mature. This paper provides but a few examples of new areas in which zeolites are being investigated for use in Green Chemistry as environmentally friendly materials that can replace potentially hazardous ones. Many new developments in zeolite science are driving the use of zeolites as substitutes in these and other applications. These developments include new compositions, the availability of formed products and favorable economics.

The number of zeolite compositions available has been extended by the addition of framework heteroatoms such as titanium in TS-1, iron, gallium and cobalt, many of which give unique properties to the material. Larger pore size zeolites are being synthesized which extend the molecular size range of the reactants that can be treated. Zeolite properties such as the degree of hydrophobicity, the amount of acidity, and the character of the surface can also be modified to make them useful for specific applications. Zeolites can also be used as carriers of homogeneous catalysts, resulting in a system that has the benefits of a heterogeneous system. There have also been instances where combinations of zeolites or, zeolites with other materials such as carbon, shows a synergy that produces unique results.

Zeolites as synthesized are fine powders, a form that is not useful in many reactions. Extruded zeolite products have been made in the shape of small cylinders with a variety of binders. In the future, in order to allow zeolite use to extend into more application areas, other forms will be needed. Delivery methods such as zeolite monoliths, foams, and non-woven fabrics containing zeolites, and zeolite membranes are some of the forms that are being actively investigated in order to extend the usefulness of zeolites.



Scheme 3 Comparison of the Raschig and Ammoxidation Reaction

In the economic area, process economics and zeolite economics drive the use of zeolites. Industries that are investigating zeolite technologies are being pressured by regulations to find economical ways to clean up their processes and are also being pressured to find cheaper methods to produce materials to compete with third world countries that do not have the same regulatory pressures. Zeolite economics have become increasingly favorable as techniques to manufacture these materials have improved, resulting in lower costs. The production capabilities of zeolite manufacturing plants have increased, and this expanded capacity has led to reduced costs.

In order to utilize new zeolite materials and to tailor existing materials for new applications in green chemistry, it is important to think “outside of the box” and to look for more new and novel ways to manipulate and utilize this versatile class of materials.

Literature Cited

1. Heck, R.M., Farrauto, R.J., Catalytic Air Pollution Control: Commercial Technology, VanNostrand Reinhold, 1995.
2. Iwamoto, M., Hamada, H., *Catalysis Today*, 10:57-71 (1991).
3. Li, Y., Armor, J. N., USP 5,149,512, “Catalytic reduction of NO_x using methane in the presence of oxygen”, 1992.
4. Engler, B.H., Leyrer, J., Lox, E.S., Ostgathe, K. SAE Paper 930735, “DeNO_x with Metal Zeolites”, Society of Automotive Engineers, Dearborn, MI, 1993.
5. Bellussi, G., et.al., EP 652,040, “Process and catalyst for reducing NO_x in combustion exhaust gas”, 1995.
6. Li, Y., Armor, J. N., USP 5,171,553, “Catalytic decomposition of N₂O”, 1992.
7. Heimrich, M.J., Smith, L.R., Kitowski, J., SAE Paper 920847, “Cold-start Hydrocarbon Collection for Advanced Exhaust Emission Control”, 1992.
8. Patil, M.D., Hertl, W., Williams, J.L., SAE Paper 960343, “Hydrocarbon Adsorber System for Cold Start Emissions”, Society of Automotive Engineers, Dearborn, MI, 1996.
9. Hertl, W., Patil, M.D., Williams, J.L., SAE Paper 960347 “Hydrocarbon Adsorber System”, Society of Automotive Engineers, Dearborn, MI, 1996.
10. Ballinger, T.H., Manning, W.A., Lafyatis, D.S., SAE Paper 970741 “Hydrocarbon Trap technology for the Reduction of Cold-Start Hydrocarbon Emissions”, Society of Automotive Engineers, Dearborn, MI, 1997.
11. Vesely, J.A., Schmerling, L., *Journal of Organic Chemistry*, 35, 4028 (1970).
12. Kharitonov, A.S., et.al., USP 5,672,777, “Catalyst for the production of phenol and its derivatives. 1997.
13. Chemical Week, January 1/8, 1997, page 11; Chemical Week, February 18, 1998, page 37.

14. Taramasso, M., Perego, G., Notari, B., USP 4,410,501, "Preparation of porous crystalline synthetic material comprised of silicon and titanium oxides", 1983.
15. Hensen, K., Mahaim, C., Holderich, W.F., Progress in Zeolite and Microporous Materials, Chon, Ihm, Uh (Editors), *Studies in Surface Science and Catalysis*, Vol 105B, 1133, Elsevier Science, B.V., 1997.

Chapter 14

Catalytic Recovery of Elemental Sulfur from Sulfur Dioxide-Laden Gas Streams

Maria Flytzani-Stephanopoulos and Tianli Zhu

Department of Chemical Engineering, Tufts University,
Medford, MA 02155

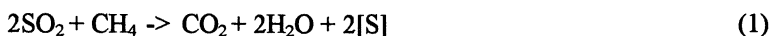
Single-stage catalytic reduction of SO_2 to elemental sulfur is a promising new technology better suited to treat SO_2 -laden streams generated in power plants and certain industries than the conventional multi-stage Claus process. The catalytic reduction of SO_2 to elemental sulfur by CH_4 over ceria and metal-modified ceria was studied in this work at atmospheric pressure and with a feed gas mixture containing a molar ratio of $\text{CH}_4/\text{SO}_2=0.5\text{--}3$. These catalysts are active in the temperature range $550\text{--}750^\circ\text{C}$. At temperatures below $\sim 550^\circ\text{C}$ the catalyst surface is capped by SO_2 . Activation of CH_4 on these surfaces is initiated after sulfate decomposition. The catalyst structure was examined by XRD, STEM/EDS and XPS. The working catalyst surface was partially sulfated even under fuel-rich conditions. CH_4 -TPR and isothermal CH_4 reduction of pre-sulfated catalysts suggest that the reaction light-off coincides with the threshold temperature for sulfate decomposition. The addition of five atomic metal percent (5 at%) of copper into La-doped ceria, $\text{Ce}(\text{La})\text{O}_x$, improved dramatically both the wet activity of the latter as well as its selectivity to elemental sulfur under fuel-rich conditions. Nickel addition, on the other hand, favored the partial oxidation of methane, and decreased the selectivity to sulfur.

Introduction

Sulfur dioxide is a major precursor of acid rain. The commercially applied control technology of sulfur dioxide emission has typically involved conventional flue gas desulfurization (FGD) systems, most of them employing wet scrubbers based on limestone, lime or sodium carbonate. More than 170 wet scrubber systems applied to 72,000 MW of U.S. coal-fired, utility boilers are in operation (1). About 1% of these systems (2) produce a usable byproduct (gypsum); the remainder generate approximately 20 million tons per annum of disposable FGD byproduct which are

transported and disposed of in landfills (3). The use of regenerative sorbent technologies has the potential to reduce or eliminate this solid waste production, transportation and disposal. In a dry regenerative process, SO₂ is first fixed by reaction with a solid oxide substrate, which is subsequently reduced back to the oxide producing a highly-concentrated SO₂-stream during the regeneration step. It is desirable to further process this SO₂-stream to obtain elemental sulfur, sulfuric acid or liquid SO₂. Single-stage catalytic reduction of SO₂ to elemental sulfur is a promising sulfur recovery approach that may also have economic benefits from the sale of sulfur, a safe material to handle, transport and store. The overall process of sulfur dioxide reduction will, accordingly, become more environmentally benign. Its success will accelerate the commercialization of regenerative FGD processes.

An attractive reductant of SO₂ is natural gas, the most environmentally benign of all fossil fuels. SO₂ can be reduced by methane (the major component of natural gas) to produce elemental sulfur. The stoichiometric overall reaction between SO₂ and CH₄ is:



where [S] represents the various elemental sulfur forms (S₂, S₆, S₈). A number of side reactions and intermediate products are, in general, possible in the SO₂ + CH₄ system. By-products, such as H₂S, COS, CS₂, CO and H₂, can be formed under certain conditions. Catalysts previously studied for this reaction include bauxite (4), alumina (5), Fe-Cu-Cr and Cu-Cr-Mn oxides (6), and more recently, transition metal sulfides, WS₂, FeS₂ and MoS₂ (7-10), and Co₃O₄/Al₂O₃ catalyst (11). However, issues of low activity and/or low selectivity to elemental sulfur are present with all these catalysts. The mechanism over the supported Co₃O₄ or MoS₂ catalysts may involve the formation of [S] via intermediate H₂S (9), as indicated by the finding that sulfur yield is maximized at very low space velocity. Effects of water vapor on the catalyst activity/selectivity have been reported only for the aluminum-chromium oxide catalysts (12). The presence of water vapor in the reacting gas mixture increases the production of hydrogen sulfide and thus, lowers the elemental sulfur yield (12).

Ceria-based materials are highly active and stable catalysts for SO₂ reduction to elemental sulfur by CO (13-16). The catalytic activity of ceria and its resistance to impurities, such as water vapor, can be significantly enhanced by addition of a small amount of transition metals, such as Cu, Ni, Co, etc. (13). The redox reaction mechanism was used to explain the catalytic behavior of ceria-based materials in SO₂ reduction by CO. Accordingly, CO creates surface oxygen vacancies that are taken by SO₂, which is thus reduced to elemental sulfur. In the redox mechanism, sulfur is a primary product and very high space velocity can be used without a decrease of the selectivity to sulfur (13-16).

In this paper, we report on the activity/selectivity of ceria-based catalysts for the reduction of SO₂ by CH₄ at the relatively high space velocity of 20,000-40,000 h⁻¹ (STP). The effect of adding a small amount of Cu or Ni on the performance of ceria was examined under both dry and wet reaction conditions.

Experimental

Bulk ceria-based catalysts were prepared by the urea gelation/co-precipitation method using metal nitrates and urea by a procedure described in detail elsewhere (16). The samples used in the SO₂ and CH₄ reaction tests were calcined in air at 720°C for 3h. The resulting surface area was 45-70 m²/g and the bulk density was 1.8-2 g/cm³.

Bulk elemental analysis was performed by Inductively Coupled Plasma (ICP) atomic emission spectrometry (Perkin Elmer Plasma 40). The BET surface area was measured in a Micromeritics Pulse ChemiSorb 2705. X-ray power diffraction (XRD) analysis of catalysts was performed on a Rigaku 300 instrument. Copper Ka1 radiation was used with a power setting of 60kV and 300mA. Tungsten was used as the internal d-spacing standard. The catalyst surface composition was determined by X-ray photoelectron spectroscopy (XPS) on a Perkin Elmer 5100C system. All measurements were carried out at room temperature and without any sample pre-treatment. A Mg Ka X-ray source typically set at 15 kV and 20 mA was used in this work. All binding energies were adjusted relative to C1s at 284.6 eV. The catalyst microstructure was studied in a Vacuum Generators HB 603 Scanning Transmission Electron Microscope (STEM) equipped with a X-ray microprobe of 0.14nm optimum resolution for Energy Dispersive X-ray Spectroscopy (EDS). For STEM analysis, the catalyst powder was dispersed on a nickel or copper grid coated with a carbon film and elemental maps were obtained on a 128×128 data matrix.

Reaction tests were conducted at atmospheric pressure in a packed-bed quartz microreactor (I.D.=10mm). A cold trap at the outlet of the reactor was used to separate and collect the elemental sulfur and water from the product gas stream. The reactants and products were analyzed by an on-line HP5880A gas chromatograph (GC) equipped with a Thermal Conductivity Detector (TCD). A 1/8"O.D.x 6' long Teflon column packed with Porapak QS was used to separate CH₄, CO, CO₂, COS, CS₂, H₂S and SO₂. The following definitions and notations are used in this paper:

Contact time (g·s/cm³) = catalyst weight/inlet gas volumetric flow rate (STP)

$$R = \text{CH}_{4\text{in}}/\text{SO}_{2\text{in}}$$

$$\text{X-SO}_2 = (\text{SO}_{2\text{in}} - \text{SO}_{2\text{out}}) / \text{SO}_{2\text{in}}$$

$$\text{Y-[S]} = \text{Sulfur}_{\text{out}}/\text{SO}_{2\text{in}}$$

$$\text{S} = \text{Y-[S]}/\text{X-SO}_2$$

where CH_{4in} and SO_{2in} are mol percentages of CH₄ and SO₂ in the feed gas, and Sulfur_{out} and SO_{2out} are mol percentages of elemental sulfur and SO₂ in the effluent gas, respectively. Typically, Sulfur_{out} was determined by subtracting the mol percentages of sulfur-containing byproducts, i.e., H₂S, COS or CS₂, in the effluent gas from SO_{2in}-SO_{2out}. H₂S was the major sulfur byproduct. A trace amount of COS or CS₂ was observed only at high temperatures and long contact times. X-SO₂ and Y-[S] are based on a constant molar gas flow rate through the catalyst bed, a plausible assumption for the dilute gas (1-3% SO₂ or CH₄) used here.

For temperature-programmed reduction (TPR) of pre-sulfated catalysts, 150mg of catalyst (720°C-calcined) was loaded into the quartz reactor. The catalyst was pre-sulfated at 400°C for 30min in a 1% SO₂/He gas mixture. After cooling down in the same stream to room temperature and purging with He, TPR was carried out in a 2%

CH₄/He mixture at a heating rate of 10 °C/min to 750°C. The gas flow rate was 50 cm³/min (STP). The effluent gas was analyzed by mass spectrometry (MS) using a quadrupole residual gas analyzer (MKS-model RS-1).

The reducibility of pre-sulfated catalysts at constant temperature was evaluated in a thermogravimetric analyzer (Cahn 121 TGA). A load of (4-5 mg) fresh sample was heated to each temperature in a flow of He and after the weight was stabilized, a 1% SO₂/He gas mixture was switched in for 30 minutes. This was followed by a gas mixture of 4% CH₄/He. A high flow rate, 600cm³/min (STP), was used in these tests to eliminate mass transfer limitations. The isothermal reduction curves are plotted as (1-conversion)×100% vs. time, where conversion is defined as $(\Delta W/\Delta W_s)$, where ΔW is the sample weight loss due to reduction, and ΔW_s is the sample weight gain at the end of sulfation, i.e., the SO₂ uptake.

Results

Ceria and La-doped Ceria

(SO₂+CH₄) reaction light-off curves of the 750°C-calcined CeO₂ and La-doped CeO₂ are shown in Figure 1. The dopant level is expressed in atomic metal percent, as La/(La+Ce)×100%. The reaction light-off temperature was about 600°C with a stoichiometric feed gas composition. Over the 750°C-calcined Ce(4%La)Ox, 87% SO₂ conversion and 75% sulfur yield were measured at 720°C at a contact time of 0.36 g·s/cm³ (STP) (S.V.~20,000 h⁻¹). No hysteresis was found in these tests, i.e., fall-off temperatures were identical to light-off. The unmodified ceria gave similar results (Figure 1). The two used samples had similar surface area (Table I). La-doped ceria was examined because of its reported resistance to sintering (17,18); this can be seen in Table I. In many other tests, we found that there was no significant difference between a La dopant level of 4 and 10 at%. Catalysts with high content of La (>10 at%), which is known to enrich the ceria surface (19), were less active than ceria. Thus, most of the catalysts reported here were doped with ~4 at% La and are denoted as Ce(La)Ox throughout the paper.

As shown in Figure 2, the addition of water vapor in the feed gas greatly affected the performance of Ce(La)Ox. With 5% H₂O addition, the SO₂ conversion was decreased from 100% to about 10% at 675°C at a contact time of 0.18 g·s/cm³ (STP) and R=2. Both the SO₂ conversion and sulfur selectivity of the catalyst were recovered upon removal of the water vapor, implying that H₂O blocked active sites on the catalyst surface without causing any permanent structural change. Thus, the wet catalyst activity increased with temperature. The product distribution was, however, affected by the presence of water vapor, which can participate in side reactions, as will be discussed below.

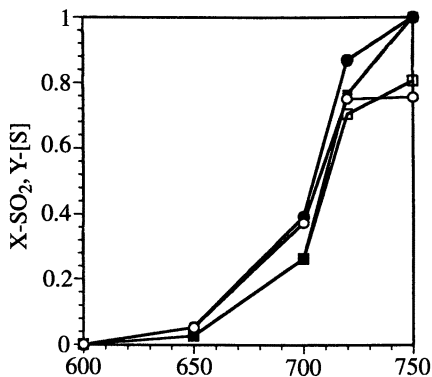


Figure 1. SO_2 conversion and sulfur yield in the SO_2 reduction by CH_4 over CeO_2 and Ce(La)Ox catalysts (750°C -calcined) ($1\%\text{SO}_2$ - $0.5\%\text{CH}_4$ -He, $0.36\text{ g}\cdot\text{s}/\text{cm}^3$ (STP) ($20,000\text{ h}^{-1}$)) (■ □) CeO_2 , (● ○) Ce(4\%La)Ox , filled symbols: X- SO_2 , open symbols: Y-[S]. (Reproduced with permission from reference 26. Copyright 1999 Elsevier Science B.V.)

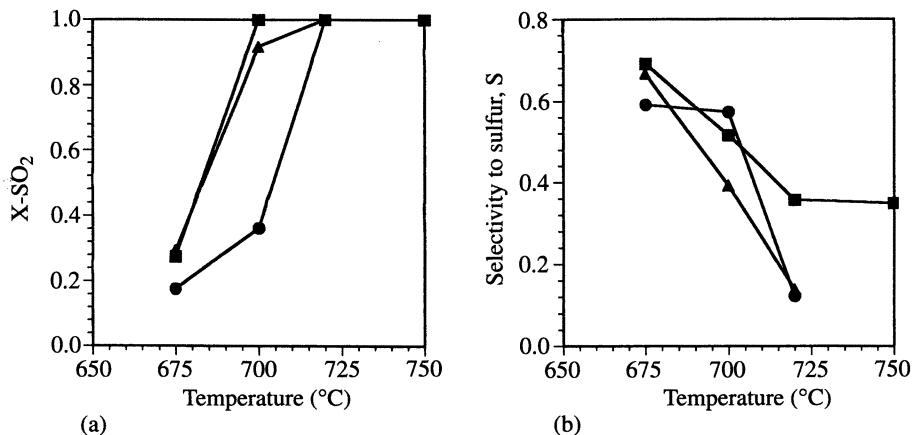


Figure 2. Effect of water on the light-off and sulfur yield of the SO_2 reduction by CH_4 over (●) Ce(La)Ox , (■) $5\%\text{Cu-Ce(La)Ox}$, (▲) $5\%\text{Ni-Ce(La)Ox}$ catalysts (720°C -calcined) ($1\%\text{SO}_2$ - $2\%\text{CH}_4$ - $5\%\text{H}_2\text{O}$ -He, $0.18\text{ g}\cdot\text{s}/\text{cm}^3$ (STP) ($40,000\text{ h}^{-1}$)). (Reproduced with permission from reference 26. Copyright 1999 Elsevier Science B.V.)

Transition Metal-Containing Ceria Catalysts

Addition of 5 at% Ni or Cu in Ce(La)Ox had a negligible effect on the SO₂ conversion under dry conditions, as shown in Figure 3. However, the Cu-modified Ce(La)Ox showed higher selectivity to elemental sulfur under fuel-rich conditions. For example, complete conversion of SO₂ and 83% sulfur yield were obtained at 675°C over 5%Cu-Ce(La)Ox at a feed gas ratio of CH₄/SO₂ = 2, which is four times the stoichiometric value for reaction 1. On the other hand, the selectivity of Ni-modified Ce(La)Ox was a complex function of feed CH₄/SO₂ ratio and temperature, as will be discussed below. The wet activity of Ce(La)Ox was enhanced by the addition of a small amount of Ni or Cu in ceria. As shown in Figure 2, complete conversion of SO₂ in the presence of 5% H₂O was measured at 700°C over the 5% Cu- or 5% Ni-modified Ce(La)Ox. Higher sulfur selectivity was obtained over the 5%Cu-Ce(La)Ox catalyst.

Table I. Physical Properties of Catalysts

Sample	BET surface area ¹ (m ² /g)			Used [#]	CeO ₂ lattice parameter ² α (Å)
	650°C calcined	720°C calcined	750°C calcined		650°C calcined
CeO ₂	75	45	40	28	5.413
Ce(4%La)Ox	90	71	59	33	5.421
Ce(10%La)Ox	106	70	64	37	5.435
Ce(20%La)Ox	120	n.a.	58	34	5.456
5%Cu-Ce(4%La)Ox	89	65	n.a.	22	5.418(5.420*)
5%Ni-Ce(4%La)Ox	98	52	42	30	5.419(5.423*)

1. Measured by single-point N₂ adsorption/desorption.

2. Calculated from the (111) reflections of ceria in XRD analysis.

* Lattice parameters of sample used in 1%SO₂-2%CH₄-He, up to 720°C for a total of 12h.

Used in 1%SO₂-0.5%CH₄-He, up to 720°C for a total of 12h.

n.a. - not available

The 5%Cu-Ce(La)Ox catalyst, which showed the highest SO₂ conversion and selectivity to sulfur in fuel-rich conditions and in the presence of water vapor, was chosen for parametric studies. Figure 4 shows the effect of contact time on the SO₂ conversion and sulfur selectivity of 5%Cu-Ce(La)Ox at R = 0.5. The SO₂ conversion increased with the contact time, while the selectivity to sulfur at the same SO₂ conversion was not affected in the range of 0.36 to 1.08 g-s/cm³ (STP). Also, the selectivity to sulfur remained high (>80%) at all conditions. Similar results were obtained at R = 1.

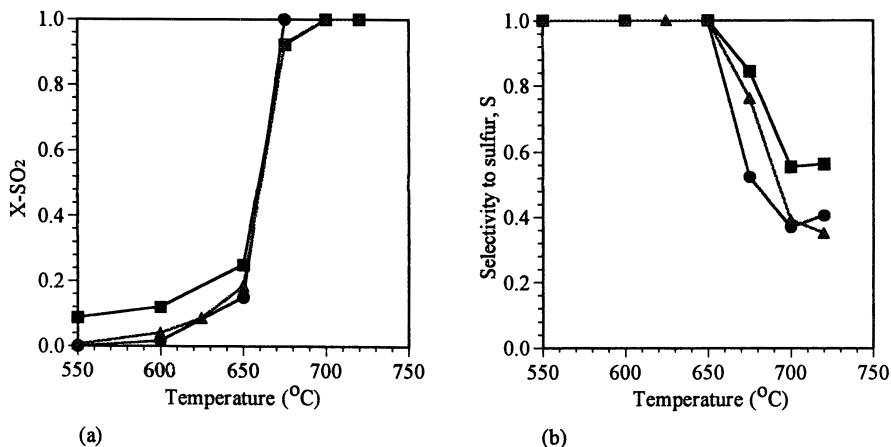


Figure 3. Effect of Cu and Ni addition on the light-off and sulfur selectivity of the SO₂ reduction by CH₄ over ceria-based catalysts (720°C-calcined) (1%SO₂-2%CH₄ He, 0.18 g·s/cm³ (STP) (40,000 h⁻¹)), (●) Ce(La)Ox, (■) 5%Cu-Ce(La)Ox, (▲) 5%Ni-Ce(La)Ox. (Reproduced with permission from reference 26. Copyright 1999 Elsevier Science B.V.)

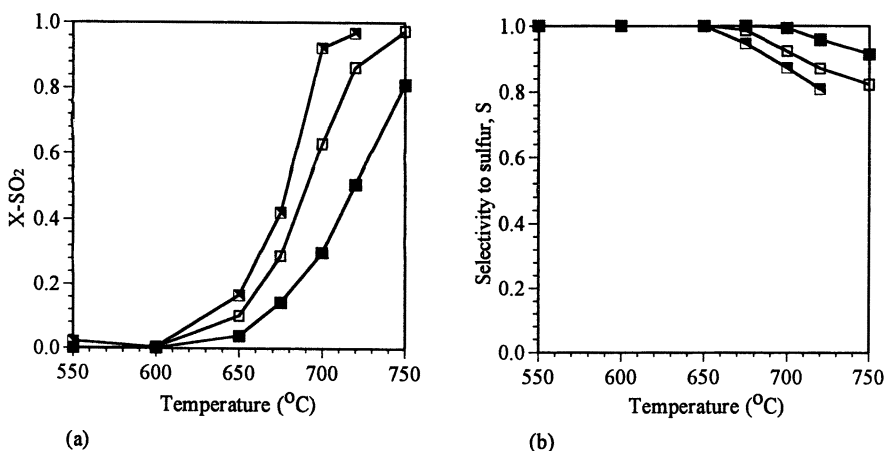


Figure 4. Effect of contact time on the light-off and sulfur selectivity of the SO₂ reduction by CH₄ over 5%Cu-Ce(La)Ox (720°C-calcined) (■) 0.36 g·s/cm³ (STP), (□) 0.72 g·s/cm³ (STP), (▣) 1.08 g·s/cm³ (STP) (1%SO₂-0.5%CH₄-He). (Reproduced with permission from reference 26. Copyright 1999 Elsevier Science B.V.)

The effect of the feed CH_4/SO_2 ratio on the SO_2 conversion and sulfur selectivity is illustrated in Figure 5 for the 5%Cu-Ce(La)Ox catalyst. The higher this ratio, the higher the SO_2 conversion and the lower the catalyst selectivity to elemental sulfur, even though no drop of selectivity was observed below 650°C . We attempted to use excess methane to further lower the reaction temperature. However, the light-off temperature could not be lowered below 550°C even at $R = 3$. Moreover, undesirable CO as well as H_2S were detected in the product gases above 650°C when the value of R exceeded unity.

Catalyst Characterization

For CeO_2 and La-doped CeO_2 with La in the range of 4 to 20 at %, only the cubic fluorite oxide-type structure was identified by XRD. No separate La_2O_3 phase was observed. However, the CeO_2 reflections shifted to lower 2θ angles at higher La levels. The lattice parameter of CeO_2 calculated from the (111) reflections is shown in Table I. The gradually increasing value of the lattice parameter of CeO_2 with La dopant content suggests oxide solid solution formation (20,21).

Only the fluorite oxide-type structure was identified on the as prepared 5%Cu-Ce(La)Ox and 5%Ni-Ce(La)Ox samples, as shown in Figure 6. No separate CuO or NiO phases are discernible by XRD. However, in previous studies of Cu-Ce(La)Ox catalysts, Liu and Flytzani-Stephanopoulos (14,19,22) have shown that at low Cu content (<10 at%), copper oxide was present in ceria, but, in highly dispersed nanoparticle form (<5nm); hence, it was not detected by XRD. Similar observations were made for Ni-Ce(La)Ox. STEM/EDS elemental mapping of the as prepared 5%Ni-Ce(La)Ox identified nickel oxide clusters well dispersed on the CeO_2 surface. At higher metal content (>15 at% Cu or 5 wt% Ni), bulk CuO and NiO particles were identified by both XRD and STEM/EDS (13,14,23,24). Values for the ceria lattice parameter obtained from the XRD reflections of Cu-, Ni-Ce(La)Ox catalysts are also shown in Table I. These values are close to the lattice parameter of Ce(La)Ox, within experimental error. Therefore, no oxide solid solution formation of Ni or Cu with CeO_2 is indicated by the XRD analysis.

After exposure to the $\text{SO}_2 + \text{CH}_4$ reaction gas mixture, CuO or NiO reflections were still absent from the XRD patterns of used 5% Cu- or 5% Ni-Ce(La)Ox samples. Only the fluorite oxide-type structure of ceria was present on the used samples, as shown in Figure 6. The lattice parameter of CeO_2 remained constant during reaction (Table I). STEM/EDS verified that the Cu or Ni phase remained highly dispersed in the used catalysts. STEM/EDS of used Ni-Ce(La)Ox is shown in Figure 7. Sulfur was found on the used samples, associated with both ceria and nickel oxide. The existence of sulfur was confirmed by electron-excited X-ray emission spectra. Selected samples were further analyzed by XPS. Figure 8 shows the O1s and S2p XP spectra of fresh (720°C calcined) and used samples (in a fuel-rich gas mixture up to 720°C for 12h). Two O1s peaks were found in the XP spectra of the used catalysts. The high binding energy peak at $\sim 531.8\text{eV}$ can be assigned to sulfate or carbonate, while the low binding energy peak at $\sim 529.4\text{eV}$ is assigned to metal oxide (25). The S2p XP spectra show a peak at $\sim 168.3\text{eV}$, assigned to metal sulfate (14). No surface metal sulfide

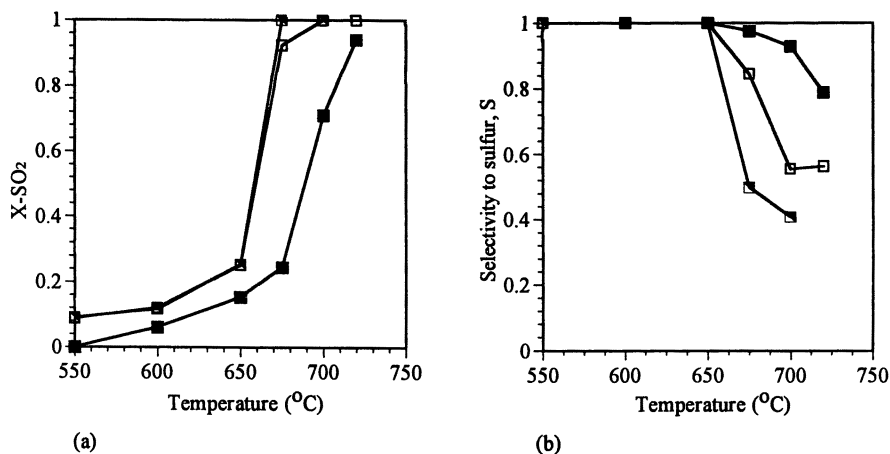


Figure 5. Effect of the CH_4/SO_2 ratio, R , on the light-off and sulfur selectivity of the SO_2 reduction by CH_4 over $5\% \text{Cu-Ce(La)Ox}$ (720°C-calcined), (■) $R=1$, (□) $R=2$, (○) $R=3$ (1% SO_2 , 0.18 g·s/cm³ (STP) (40,000 h⁻¹)). (Reproduced with permission from reference 26. Copyright 1999 Elsevier Science B.V.)

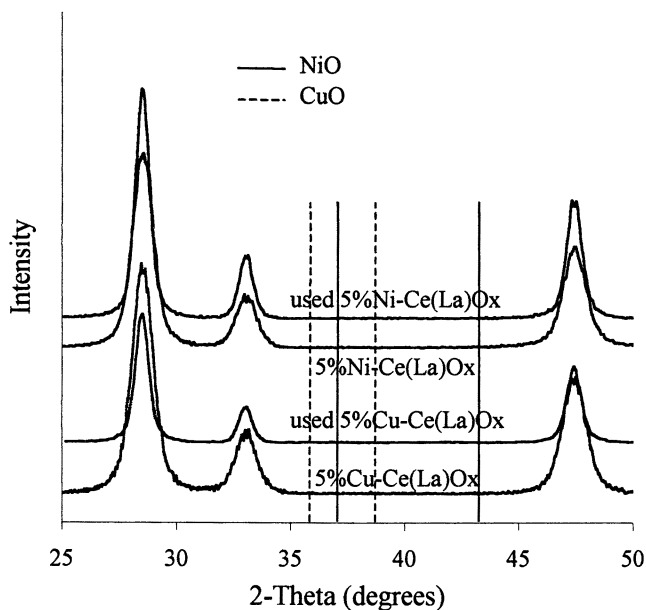


Figure 6. XRD patterns of metal-modified ceria before and after 12 h use in 1% SO_2 -2% CH_4 -He up to 720°C; reflections shown are for CeO_2 . (Reproduced with permission from reference 26. Copyright 1999 Elsevier Science B.V.)

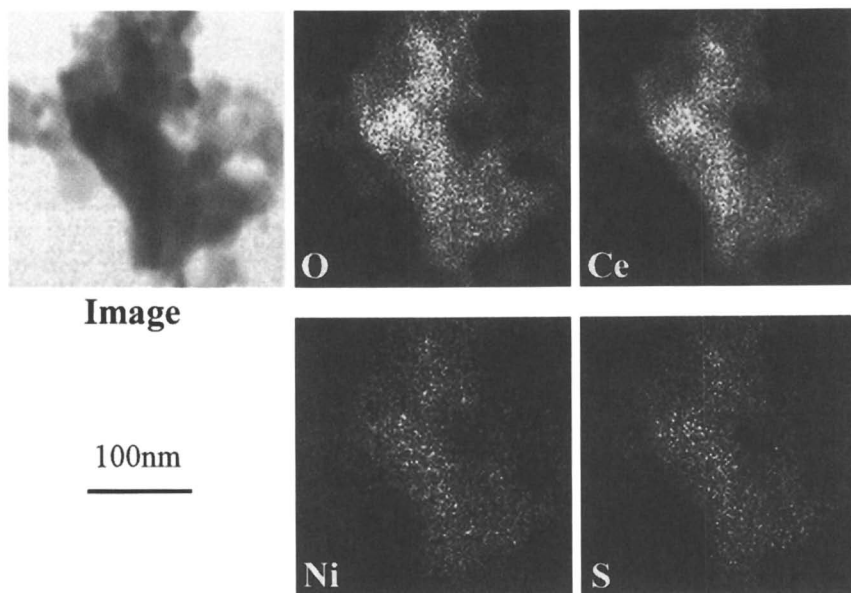


Figure 7. STEM/EDS elemental mapping of used 5%Ni-Ce(La)Ox in 1%SO₂-2%CH₄-He up to 720°C for a total of 12 h.

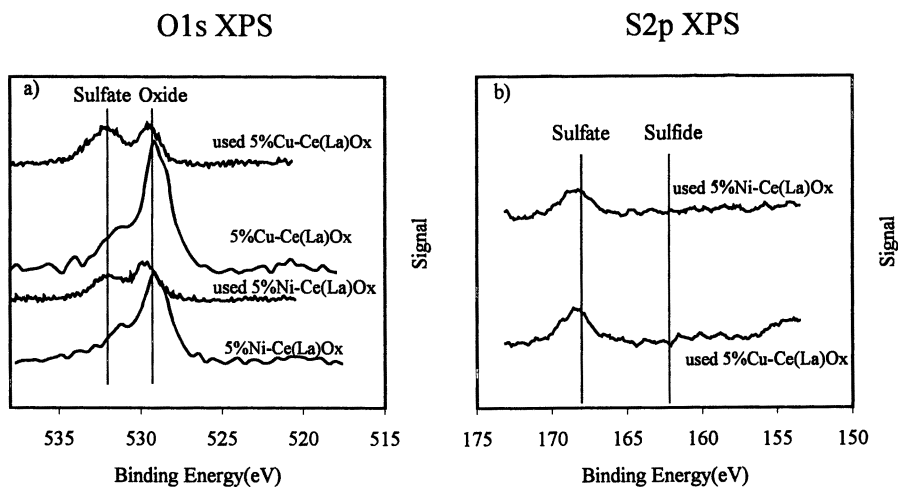


Figure 8. XP spectra of (a) O1s and (b) S 2p of 5%Cu-Ce(La)Ox and 5%Ni-Ce(La)Ox catalysts; fresh (after 720°C-calcined), used (in 1%SO₂-2%CH₄-He up to 720°C for a total of 12 h).

was observed by XPS. A similar observation was made for 2%Cu-Ce(La)Ox used in the SO₂+CO reaction, while metal sulfide was present on 15%Cu-Ce(La)Ox after the same reaction (13,14). Therefore, in a working catalyst, some cerium is present as sulfate, while bulk metal oxides form sulfide species. However, nickel or copper oxide clusters may remain sulfur-free during the SO₂ reduction by CH₄ or CO.

Reduction of Pre-sulfated Catalysts by CH₄

The working catalyst surface is only partially sulfated during the SO₂-CH₄ reaction, as indicated by the XPS and STEM/EDS analyses, while the deactivated catalyst is fully sulfated (14). Studying the reducibility of pre-sulfated catalysts has, thus, an important scope for elucidating the SO₂ reduction by CH₄. CH₄-TPR experiments of pre-sulfated catalysts were carried out in the reactor with on-line analysis of the product gases by mass spectrometry.

Figure 9a shows the results of CH₄-TPR of pre-sulfated Ce(La)Ox catalyst. Oxygen started to desorb at 600°C before the elution of SO₂. This oxygen desorption was also observed in He-TPD of pre-sulfated Ce(La)Ox, as shown in Figure 9d. However, this was not observed in CH₄-TPR experiments of fresh catalysts. Therefore, it is attributed to the decomposition of sulfate species. The decrease of the methane signal (*m/e* = 15) began at the same time as the O₂ elution at 600°C. Similar results were obtained in CH₄-TPR and He-TPD experiments of the pre-sulfated Ce(La)Ox material carried out in the TGA, i.e., the catalyst weight started to decrease at the same temperature. During CH₄-TPR, incomplete combustion products, H₂ and CO, began to evolve at 680°C (Figure 9a). At the same time, the signal from CO₂ and H₂O began to decrease in the temperature range 680°-720°C.

The CH₄-TPR profiles of pre-sulfated catalysts were different for the metal-modified ceria materials, as shown in Figure 9b-c. The desorption temperatures of O₂ and SO₂ as well as the elution temperature of CO₂ were lower for 5%Ni-Ce(La)Ox (Figure 9c) than for Ce(La)Ox (Figure 9a), suggesting an increase of the reducibility of the pre-sulfated material in the presence of nickel. However, there was no significant shift in the temperature of H₂ and CO elution from that of Ce(La)Ox. On the other hand, the evolution of H₂ and CO over 5%Cu-Ce(La)Ox was shifted to higher temperature (Figure 9b), suggesting suppression of the partial oxidation of methane by the addition of copper.

The same catalyst compositions were also tested in isothermal reduction by CH₄ after pre-sulfation at each temperature for 30min. The reduction of pre-sulfated 5%Cu-Ce(La)Ox by CO or CH₄ at 550°C is shown in Figure 10 along with thermal decomposition in He. The reduction curve in CH₄ has the same initial slope as the decomposition in He, although the former showed a much higher reduction extent after 300s. On the other hand, the reduction in CO is a much faster process, showing a higher slope throughout the reduction period. The initial rate of reduction is similar for pre-sulfated Ce(La)Ox and Cu- or Ni-containing Ce(La)Ox catalysts in the temperature range of 500°-700°C (24). An activation energy of 143±5 kJ/mol was measured, the same for all three catalysts. Thus, it appears that the key step in the

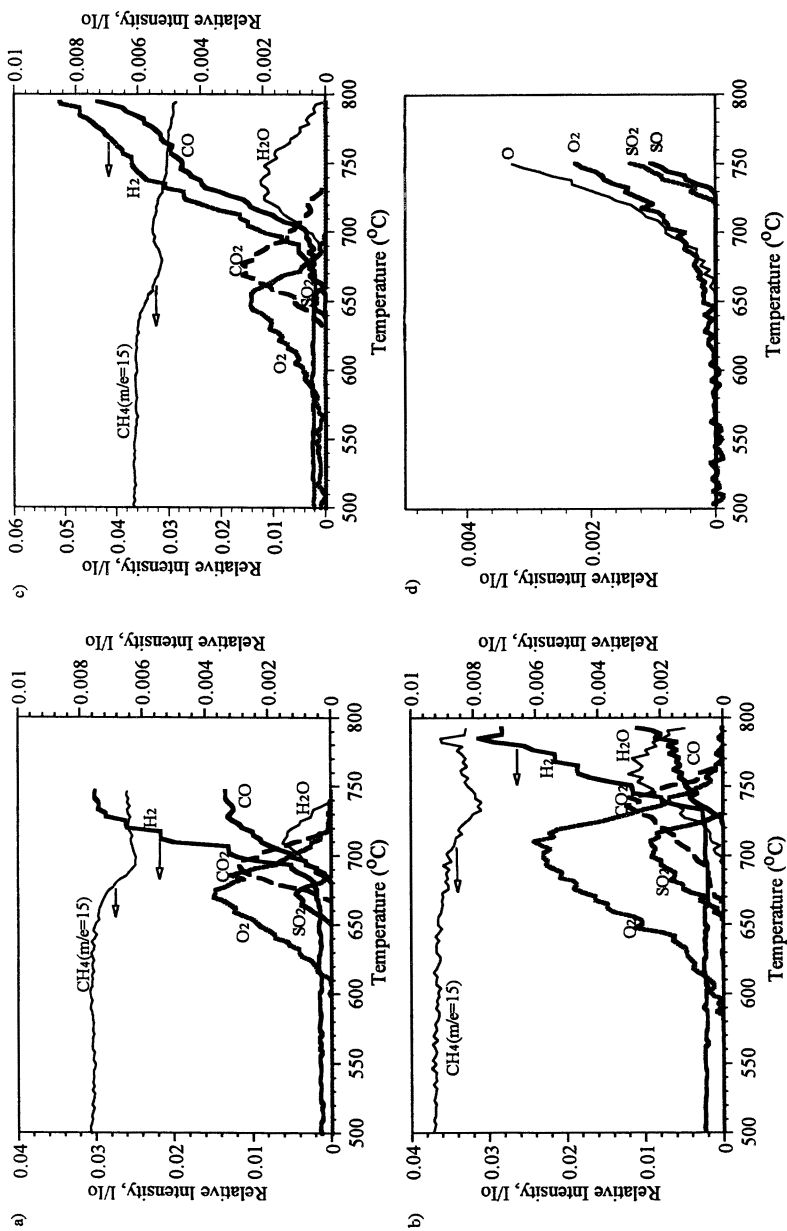


Figure 9. TPR profiles (reactor/MS) of pre-sulfated catalysts in 2%CH₄/He, (a) Ce(la)Ox, (b) 5%Cu-Ce(La)Ox, (c) 5%Ni-Ce(La)Ox, (d) He-TPD of pre-sulfated Ce(La)Ox, all catalysts pre-sulfated with 1%SO₂/He at 400°C for 30 min (10°C/min, 150 mg, 50 cm³/min(STP)). (Reproduced with permission from reference 26. Copyright 1999 Elsevier Science B.V.)

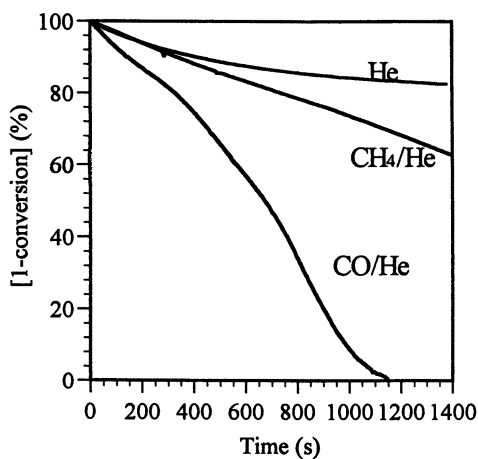


Figure 10. Reduction/decomposition of pre-sulfated (400°C, 30 min in 1% SO₂/He) 5%Cu-Ce(La)Ox at 550°C. Reduction with 4%CH₄/He or 2%CO/He (600 cm³/min(STP)), decomposition in He (600 cm³/min(STP)), both in the TGA. (Reproduced with permission from reference 26. Copyright 1999, Elsevier Science B.V.)

reaction between CH_4 and pre-sulfated ceria catalysts is the thermal decomposition of the sulfate.

Discussion

$\text{Ce}(\text{La})\text{Ox}$ and Cu- or Ni-containing $\text{Ce}(\text{La})\text{Ox}$ materials have similar dry-gas activity in CH_4 - SO_2 -He mixtures, as shown in Figure 1 and 3, and reported elsewhere (26). Thus, the light-off temperature in the reaction gas mixture is approximately the same for all three types of catalysts, as is the temperature at high SO_2 conversion. Metal addition at ~ 5 at% does not affect the light-off performance of ceria. This is contrasted with the reduction of SO_2 by CO, where addition of the same amount of these metals in $\text{Ce}(\text{La})\text{Ox}$ has a measurable shift of the light-off temperature to lower values (13-16).

The working catalyst surface is partially sulfated in both the $\text{CO} + \text{SO}_2$ and the $\text{CH}_4 + \text{SO}_2$ reaction mixtures. This was identified by XPS and STEM/EDS for Cu-Ce(La)Ox (13-15) in the $\text{CO} + \text{SO}_2$ reaction system, and again in this work for Ni-Ce(La)Ox (Figure 7-8) in the $\text{CH}_4 + \text{SO}_2$ reaction system. Thus, a partially sulfated catalyst surface is active for the reduction of SO_2 by CO or CH_4 . A completely sulfated surface is inactive for either reaction (13-16,26). However, the onset of reduction of pre-sulfated catalysts by CO is at a lower temperature than that by methane. For the Cu-Ce(La)Ox catalyst, the threshold temperature for sulfate reduction is $\sim 400^\circ\text{C}$ in CO/He (16) and $\sim 500^\circ\text{C}$ in CH_4/He gas mixtures. The rate of sulfate reduction in CO is higher than that of methane, as shown in Figure 10 at 550°C . The initial reduction in the CH_4/He gas is the same as the thermal decomposition of the sulfated Cu-Ce(La)Ox surface at 550°C . Once the surface is partially oxidized, however, reduction in $\text{CH}_4 + \text{He}$ is faster than the thermal decomposition (Figure 10). These results are used to explain the limit of $\sim 550^\circ\text{C}$ for the light-off temperature of the $\text{SO}_2 + \text{CH}_4$ reaction over the ceria-based catalysts used in this work. Activation of CH_4 does not occur over a fully sulfated surface.

The initial reduction rate measurements also indicate that sulfate reduction is not sensitive to the presence of Cu or Ni on the ceria surface. The CH_4 -TPR data in Figure 9 corroborate these findings. Thus, consumption of methane began upon decomposition of the sulfate at $\sim 600^\circ\text{C}$, as indicated by oxygen elution at the same temperature. There is a difference of $\sim 50^\circ\text{C}$ between the onset of sulfate reduction in the reactor system (Figure 9, TPR conditions) and the TGA (isothermal reduction, as in Figure 10 and other work (24)), which may be due to an activation time lag.

Ceria can react with SO_2 over a wide temperature range with or without O_2 to form surface or bulk sulfates (27,28). Also, NiO and CuO can form bulk sulfates in the presence of SO_2 and O_2 at 380°C and 325°C , respectively (29). Although there is no O_2 present in the $\text{CH}_4 + \text{SO}_2$ reaction gas mixture, stable surface sulfates of Ni and Cu may still be formed, as SO_2 adsorbs on these oxides at low temperature (29). In separate experiments, formation of stable sulfate species has been confirmed on ceria and metal-modified ceria at $T < 550^\circ\text{C}$ after the introduction of SO_2 (16,24,26). The addition of copper enhanced the adsorption of SO_2 on ceria (24). Therefore, at low temperatures, stable metal sulfates on the catalyst surface prevent the activation of

methane. This explains the negligible effect of Cu and Ni addition on the light-off temperature of Ce(La)Ox.

However, the addition of Cu or Ni was found to have appreciable effect on the selectivity of Ce(La)Ox to elemental sulfur at fuel-rich conditions, and also in wet gas mixtures ($\text{CH}_4 + \text{SO}_2 + \text{H}_2\text{O}$), as can be seen in Figures 2, 3. This is attributed to secondary reactions catalyzed by the presence of these metals/metal oxides. As shown in Figure 6 and Table I, no oxide solid solution of either metal with ceria is evident by XRD. STEM/EDS, on the other hand, has identified the presence of copper or nickel-rich cluster/particles dispersed in the Ce(La)Ox matrix (14,19,22,24). These are shown in Figure 7 for used Ni-Ce(La)Ox. These nanoparticles are too fine to be detected by XRD, which only shows CeO_2 reflections in Figure 6.

What is then the role of these metal/metal oxide clusters in the working catalyst, and how do they change the selectivity of ceria under fuel-rich conditions (Figure 3) or the activity/selectivity of ceria in wet reaction gas mixtures (Figure 2)? In the absence of SO_2 , ceria-based catalysts are active for deep oxidation of methane (14,17). Kundakovic, et al. (17,30) recently reported that Cu or Ag-modified ceria is very active for deep oxidation of methane with a light-off temperature of $\sim 300^\circ\text{C}$ as compared to $\sim 450^\circ\text{C}$ for the unmodified ceria. Even under fuel-rich conditions, the Cu- CeO_2 catalyst did not catalyze the partial oxidation of methane (to syngas). This is not the case for Ni-Ce(La)Ox. As reported elsewhere, this material catalyzes the partial oxidation of methane to synthesis gas (26) at a temperature (550°C) where both Ce(La)Ox and Cu-Ce(La)Ox have negligible activity for this reaction.

Otsuka and co-workers (31,32) have reported the direct conversion of methane into syngas with $\text{H}_2/\text{CO} = 2$ using CeO_2 at $600\text{--}800^\circ\text{C}$. The reduced ceria surface was suggested to be active for partial oxidation of methane. In the present study, CO was detected in the product gases under fuel-rich conditions ($R > 0.5$) of SO_2 reduction by CH_4 (24). The CH_4 -TPR experiments also confirmed the production of CO and H_2 on pre-sulfated catalysts (Figure 9). Over the fresh materials, production of hydrogen and carbon monoxide was observed at lower temperature (24). Apparently, methane was consumed to produce CO and H_2 at high temperatures. This can explain the low sulfur yield at high temperature, since the H_2 produced would further react with surface sulfur to form H_2S . Finally, both Cu- and Ni- modified ceria are very good catalysts for the $\text{CO} + \text{SO}_2$ reaction to elemental sulfur (13-15).

These findings were used to elucidate the different activity/selectivity of the Cu- and Ni-Ce(La)Ox catalysts for the $\text{SO}_2 + \text{CH}_4$ reaction in the presence and absence of water vapor. While a large number of reactions may be written for the $\text{SO}_2 + \text{CH}_4$ reaction system, the above results suggest the following two overall reactions:



COS and CS_2 may be also formed through various reactions, but they are rapidly hydrolyzed to H_2S (14). This is indicated by the trace amounts of CS_2 or COS observed here, and only at high temperatures and long contact times. No formation of H_2S , COS, or CS_2 was observed in low SO_2 -conversion ($\sim 10\%$) experiments over the whole temperature range and with $\text{CH}_4/\text{SO}_2 = 0.5\text{--}1.5$. Furthermore, 5%Cu-Ce(La)Ox

had the same sulfur selectivity at different temperatures, but at fixed SO₂ conversion level (Figure 4). Thus, elemental sulfur is a primary product of reaction 1 and not a result of secondary reactions of H₂S (or COS) intermediates. Similar observations were made in the SO₂ reduction by CO over this type of catalyst (14,15). The redox reaction mechanism can be invoked to explain these findings.

From the results of the present work, it appears that the addition of Cu into Ce(La)Ox catalyzes reaction 1 rather than reaction 2, thus, improving the sulfur yield. On the other hand, Ni-Ce(La)Ox materials may be more active for reaction 2 than Ce(La)Ox. The partial oxidation of methane on Ni-Ce(La)Ox may be suppressed in the presence of SO₂ at low temperature. However, at high temperature, the partial oxidation of methane will take place preferentially on the Ni-Ce(La)Ox surface.

H₂O has been reported to inhibit the methane adsorption on the ceria surface (33) and it can, thus, change the catalyst activity/selectivity. Water vapor may participate in other reactions catalyzed by some ceria-based materials. For example, steam reforming of methane occurs readily on Ni-Ce(La)Ox (16) but not on Ce(La)Ox or the Cu-Ce(La)Ox catalysts. While negligible activity was observed over Ce(La)Ox and 5%Cu-Ce(La)Ox, Ni-Ce(La)Ox is a very active catalyst for steam reforming of methane (16). The H₂ and CO produced from steam reforming may further react with elemental sulfur or SO₂, and thus change the product gas distribution. No effect of the presence of H₂O on the SO₂ adsorption by 5%Cu-Ce(La)Ox has been found (24).

Overall, the activity of ceria for the SO₂ reduction by CH₄ under wet conditions is enhanced by the addition of Cu and Ni. However, the presence of nickel is deemed undesirable in view of its high activity for steam reforming of methane, and the resulting very low selectivity to elemental sulfur. On the other hand, the addition of copper enhances both the activity and the sulfur selectivity of Ce(La)Ox under wet gas reaction conditions. Copper does not catalyze the steam reforming of methane. Accordingly, the sulfur selectivity of 5%Cu-Ce(La)Ox under wet conditions (Figure 2) is very close to that under the corresponding dry conditions (Figure 3). Further efforts to develop the Cu-Ce(La)Ox catalyst for elemental sulfur recovery from SO₂-laden streams are warranted on the basis of these findings.

Conclusion

Ceria-based materials are active catalysts for the SO₂ reduction by CH₄ at temperatures above 550°C. SO₂ capping of the surface inhibits methane activation at temperatures below 550°C. The reaction between SO₂ and CH₄ begins on a partially reduced sulfated catalyst. Thus, the light-off temperature of ceria-based catalysts depends on the thermal stability of the sulfates.

The addition of the transition metals nickel and copper has a different effect on the sulfur selectivity of ceria under fuel-rich conditions, through catalyzing different pathways of methane activation. Copper catalyzes the deep oxidation of methane by SO₂, which leads to elemental sulfur production. In contrast, nickel provides sites for methane dissociation at high temperature and gives low yields of elemental sulfur under fuel-rich conditions. In the presence of water, unmodified ceria is a poor catalyst. The incorporation of 5at% Cu or Ni enhances the activity and sulfur yield of

the catalyst. The 5%Cu-Ce(La)Ox has better sulfur selectivity than 5%Ni-Ce(La)Ox. The Cu-modified ceria is, therefore, a preferred catalyst under both dry and wet conditions. Further work will focus on composition optimization of this type catalyst for SO₂ reduction to sulfur in industrial applications.

Acknowledgement

This work was partially supported by the U.S. Department of Energy under Contract No. DE-AC-95PC95252 to Arthur D. Little, Inc., and a subcontract to Tufts University.

Literature Cited

1. *Steam Electric Plant Factors*; 1992 Edition, National Coal Association.
2. Henzel, D.S., and Ellison, W. *Commercial Utilization of SO₂ Removal Wastes in the Application of New Advanced Control Technology*; Proceed. 1990 SO₂ Control Symposium; Vol 1, 3B-27.
3. Tyson, S. *Guidance for Coal Ash Use: Codes and Standards Activities for High Volume Applications*; Proceed. of the 9th Ann. Intern. Pittsburgh Coal Conference, Oct. 1992.
4. Helstrom, J.J. and Atwood, G.A. *Ind. Eng. Chem. Process Des. Dev.* 1978, 17, 114-117.
5. Sarlis, J. and Berk, D. *Ind. Eng. Chem. Res.* 1988, 27, 1951-1954.
6. Nekrich, E.M.; Kontsevaya, A.N and Ganzha, G.F. *J. of Appl. Chem. of U.S.S.R.* 1978, 51, 517-520.
7. Mulligan, D.J. and Berk, D. *Ind. Eng. Chem. Res.* 1989, 28, 926-931.
8. Mulligan, D.J. and Berk, D. *Ind. Eng. Chem. Res.* 1992, 31, 119-125.
9. Sarlis, J. and Berk, D. *Chem. Eng. Comm.* 1996, 140, 73-85.
10. Wiltowski, T.S.; Sangster, K. and O'Brien, W.S. *J. Chem. Tech. Biotech.* 1996, 7, 204-212.
11. Yu, J.J.; Yu, Q.; Jin, Y. and Chang, S.G. *Ind. Eng. Chem. Res.* 1997, 36, 2128-2133.
12. Akhmedov, M.M.; Shakhtakhtinskii, G.B.; Agaev, A.I. and Gezalov, S.S. *Zhurnal Prikladnoi Khimii* 1986, 59, 504-508.
13. Liu, W.; Sarofim, A. F. and Flytzani-Stephanopoulos, M. *Appl. Catal. B: Environ.* 1994, 4, 167-186.
14. Liu, W. Sc. D. thesis, Massachusetts Institute of Technology, Cambridge, Massachusetts, 1995.
15. Liu, W.; Wadia, C. and Flytzani-Stephanopoulos, M. *Catal. Today* 1996, 28, 391-403.
16. Zhu, T; Kundakovic, Lj. and Flytzani-Stephanopoulos, M. *Catal. Today* 1999, 50, 381-397.
17. Kundakovic, Lj. and Flytzani-Stephanopoulos, M. *Appl. Catal. A: General* 1998, 171, 13-29.

18. Pijolat, M.; Prin, M.; and Soustelle, M. *Solid State Ionics*, 1993, 63-65, 781-785.
19. Liu, W. and Flytzani-Stephanopoulos, M. *J. Catal.* 1995, 153, 304-316.
20. Hong, S.J. and Virkar, A.V. *J. Am. Ceram. Soc.* 1995, 78(2), 433-439.
21. Bernal, S.; Blanco, G.; Cifredo, G.; Perez-omil, J.A.; Pintado, J.M. and Rodriguez-Izquierdo, J.M. *J. Alloys and Compounds* 1997, 250, 449-454.
22. Liu, W. and Flytzani-Stephanopoulos, M. *J. Catal.* 1995, 153, 317-332.
23. Li, Y. M.S. thesis, Tufts University, Medford, Massachusetts, 1999.
24. Zhu, T. Ph.D. thesis, Tufts University, Medford, Massachusetts, in progress.
25. Wagner, C.D.; Rigg, W.M.; Davis, L.E.; Moulder, J.F. and Muilenberg, G.E. *Handbook of X-ray Photoelectron Spectroscopy*, Perkin-Elmer, 1978.
26. Zhu, T. and Flytzani-Stephanopoulos, M. *Appl. Catal. B: Environ.* 1999, 21, 103-120.
27. Lundgren, S.; Spiess, G.; Hjortsberg, O.; Jobson, E.; Gottberg, I. and Smedler, G. *Stud. in Surf. Sci. and Catal.* 1995, 96, 763-774.
28. Waqif, M.; Bazin, P.; Saur, O.; Lavalley, J.C.; Blanchard, G. and Touret, O. *Appl. Catal. B: Environ.* 1997, 11, 193-205.
29. Deberry, D.W. and Sladek, K. J. *The Canad. J. Chem. Eng.* 1971, 49, 781-785.
30. Kundakovic, Lj. and Flytzani-Stephanopoulos, M. *J. Catal.* 1998, 179, 203-221.
31. Otsuka, K.; Ushiyama, T. and Yamanaka, I. *Chem. Lett.* 1993, 1517-1520.
32. Otsuka, K.; Sunada, E.; Ushiyama, T. and Yamanaka, I. *Stud. in Surf. Sci. and Catal.* 1997, 107, 531-536.
33. Li, C. and Xin, Q. *J. Phys. Chem.* 1992, 96, 7714-7718.

Chapter 15

Kinetics for the Hydrodechlorination of Chlorofluorocarbons over Model Palladium Catalysts

Fabio H. Ribeiro^{1,3} and Gabor A. Somorjai²

¹Department of Chemical Engineering, Worcester Polytechnic Institute, Worcester, MA 01609-2280

²Department of Chemistry, University of California at Berkeley, Berkeley, CA 94720

The kinetics for the hydrodechlorination reaction of 2-chloro-1,1,1,2-tetrafluoroethane (CF₃-CFCIH), 1,1-dichlorotetrafluoroethane (CF₃-CFCI₂), and 1,1,1-trichloro-2,2,2-trifluoroethane (CF₃-CCl₃) are reported on three model catalysts: a palladium foil and two Pd single crystals of (111) and (100) orientation. The turnover rates for the hydrodechlorination of 1,1-dichlorotetrafluoroethane were similar for the three model catalysts tested, suggesting that the reaction is not sensitive to the structure of the catalyst. However, the turnover rates for hydrodechlorination of the three compounds tested are very dependent on the structure of the reactant, spanning a range of seven orders of magnitude. The experimentally determined reaction orders for the main products are about 1 in the reactant, 0.5 in H₂ and -1 in HCl. The derived reaction steps based on these orders consist of the adsorption of the chlorofluorocarbon (rate determining step) and equilibrated steps between gas phase H₂, gas phase HCl and adsorbed hydrogen and chlorine atoms. This chemistry is important in the manufacture of many new compounds that use hydrodechlorination as an intermediate step.

³Corresponding author (fabio@wpi.edu)

Introduction

Hydrodechlorination involves the substitution of a chlorine by a hydrogen in a chloro-containing organic compound. The reaction is carried out in the presence of H_2 and a catalyst, with the production of HCl. The catalytic chemistry related to the understanding of hydrodechlorination has not followed the pace of other areas in catalysis. The main reason is that there appears to have been no economic stimulus for the study of the catalytic chemistry of these compounds. This situation has changed greatly in the past few years with the realization that the ubiquitous chlorofluorocarbons, some produced in millions of pounds per year, can be very damaging to the environment (1).

Heterogeneous catalysis can be used to alleviate the problem of pollution by chloro-containing compounds in two ways: (1) synthesis of new environmentally friendly compounds or (2) the transformation of undesired compounds into desirable or easier to dispose of compounds. As an example of the first application, the new substitutes for chlorofluorocarbon refrigerants contain no chlorine (for example, CF_3-CFH_2) but one of the methods of preparing new refrigerants still use chlorine containing molecules as intermediates (CF_3-CFCl_2), which are removed in a hydrodechlorination step. In fact, chlorine-containing molecules are very common intermediates in many syntheses, the chlorine being eventually removed by a hydrodechlorination step (2). The second application of hydrodechlorination is the conversion of a waste compound into a non-environmentally damaging compound or to other useful compounds. For example, Makkee and co-workers (3) presented an industrial process for the conversion of recovered CF_2Cl_2 (a banned refrigerant) into CF_2H_2 and Harley *et al.* (4) presented a process to convert waste 1,2-dichloropropane into propylene. Hydrodechlorination can be carried out over noble metals, with palladium showing the best selectivity in most applications. The objective of this work is to study the kinetics of hydrodechlorination on model catalysts so that more efficient processes for the manufacture and destruction of chlorofluorocarbons may be achieved.

Reviews of the catalytic chemistry involved in chlorofluorocarbon synthesis in general (5) and also in hydrofluorocarbon synthesis (6) are available. The literature available on hydrodechlorination of chlorofluorocarbons is still very limited with most of the papers dealing with the hydrodechlorination of chlorocarbons. Some of the papers are on metal films (7-10), but most of the literature deals with metal-supported catalysts (e.g., (11-30)). There are also numerous papers on aqueous systems (e.g. (31-33)), but these cases are not covered here.

In addition to the lack of papers that report on the reaction kinetics, the accumulated wisdom for other catalytic reactions does not seem to apply to hydrodechlorination. For example, as is described below, the reactivity of a C-Cl bond is very dependent on the other atoms attached to the carbon and can vary by a factor of 10^7 . The reaction orders for the hydrodechlorination of CF_3-CFCl_2 are also surprising: the reaction order is 1 in CF_3-CFCl_2 , 0.5 in H_2 , and -1 in HCl. Although the strong inhibition by HCl hints to a surface covered by chlorine under reaction

conditions, after the reaction there is no detectable chlorine, fluorine, or carbon on the surface (34,35).

Understanding the reaction selectivity has also been challenging. Because of the number of distinct atoms in the molecule (hydrogen, carbon, fluorine, and chlorine), many more reaction products are possible than with, for example, hydrocarbon reactions. As an example, with $\text{CF}_3\text{-CFCl}_2$ on Pd, the products and selectivity (in parentheses) are $\text{CF}_3\text{-CH}_3$ (5%), $\text{CF}_3\text{-CFHCl}$ (10%), and $\text{CF}_3\text{-CFH}_2$ (85%) independent of the conversion level. Because only one of the products is usually desired, how may the reaction selectivity be controlled? This chemistry presents many questions for research.

In this project, the kinetics of hydrodechlorination of a family of three compounds was studied in detail. The objective was to understand the surface chemistry and find out the reaction kinetics for these compounds. The main finding is that the hydrodechlorination reaction is not sensitive to the structure of the catalysts but is very sensitive to the structure of the molecule undergoing hydrodechlorination.

Experimental Methods

This work is a continuation of the results described in Ribeiro et al. (35) and for this reason the experimental methods will be only briefly described here. The rates on the foil and single crystals were carried out in a high pressure (atmospheric pressure) batch reactor attached to an ultrahigh vacuum (UHV) chamber with a base pressure of 8×10^{-10} Torr (1 Torr = 133 Pa). The chamber had facilities for measurement of low energy electron diffraction (LEED), Auger electron spectroscopy (AES) and temperature programmed desorption (TPD) of CO. The sample was transferred between the UHV chamber and the high pressure reactor using a welded bellows assembly capable of maintaining an UHV environment during sample transfer. The samples were attached to a sample cart containing two pins for resistive heating and two pins (chromel and alumel) for thermocouple temperature readings so the sample could be heated and the temperature measured both in the UHV chamber and in the reactor. The foil was spot-welded directly to the pins, and for the single crystal samples, stainless steel tabs were used to spot-weld the side of the crystal to the pins. The type K thermocouple was spot-welded to the center of the rear of the foil and to the side of the single crystals.

The reactants were mixed with a metal bellows pump (Senior Flexonics - Model MB21) with a flow rate of about 1 L min^{-1} . This flow rate permitted a small conversion per pass. Heat and mass transfer limitations are of no concern in this type of experiment since all the active surface area is exposed.

The Pd polycrystalline foil used in this study was 0.1 mm thick, had a total surface area of about 0.5 cm^2 , and had a purity of 99.99% (Johnson Matthey). The single crystals were about 1 mm thick, had a surface area of 0.5 to 0.8 cm^2 , and were cut from bulk material (single crystal rods, Goodfellow) with 0.5° precision and polished with standard techniques. Due to the sample cart design, only one side of the

samples could be cleaned by Ar sputtering. The samples were cleaned by cycles of Ar sputtering at 1000 K and 5×10^{-5} Torr, and annealing at 1000 K until no foreign peaks were found by Auger electron spectroscopy (AES). The LEED pattern of each single crystal, was also examined before reaction to verify its structure. After each reaction, Ar sputtering for 15 min followed by annealing at 1000 K was sufficient, as shown by AES, to clean the surface.

After the sample was transferred into the reactor, it was heated to 373 K and then H_2 was introduced followed by CFC 114a and Ar (make-up gas) to achieve 770 Torr total pressure. The sample was heated to 373 K before the introduction of reactants because previous experience (34) demonstrated that a combination of high hydrogen pressures (such as 500 Torr) and low temperatures (RT) would warp the Pd foil, probably due to the formation of palladium hydride.

The chlorofluorocarbons used in this study were obtained from DuPont Co. and had a purity of greater than 99.9%. The impurities detected did not change their concentration during the experiments, indicating that they are less reactive than the reactant. The reactants were degassed by freeze-pump-thaw cycles and then stored in a glass vial filled with a previously-reduced 0.5% Pd on carbon supported catalyst. This was done to scavenge any sulfur-containing compounds from the reactant feed. Hydrogen (Matheson, Prepurified) was passed through a liquid nitrogen cold trap to remove any condensable impurities. The Ar (Liquid Carbonic, 99.995%) was used without further purification. For CF_3-CFCl_2 , the reaction rates were measured in the temperature range of 350 to 470 K, pressure range of 23 to 670 Torr in H_2 , 21 to 511 Torr in CF_3-CFCl_2 and balance Ar to a total pressure of 770 Torr. For $CF_3-CFClH$, the ranges were 483-543 K, HCFC 20-500 Torr, and H_2 60-300 Torr. For CF_3-CCl_3 , the ranges were 363-383 K, CFC 10-100 Torr, and H_2 25-200 Torr. The reaction products were analyzed with a gas chromatograph (Hewlett-Packard 5790A) with a flame ionization detector. The products were separated in a 5% Krytox™ 143AC, 60/80 Carbopack B HT 20' x 1/8" column (Supelco, Inc.). The first analysis was made after 3 min of reaction and subsequent analyses were carried out at intervals of about 18 min.

Blank experiments were carried out to certify that the background catalytic activity was not significant. Those experiments were run on a stainless steel foil with a feed of 150 Torr of CF_3-CFCl_2 (CFC 114a) and 630 Torr of H_2 . At 423 K, where most of the experiments were run for CFC 114a, background reactions could not be detected, to a level at least 1000 times lower than the level obtained with a Pd foil.

In the calculation of turnover rates an atom surface density of 1.0×10^{15} atoms cm^{-2} is assumed for the foil and that each surface Pd atom is considered to be an active site.

Results and Discussion

The reactivity studies were carried out in a batch reactor at very low (about 1%) final total conversion and thus the reaction should behave as pseudo-zero-order. By plotting the amount converted as a function of time, a straight line should be obtained.

However, as illustrated in Figure 1-A there is a curvature on the line indicating that the rates decrease as the conversion is increased. As will be discussed in more detail below, the curvature in the plot is due to the inhibition by the reaction product, HCl, which has a reaction order of -1 . To account for the effect of HCl, the kinetic expression can be integrated. The resulting equation shows a linear relationship between the square of concentration and time (34,35) as illustrated in Figure 1-B. The rate is calculated from the slope of the line, which will be proportional to the reaction rate constant.

To optimize the catalyst performance for the chemistry of hydrodechlorination, it is important to determine how much the structure of the Pd catalyst affects the rate. To answer this question, the reaction of hydrodechlorination of $\text{CF}_3\text{-CFCl}_2$ was carried out over a Pd foil and two palladium single crystals of orientation (111) and (100). These three samples provided a range of surface structures. The (111) orientation has a surface with hexagonal symmetry, (100) has square symmetry, and the foil is probably composed of (111) domains with many surface defects. If the reaction were sensitive to the structure, we expected that a difference in rates and selectivity would be apparent among the different samples. The results are collected in Table 1 (35). For the three catalysts tested, the variation in the rates for each product were not significant. Note also that the selectivity is not a function of conversion, which implies that the reactions occur in parallel (34,35). Based on this result it was proposed that the reaction of hydrodechlorination is not sensitive to the structure of the palladium catalyst for $\text{CF}_3\text{-CFCl}_2$. We hypothesize that this is also true for other chloro-containing organic molecules since the kinetics of reaction is similar for a family of compounds as we will discuss below. In addition, this result may also be true for the other halogens and for other metals as suggested by Fung and Sinfelt (18).

Table 1 - Hydrodechlorination rates for $\text{CF}_3\text{-CFCl}_2$ (CFC114a) over Pd catalysts.

Catalyst	Turnover Rate ^a / s ⁻¹ (selectivity ^b / %)		
	Reaction Products		
	$\text{CF}_3\text{-CH}_3$ (HFC 143a)	$\text{CF}_3\text{-CFH}_2$ (HFC 134a)	$\text{CF}_3\text{-CFClH}$ (HCFC 124)
Pd foil	6.4×10^{-2} (3)	2.1 (85)	3.0×10^{-1} (12)
Pd(100)	8.0×10^{-2} (6)	1.2 (84)	1.4×10^{-1} (10)
Pd(111)	18.0×10^{-2} (10)	1.3 (74)	2.8×10^{-1} (16)

Reproduced with permission from reference (35). Copyright 1998.

^aRates corrected for 50 Torr of CFC, 100 Torr H₂, 0.1 Torr HCl, 423 K.

^bSelectivity is constant for conversion lower than 50%.

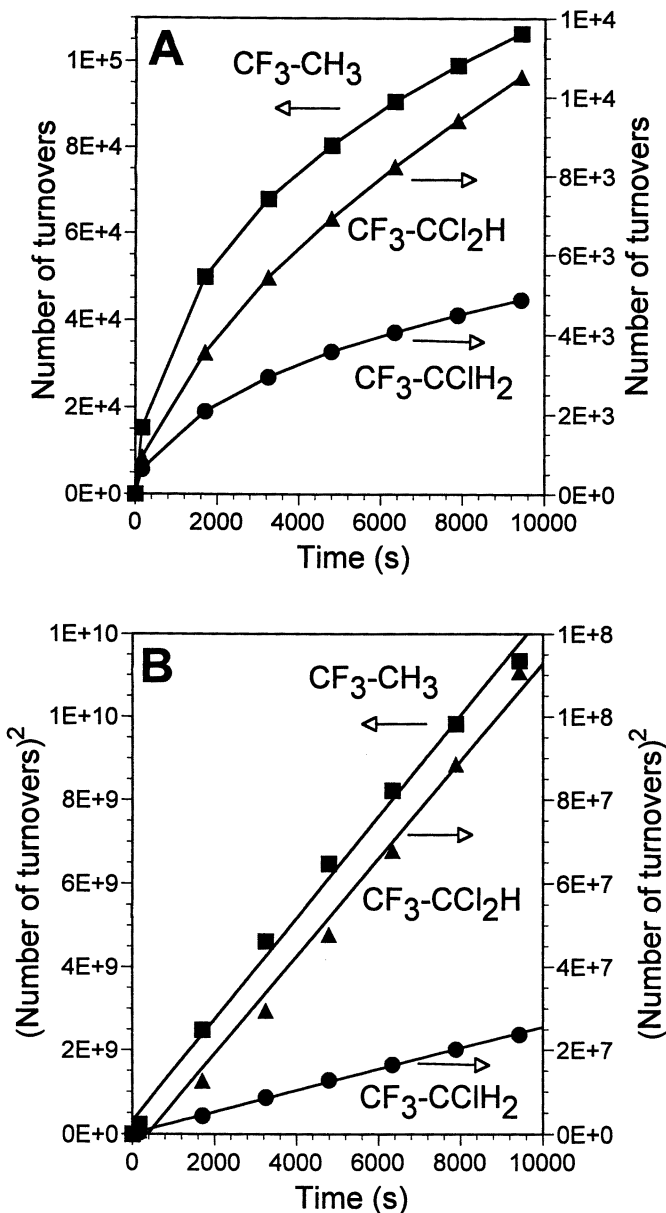
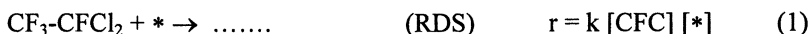


Figure 1. (A) Accumulation plot (Number of turnovers versus time) and (B) integrated equation plotted in linear form (effect of HCl accounted for) for the reaction of CF₃-CCl₃ (49.9 Torr) and H₂ (25.7 Torr) at 100°C on a Pd foil. The reaction products were CF₃-CH₃ (■), CF₃-CCl₂H (▲), and CF₃-CClH₂ (●).

The reaction orders and turnover rates will be presented in turn for the hydrodechlorination of $\text{CF}_3\text{-CFCl}_2$, $\text{CF}_3\text{-CFClH}$, and $\text{CF}_3\text{-CCl}_3$ carried out over a Pd foil.

The results of the hydrodechlorination of $\text{CF}_3\text{-CFCl}_2$ are presented in Table 2. The kinetics of this reaction has been described in detail before (34,35). The reaction orders of the two most abundant reaction products, $\text{CF}_3\text{-CFH}_2$ and $\text{CF}_3\text{-CFHCl}$, are approximately 1 in the CFC, 0.5 in H_2 , and -1 in HCl. These orders suggest the following sequence of steps over the catalyst:

The rate determining step (RDS) is the adsorption of the reactant CFC 114a on a single Pd atom:

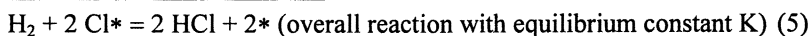


(Other steps for the CFC hydrodechlorination are not kinetically significant)

For the calculation of the number of free sites $[*]$, it is assumed that Cl^* is the most abundant reaction intermediate

$$[*] + [\text{Cl}^*] = [\text{L}] \quad (2)$$

where $[\text{L}]$ is the total number of sites, and that the surface is equilibrated with H_2 and HCl in the gas phase:



The number of free sites can then be calculated from (2) and (5) and it is equal to $[*] = [\text{L}]/(1 + [\text{HCl}]/K [\text{H}_2]^{0.5})$. Assuming that the second term in the denominator is much bigger than 1 for practical conditions, the final rate will then be

$$r = k K [\text{L}] [\text{CFC}] [\text{H}_2]^{0.5} / [\text{HCl}] \quad (6)$$

which is a good approximation to the experimentally observed rate dependencies reported in Table 2.

Table 2- Hydrodechlorination of $\text{CF}_3\text{-CFCl}_2$ (CFC 114a) on a Pd foil.

Products	TOR ^a (s ⁻¹)	E _a (kJ mol ⁻¹)	Reaction order dependence		
			CFC 114a	H ₂	HCl
CF ₃ -CH ₃	1.4x10 ⁻³	94	0.9	-0.20	-0.7
CF ₃ -CFH ₂	4.5x10 ⁻²	109	0.8	0.44	-1.2
CF ₃ -CFHCl	6.3x10 ⁻³	97	0.9	0.52	-0.9

^aTurnover Rate (TOR) corrected for 150 Torr $\text{CF}_3\text{-CFCl}_2$, 200 Torr H_2 , 20 Torr HCl, 150°C.

The rate expression (6) does not conform with the observed hydrogen order on the product $\text{CF}_3\text{-CH}_3$ in Table 2. There are at least two possibilities: (1) the reaction mechanism is different for the over-hydrogenated species, (2) this particular catalyst (a foil) has an ability to store hydrogen and modify the reaction rates. For example, Rupprechter and Somorjai (36) suggested that an anomalous H_2 order for the hydrodechlorination of $\text{CF}_3\text{-CFCl}_2$ on Pd single crystals was due to hydrogen dissolved in the bulk of the crystal.

Another distinctive fact in this chemistry is that the reaction product, HCl, is a strong inhibitor of the reaction. As described in the mechanism above, the reason is that chlorine adsorbs and occupies most of the available sites. The practical consequence of this inhibition is that the reaction rate is a function of the concentration of HCl and thus a function of conversion. Thus, care then must be exercised when reporting rates to specify the concentration of HCl.

The kinetic data for hydrodechlorination of $\text{CF}_3\text{-CFCIH}$ is presented in Table 3. In this case the selectivity to one of the products, $\text{CF}_3\text{-CFH}_2$, is 99.7%. The over-hydrogenated product ($\text{CF}_3\text{-CH}_3$) has a much lower reaction rate and a higher activation energy, as expected from the higher bond strength of the carbon-fluorine bond. The reaction order of HCFC 124 is about first order on the most abundant product but much lower in the over-hydrogenated product. As is for the case of CFC 114a, the reaction kinetics for the over-hydrogenated product does not follow the kinetic orders presented above in CFC order or H_2 order. The reaction order in H_2 is zero for both products. This result may be due to a different mechanism of reaction for this reactant or an artifact of the Pd foil, as discussed above. The HCl order could not be measured directly because the addition of excess HCl caused a severe poisoning by sulfur. However, because the experiments were carried out in a batch reactor, the concentration of HCl increased as a function of time and it was possible to fit the rate data with an assumed order dependence as illustrated above in Figure 1. The same procedure works for $\text{CF}_3\text{-CFCIH}$ and the curvature observed in Figure 2A is again due to the inhibition of the reaction by HCl. Assuming an HCl order dependence of -1 implies that plotting the square of the number of turnovers versus time will produce a straight line, as observed experimentally (Figure 2B).

Table 3- Hydrodechlorination of $\text{CF}_3\text{-CFCIH}$ (CFC 124) on a Pd foil.

Products	TOR ^a (s ⁻¹)	E _a (kJ mol ⁻¹)	Reaction order dependence		
			CFC 124	H ₂	HCl
$\text{CF}_3\text{-CH}_3$	6.4x10 ⁻⁷	120	0.6	0	-1
$\text{CF}_3\text{-CFH}_2$	1.9x10 ⁻⁴	96	0.9	0	-1

^aTurnover Rate (TOR) corrected for 150 Torr $\text{CF}_3\text{-CFCIH}$, 200 Torr H_2 , 20 Torr HCl, 150°C

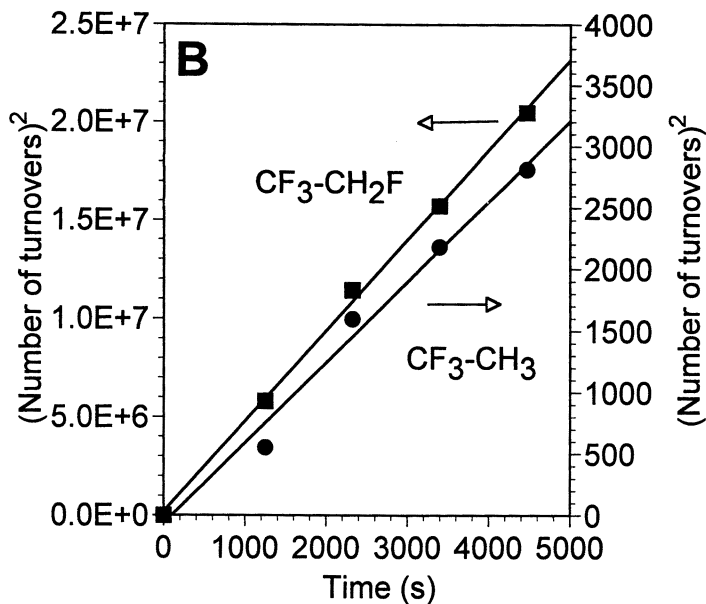
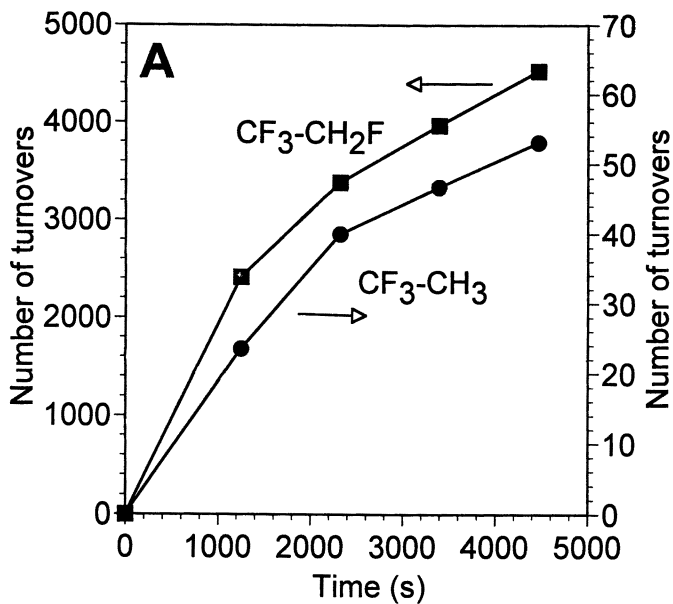


Figure 2. (A) Accumulation plot (Number of turnovers versus time) and (B) integrated equation plotted in linear form (effect of HCl accounted for) for the reaction of CF₃-CFCIH (260 Torr) and H₂ (510 Torr) at 225°C on a Pd foil. The reaction products were CF₃-CFH₂ (■), and CF₃-CH₃ (●).

The kinetic data for hydrodechlorination of $\text{CF}_3\text{-CCl}_3$ are presented in Table 4. This is the most reactive of the compounds tested and for this reason the temperature chosen to report the turnover rates is lower than for the other compounds. Reporting the data at 150 °C would require extrapolating the results. The product distribution is peculiar in this case in that the under-hydrogenated product with only one chlorine exchanged is formed with a high selectivity (27%). The activation energy increases as the number of chlorine atoms removed increases. The reaction order dependence for CFC 113a is the same for the two most abundant products but lower than the first order assumed by our model. The reaction order in H_2 is close to the expected value of 0.5 for the most abundant product but much higher than expected for the other two. Again, this may be an artifact due to the interaction of hydrogen with the palladium foil. The HCl reaction order was measured from the accumulation plots as exemplified in Figure 1 and is about -1 order.

Table 4- Hydrodechlorination of $\text{CF}_3\text{-CCl}_3$ (CFC 113a) on a Pd foil.

<i>Products</i>	<i>TOR^a (s⁻¹)</i>	<i>E_a (kJ mol⁻¹)</i>	<i>Reaction order dependence</i>		
			<i>CFC 113a</i>	<i>H₂</i>	<i>HCl</i>
$\text{CF}_3\text{-CH}_3$	2.4×10^{-1}	100	0.6	0.6	-1
$\text{CF}_3\text{-CH}_2\text{Cl}$	1.9×10^{-2}	82	0.8	1.0	-1
$\text{CF}_3\text{-CHCl}_2$	9.6×10^{-2}	70	0.6	1.2	-1

^aTurnover Rate (TOR) corrected for 30 Torr $\text{CF}_3\text{-CCl}_3$, 120 Torr H_2 , 20 Torr HCl, 70°C.

The last task was to compile the rates for the family of compounds presented for a standard reaction condition. The results are presented in Table 5. There is a rate change of seven orders of magnitude as the structure of the molecule is varied. The important conclusion is that the rate of hydrodechlorination is a strong function of molecular structure. Because there are many possible combinations of organic compounds containing hydrogen, fluorine, and chlorine and the rates are very dependent on the structure, it is important to find a way to correlate the structure of the catalyst with its rate of hydrodechlorination. It will be shown in a forthcoming publication (37) that the rate of hydrodechlorination correlates well with the strength of the C-Cl bond.

Table 5 – Overall rate of hydrodechlorination on a Pd foil for three compounds

<i>Compound</i>	<i>Overall Turnover Rate^a / s⁻¹</i>
CF ₃ -CFCIH (HCFC 124)	2x10 ⁻⁴
CF ₃ -CFCl ₂ (CFC 114a)	5x10 ⁻²
CF ₃ -CCl ₃ (CFC 113a)	1x10 ³

^aTurnover Rate corrected for 150 Torr of CFC, 200 Torr H₂, 20 Torr HCl, 150°C

Conclusions

The reaction of hydrodechlorination of CF₃-CFCl₂ over Pd is not sensitive to the structure of the catalyst. It is proposed that this reaction is also insensitive to the Pd structure for other halogen-containing organic compounds. The reaction may also be structure insensitive for other metal catalysts.

A sequence of steps was proposed for this reaction that consists of the adsorption of the CFC on the Pd surface as the rate limiting step, equilibrated steps of H₂ and HCl chemisorption on the surface, and adsorbed Cl as the most abundant reaction intermediate. This sequence implies that the reaction is 1 order in CFC, 0.5 in H₂, and -1 order in HCl. The experimental results for CF₃-CFCl₂ agree with the model very well. For the other two compounds tested, the agreement is not as good. The explanation may be a different reaction mechanism or just an artifact because a bulk palladium sample is used for these studies. Experiments with supported catalysts (37) agree with the reaction orders proposed here and thus the property of bulk Pd to store hydrogen may affect the kinetic orders. The rates and the selectivity on the foil and the supported catalysts are, however, very similar (37).

The rates of hydrodechlorination are very dependent on the CFC molecule considered. The rates span seven orders of magnitude for the three compounds tested. Because there are a vast number of organic molecules that can be synthesized with a given combination of hydrogen, chlorine, and fluorine, it is necessary to predict how the structure of the molecule relates to its rate of hydrodechlorination.

Acknowledgements

This work was supported by the National Science Foundation, CTS-9702699 and by the Director, Office of Energy Research, Office of Basic Energy Sciences, Materials Sciences Division, of the U.S. Department of Energy under Contract DE-AC03-76SF00098. We also thank Drs. L. Abrams, C.S. Kellner, L.E. Manzer, M. Nappa, and B.E. Smart from DuPont for help with technical and material issues.

Literature Cited

1. Molina, M. J.; Rowland, F. S. *Nature* **1974**, *249*, 810.
2. Rylander, P. N. *Catalytic Hydrogenation in Organic Synthesis*; Academic Press: New York, 1979, p. 235.
3. Wiersma, A.; vandeSandt, E.; denHollander, M. A.; vanBekum, H.; Makkee, M.; Moulijn, J. A. *J. Catal.* **1998**, *177*, 29-39.
4. Harley, A. D.; Holbrook, M. T.; Smith, D. D.; Cisneros, M. D.; Ito, L. N.; Murchison, C. B., US Patent 5,453,557, The Dow Chemical Company (1995).
5. Manzer, L. E.; Rao, V. N. M. *Adv. Catal.* **1993**, *39*, 329-350.
6. Ainbinder, Z.; Manzer, L. E.; Nappa, M. In *Handbook of Heterogeneous Catalysis*; Ertl, G., Knözinger, H., Weitkamp, J., Eds.; VCH: Weinheim, 1997; Vol. 4; pp 1677-1685.
7. Campbell, J. S.; Kemball, C. *Trans. Faraday Soc.* **1961**, *57*, 809-820.
8. Campbell, J. S.; Kemball, C. *Trans. Faraday Soc.* **1963**, *59*, 2583-2593.
9. Campbell, J. S.; Kemball, C. *Kinet. Katal.* **1964**, *5*, 4.
10. Anderson, J. R.; McConkey, B. H. *J. Catal.* **1968**, *11*, 54 - 70.
11. Lacher, J. R.; Kianpour, A.; Oetting, F.; Park, J. D. *Trans. Faraday Soc.* **1956**, *52*, 1500-1508.
12. Lacher, J. R.; Kianpour, A.; Park, J. C. *J. Phys. Chem.* **1956**, *60*, 1454-1455.
13. Witt, S. D.; Wu, E. C.; Loh, K. L.; Tang, Y. N. *J. Catal.* **1981**, *71*, 270 -277.
14. Dodson, D. A.; Rase, H. F. *Ind. Eng. Chem. Prod. Res. Dev.* **1978**, *17*, 236 -41.
15. van Barneveld, W. A. A.; Ponec, V. *J. Catal.* **1984**, *88*, 382.
16. Gervasutti, C.; Marangoni, L.; Marra, W. *J. Fluorine Chem.* **1981/82**, *19*, 1-20.
17. Coq, B.; Ferrat, G.; Figueras, F. *J. Catal.* **1986**, *101*, 434 -45.
18. Fung, S. C.; Sinfelt, J. H. *J. Catal.* **1987**, *103*, 220 -223.
19. Sinfelt, J. H. *Catal. Lett.* **1991**, *9*, 159 -171.
20. Bodnariuk, P.; Coq, B.; Ferrat, G.; Figueras, F. *J. Catal.* **1989**, *116*, 459 -66.
21. Srinivas, S. T.; Lakshmi, L. J.; Lingaiah, N.; Prasad, P. S. S.; Rao, P. K. *App. Catal. A* **1996**, *135*, L201-L207.
22. Ohnishi, R.; Suzuki, I.; Ichikawa, M. *Chem. Lett.* **1991**, 841 -4.
23. Coq, B.; Hub, S.; Figueras, F.; Tournigant, D. *Appl. Catal., A* **1993**, *101*, 41 -50.
24. Ohnishi, R.; Wang, W.-L.; Ichikawa, M. *Appl. Catal., A* **1994**, *113*, 29 - 41.
25. Suzdorf, A. R.; Morozov, S. V.; Anshits, N. N.; Tsiganova. *Catal. Lett.* **1994**, *29*, 49 -55.
26. Dhandapani, B.; Oyama, S. T. *Catal. Lett.* **1995**, *35*, 353 -60.
27. Wiersma, A.; Van de Sandt, E. J. A. X.; Makkee, M.; Luteijn, C. P.; Van Bekum, H.; Moulijn, J. A. *Catal. Today* **1996**, *27*, 257-264.
28. Mori, T.; Ueda, W.; Morikawa, Y. *Catal. Lett.* **1996**, *38*, 73-76.
29. Karpinski, Z.; Early, K.; d'Itri, J. L. *J. Catal.* **1996**, *164*, 378-386.
30. Early, K.; Kovalchuk, V. I.; Lonyi, F.; Deshmukh, S.; d'Itri, J. L. *J. Catal.* **1999**, *182*, 219-227.
31. Hoke, J. B.; Gramiccioni, G. A.; Balko, E. N. *Appl. Catal., B* **1992**, *1*, 285 -96.

32. Kovenklioglu, S.; Cao, Z. H.; Shah, D.; Farrauto, R. J.; Balko, E. N. *AIChE J.* **1992**, *38*, 1003-1012.
33. Marques, C. A.; Rogozhnikova, O.; Selva, M.; Tundo, P. *J. Mol. Cat. A* **1995**, *96*, 301-309.
34. Ribeiro, F. H.; Gerken, C. A.; Somorjai, G. A.; Kellner, C. S.; Coulston, G. W.; Abrams, L.; Manzer, L. E. *Catal. Lett.* **1997**, *45*, 149-153.
35. Ribeiro, F. H.; Gerken, C. A.; Rupprechter, G.; Somorjai, G. A.; Kellner, C. S.; Coulston, G. W.; Abrams, L.; Manzer, L. E. *J. Catal.* **1998**, *176*, 352-357.
36. Rupprechter, G.; Somorjai, G. A. *Catal. Lett.* **1997**, *48*, 17-20.
37. Thompson, C. D.; Rioux, R. M.; Chen, N.; Ribeiro, F. H. **Submitted.**

Chapter 16

Green Separation Science and Technology: Replacement of Volatile Organic Compounds in Industrial Scale Liquid–Liquid or Chromatographic Separations

Scott K. Spear, Ann E. Visser, Heather D. Willauer, Richard P. Swatloski,
Scott T. Griffin, Jonathan G. Huddleston, and Robin D. Rogers¹

Department of Chemistry and Center for Green Manufacturing,
The University of Alabama, Tuscaloosa, AL 35487

One area of opportunity for new chemical science and engineering technology which will help meet the goals of the U.S. Chemical Industry's *Technology Vision 2020* is the development of new separations technologies that eliminate the use of flammable, toxic VOCs as industrial solvents. Alternative technologies currently under investigation in our laboratories include those based on the use of water soluble polyethylene glycol polymers in either liquid/liquid (aqueous biphasic systems - ABS) or chromatographic (aqueous biphasic extraction chromatographic resins - ABEC) separations, and those based on air and moisture stable, water immiscible room temperature ionic liquids (RTIL). The ABS and ABEC applications are highlighted with two patented technologies for pertechnetate separation including: a) applications in radiopharmacy where the use of cleaner neutron-irradiated isotopes rather than fission-produced isotopes is possible, and b) applications in nuclear waste remediation where reduction of secondary waste streams produced by conventional technologies are anticipated. The potential and challenges for using the much less studied RTIL in novel separations will also be discussed. Within a new paradigm of pollution prevention and with industry participation, it is anticipated that a tool-box approach to Green Separation Science & Technology will lead to new technologies which do not utilize VOCs.

¹Corresponding author

Introduction

One of the goals of *Technology Vision 2020: The U.S. Chemical Industry* is to "enable the (chemical) industry to continue to lead in technology development, manufacturing and profitability, while optimizing health and safety and ensuring environmental stewardship" (1). The *Technology Vision 2020* initiative is further evidence of the recent upsurge of interest in 'green chemistry': research and development of new processes or new products that are environmentally benign and prevent pollution (2-6). The objective of this approach is to eliminate pollution at the source without compromising product quality or profitability.

Separations are ubiquitous in every industry, yet are rarely considered when determining the environmental impact of a manufacturing process. Thus, one area of opportunity for new chemical science and engineering technology which will help meet the goals of *Technology Vision 2020* is the development of new separations technologies that eliminate the use of flammable, toxic volatile organic compounds (VOCs) as solvents (7). Used in conjunction with, or instead of appropriate current manufacturing processes, such technologies would help to prevent pollution and increase safety.

Traditional solvent extraction employs partitioning of a solute between two immiscible phases, typically an organic solvent and aqueous solution (8). The ability to utilize a number of different diluents, extractants, and aqueous phases makes solvent extraction a powerful separations method possessing a number of favorable characteristics including rapid extraction kinetics for many separations, the adaptability of the method to a wide variety of solutes, and back extraction or stripping of the solute and recycling of the solvent and/or diluent. Further, liquid/liquid extraction is capable of large volume throughput and is amenable to large-scale separations, and can be engineered for high selectivity and efficiency by the use of multistage contactors.

Liquid/liquid extraction has often been a favorite choice for the development of separations processes, and typically this involves the use of an organic solvent into which the organic molecules partition or in which the extractant resides for the complexation and removal of metal ions from an aqueous phase. A characteristic of many VOCs that has been exploited in this regard is their water immiscibility that induces the formation of a two-phase system when contacted with water. As over 90% of hazardous waste is aqueous (9), considerable emphasis has been placed on processes that provide efficient means for solute separations from liquid media. Liquid/liquid extractions employing an organic solvent have become a common industrial separation process due to the ability to fine-tune both the hydrophobic and complexing properties of the extracting phase through the use of various organic solvents available. Worldwide usage of solvent at a cost of 5 billion dollars indicates the large quantity of VOCs consumed per annum (10).

Despite the widespread use of organic diluents, the abbreviation VOC has become synonymous with a plethora of social, economic, and ecological hazards. (When the diluent is coupled with a highly selective extractant the cost of the solvent system can become very expensive, not to mention the costs of safely designing a system to operate with a volatile or flammable diluent and the high costs of disposal.)

With the increased emphasis on the adoption of clean manufacturing processes and environmentally benign technologies, such use seems increasingly anachronistic. It is thus worth exploring the inherent benefits of alternative technologies to replace VOCs and reduce the associated health risks, volatility, environmental, and human health and safety concerns that accompany exposure to organic solvents. In environmental remediation and hazardous waste treatment, the generation of additional toxic or hazardous waste, doesn't present itself as a logical solution to the problem.

Several separations technologies, some of which have been intensively studied and others which are only now getting attention in the separations community, have the potential to reduce VOC use in industrial application. Two such technologies will be considered here, the use of environmentally benign polymer systems (7) and room temperature ionic liquids (RTIL) (11). The relationships between these techniques and traditional solvent extraction or ion exchange will be highlighted where possible. In addition, we will present areas which need immediate attention for any true industrial application of these technologies and point out some of the barriers to the introduction of new technologies into industrial practice, whether 'green' or not.

Aqueous Biphasic Systems

Separations scientists have employed the solubilizing power of aqueous solutions of certain polymers to extract and fractionate a variety of solutes (12-16). In the context of environmentally benign separations technologies, several techniques are worthy of note; including cloud point extraction, micellar extraction, aqueous biphasic systems (ABS), thermoseparating polymers, and chromatographic separations involving aspects of these (e.g., aqueous biphasic extraction chromatography - ABEC). (These techniques as applied to environmentally benign separations technologies are reviewed in reference 7.)

Two of these techniques have been extensively investigated in our laboratories (ABS and ABEC); however, all of these liquid/liquid extraction methods, each of which has its own specialized literature, have many common features which could be used to design industrial separations technologies (7). Some of these common features include: a) all represent anisotropic or multiphase systems and thus lend themselves to development in solvent extraction technologies; b) all may be applied to the solubilization of otherwise relatively insoluble hydrophobic species; c) none require VOCs for use in liquid/liquid extraction; d) all may be formed by addition of polymers to water; e) all rely on the structuring properties of liquid water for the formation of heterogeneous multiphase systems and also for their solubilizing power; and f) all seem to depend on the properties of the poly(oxyalkylenes) and similar polymers, to be effective.

Until recently, the utility in industrial scale separation of metal ions and organic solutes of polyethylene glycol (PEG)-based ABS, formed by salting-out polyethylene glycol to form two immiscible aqueous phases (Fig. 1), had been all but overlooked except for their original applications in gentle, nondenaturing separations of biomolecules (12-16). This was in part due to the lack of a fundamental understanding of these systems and well defined applications of this technology. Our

research effort has thus aimed to understand ABS and demonstrate potential selective batch or chromatographic applications for removal and recovery of solutes and particulates.

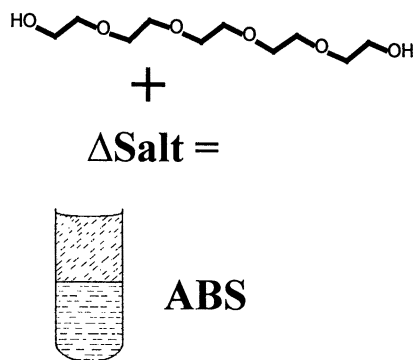


Figure 1. The salting-out of polymers such as PEG-2000 with cosmotropic salts produces ABS.

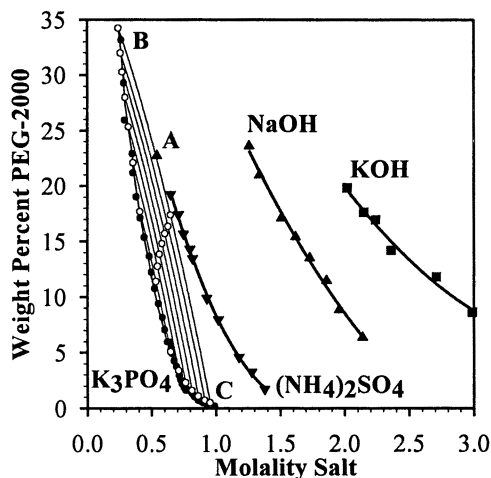


Figure 2. Phase diagrams of four PEG/salt ABS; system compositions (salt and PEG) to the left of each binodal are monophasic, while those to the right of the binodal are biphasic. Increasing salt and/or PEG concentrations to the right of the binodal leads to longer tie line lengths and increasingly divergent phase compositions.

A number of different water soluble polymers may be utilized to form ABS, with PEGs, dextrans, and ficolls receiving the most attention (12-17). An even wider variety of polymer/salt combinations exists, usually with Na^+ , K^+ , or NH_4^+ salts of mono- through trivalent anions like OH^- , CO_3^{2-} , SO_4^{2-} , and PO_4^{3-} (18). As two-phase systems they are suitable for carrying out liquid/liquid separations of various solutes such as biomolecules, metal ions, and particulates, and yet, *the major component in each of the two phases is water.*

Aqueous biphasic systems retain all of the practical advantages of liquid/liquid extraction and also have a number of unique advantages due, in large part, to their aqueous nature. Polyethylene glycol-based ABS are virtually nontoxic and nonflammable. All components are commercially available in bulk quantities, are inexpensive, and the systems have reasonable phase separation characteristics that can even be used with traditional solvent extraction equipment. In addition, the PEG-rich phases in PEG-ABS appear to be tunable; their phase characteristics can be changed to match the hydrophobicity and water content of a number of organic solvents.

A phase diagram with data for four salt/PEG-2000 systems is presented in Fig. 2. The curves represent the binodal for each salt/polymer combination. System compositions below the curves result in homogeneous solutions, while compositions

above the binodals result in two immiscible aqueous phases. The straight lines connecting two points (nodes) on the binodal are tie lines. Preparing a system by adding the individual components in amounts anywhere along a given tie line will result in individual phase compositions represented by the nodes. (The upper node (B) refers to the upper phase and the lower node (C) to the lower phase.) The approximate phase ratio can be estimated as the ratio of the length along the tie line from the upper phase composition to the system composition (BA), over the system composition to the lower phase (AC). The phase ratio (BA/AC) is equal to the volume ratio which is an important characteristic to be considered in optimizing any liquid-liquid separation using ABS. Concentrations of solutes in each phase are independent of phase volume.

We have related both the ability of salts to form ABS and their partitioning in ABS to their Gibbs free energy of hydration (19,20). Separation of the phases is most strongly promoted by anions having large negative ΔG_{hyd} (i.e., by cosmotropic, water-structuring anions, typically of high charge density). The effect of the cation on phase separation is in general much less than the anion (18), however, the more negative the combined ΔG_{hyd} of the salt, the lower the concentration of PEG and salt required to form a biphasic system.

The relative ordering in salting-out ability of both the cations and anions present can be directly correlated with their ΔG_{hyd} values. The salting-out effects are additive and the cations also have a contribution. When comparing salts having the same anion, the one whose cation has a more negative ΔG_{hyd} value is better at salting-out PEG.

Chaotropic (water-destructuring) ions with small negative ΔG_{hyd} (e.g., TcO_4^-) tend to partition quantitatively to the PEG-rich phase of an ABS (21,22). Hydrated metal cations can also be partitioned to the PEG-rich phase, but only if a suitable extractant (e.g., halide, dye, crown ether, etc.) is used to produce a more chaotropic ion-complex (22,23).

The effectiveness of a given ABS for separation may be qualitatively estimated from the sum of ΔG_{hyd} of all salting-out ions present (Fig. 3) and the partitioning of a chaotropic ion can be approximated from a knowledge of its ΔG_{hyd} . In a similar manner (Fig. 4), the partitioning of organic solutes can be estimated from a knowledge of their hydrophobicity (e.g., as measured by their 1-octanol/water partition coefficients, $\log P$) (24). Thus, knowledge of the composition of the matrix containing the solutes to be separated enables a qualitative prediction of the performance of a proposed extraction.

We have utilized PEG-ABS in the majority of our studies due to the favorable properties of PEG. It is the most hydrophilic of several possible alternatives (PEG > polyethylene oxide/propylene oxide block and random copolymers > polypropylene glycol (PPG) > polytetramethylene glycol) (13,25). PEG is also a commodity chemical, readily available, inexpensive, and FDA-approved for internal consumption, thus making PEGs ideally suited to development of green separation technologies.

Of the many available PEG molecular weights, we have used MW 2000 most often (22). This selection was based on the fact that PEG-2000/ABS provide two-phase systems with phase viscosities, phase ratios, etc., all within the range of many

oil/water systems currently in use. This is supported by the demonstrated ability to use PEG-ABS effectively in a thin-layer countercurrent distribution apparatus for separations (12).

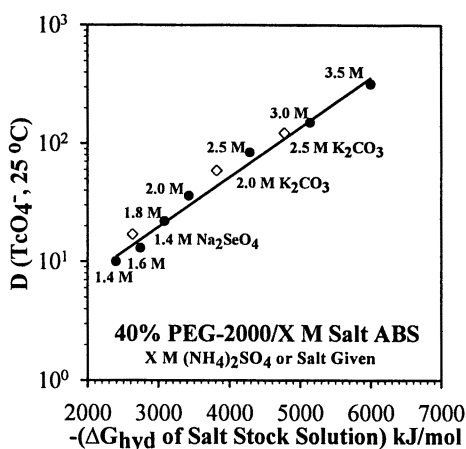


Figure 3. The effectiveness of a given ABS at partitioning a chaotropic ion to the PEG-rich phase can be approximated from a knowledge of the ΔG_{hyd} for the ions involved. Here the distribution ratio (D) is defined as the activity in the upper PEG-rich phase divided by the activity in the lower salt-rich phase as measured from equal volume aliquots of each phase. The total ΔG_{hyd} of the salt stock solution has been calculated by adding the products of each ion's concentration in molarity times its calculated ΔG_{hyd} from reference 19.

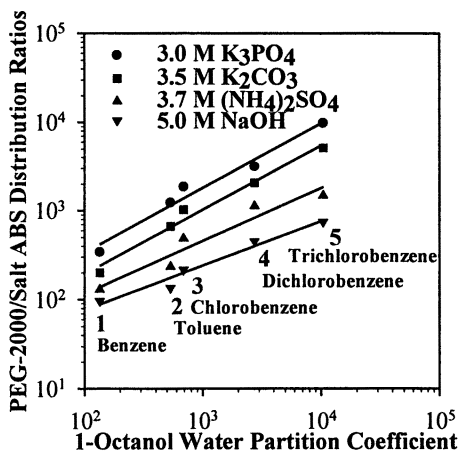


Figure 4. The partitioning of organic solutes to the PEG-rich phase of an ABS is correlated with the solutes $\log P$ 1-octanol/water partition coefficient. The ABS were prepared by mixing equal aliquots of the salt concentrations indicated with 40% PEG-2000.

ABS have been criticized for some applications because of the necessity to strip into a salt solution so that a two-phase system is maintained. Difficulties with stripping, however have been overcome by successfully adapting PEG-ABS to solid chromatographic separations processes via covalent attachment of monomethylated-PEG to an inert polystyrene-divinylbenzene backbone (22,26). Thus, in column chromatographic mode, stripping can be accomplished simply by elution with water (Fig. 5).

Although attachment of PEGs to a solid support is not new, by relating the resin behavior directly to liquid/liquid ABS (27), we have been able to utilize these resins in unique separations technologies. Importantly, these tunable, affinity adsorbents can be stripped simply by elution with water. Given the current emphasis on green chemistry and the desire to prevent pollution by redesign of industrial processes, ABS and ABEC represent an economical avenue for 'clean' separations. Three patented

technologies (28-30) offer evidence of the applicability of these technologies to a wider industrial sector. These include the following, of which the first two applications will be discussed in this chapter:

- $\text{TcO}_4^-/\text{MoO}_4^{2-}$, $\text{ReO}_4^-/\text{MoO}_4^{2-}$, and $\text{ReO}_4^-/\text{WO}_4^{2-}$ separations for radiopharmacy and hydrometallurgy (22,31)
- Separation and recovery of TcO_4^- from Hanford tank wastes (22,32,33)
- Separation and recovery of food coloring dyes or textile dyes (34)
- Separation and stripping of metal halide complex anions for hydrometallurgy applications (23,35)
- Adaptation of liquid/liquid PEG-ABS to a solid-supported chromatographic mode (22,26,36)
- Proving that ionophores capable of metal ion recognition can be used in PEG-ABS (22,37)
- Development of iodine specific resins (38)

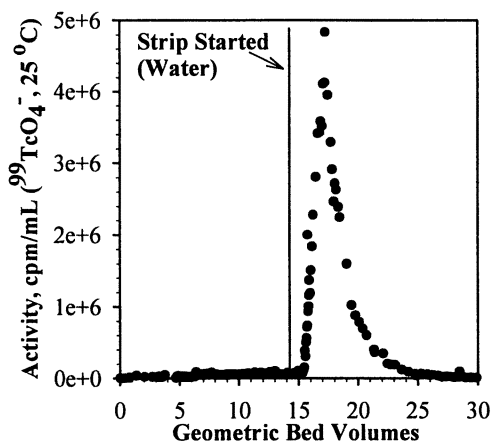


Figure 5. Chromatographic separation of $^{99}\text{TcO}_4^-$ from 4 M NaOH (the major constituent of the Hanford tank waste) demonstrates recovery of the radioactive $^{99}\text{TcO}_4^-$ simply by washing the column with water. The geometric bed volume was 1.005 mL.

$\text{TcO}_4^-/\text{MoO}_4^{2-}$, $\text{ReO}_4^-/\text{MoO}_4^{2-}$, and $\text{ReO}_4^-/\text{WO}_4^{2-}$ Separations for Radiopharmacy and Hydrometallurgy

Although $^{99\text{m}}\text{Tc}$ is used in the vast majority of all diagnostic nuclear medicine, its continued supply is at best uncertain (39). Current generators for $^{99\text{m}}\text{Tc}$ (the daughter of radioactive decay of the ^{99}Mo parent), the most widely used radionuclide in diagnostic nuclear medicine, are primarily based on the adsorption of molybdate on alumina from which pertechnetate is eluted with saline solution (40). These generators require high specific activity ^{235}U fission-produced ^{99}Mo (which is expensive, requires extensive purification prior to use, produces radioactive waste, and has few suppliers) and still suffer from radiomolybdate and aluminum contamination of the eluate.

Methyl ethyl ketone-based solvent extraction generators can utilize low specific activity neutron irradiation-produced ^{99}Mo (which is less expensive and cleaner), but require a flammable, toxic organic solvent, and are more complicated (40). Given the

expense and dwindling number of suppliers of fission-produced ^{99}Mo , economically viable technologies for the separation of $^{99\text{m}}\text{Tc}$ from neutron irradiation-produced, low specific activity ^{99}Mo are needed to maintain current supplies and meet the continually growing demand for $^{99\text{m}}\text{Tc}$ in medicine.

We developed two new separation schemes (liquid/liquid and chromatographic) for this important problem. We were able to demonstrate that partitioning behavior correlated to phase incompatibility and that the phase forming salt's ability to salt-out PEG, and thus its influence on the distribution ratio of TcO_4^- (D_{Tc}) was related to the anion's Gibbs free energy of hydration (ΔG_{hyd}) (27). This led directly to the discovery of new salt systems capable of salting out PEG in an ABS including VO_4^{3-} , CrO_4^{2-} , MoO_4^{2-} , and WO_4^{2-} (31). It also led to the stripping of TcO_4^- by recognizing that reduction with SnCl_2 to an oxy-chloro cationic species would change technetium's hydration environment and force it back to the salt-rich phase.

With the knowledge that MoO_4^{2-} salts-out PEG and that TcO_4^- quantitatively partitions to the PEG-rich phase, we designed a $\text{TcO}_4^-/\text{MoO}_4^{2-}$ separation (31,41). The results are shown in Fig. 6. Pertechnetate can be separated from molybdate with separation factors as high as 10,000. The two most important salt solutions are OH^- and MoO_4^{2-} . As shown in Fig. 6, high concentrations of MoO_4^{2-} (as would be needed to produce enough $^{99\text{m}}\text{Tc}$ activity from low specific activity neutron irradiation-produced $^{99}\text{MoO}_4^{2-}$) are not deleterious, but actually enhance the separation. Stripping is accomplished by reduction of the TcO_4^- and back extraction into a salt solution. The strip solution can be the salt of an imaging agent (e.g., Na_4HEDPA) and thus may, under the appropriate conditions, be injected directly into the human body.

Using the knowledge obtained from the liquid/liquid studies, we were able to design and test, batch and column chromatographic separations of pertechnetate from molybdate using ABEC. A 5 M NaOH solution containing the parent salt Na_2MoO_4 was passed through the ABEC column with immediate breakthrough of molybdate (Fig. 7). The daughter pertechnetate ion is retained on the column until stripped with water. A major advantage of the chromatographic technique is that the pure $^{99\text{m}}\text{TcO}_4^-$ can be eluted with either water or saline.

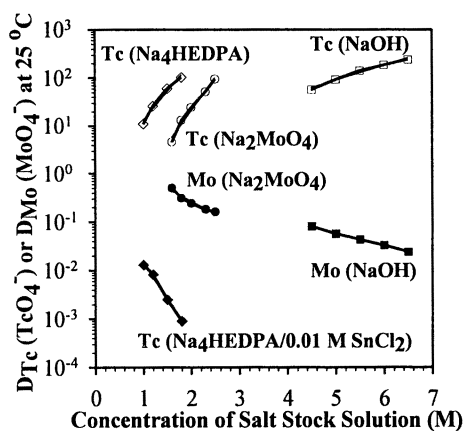


Figure 6. The separation of TcO_4^- from MoO_4^{2-} improves with higher molybdate, hydroxide, or HEDPA $^+$ concentrations as a result of the increasing phase divergence of the PEG-rich and salt-rich phases. Note that in the presence of SnCl_2 , the reduced technetium species prefers the salt-rich phase.

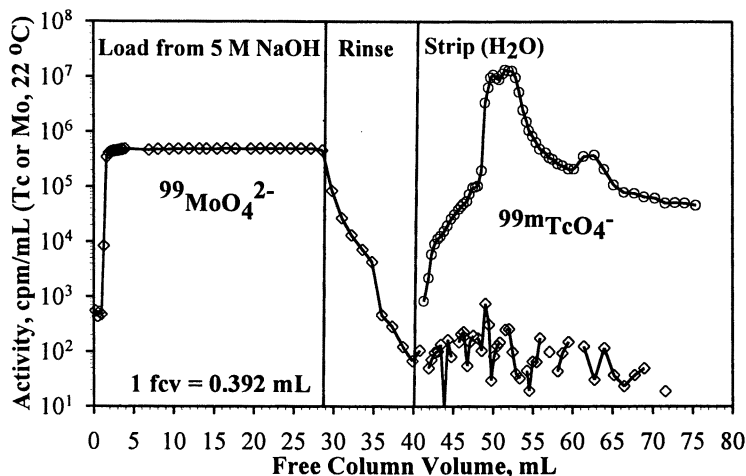


Figure 7. The elution curves for $^{99}\text{MoO}_4^{2-}$ and $^{99\text{m}}\text{TcO}_4^-$ using ABEC-5000 demonstrates efficient separation and recovery. Note the immediate breakthrough of $^{99}\text{MoO}_4^{2-}$ and the ready stripping of $^{99\text{m}}\text{TcO}_4^-$ when the column is rinsed with water.

An additional benefit of this technology is the adaptation to the separation of perrhenate (ReO_4^-) from molybdate or tungstate (42). Given the similarity in perrhenate and pertechnetate, we reasoned that the $\text{ReO}_4^-/\text{MoO}_4^{2-}$ or $\text{ReO}_4^-/\text{WO}_4^{2-}$ separation should also be equally efficient, and indeed this has proven to be true (42). Thus, this technology can be applied to a hydrometallurgical process which currently uses organic solvents to accomplish the purification of rhenium from molybdenum ores. In addition, it can be applied to the separation of Re isotopes for radiopharmacy where high specific activity tungsten parent sources are not available, thus complicating the adaptation of technetium-generator technologies to rhenium.

Separation and Recovery of TcO_4^- from Hanford Tank Wastes

Remediation efforts often produce secondary waste streams which further complicate clean-up. Introduction of the Green Chemistry paradigm into remediation efforts could thus, also have a significant impact on pollution prevention. We were able to demonstrate that simulants of Hanford, WA radioactive tank wastes form an ABS with PEG-2000 due to the salting-out action of NaOH (43). We also demonstrated that TcO_4^- quantitatively partitions to the PEG-rich phase from these ABS. (This is noteworthy since many oil/water separations do not work well under highly alkaline conditions.) We demonstrated stripping by SnCl_2 reduction, however, stripping back into a salt solution would not be acceptable in this case, and thus, ABEC resins were utilized for their ability to directly remove TcO_4^- from the Hanford

wastes (26,32,33). The chromatogram in Fig. 5 is representative of pertechnetate removal from the alkaline Hanford waste tanks which are typically 2-4 M NaOH.

ABEC resins are currently being tested with actual Hanford tank wastes under the direction of the Tank Focus Group at Pacific Northwest National Laboratory (44). The utilization of ABEC for this process has a significant secondary waste reduction aspect. The resin initially chosen for this task was Reillex-HPQ, a methylated, divinylbenzene/4-vinylpyridine copolymer. Reillex-HPQ requires the addition of SnCl_2 to reduce Tc(VII) and a chelating agent (e.g., ethylenediamine) in a high ionic strength solution (e.g., 1 M NaOH) to strip the loaded pertechnetate anion (45). This produces a significant radioactive secondary waste stream. By recognizing the relationship between ABS and ABEC and the strongly salting-out composition of the alkaline wastes, we were able to demonstrate that the ABEC resins would selectively remove TcO_4^- (other metal cations were shown not be retained by the resin) and could be stripped using only water. This technology, thus removes the radioactive technetium from a large volume of mixed, radioactive waste and concentrates it into a small volume of water for recycle or disposal (32,33).

Room Temperature Ionic Liquids

To add to the growing toolbox of green separations technologies, separations scientists are now starting to look at 'neoteric solvents' for VOC replacement such as RTIL (10,46-48). Although much work remains to be done, RTIL show promise for novel liquid/liquid separations strategies (11). These liquids, as discussed below, have no vapor pressure, thus eliminating a major pollutant and fire hazard from solvent extraction.

Room temperature ionic liquids, in the strictest sense, may conjure the image of molten NaCl at temperatures above 800 °C, however, RTIL simply represent ionic salts that are liquid at room temperature. These ionic liquids offer a highly solvating, yet non-coordinating medium in which a number of organic and inorganic solutes may be dissolved (47). RTIL are non-volatile, non-flammable, and have high thermal stability. Importantly, RTIL are relatively undemanding and inexpensive to manufacture.

Many RTIL are liquids over a wide temperature range (for some this range may exceed 300 °C) and RTIL with melting points as low as -96 °C are known (47). The constituents of RTIL (being ionic) are constrained by high coulombic forces and thus, exert practically no vapor pressure above the liquid surface. These features, and the potential to reduce pollution in industrial processes, have led to current investigations of RTIL as alternative reaction media for a variety of applications that use organic solvents.

The low melting nature of RTIL can be engineered by the choice of anionic and cationic species to produce salts with low lattice energies. The majority of RTIL studies reported in the literature to date have utilized large, asymmetric organic cations to produce this effect. The most common examples include *N*-alkylpyridinium and 1-alkyl-3-methylimidazolium (Rmim, Fig. 8) cations in which the alkyl group may be varied to fine-tune the physical properties of the RTIL. For

example, notable changes in melting point are observed as the length of the alkyl chain increases in $[\text{Rmim}][\text{PF}_6]$ ionic liquids; the ethyl derivative ($[\text{emim}][\text{PF}_6]$) melts at 58-60 °C (49) while at room temperature, the butyl (mp = 4 °C), hexyl (mp = -78 °C), and octyl (mp = -72 °C) derivatives are liquids (50). When R is increased to the decyl group ($[\text{dmim}][\text{PF}_6]$), the salt is a solid at room temperature (mp = 37 °C).

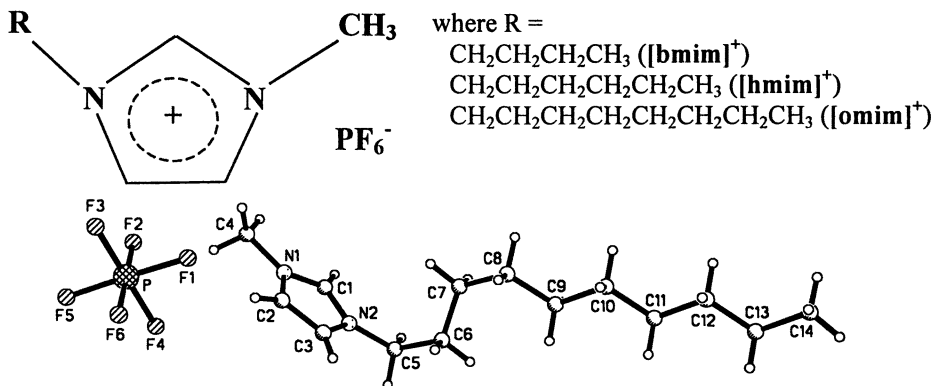


Figure 8. Examples of structural variation in 1-alkyl-3-methylimidazolium-based RTIL including the crystal structure of the low melting decyl derivative, $[\text{dmim}][\text{PF}_6]$.

The choice of cation need not be limited to pyridinium or imidazolium salts and the range of potential cations is exceedingly large. For example, asymmetric tetralkylammonium or phosphonium salts may also form RTIL. Choice of cation, their modification (e.g., fluorinated or chiral alkyl groups), and the determination of chemical and physical properties offers a fertile field of research, where the possible permutations may only be limited by imagination.

Recently, RTIL have been identified in which the anion is not only stable to moisture, but imparts water immiscibility as well, hence rendering them capable of forming a two-phase system with aqueous media (47,49,51). The anions reported in this category include PF_6^- , BF_4^- , triflate (CF_3SO_2^-), nonaflate ($\text{CF}_3(\text{CF}_2)_3\text{SO}_2^-$), bis(triflyl)amide ($(\text{CF}_3\text{SO}_2)_2\text{N}^-$), trifluoroacetate (CF_3CO_2^-), and heptafluorobutanoate ($\text{CF}_3(\text{CF}_2)_3\text{CO}_2^-$) (51).

We have chosen to study the 1-alkyl-3-methylimidazolium salts of PF_6^- due to ready availability of reagents, ease of synthesis, ability to readily vary the alkyl chain length in the cation (and thus the physical properties), and the convenient melting points and viscosities. Three of the four salts depicted in Fig. 8 are liquids at room temperature and all three form biphasic systems with water in which the RTIL forms the heavy lower phase.

Three communications have appeared involving the use of RTIL in separations. Brennecke and Beckman demonstrated stripping of nonvolatile aromatic solutes from a RTIL-loaded phase using supercritical CO_2 (52). In another paper, Dai, *et al.* used a crown ether extractant to enhance metal ion partitioning to a RTIL phase from water (53). We have recently demonstrated that aromatic organic solutes partition to RTIL

from water in relationship to their hydrophobicity as measured by their 1-octanol/water partition coefficients (Fig. 9) (11). Based upon these results one would predict that hard metal cations would prefer the aqueous phase of a RTIL/aqueous system and the partitioning data obtained for metal cations between [Rmim][PF₆] and neutral, acidic, and basic aqueous phases thus far bear this out (54). If metal ions are to be extracted from aqueous solution into the RTIL, extractants (e.g., PAN; Fig. 10) will be needed in direct analogy to the use of extractants in traditional solvent extraction.

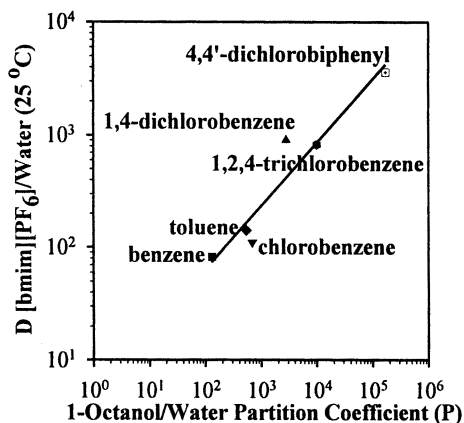


Figure 9. Correlation of distribution ratios for ¹⁴C-labeled aromatic solutes in [bmim][PF₆]/water with 1-octanol/water biphasic systems. The distribution ratios for these systems were calculated as the activity in the lower RTIL phase divided by the activity in the upper aqueous phase as measured from equal volume aliquots of each phase.

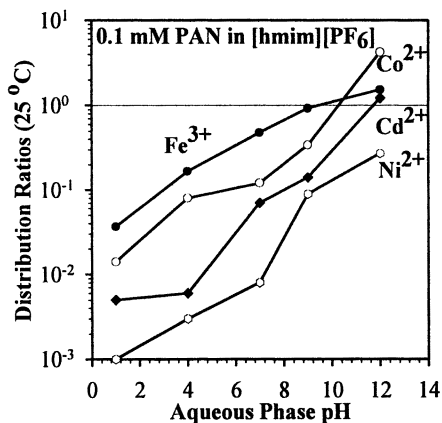


Figure 10. Metal cations can be extracted from aqueous solution into RTIL by using extractants (e.g., PAN: 1-(2-pyridylazo)-2-naphthol). Note as in traditional solvent extraction, the ionizing ligand extracts metal cations at high pH, but not at low pH.

Studies on the partitioning behavior of organic solutes in RTIL are just now beginning to appear in the literature, although this is essential information for developing metal ion extractants for RTIL. Although several aromatic solutes have been shown to prefer the RTIL phase, the partitioning data suggest that the observed phase preference often depends upon the degree of ionization (11). Thus ionizable extractants may not be retained in the extracting phase during both loading and stripping, although this has yet to be studied in detail.

Conclusions: Implementation of Green Separations Technologies

New separations technologies that reduce the reliance on VOCs have potential for application in pollution prevention, pollution remediation, and in the reduction of secondary waste streams. Certainly the recent flurry of activity in the field of RTIL will result in a number of new applications for the exploitation of the unusual properties of these neoteric solvents. Room temperature ionic liquids and ABS/ABEC processes are expected to result in lower utilization of VOCs with relatively safe, nonvolatile, nonflammable systems.

Despite the promise of these technologies, however, much research remains to be carried out in order to realize this promise. Comprehensive toxicity data is not always available and a general database of physical properties is needed. In addition, with literally millions of different combinations of ions which may produce RTIL or polymers and salts for ABS, a new combinatorial approach to identification may lead to a variety of useful liquid/liquid systems. Other roadblocks to successful development, especially for RTIL, include limited commercial availability and the development of more economic synthetic pathways.

It will also be important to have greater industrial input into the research agenda for these fields. Barriers to implementation include education, cost of testing, and perhaps resistance to new ideas. Comparative scientific and economic data must be collected for direct comparison with traditional solvents. A fundamental understanding of the new technologies is needed, for example system design and a knowledge of solute transport mechanisms, would allow model development. This research should continue in a scientific-engineering/problem solving approach and must be supported by industrial participation and support for a new paradigm of pollution prevention. All of these will be needed to educate potential users and overcome the inherent barriers to new technologies, but the current emphasis on sustainable development may be just the catalyst needed to see these new technologies to fruition.

Acknowledgements

This research was supported by the Division of Chemical Sciences, Office of Basic Energy Sciences, Office of Energy Research, U.S. Department of Energy (Grant No. DE-FG02-96ER14673). Portions of this work involving metal ion separations in ABS and with ABEC resins were supported by the U.S. National Science Foundation (Grant No. CTS-9522159).

Literature Cited

1. *Technology Vision 2020: The U.S. Chemical Industry*, American Chemical Society, American Institute of Chemical Engineers, Chemical Manufacturers Association, Council for Chemical Research, Synthetic Organic Chemical Manufacturers Association; Washington, DC, 1996.

- Collins, T. J. In *Macmillan Encyclopedia of Chemistry*; Lagowski, J. J., Ed.; Macmillan, Inc.: New York, 1997; Vol. 2, pp. 691-697.
- Benign by Design: Alternative Synthetic Design for Pollution Prevention*; Anastas, P. T.; Farris, C. A., Eds.; ACS Symposium Series 577, American Chemical Society: Washington, DC, 1994.
- Green Chemistry: Designing Chemistry for the Environment*; Anastas, P. T.; Williamson, T. C., Eds.; ACS Symposium Series 626, American Chemical Society: Washington, DC, 1996.
- Green Chemistry: Frontiers in Benign Chemical Syntheses and Processes*; Anastas, P. T.; Williamson, T. C., Eds.; Oxford University Press: Oxford, 1998.
- Healey, M. J.; Watts, D.; Battista, L. L.; Grosvenor, T.; Kretkowski, D. A.; Lewis, J.; Pico, J. D. *Pollution Prevention Opportunity Assessments: A Practical Guide*; John Wiley & Sons: New York, 1998.
- Huddleston, J. G.; Willauer, H. D.; Griffin, S. T.; Rogers, R. D. *Ind. Eng. Chem. Res.* **1999**, *38*, 2523-2539.
- Rydberg, J.; Musikas, C.; Choppin, G. R. *Principles and Practices of Solvent Extraction*; Marcel Dekker: New York, 1992.
- Lo, T. C. In *Handbook of Separations Techniques for Chemical Engineers*; Schwietzer, P. A., Ed.; McGraw-Hill: New York, 1996; pp. 1-450-1-529.
- Seddon, K. R. *J. Chem. Tech. Biotechnol.* **1997**, *68*, 351-356.
- Huddleston, J. G.; Willauer, H. D.; Swatloski, R. P.; Visser, A. E.; Rogers, R. D. *Chem. Commun.* **1998**, 1765-1766.
- Partitioning of Aqueous Two-Phase Systems: Theory, Methods, Uses, and Applications to Biotechnology*; Walter, H.; Brooks, D. E.; Fisher, D., Eds.; Academic Press: Orlando, FL, 1985.
- Aqueous Two-Phase Systems*; Walter, H.; Johansson, G., Eds.; In *Methods in Enzymology*; Abelson, J. N.; Simon, M. I., Eds.; Academic Press: New York, 1994; Vol. 228.
- Aqueous Biphasic Separations: Biomolecules to Metal Ions*; Rogers, R. D.; Eiteman, M. A., Eds.; Plenum: New York, 1995.
- Albertsson, P. Å. *Partition of Cell Particles and Macromolecules*; 3rd ed.; John Wiley & Sons: New York, 1986.
- Zaslavsky, B. Y. *Aqueous Two-Phase Partitioning: Physical Chemistry and Bioanalytical Applications*; Marcel Dekker: New York, 1995.
- Tjerneld, F. In *Poly(Ethylene Glycol) Chemistry*; Harris, J. M., Ed.; Plenum Press: New York, 1992; pp. 85-102.
- Ananthapadmanabhan, K. P.; Goddard, E. D. *J. Colloid Interface Sci.* **1986**, *113*, 294-296.
- Marcus, Y. *J. Chem. Soc., Faraday Trans.* **1991**, *87*, 2995-2999.
- Rogers, R. D.; Bond, A. H.; Bauer, C. B.; Zhang, J.; Griffin S.T. *J. Chromatogr. B* **1996**, *680*, 221-229.
- Rogers, R. D.; Zhang, J.; Griffin, S. T. *Sep. Sci. Technol.* **1997**, *32*, 699-707.
- Rogers, R. D.; Zhang, J. In *Ion Exchange and Solvent Extraction*; Marinsky, J. A.; Marcus, Y., Eds.; Marcel Dekker: New York, 1997; Vol. 13, pp. 141-193.

23. Rogers, R. D.; Bond, A. H.; Bauer, C. B. In *Solvent Extraction in the Process Industries, Proceedings of ISEC '93*; Logsdail, D. H.; Slater, M. J., Eds.; Elsevier: London, 1993; pp. 1641-1648.
24. Rogers, R. D.; Willauer, H. D.; Griffin, S. T.; Huddleston, J. G. *J. Chromatogr. B* **1998**, *711*, 255-263.
25. Rogers, R. D.; Zhang, J. *J. Chromatogr. B* **1996**, *680*, 231-236.
26. Rogers, R. D.; Bond, A. H.; Griffin, S. T.; Horwitz, E. P. *Solvent Extr. Ion Exch.* **1996**, *14*, 919-946.
27. Huddleston, J. G.; Griffin, S. T.; Willauer, H. D.; Rogers, R. D. In *Metal-Ion Separation and Preconcentration, Progress and Opportunities*; Dietz, M. L.; Bond, A. H.; Rogers, R. D., Eds.; ACS Symposium Series 716, American Chemical Society: Washington, DC, 1999; pp. 79-100.
28. Rogers, R. D.; Horwitz, E. P.; Bond, A. H. "Process for Recovering Pertechnetate Ions from an Aqueous Solution also Containing Other Ions," 2/18/1997, U. S. Patent No. 5,603,834.
29. Rogers, R. D.; Horwitz, E. P.; Bond, A. H. "Process for Separating and Recovering an Anionic Dye from an Aqueous Solution," 1/13/1998, U. S. Patent No. 5,707,525.
30. Rogers, R. D.; Horwitz, E. P.; Bond, A. H. "Process for Recovering Chaotropic Ions from an Aqueous Solution also Containing Other Ions," 3/10/1999, U. S. Patent No. 5,888,397.
31. Rogers, R. D.; Bond, A. H.; Zhang, J.; Bauer, C. B. *Appl. Radiat. Isot.* **1996**, *47*, 497-499.
32. Bond, A. H.; Gula, M. J.; Harvey, J. T.; Duffey, H. M.; Horwitz, E. P.; Griffin, S. T.; Rogers, R. D.; Collins, J. L. *Ind. Eng. Chem. Res.* **1999**, *38*, 1683-1689.
33. Bond, A. H.; Chang, F. W. K.; Thakkar, A. H.; Williamson, J. M.; Gula, M. J.; Harvey, J. T.; Griffin, S. T.; Rogers, R. D.; Horwitz, E. P. *Ind. Eng. Chem. Res.* **1999**, *38*, 1676-1682.
34. Huddleston, J. G.; Willauer, H. D.; Boaz, K.; Rogers, R. D. *J. Chromatogr. B* **1998**, *711*, 237-244.
35. Visser, A. E.; Griffin, S. T.; Ingenito, C. C.; Hartman, D. H.; Huddleston, J. G.; Rogers, R. D. In *Metal Separation Technologies Beyond 2000: Integrating Novel Chemistry with Processing*; Liddell, K.; Chaiko, D. J., Eds.; The Minerals, Metals & Materials Society: Warrendale, PA, 1999; pp 119-130.
36. Rogers, R. D.; Griffin, S. T.; Horwitz, E. P.; Diamond, H. *Solvent Extr. Ion Exch.* **1997**, *15*, 547-562.
37. Rogers, R. D.; Bond, A. H.; Bauer, C. B. *Pure Appl. Chem.* **1993**, *65*, 567-572.
38. Spear, S. K.; Griffin, S. T.; Rogers, R. D. *J. Chromatogr. B* **1999**, Submitted for Publication.
39. Carretta, R. F. *J. Nucl. Med.* **1994**, *35*, 24N-25N.
40. Steigman, J.; Eckelman, W. C. *The Chemistry of Technetium in Medicine*; National Academy Press: Washington, DC, 1992.
41. Rogers, R. D.; Bond, A. H.; Zhang, J.; Horwitz, E. P. *Sep. Sci. Technol.* **1997**, *32*, 867-882.
42. Spear, S. K.; Griffin, S. T.; Huddleston, J. G.; Rogers, R. D. *Ind. Eng. Chem. Res.* **1999**, Submitted for Publication.

43. Rogers, R. D.; Bond, A. H.; Bauer, C. B.; Zhang, J.; Rein, S. D.; Chomko, R. R.; Roden, D. M. *Solvent Extr. Ion Exch.* **1995**, *13*, 689-713.
44. Blanchard, D. L.; Brown, G. N.; Conradson, S. D.; Fadeff, S. K.; Golcar, G. R.; Hess, N. J.; Klinger, G. S.; Kurath, D. E. *Technetium Removal and Characterization: A Progress Report*; Pacific Northwest National Laboratory: Richland, WA, 1996.
45. Schroeder, N. C.; Radzinski, S. D.; Ball, J. R.; Ashley, K. R.; Whitener, G. D. In *Metal-Ion Separation and Preconcentration, Progress and Opportunities*; Dietz, M. L.; Bond, A. H.; Rogers, R. D., Eds.; ACS Symposium Series 716, American Chemical Society: Washington, DC, 1999; pp. 219-233.
46. Chauvin, Y.; Olivier-Bourbigou, H. *CHEMTECH* **1995**, *25*, 26-30.
47. Freemantle, M. *Chemical and Engineering News* **1998**, *June 30*, 32-37.
48. Hussey, C. L. *Pure Appl. Chem.* **1988**, *60*, 1763-1772.
49. Fuller, J.; Carlin, R. T.; De Long, H. C.; Haworth, D. *Chem. Commun.* **1994**, 299-300.
50. Seddon, K. R., **1999**, private communication.
51. Bonhôte, P.; Dias, A.-P.; Papageorgiou, N.; Kalyanasundaram, K.; Grätzel, M. *Inorg. Chem.* **1996**, *35*, 1168-1176.
52. Blanchard, L. A.; Hancu, D.; Beckman, E. J.; Brennecke, J. F. *Nature* **1999**, *399*, 6 May, 28-29.
53. Dai, S.; Ju, Y. H.; Barnes, C. E. *J. Chem. Soc., Dalton Trans.* **1999**, 1201-1202.
54. Rogers, R. D.; Visser, A. E.; Swatloski, R. P.; Hartman, D. H. In *Metal Separation Technologies Beyond 2000: Integrating Novel Chemistry with Processing*; Liddell, K.; Chaiko, D. J., Eds.; The Minerals, Metals & Materials Society: Warrendale, PA, 1999; pp 139-147.

Chapter 17

Separations Research at the U.S. Environmental Protection Agency

Toward Recovery of VOCs and Metals Using Membranes and Adsorption Processes

Teresa M. Harten, Leland M. Vane, and David Szlag

**Clean Processes and Products Branch, Sustainable Technology Division,
National Risk Management Research Laboratory,
Office of Research and Development
U.S. Environmental Protection Agency,
26 West Martin Luther King Drive, Cincinnati, OH 45268**

The United States Environmental Protection Agency's National Risk Management Research Laboratory (NRMRL) is investigating new separations materials and processes for removal and recovery of volatile organic compounds (VOCs) and toxic metals from wastestreams and industrial process streams. Research applying membrane-based pervaporation to recovery of VOCs from surfactant-containing solutions has yielded results indicating that existing models for predicting required membrane surface area underestimate VOC flux across the membrane. Other research evaluated the new application of a modified commercial vibratory membrane for pervaporative removal of VOC. A software program is also being developed in NRMRL to predict pervaporation performance of commercial and research membranes for a variety of VOCs and user-selected conditions. In metals recovery research, NRMRL has targeted the metals copper, lead, nickel, and recently, mercury. Development of novel ion exchange and adsorbents for these metals and utilization of newer processes such as electrochemical ion exchange and adsorption are being investigated for some of them. Industrial streams of interest are those from metal finishing and electronics for copper, nickel and lead and from boilers, incinerators, and medical facilities for mercury.

To achieve a sustainable world, there is increasing pressure to move towards multimedia zero emissions industrial processing. Separations technologies enable

process lines to more closely approach zero emission through in-process recycling and reuse of resources that would otherwise be emitted to air, water, and solid wastes. More needs to be done however to improve options for separations and make technologies more efficient and user friendly. Mature separations technologies like distillation have been around for over 100 years; others have a much shorter history. Technologies like adsorption, extraction, membrane processes and hybrid processes offer areas of research opportunity for improving resource recovery. As energy costs increase, alternatives to distillation such as membranes and adsorption become more attractive. However, the knowledge base regarding these newer technologies is limited and needs to be expanded with basic and applied research to further advance separation processes, which in turn will encourage industry adoption. This view is consistent with the recommendations for research contained in the chemical industry's *Technology Vision 2020: the US Chemical Industry*. Under *Enabling Technologies, Process Science and Engineering Technology* (PS&ET) the report specifically calls for "nontraditional" separations systems research (1).

The Environmental Protection Agency's (EPA), Office of Research and Development, National Risk Management Research Laboratory (NRMRL) scientists and engineers are building on their existing expertise in separations technologies for removal of organics and metals from wastestreams to new applications in direct recycling and recovery in industrial process streams. This area of research is a logical evolution for an environmental engineering laboratory whose past focus in command and control technologies is changing to one of pollution prevention. Our group has recently completed two projects in remediation oriented separations. We are now extending this work to potential industrial applications for in process recycling.

Pervaporation for Volatile Organic Compound (VOC) Recovery

Background

Pervaporation is a membrane process in which a liquid containing two or more components contacts one side of a non-porous polymeric membrane while a vacuum or gas purge is applied to the other side. Components in the liquid stream sorb into the membrane, permeate through the membrane and evaporate into the vapor phase, hence the name pervaporation. The vapor, referred to as permeate, is then condensed. Literature concentration factors range from single digits to over 1000, depending on the compounds, the membrane, and process conditions. Advantages over conventional air stripping/activated carbon processes are that there are no fugitive emissions, no regeneration costs, and the VOCs can potentially be recovered for reuse (2).

NRMRL has maintained an active in-house pervaporation research program for over seven years. Early work dealt with the removal of multiple VOCs from water using existing and novel membranes. Today, we continue to develop and evaluate new membranes for pervaporation of organic compounds that aid in the recovery and reuse of those compounds. The focus of this work has been on membranes with

superior separation properties and resistance to extreme environments, such as ceramic-supported polymeric membranes.

Pervaporation to Recover Surfactant in a Contaminated Groundwater Cleanup Process

In 1995, research was initiated to determine if VOCs could be recovered from surfactant solutions. The initial focus of the work was surfactant solutions generated during a surfactant enhanced aquifer remediation (SEAR) project where surfactants are used to solubilize organic contaminants in soils/aquifers. SEAR researchers have found that efficient surfactant recycle is essential for the cost-effectiveness of this soil remediation technology. Unfortunately, serious foaming problems result when conventional technologies such as vacuum stripping are used to remove VOCs from surfactant solutions. Since a nonporous membrane separates the liquid and vapor streams in pervaporation, foam should not be generated.

After bench scale work with pervaporation processes using simulated and actual contaminated streams containing surfactant (3), NRMRL's first pilot scale testing of the technology came with a Department of Defense project. Five thousand gallons of surfactant-based soil remediation fluid containing VOCs from a test plot at Hill Air Force Base in Layton, Utah, were transported and treated at EPA's Cincinnati pilot unit which was equipped with, at first, spiral wound and, then, hollow fiber pervaporation modules. The VOC contaminated groundwater also contained an anionic surfactant (Cytec MA-80) present at 2.4wt%, isopropyl alcohol present at 1.5 wt%, and approximately 2000 mg/l sodium chloride. At a feed flow rate of 0.25 gallons per minute, 50 °C feed temperature, and 55 torr permeate pressure, up to 96% 1,1,1-trichloroethane, 95% trichloroethylene, and 88% tetrachloroethylene was removed in a single pass through the four commercial spiral wound modules. The average feed concentrations for the demonstration were 400 mg/l 1,1,1-trichloroethane, 2800 mg/l trichloroethylene, and 400 mg/l tetrachloroethylene. Similar results were seen with the hollow fiber membrane modules; however, operational advantages of the hollow fiber modules made them the module of choice for scale up.

Impact of Surfactant on Removal of VOC

As part of designing a full scale system for demonstrating pervaporation in the removal of VOCs and recovery of surfactant in SEAR processes, NRMRL has conducted additional research in NRMRL's lab to understand the impact of surfactant on VOC removal. In SEAR processes, surfactant is added at concentrations above that required to create surfactant micelles, that is, above the critical micelle concentration (CMC). These micelles act as high capacity reservoirs where organic compounds can accumulate, thereby creating a high apparent solubility of the organic compounds in the surfactant solution. Extramicellar VOC concentration is much lower than the apparent concentration and may only be a small fraction of the total VOC in the system. The flux across the pervaporation membrane is highly dependent on concentration of VOC on the liquid side of the membrane as will be explained below.

Methods for determining micellar partitioning include vapor pressure and headspace measurements, which are referenced to systems without surfactant.

NRMRL used the equilibrium partitioning in closed systems (EPICS) method to determine the micellar partitioning of VOCs (4). The method has been used to determine Henry's law constants for several VOCs using a variety of surfactants over a range of temperatures. The Henry's law constant (H_c) represents the ratio of the gas phase concentration of a VOC to that in the liquid phase. Further, the fraction of VOC in the solution which is extramolecular can be calculated from the H_c measured with surfactant and that measured without:

$$f_{ex} = H_c \text{ [with surfactant]} / H_c \text{ [no surfactant]}$$

where f_{ex} is the extramolecular fraction of VOC in the system. These experiments have confirmed the theoretical assumption that the more hydrophobic the VOC the more readily it will partition into the micelles. An example result shows that in the presence of forty times the CMC DowFax 8390, only 10% of tetrachloroethylene is extramolecular, while 40% of trichloroethane (TCA) is outside the micelles. Temperature does not appear to affect the f_{ex} .

Flux across the pervaporation membrane is often modeled as the diffusion of VOC from the bulk liquid phase through a stagnant or laminar boundary layer to the membrane surface. As a result, a steep concentration gradient develops on the liquid side of the membrane, referred to as "concentration polarization". When surfactant is added to the system, keeping constant the total VOC concentration at the membrane surface, the net effect would be to reduce the amount of VOC the membrane "sees" by a factor of f_{ex} . The activity of the VOC is reduced due to the partitioning of the VOC into the micelle. The implication for determining required membrane area for a given VOC removal is this: the membrane area required in the presence of surfactant would be $1/f_{ex}$ times the membrane area required when surfactant is not present.

NRMRL tested this simple model for predicting the change in flux due to micellar partitioning and found that it underestimated VOC flux. For example, for a system containing TCA with and without DowFax 8390 (40xCMC), we found that for TCA removal an actual value of 91% compared to the predicted 83%. Similarly, for toluene removal the actual value was 82%, whereas the predicted value was 61%. The differences between observed performance and that predicted from a simple application of the extramolecular fraction to existing pervaporation models was observed for bench and pilot scale experiments with a variety of membrane configurations. NRMRL researchers are in the process of modeling the pervaporation of VOCs from surfactant systems. The current focus of the modeling effort is to describe the effect of surfactant micelles on the transport of VOCs through the liquid boundary layer. Early indications are that the micelles act as a source of VOC in the boundary layer, yielding a less steep gradient in the boundary layer and a higher concentration of VOC at the membrane surface than predicted by current models.

This translates to a higher VOC flux and greater %VOC removal in surfactant systems than that predicted. A pictorial representation of the VOC concentration in the liquid boundary layer in the presence and absence of surfactants is shown in Figure 1 (5).

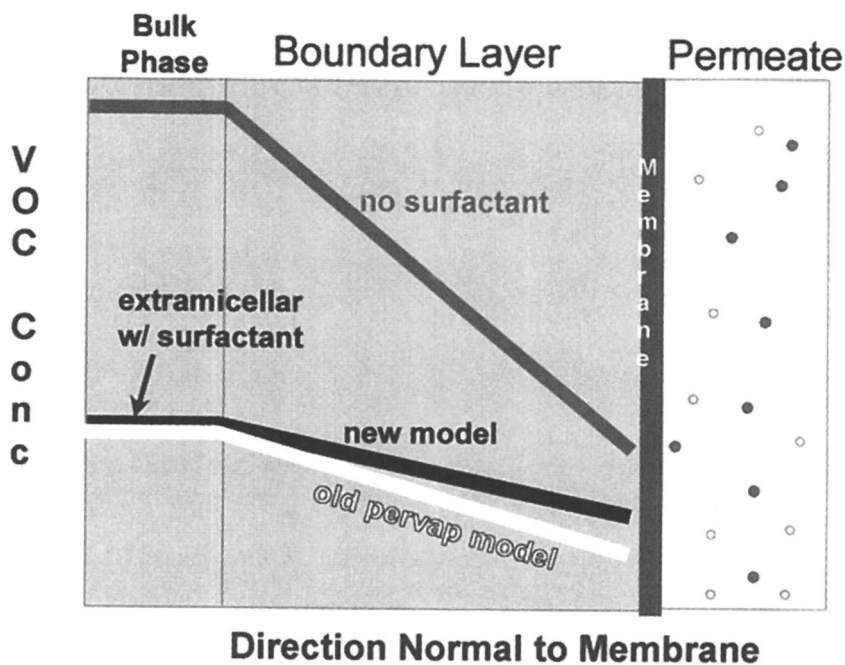


Figure 1. Qualitative Illustration of the Effect of Surfactants on the VOC Concentration in the Liquid Boundary Layer and at the Membrane Surface.

Application of a Novel Pervaporation Vibratory Membrane Module

In further preparation for scale-up of the SEAR process using pervaporation, NRMRL evaluated a variety of standard pervaporation module configurations, as well as a new vibratory membrane module. The vibratory membrane, and its novel application to a pervaporation process, was one of the most promising of module configurations. It met the dual challenge of reducing membrane fouling and reducing concentration polarization at the membrane liquid interface, thereby improving VOC mass transfer across the membrane.

The impact of concentration polarization on the performance of pervaporation processes is well known and, in particular, polarization observed during the separation of VOCs from aqueous solutions by pervaporation is particularly severe. Often, the rate of mass transfer of the VOC from the feed solution is controlled solely by the rate of diffusion through the liquid boundary layer next to the membrane surface. As a result, a significant amount of effort has been expended attempting to understand the role of the boundary layer and to engineer systems to minimize the magnitude of concentration polarization. For the traditional pervaporation modules (spiral wound, hollow fiber with lumen feed, hollow fiber with crossflow shell-side feed, and plate & frame), the liquid boundary layer mass transport coefficient is a direct function of the liquid bulk velocity. Increasing flow rates through the membrane module also increases mass transfer. For a vibratory module mass transfer improvements are achieved through an entirely different mechanism.

The vibrating membrane module was obtained from New Logic International (Emeryville, California). This module is designated as the VSEP (Vibrational Shear Enhanced Process) Series *L*. The module is similar to a plate & frame system with open channel flow. The main difference is that the entire stack of membrane "plates" vibrates rotationally about the axis of the stack at approximately 60 Hz. The edge of the stack moves a maximum distance of 1" (2.54 cm) per cycle (approx. 10° rotational amplitude for an 11" (28 cm) OD disk). Because the membrane is actually moving at the same rate as the plate, high shear rates are developed at the membrane surface. In addition, because the plate vibrates back and forth, a high level of turbulence results. Most experiments conducted at NRMRL labs were performed in the vicinity of 54 Hz. Specific travel distances were monitored and maintained for a given experiment.

Experiments were conducted for the VSEP system using several commercially available membranes and feed streams containing TCA, TCE, and PCE with and without surfactant. Similar experiments were conducted using spiral wound and hollow fiber membrane modules. In total, these experiments yielded several notable conclusions. First, the vibrating membrane produces high surface shear rates, which greatly enhance boundary layer mass transport. In this work, as little as 1/4" travel distance (approx. 3° rotational amplitude) yielded as much as a 10-fold increase in the rate of VOC mass transport. Levels of mass transport observed with the VSEP Series *L* reached and generally exceeded those observed with spiral wound modules for characteristic operating conditions. Of equal significance was the decoupling of mass transport from liquid flow rate in the VSEP system, since the shear-energy is not provided by the feed fluid. A seven-fold increase in fluid flow rate resulted in only a 10 to 30% increase in the mass transport coefficient. If mass transport could be completely decoupled from flow rate, then any configuration of a given set of

membrane modules (i.e. all in series vs. all in parallel) would yield the same level of removal. The current VSEP may have to be modified to accept existing pervaporation membrane materials or new membranes developed to work specifically with a vibrating membrane unit (6).

Novel Membrane Development

A novel elastomeric membrane for recovery of VOCs from industrial aqueous streams has been developed in at NRMRL. The new membrane can achieve a separation factor of 3000 for TCA at concentrations up to 450 mg/l. This is a 30% improvement in the separation factor of 2300 of a commercial silicone membrane used for TCA separation from water. When toluene was tested, separation factors of 3500 to nearly 6000 were seen at feed concentrations between 50 to 300 mg/l. Additional experiments using TCE showed separation factors of between 4000 and 6000 at concentrations of 50 to 300 mg/l in the feed. Permeate concentrations increased with increasing feed concentrations and at the highest feed concentration, 300 mg/l, 50 wt % and 60 wt % toluene and TCE were achieved, respectively. Generally the VOC flux was similar to commercial membranes, while the water flux was lower, hence the improved selectivity. A patent application is in progress for the new membrane and it is currently being tested in electronic chip manufacturing for removal and recovery of both VOCs and ultrapure water.

Software Development

In 1996, NRMRL began development of the Pervaporation Performance Prediction Software and Database (PPPS&D). This program is intended for membrane researchers and users of pervaporation equipment to assist in predicting the performance of the process for user-selected conditions as well as provide a database of performance characteristics of membrane materials reported in the literature. The database provides support to the simulation software by conducting physical property and performance data calculations and serving as a repository for commercial membrane information. The PPPSD is a graphical interface program designed to allow the user to determine the effect of membrane and process design changes on pervaporation performance and to provide a database of performance for commercial and research membranes. The program will also be used as a tool to educate potential users about how pervaporation works and where it can be applied. In 1998 the educational module was completed and a cooperative research and development agreement between EPA and an industrial partner, MemPro, was established to further develop and commercialize the software program. Plans are to release a bench-scale performance prediction module by the end of 1999.

Emerging Research Direction

In November 1996, NRMRL hosted a workshop in Cincinnati to discuss the potential for pervaporation in industrial organics recycle. About twenty participants from academia, government and industry drafted a list of research needs. The recommendations included the need for development of new membrane and module materials, which are capable of withstanding harsh industrial environments, for

example, development of modules for amine dehydration. Another recommendation was to investigate in-process recycle of certain industrial streams, such as acetic acid in pulp manufacturing. The use of pervaporation to dehydrate organic solvents and process streams was identified as focus area for future pervaporation research. Bench scale research was initiated in 1998 to develop performance benchmarks for existing dehydration membranes and to develop new membranes.

Adsorption for Metals Recovery

Previous Work

In 1996 NRMRL began an in-house research program to identify low-cost, highly selective adsorbents for recovery of copper and lead. This work formed the nucleus of our current in-house program directed at the recovery and in-process recycle of copper, nickel and chromium in the printed wire board and electroplating industries with possible extension to mining and primary metals manufacturing industries. Although the original program was narrowly focused on remediation applications, the capabilities and methods that were developed have many pollution prevention applications.

NRMRL's early research for low cost lead and copper adsorbents screened a variety of inexpensive alternatives, such as 1) forestry and pulp industry byproducts, such as steam exploded wood and lignin, 2) modified granular activated carbon (GAC), 3) granulated tires, 4) hydroxyapatite, and 5) chitosan beads. On the basis of cost versus metal capturing capacity, lignins proved to be particularly effective lead sorbents. Studies were undertaken to identify the best way to use these types of materials. The adsorption of lead, copper, cadmium, zinc, and calcium ions from aqueous solution onto a variety of lignochemicals was investigated (7). Metal capacities were determined from Langmuir adsorption isotherms. The adsorption capacity for Pb(II) from a 0.02 M total acetate solution at pH 4.7 was highest for a carboxymethyl ether lignin (CML) followed by: hardwood Kraft Lignin > hydroxymethyl lignin (hydrolytic sugar cane bagasse) > hydrolytic peanut hull lignin > Kraft pine lignin > hydrolytic yellow poplar lignin > hydroxypropyl ether Kraft pine lignin. Capacities ranged from a high of 192 mg Pb / gram lignochemical to approximately 20 mg Pb /gram lignochemical. The adsorption process was pH-dependent in the range 3.7 to 4.7 and was believed to be primarily due to ion exchange. At subsaturating conditions, the carboxymethyl ether lignin derivative displayed the following selectivity sequence: Pb > Cu > Cd > Zn >> Ca. Although they do not have as high a capacity nor are they as chemically stable as commercial resins, many lignochemicals and in particular the carboxymethyl ether lignin derivatives, might prove cost-effective in applications where the adsorbent is not regenerated after it is exhausted.

Many waste or agricultural by-products that have been investigated as low-cost sorbents by USEPA and other groups are powdered materials with particle sizes from 10 μm to 100 μm . These types of materials do not perform well in long fixed beds because of the high-pressure drops associated with small particle sizes and/or

compressible materials. Multi-stage mixer-settler operations with these materials are also difficult due to the small particle size and slow settling. To circumvent these problems, we demonstrated that it is possible to immobilize a variety of fine powdered sorbent materials in reticulated polyurethane foam (RPF) while retaining metal binding capacity. The composite can contain up to 50% sorbent and still maintain a reticulated foam morphology. If the polyurethane is used as a binder only, than loadings up to 90% are possible.

In September 1996, EPA and NASA conducted a joint pilot-scale soil washing/adsorption study at a small arms firing range. Two ion exchange materials were tested for their ability to remove lead from the soil washing solution so that it may be recycled back to the process. One ion exchange material was the EPA-developed RPF-CML discussed above, and the other was a NASA-developed ion exchange material made from polyacrylic acid entrapped in cross-linked polyvinyl alcohol beads. The pilot unit consisted of two 0.8 ft³ columns, operated at a flow rate of 1 gpm and successfully removed lead from the soil wash solution. The estimated cost to treat the soil wash solution was \$26/1000 gallons and \$60/1000 gallons, for the RPF-CML and NASA material respectively. Although adsorbents were not regenerated in the pilot scale demonstration, regeneration of these same materials was demonstrated in the laboratory. The lab-scale regeneration studies indicated that costs could be significantly reduced if regeneration were employed in the field.

Ongoing Research

NRMRL's current focus is on the recovery of metals and the maintenance of process solutions used in the metal finishing and other industries. This has become important not only as a means of meeting stricter regulations but also as a means of improving competitiveness. A nearly zero discharge or closed-loop process is usually desired. This is illustrated schematically in Figure 2. To achieve closed-loop operation: 1) water use must be minimized, 2) metals must be recycled "in-process" or recovered, and 3) contaminants must be removed from the process bath. The reversible nature of ion exchange and sorption processes make them particularly suited to these applications. Two key factors determine the effectiveness of a given sorbent material: selectivity for the target metal ion and the number of active sites available for exchange. Regeneration of the sorbent material lowers costs and allows the target metal ions to be concentrated and purified in the regeneration effluent. The general objective of this program is to address pollution risk by advancing the understanding of the chemistry and the engineering of sorption based metals separations. Through our sorption based separation projects NRMRL hopes to identify new and novel pollution prevention applications, provide tools and information to evaluate the performance of sorption based unit operations, and increase end-user confidence in these technologies through small-scale demonstrations.

NRMRL's separation program for metals recovery can be divided into four main project areas. The first project area is the investigation of new adsorbents for plating bath maintenance and metals separation. A variety of functional groups including hydroxamic acids, thiosemicarbazides, and ionic polymers are being attached to polyurethane films and foams, cellulosic particles for filter aids, and membranes (8). The second project area is focused on the investigation of a continuous ion exchange

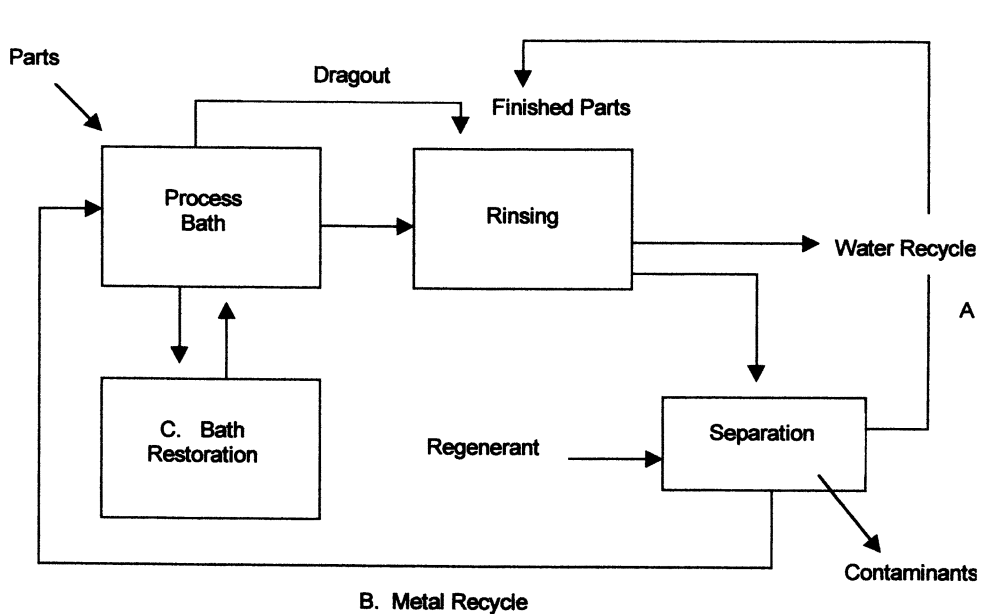


Figure 2. Recycle Opportunities in Metal Finishing

process based on a continuous moving belt which passes through separate sorption, regeneration, and conditioning stages. The third project area is focused on combining electrochemical and ion exchange systems into hybrid unit operations. The fourth project area is focused on sorbents and systems for the recovery of mercury from liquid streams originating in boilers, incinerators and medical facilities.

Novel Ion Exchange Materials

NRMRL is investigating the properties of polymeric ion exchangers attached to cellulose, membranes and small silica particles. Current focus is on synthesizing a number of sorbents based on hydroxamic acid and polyethylenimine. These groups are highly selective for copper/iron and copper respectively. In the future NRMRL will investigate the possibility of using molecular imprinting to enhance the selectivity of these functional groups or to switch the metal selectivity. Metal ion imprinted polymers (MIIPs) can be derivatized from polymeric particles with a ligand imprinted with a metal ion. Alternatively, MIIPs can be formed by seed polymerization with a metal-ligand complex as a monomer; the imprinted ligand groups reside predominantly on the surface of the polymeric particles. Seed polymerization is capable of yielding highly uniform polymeric particles. Pore size, particle size, and surface area can be controlled. Some of the imprinting work is being done in collaboration with the University of Arizona through a cooperative research agreement.

One of the novel aspects of this research is that it involves attaching a variety of highly selective functional groups to unconventional sorbent forms such as foams and derivatized membranes. These sorbents when incorporated into hybrid systems offer the potential benefits of faster kinetics, smaller size and lower cost. The main project objectives are: (1) to synthesize highly selective and high capacity ion exchange materials from ionic polymers and (2) to incorporate them into novel mass transfer unit operations such as membranes and continuous ion exchange systems. At present NRMRL has synthesized several types of polyethylenimine-cellulose and hydroxamic acid-cellulose ion exchangers. Both materials show a remarkable selectivity for copper over a broad range of conditions.

The mercury projects are exploratory in nature and are focused on the development of sulfur containing membranes and sorbent particles. The objective of this sub-project is to rapidly evaluate existing thiol and thiourea functional groups for Hg selectivity and ease of regeneration.

Integration of Electrochemical Processes

Two commercial electrochemical processes are currently being evaluated. The Electrochange system developed by Faratec, Inc. is pilot scale electrochemical ion exchange cell. The RenoCell developed by Renovare International Inc. is a high surface-area electrowinning cell based on novel radial flow design through a carbon felt cathode. Ultimately, NRMRL will incorporate highly selective ion exchange electrodes into both devices and apply them to bright nickel rinse water and electroless copper and electroless nickel plating rinses and plating baths. The main objectives of this project are:

1. Determine the composition of the effluent from the Electrochange and

RenoCell as a function of waveform applied, ion exchange functionality, and starting composition.

2. Determine the composition of the regenerant from the Electrochange and RenoCell as a function of waveform applied, ion exchange functionality, and starting composition.
3. Determine the cost effectiveness of the basic technology and the EPA modified technology on both acid copper and electroless copper plating processes and bright nickel and electroless nickel plating baths and rinses.

Pilot units from Faratech and Renovare have been constructed and delivered. Batch tests with the RenoCell have been completed on acid copper plating bath rinse water and Watts nickel plating bath rinse water. Very rapid and almost complete removal of copper was achieved with the RenoCell at moderate current densities. Removal of nickel was demonstrated but was less efficient due to the competing reaction generating hydrogen gas.

Continuous ion exchange (CIX)

For some applications of ion exchange, beads or particles may not be the best configuration (9). The advantage of a foam is the ability to utilize different unit designs. Continuous moving beds (i.e., an endless belt) can be used, or floating particles (similar to duck weed floating on a pond) can be utilized. The continuous ion exchange concept for these resins involves immobilizing the resin on a moving belt that passes through an adsorption stage, a regeneration stage combining acid regeneration with electrowinning and a rinse or conditioning stage during which any residual acid is neutralized (10). This system is simple to operate (one motor to drive the belt) and easy to understand mechanically. For the bench-scale tests, the system was run in batch mode (300 ml capacity). In this mode of operation, the adsorption stage is charged with rinse water containing the target metal and then the belt is allowed to make repeated passes through the same solution. An exponential decrease in the metal concentration occurs. In actual practice, the system would be operated with continuous flow to and from the adsorption stage. Proof of concept experiments have shown that metals are removed according to their affinity series and that polyurethane belts containing immobilized polyacrylic acid can achieve very rapid and almost complete removal of Pb and Cu. Nickel is generally not removed by the polyacrylic acid ion exchange material in the presence of lead and copper. Regeneration of the belt with acid (0.2 M HCl) achieved only a moderate fraction of regeneration (50%). These results show the feasibility of this approach. However, more work needs to be done to minimize the carryover and cross contamination of the regeneration and rinsing stages. In the next phase of this project NRMRL will incorporate functional groups that are selective for copper, iron, and/or zinc into the belt and use CIX for the continuous purification of nickel plating baths. Simultaneously, NRMRL is investigating conductive belt materials to facilitate electrochemical regeneration.

Summary

The NRMRL research program in separations has emphasized work in pervaporation for VOC removal and recovery and adsorption for metals removal and recovery. In pervaporation research a key recent finding is that a simple model for predicting VOC removal in the presence of surfactant underestimated the actual amount VOC removed. In NRMRL experiments the underestimate was 8% for TCA and 21% for toluene. In other experiments a vibratory membrane showed promising performance in terms of VOC mass transfer, apparently through reduction in membrane fouling and reduction in the concentration polarization effect. Investigation of a new elastomeric membrane showed significant improvements in VOC selectivity as compared to commercial membranes, primarily through a lower water flux. In metals adsorption and recovery research NRMRL has synthesized polyethylenimine-cellulosic and hydroxamic acid-cellulose ion exchangers, some of which show selectivity for copper over a range of conditions relevant to metal finishing rinse stream recovery. In addition, an electrochemical ion exchange hybrid system demonstrated complete removal of copper at moderate current densities; nickel was more difficult to remove.

Separations research at EPA-NRMRL is being redirected from remediation applications to in-process recycling applications, making separations research a cornerstone of in-house pollution prevention research. The focus of this pollution prevention research in the past has been on source reduction through substitution of less toxic chemicals and processes. However, in cases where more environmentally benign substitute chemicals and chemical processing methods are either not available or are not accepted by the manufacturing community, separations technologies which allow industrial processes to approach zero emissions are needed immediately. In addition, even in cases where processes have been modified by substitution of cleaner chemicals, there will be a need to insure resource conservation through near zero emissions processing.

Literature Cited

1. American Chemical Society, American Institute of Chemical Engineers, Chemical Manufacturers Association, Council for Chemical Research, Synthetic Organic Chemical Manufacturers Association, *Technology Vision 2020 The US Chemical Industry*, Dec., 1996.
2. Vane, L.M. In *Standard Handbook of Hazardous Waste Treatment and Disposal, 2nd Edition*, Freeman, H., Ed., Mc Graw Hill: NY, 1997; pp 7.60-7.72.
3. Jiang, J.S.; Vane, L.M.; Sikdar, S.K.; *J. Mem. Sci.*, **1997**, *136*, 233-247.
4. Vane, L.M.; Giroux, E.L. *J. Chem. Eng. Data*, **2000**, *45*, 38-47.

5. Vane, L.M.; Giroux, L.; Alvarez, R.; Hitchens, L. *Surfactant-Based Separations: Science and Technology*, ACS Symposium Series No. 740, American Chemical Society: Washington, DC, 2000, pp 57-75.
6. Vane, L.M.; Alvarez, F.R.; Giroux, E.L. *J. Mem. Sci.* **1999**, *153*, 233-241.
7. Szlag, D.C.; Bless D.R.; unpublished.
8. Szlag, D.C.; Rotching K.; and Bedrossian M.; AIChE Spring Meeting, New Orleans, LA, March, 1998.
9. Szlag, D.C.; Wolf, N.J. *Clean Products and Processes*, **1999**, *2*, 117-131.
10. Szlag, D.C.; Wolf, N.J. Poster presented at the 41st Gordon Research Conference on Separation and Purification, New-London, NH, 1998.

Author Index

- Anastas, Paul T., 1
Beckman, E. J., 78
Bersin, Richard L., 29
Chuang, Steven S.C., 136
Cormier, W. E., 159
Dong, H., 8
Ellison, Matthew M., 18
Farrauto, Robert J., 149
Flytzani-Stephanopoulos, Maria, 174
Gooch, J. W., 8
Griffin, Scott T., 206
Hâncu, D., 78
Harten, Teresa M., 222
Heine, Lauren, 1
Hobb, Terry, 111
Huang, Y. L., 42
Huddleston, Jonathan G., 206
Huh, Jin Young, 18
Jones, Roger, 124
Kondura, Mahesh V., 136
Lesser, Alan J., 111
Li, Y. E. David, 62
Lou, H. H., 42
Marcus, B. K., 159
Nikles, David E., 18
Paganessi, Joseph E., 62
Parakka, James P., 18
Poehein, G. W., 78
Powell, C., 78
Power, Adam, 18
Rajewski, Roger, 96
Ribeiro, Fabio H., 192
Rogers, Robin D., 206
Rufin, Denis, 62
Saim, Said, 96
Schork, F. J., 8
Stella, Valentino J., 96
Somorjai, Gabor A., 192
Spear, Scott K., 206
Subramaniam, Bala, 96
Swatloski, Richard P., 206
Szlæg, David, 222
Visser, Ann E., 206
Wang, S. T., 8
Willauer, Heather D., 206
Williamson, Tracy C., 1
Wu, X., 8
Zhu, Tianli, 174

Subject Index

A

- Acid rain. *See* Sulfur dioxide
- Acids elimination. *See* Wafer processing
- Acrylate formulations
- magnetic tape, 22*t*, 23
 - monomers for magnetic tape preparation, 20–21
 - tensile properties of cured, 23*t*
- Aerosol spray extraction system (ASES), spray process, 98
- Ag-Pd/C catalyst. *See* Oxidative carbonylation of aniline
- Amorphous orientation, poly(ethylene terephthalate) (PET) fibers, 120–121
- Aniline. *See* Oxidative carbonylation of aniline
- Anthraquinone/anthrahydroquinone process
- producing hydrogen peroxide, 80
 - target for CO₂ technology, 81*f*
- See also* Hydrogen peroxide
- Aqueous biphasic extraction chromatography (ABEC), resins, 208, 214–215
- Aqueous biphasic systems (ABS)
- binodals for salt/polymer combination, 209–210
 - chaotropic (water-destructuring) ions, 210
 - chromatographic separation of ⁹⁹TcO₄⁻ from 4M NaOH, 212*f*
 - common features of liquid/liquid extraction methods, 208
 - elution curves for ⁹⁹MoO₄²⁻ and ^{99m}TcO₄⁻; demonstrating separation and recovery, 214*f*
 - estimating effectiveness of given ABS for separation, 210, 211*f*
 - favorable properties of poly(ethylene glycol) (PEG), 210, 212
 - partitioning of organic solutes to PEG-rich phase of ABS correlation with 1-octanol/water partition coefficient, 211*f*

- phase diagrams of four PEG/salt ABS, 209*f*
 - retaining practical advantages of liquid/liquid extraction, 209
 - salting-out of polymers (PEG-2000) with cosmotropic salts producing ABS, 209*f*
 - separation and recovery of TcO₄⁻ from Hanford tank wastes, 214–215
 - separation of TcO₄⁻ from MoO₄²⁻, 213*f*
 - TcO₄⁻/MoO₄²⁻, ReO₄⁻/MoO₄²⁻, and ReO₄⁻/WO₄²⁻ separations for radiopharmacy and hydrometallurgy, 212–214
 - utilizing ABS-PEG, 210, 212
 - water soluble polymers forming ABS, 209
- See also* Separations research
- Automobile cold start, zeolite as trap, 165

B

- Benign chemicals, ENVIRO™ process, 38
- Birefringence, poly(ethylene terephthalate) fibers, 120
- 2-Butanone (MEK), magnetic tape coating formulations, 19

C

- Capture and recycle
- emission reduction technology, 68*t*
 - perfluorocompound (PFC) emission reduction, 67
- See also* Perfluorocompounds (PFCs)
- Carbamate synthesis
- formation of methyl *N*-phenyl carbamate, 142
 - reaction, 137
- See also* Oxidative carbonylation of aniline

Carbon dioxide technology

- capital and operating costs, 78
- critical point for CO₂, 113
- hydrogenation of functionalized anthraquinone (FAQ) in CO₂, 84, 86
- hydrogen peroxide, 80–89
- metal refining, 89, 91–93
- oxidation of functionalized anthrahydroquinone (FAQH₂) in CO₂, 89, 90*f*
- process characteristics amenable to use of CO₂, 79
- process constraints minimizing energy and capital costs, 79
- subcritical and supercritical CO₂ as drawing media, 112–113
- See also* Hydrogen peroxide; Poly(ethylene terephthalate) (PET) fibers; Refining of metals; Supercritical carbon dioxide; Supramics® process technology
- Carbonation of cement. *See* Cement and cement/fiber composites
- Carbonylation catalysis. *See* Oxidative carbonylation of aniline
- Catalysis. *See* Oxidative carbonylation of aniline
- Catalytic combustion, perfluorocompound (PFC) emission reduction, 66
- Cement and cement/fiber composites
 - calcium carbonation reactions in portland cements, 127
 - carbonating hydrated or cured product with carbon dioxide, 130
 - cedar shake look-alike, 130–131
 - coal ash for producing, 125
 - economics of Supramics® process, 131–133
 - efficiency of Supramics® process, 131–132
 - fiberglass-reinforced ceramic wall-board, 131
 - fully carbonated, fiberglass-reinforced hydraulic cement/fiber composites, 126–127
 - green business/green manufacturing, 125
 - ground rules for manufacturing by Supramics® process technology, 125–126
 - hindrances to ash and CO₂ use, 132–133
 - industrializing reaction, 128, 130
 - project test site, 126
 - reaction of supercritical carbon dioxide with metal hydrates, 128

- sample mix design for Supramics® precursors, 128*t*
- schematic of Supramics® process, 129*f*
- separating CO₂ for use in manufacturing process, 130
- supercritical carbon dioxide for carbonation, 127
- use of fly ash, 132
- See also* Supramics® process technology

Ceria catalysts

- activity/selectivity of Cu- and Ni-Ce(L-a)Ox catalysts for SO₂ + CH₄, 188
- addition of Ni or Cu to Ce(La)Ox, 179, 181
- ceria and La-doped ceria for SO₂ reduction, 177
- CH₄-TPR (temperature-programmed reduction) of pre-sulfated Ce(L-a)Ox, 5%Ni-Ce(La)Ox, 5%Cu-Ce(L-a)Ox, 185*f*
- characterization, 181, 184
- direct conversion of methane into syngas using CeO₂, 188
- experimental, 176
- fluorite oxide-type structure for 5%Cu- and 5%Ni-Ce(La)Ox samples, 182*f*
- O1s and S2p XP spectra of fresh and used catalysts, 183*f*
- physical properties, 179*t*
- reduction of pre-sulfated catalysts by CH₄, 184, 186*f*, 187
- scanning transmission electron microscope/energy dispersive X-ray spectroscopy (STEM/EDS) of used Ni-Ce(La)Ox, 183*f*
- SO₂ reduction to elemental sulfur by CO, 175
- See also* Sulfur dioxide
- Chemical synthesis, cumene using zeolites, 166–168
- Chlorofluorocarbons (CFC)
 - optimizing catalyst performance for hydrodechlorination, 196
 - rate determining step for hydrodechlorination, 198
 - reactivity of C–Cl bond, 193–194
 - reviews of catalytic chemistry, 193
 - See also* Hydrodechlorination of chlorofluorocarbons (CFC)
- Cleaning model, dirt removal and chemical consumption, 45
- Coal ash, production of ceramic composites, 125

- Coating process
 suspension using supercritical CO₂,
 106–107
See also Supercritical carbon dioxide
- Cold start, automobile, zeolite as trap,
 165
- Combustion, clean
 air-to-fuel weight ratio, stoichiometric($I=1$), 150
 catalytic assisted thermal combustion
 in gas turbine, 155–156
 conversion of pollutants at $I=1$, 151*f*
 Cu on zeolite as catalyst for HC–NO₂
 reduction, 152
 developing lean burn gasoline engines,
 150
 development of suitable catalysts for
 reducing NO_x with hydrocarbons,
 150, 152
 fuel cell, 152–155
 hydrocarbon reaction with O₂, 152
 lean burn engines, 150–152
 natural gas as preferred fuel, 154
 nickel catalyzed steam reforming, 154
 operation of fuel cell, 153*f*
 producing H₂ from sulfur-containing
 hydrocarbons, 154–155
 proton exchange membrane (PEM)
 fuel cell, 154
 secondary reformer generating more
 heat and H₂, 155
 status of current platinum and copper/
 zeolite (Cu-ZSM-5) catalyst technol-
 ogies using propylene, 151*f*
 transportation consuming energy and
 generating pollution, 149
 turbine generating electricity, 157*f*
 weight, size, and transit operations for
 fuel cell systems, 155
- Combustion abatement
 emission reduction, 68*t*
 perfluorocompound (PFC) emission re-
 duction, 65–66
- Computer-chip industry. *See* Wafer pro-
 cessing
- Contaminated groundwater cleanup, sur-
 factant recovery, 224
- Continuous ion exchange (CIX), metals
 recovery, 233
- Copper
 early research for low cost adsorbents,
 229–230
See also Metals recovery
- Crystallization, poly(ethylene terephthal-
 ate) fibers, 115–117
- Cumene
 catalysts, 166*t*
 precursor for synthesis of phenol, 167,
 168
 synthesis using zeolites, 166–168
 synthetic scheme, 167
 zeolite-based catalysts, 168*t*
See also Zeolites
- Cupping, curling magnetic tape, 20
- Curing mechanism, oil-based coatings, 8
- Cyclosporin A, dosage forms, 97
- ## D
- Diesel engines
 lean burn, 150
 NO_x conversion, 163, 165
- Dimethyl sulfoxide (DMSO)
 producing solvent-free drug micro-
 and nanoparticles, 103, 106
See also Supercritical carbon dioxide
- Drawing fibers. *See* Poly(ethylene tereph-
 thalate) (PET) fibers
- Drop nucleation, miniemulsion polymer-
 ization, 9
- Drug delivery, nanoparticles, 97
- Drugs. *See* Pharmaceutical industry
- Ductility, poly(ethylene terephthalate)
 (PET) fibers, 117–119
- ## E
- Economics
 analysis of magnetic tape manufactur-
 ing, 26–27
 capital and operating costs with CO₂
 in hydrogen peroxide preparation,
 80
 minimizing operating costs in oxida-
 tive carbonylation of aniline, 146
 potential cost savings of ENVIRO™,
 40
 process constraints minimizing energy
 and capital costs in CO₂ technology,
 79
 Supramics® process technology,
 131–133
- Electrochemical processes, integration,
 metals recovery, 232–233
- Electron beam-cured process, sol-
 ventless, magnetic tape manufacturing,
 19–20
- Electroplating operations
 applications, 52, 59

- classifications of current source reduction strategies, 43, 48
- cleaning model, 45
- collaboration for green engineering in industry, 43
- complete dynamic simulation of 20 barrels of parts cleaning in soak cleaning tank, 60*f*
- consumption of chemicals and water, 42
- data input window for parts, 57*f*
- drag-out minimization during zinc-acid plating, 54*f*
- estimating surface tension based on experience, 48
- example of cleaning and rinsing steps, and plating unit, 56*f*
- first window of OP2EP (optimal pollution prevention in electroplating plants) system, 53*f*
- fuzzy rules for qualitative analysis, 47–48
- illustration of rule evaluation by fuzzy logic, 49*f*
- limited success in source reduction strategies, 43
- minimizing consumption of freshwater, chemicals, and energy, 50
- OP2EP–environmental decision support system, 48, 50
- plating model, 46–47
- process modeling for quantitative analysis, 45–47
- process waste and source reduction, 43, 45
- qualitative analysis, 52
- quantitative analysis, 52, 59
- rinsing model, 46
- rule for drag-out minimization, 47
- soak cleaning tank, 58*f*
- structure of tool OP2EP, 51*f*
- system analysis of waste minimization, 55*f*
- typical electroplating process, 44*f*
- Emission reduction
- comparison of different PFC technologies, 68*t*
 - strengths and weaknesses of strategy, 68*t*
 - See also* Perfluorocompounds (PFCs)
- Emulsion polymerization, particle nucleation and monomer transport, 9
- Energizing gas, ultrasonic nozzles, 99, 101
- Engines, lean burn, 150–152
- Environment, green chemistry protecting, 1
- Environmental benefits, CO₂ processing for fibers, 112
- Environmental Protection Agency's National Risk Management Research Laboratory (NRMRL). *See* Separations research
- Environmental research, reduction of nitrogen oxide gases, 163
- Environmentally benign. *See* Electroplating operations
- ENVIRO™ processing
- introduction, 34, 36, 38
 - potential cost savings, 40
 - stripping process, 36
 - using benign chemicals, 38
 - See also* Wafer processing
- Equilibrium partitioning in closed systems (EPICS) method, determining micellar partitioning of volatile organic compounds, 225
- Etching. *See* Wafer processing
- Extraction methods, common features of liquid/liquid, 208
- F**
- Fiber-reinforced cement, Supramics® product, 126–127
- Fibers
- development of high strength, 112
 - See also* Poly(ethylene terephthalate) (PET) fibers
- Flavors, zeolites, 168–169
- Flue gas desulfurization (FGD) systems
- sulfur dioxide emissions, 174
 - See also* Sulfur dioxide
- Fly ash, use in concrete, 132–133
- Fragrances, zeolites, 168–169
- Fuel cells
- alternative to combustion, 152
 - natural gas preferred fuel, 154
 - nickel catalyzed steam reforming, 154 operation, 153*f*
 - producing H₂ from sulfur-containing hydrocarbon, 154–155
 - proton exchange membrane (PEM), 154
 - secondary reformer generating heat and H₂, 155
 - weight, size, and transit operations, 155
 - See also* Combustion, clean

Functionalized anthraquinones. *See* Hydrogen peroxide

G

Garbage to goods, Supramics® process, 133

Gas antisolvent (GAS), recrystallization process, 98

Gases, global warming potentials, 63*t*

Gas turbine

catalytic assisted thermal combustion, 155–156

electricity generation, 157*f*

Glass fiber-reinforced cement, Supramics® product, 126–127

Global perspectives

conference theme, 2

Supramics® process technology, 133

Global warming

natural “greenhouse effect”, 63

United States pursuing course to limit gases, 64

Global warming potentials, gases, 63*t*

Green chemistry

adoption by industry, 1

categorizing approaches, 3–5

definition, 1

economics driven, 125

ENVIRO™ process, 38

protecting human health and environment, 1

Green Chemistry and Engineering Conference

“Global Perspectives” theme, 2

“Implementing Vision 2020 for Environment” theme, 2

organizing committee, 2

Greenhouse effect, gases, 63

Greenhouse gases

absorbing emitted infrared, 63

altering climate, 63–64

Groundwater cleanup, contaminated, per-vaporation to recover surfactant in, 224

H

Hanford radioactive tank wastes, separation and recovery of TcO_4^- , 214–215

Hazardous air pollutants, magnetic tape manufacturing, 19

Homogeneous catalysts, zeolites, 169

Human health, green chemistry protecting, 1

Hybrid miniemulsion polymerization definition, 10

See also Water-borne coatings via hybrid miniemulsion polymerization

Hydrocarbons, development of catalysts for reducing NO_x , 150, 152

Hydrocortisone

scanning electron micrograph (SEM)

of particles recrystallized from dimethyl sulfoxide (DMSO) using capillary nozzle, 102*f*, 103

SEM of particles recrystallized from DMSO using ultrasonic nozzle and CO_2 , 103, 104*f*

whisker-shaped particles, 103, 104*f*

See also Supercritical carbon dioxide

Hydrodechlorination of chlorofluorocarbons (CFC)

blank experiments, 195

calculating number of free sites, 198

CFCs in study, 195

conversion as function of time for reactivity studies, 195–196

experimental methods, 194–195

HCl inhibiting reaction, 199, 200*f*

heterogeneous catalysis alleviating pollution problem, 193

hydrodechlorination of CF_3-CCl_3 (CFC 113a) on Pd foil, 201*t*

hydrodechlorination of CF_3-CFCl_2 (CFC 114a) on Pd foil, 198*t*

hydrodechlorination of $CF_3-CFClH$ (CFC 124) on Pd foil, 199*t*

linear relationship between square of concentration and time, 197*f*

optimizing catalyst performance for chemistry of hydrodechlorination, 196

Pd polycrystalline foil in study, 194–195

rate determining step, 198

rates decreasing with increasing conversion, 197*f*

rates for CF_3-CFCl_2 (CFC114a) over Pd catalysts, 196*t*

rates for family of compounds for standard reaction condition, 201, 202*t*

rates on foil and single crystals in high pressure batch reactor, 194

reactivity of C–Cl bond, 193–194

square of number of turnovers versus time, 200*f*

- substitution of chlorine by hydrogen, 193
- understanding reaction selectivity, 194
- Hydrogen peroxide
 - anthraquinone/anthrahydroquinone process, 80, 81*f*
 - capital and operating costs with CO₂, 80
 - cloud point curves of di-amido FAQ (functionalized anthraquinone), 85*f*
 - dependence of cloud point curves on molecular weight of CO₂-philic tail, 84
 - experimental, 82
 - experimental and regressed effect rate constant for group of amide-FAQs with different length CO₂-philic tails, 87*f*
 - FAQ with CO₂-philic tail and spacer, 82, 83*f*
 - hydrogenation of FAQ in CO₂, 84, 86
 - influence of linker on phase behavior of FAQ, 84, 85*f*
 - kinetic and mass transfer parameters determined by regression, 88*t*
 - mass transfer effects, 86, 89
 - overall effectiveness factors for hydrogenation of FAQs in CO₂, 88*t*
 - oxidation of functionalized anthrahydroquinone (FAQH₂) in CO₂, 89, 90*f*
 - phase diagrams of FAQs in study, 83*f*
 - use of CO₂-based process, 80
 - See also* Carbon dioxide technology
- Hydrometallurgy, TcO₄/MoO₄²⁻, ReO₄/MoO₄²⁻, and ReO₄/WO₄²⁻ separations, 212–214
- Hydrophobe/surfactant system
 - miniemulsion polymerization, 9
 - retarding Ostwald ripening, 9

I

- Ibuprofen, scanning electron micrograph (SEM) of particles recrystallized from dimethyl sulfoxide (DMSO) using ultrasonic nozzle and CO₂, 103, 105*f*
- Industry, adoption of green chemistry, 1
- Information superhighway, high technology industry, 19
- Ion exchange materials, metals recovery, 232
- Isocyanate, route without phosgene, 137

L

- La-doped catalysts. *See* Ceria catalysts
- Lead
 - early research for low cost adsorbents, 229–230
 - See also* Metals recovery
- Lean burn conditions, NO_x conversion, 163
- Lean burn engines, 150–152
- Liquid/liquid extraction methods
 - common features, 208
 - favorite choice for separation processes, 207
 - practical advantages, 209

M

- Magnetic tape manufacture
 - accelerated aging study of Formulotion 1 using 60°C and 90% relative humidity, 24*f*
 - acrylate formulations, 22*t*, 23
 - acrylate monomer and oligomers in study, 21*t*
 - anchoring coupling agent to particle surface, 25
 - coating fluid with rheology comparable to conventional solvent-based, 24*f*
 - commercial acrylate-functionalized silane coupling agent (Z-6030) bonded to surface of iron particles, 25
 - comparison of hourly cost of operation, 27*t*
 - composition, 18
 - cupping problem, 20
 - dispersions preparation using particles treated with Z-6030, 25
 - economic analysis, 26–27
 - experimental, 20–22
 - film curing method, 21
 - film testing methods, 21
 - hourly materials consumption and costs for solventless process, 27*t*
 - magnetic dispersions preparation, 21
 - magnetic particles, 21
 - material problems to be solved, 20
 - organic solvents in formulations, 19
 - preparation, 19
 - rheological properties of magnetic dispersions by oscillating shear rheometry, 21–22

- rheology of magnetic coating fluids, 25–26
- solvent capture versus release, 19
- solvent recovery, 19
- solventless dispersions, 23, 25–26
- solventless electron beam-cured process, 19–20
- tensile properties of cured acrylate formulations, 23*t*
- two-fold approach for environmentally friendly processes, 19–20
- waterborne tape coating process, 19–20
- Membrane technology**
- advantages, 74
- chemical species in process exhaust as function of time, 73*f*
- concentrations of CF₄ and C₂F₆ at inlet and outlet of membrane unit, 73*f*
- hollow fiber separation systems, 70
- kinetic diameter of different gas molecules, 70*t*
- parameters characterizing membranes, 69
- performance of Air Liquide perfluorocompound (PFC) recycle system, 71–74
- PFC recycle system, 67, 69–71
- recovery of volatile organic compounds with elastomeric, 228
- See also* Perfluorocompounds (PFCs)
- Metals.** *See* Refining of metals
- Metals recovery**
- continuous ion exchange (CIX), 233
- early research by National Risk Management Research Laboratory (NRMRL), 229–230
- integration of electrochemical processes, 232–233
- novel ion exchange materials, 232
- ongoing NRMRL's research, 230–233
- recycle opportunities in metal finishing, 231*f*
- See also* Refining of metals; Separations research
- Methane.** *See* Sulfur dioxide
- 4-Methyl-2-pentanone (MIBK), magnetic tape coating formulations, 19
- Miniemulsion polymerization**
- particle nucleation and monomer transport, 9
- polymerization mechanism, 9–10
- surfactant/hydrophobe system, 9
- See also* Water-borne coatings via hybrid miniemulsion polymerization
- Modeling**
- cleaning, 45
- flux across pervaporation membrane, 225
- plating, 46–47
- rinsing, 46
- See also* Electroplating operations
- Molecular sieve zeolites**
- properties, 160, 162*t*
- See also* Zeolites
- N**
- Nanoparticles**
- drug delivery, 97
- pharmaceutical applications, 97
- See also* Supercritical carbon dioxide
- National Risk Management Research Laboratory (NRMRL).** *See* Separations research
- Natural gas**
- fuel cell, 154
- reductant of SO₂, 175
- Nitrogen oxides (NO_x) reduction**
- development of catalysts with hydrocarbons, 150, 152
- status of Pt and Cu/zeolite using propylene, 151*f*
- use of zeolites, 163, 165
- Nitrous oxides (N₂O)**
- oxidant in direct oxidation of benzene to phenol, 168
- zeolites decomposing, 165
- O**
- One-stage drawing, poly(ethylene terephthalate) fibers, 117–119**
- Optimal pollution prevention in electroplating plants (OP2EP)**
- applications, 52, 59
- data input window for parts, 57*f*
- dynamic simulation of 20 barrels of parts cleaning in soak cleaning tank, 60*f*
- environmental decision support system, 48, 50
- example of number of cleaning and rinsing steps and plating unit, 56*f*
- qualitative analysis, 52
- quantitative analysis, 52, 59
- soak cleaning tank, 58*f*
- system analysis of waste minimization, 55*f*

tool structure, 51*f*
See also Electroplating operations
 Orientation, amorphous, poly(ethylene terephthalate) fibers, 120–121
 Ostwald ripening, hydrophobe retarding, 9
 Oxidative carbonylation of aniline
 activity of Ag promoted Pd/C (Ag-Pd/C), 146, 147*f*
 Ag-Pd/C revealing potential effect of Ag, 142
¹³C NMR analysis confirming carbamate formation, 145*f*
 carbamate synthesis, 137
 differences between oxidative and reductive carbonylation, 137–138
 experimental, 138–139
 formation of methyl *N*-phenyl carbamate, 142
 infrared (IR) spectra of dried solid diphenyl urea, 144*f*
 IR spectra of reactant/product mixture for first step of run 1, 141*f*
 major function of O₂ in reaction, 146
 minimizing operating costs, 146
 NaI in catalyst, 146
 Pd/C and Ag-Pd/C catalysts preparation, 138
 reactant and product analysis methods, 139
 reaction conditions using Pd/C and Ag-Pd/C, 140*t*
 reaction procedure, 139
 reductive carbonylation steps, 137
 route to isocyanate without phosgene, 137
 safety, 139
 solid diphenyl urea in reactant solution, 139, 142
 solving problems associated with removal of corrosive solution, 138
 transmission IR spectra of liquid samples from first step of run 2, 143*f*
 utilizing aniline, alcohol, CO, and O₂, 137

P

Palladium catalysts. *See* Hydrodechlorination of chlorofluorocarbons (CFC)
 Palladium/C catalyst. *See* Oxidative carbonylation of aniline
 Particle formation. *See* Supercritical carbon dioxide

Particle nucleation, emulsion and miniemulsion polymerizations, 9
 Perfluorocompounds (PFCs)
 advantages of membrane system, 74
 capture and recycle, 67
 cascaded membrane system, 71
 catalytic combustion, 66
 combustion abatement, 65–66
 concentrations of CF₄ and C₂F₆ at inlet and outlet of membrane unit, 73*f*
 destructive abatement, 65–67
 emission reduction options, 64–67
 etching and reactor cleaning in semiconductor manufacturing, 64
 flux, 69
 gas permeability, 69
 greenhouse gases, 63
 hollow fiber separation systems, 70
 performance of Air Liquide PFC recycle system, 71–74
 PFC capture unit, 72*f*
 PFC recycle system: membrane technology, 67, 69–71
 plasma abatement, 67
 process chemistry alteration, 64–65
 process improvement, 65
 quantification test of PFC recovery system, 73–74
 selectivity (separation factor) of membrane, 69
 strengths and weaknesses of emission reduction strategy, 68*t*
 thermal-chemical abatement, 67
See also Semiconductor manufacture
 Pervaporation
 emerging research direction, 228–229
 membrane process, 223–224
 recovering surfactant in contaminated groundwater cleanup process, 224
 software development, 228
 vibrating membrane module, 227–228
See also Volatile organic compound (VOC) recovery
 PET. *See* Poly(ethylene terephthalate) (PET) fibers
 Pharmaceutical industry
 hydrocortisone particles, 102*f*, 103, 104*f*
 ibuprofen particles, 103, 105*f*
 nanoparticles, 97
 organic solvents for recrystallizing drugs, 97
 particle formation using supercritical CO₂ (scCO₂), 97–98
 SEM micrographs of coated nonpareil

- sugar beads uniformly coated with RG503H microparticles, 108*f*
 suspension coating using $scCO_2$, 106–107
 use of ultrasonic nozzles for spray atomization, 99–106
See also Supercritical carbon dioxide
- Phenol, cumene precursor to synthesis, 168
- Phosgene, route to isocyanate without, 137
- Plasma abatement
 decomposing perfluorocompounds, 67
 emission reduction technology, 68*t*
- Plating model, quality and production rate, 46–47
- Platinum group metals (PGMs)
 purification, 89, 91
See also Refining of metals
- Poly(ethylene terephthalate) (PET)
 fibers
 amorphous orientation, 120–121
 birefringence, 120
 comparing traditional or uniaxial drawing with drawing in CO_2 , 112
 comparison of CO_2 treated, solvent treated, and untreated fibers, 122*t*
 comparison of structure and mechanical properties, 121
 crystallinity measurements, 115
 crystallization, 115–117
 crystallization differences using CO_2 compared to acetone, 116–117
 development of orientation in amorphous and crystalline phases, 120*f*
 drawability using CO_2 as drawing media, 117–118
 drawing behavior for high strength fibers, 111
 ductility and one-stage drawing, 117–119
 environmental benefits of CO_2 processing for fibers, 112
 experimental, 113–115
 fiber bundles drawn in supercritical CO_2 , 118–119
 first stage drawing procedure, 114–115
 measurements, 114–115
 melt spinning, 111
 physical characterization of two-stage drawn PET fibers, 119–121
 plasticization effect of CO_2 in amorphous phase, 119
 production of high strength fibers, 112
 sample preparation, 113
 second draw stage procedure, 115
 stainless steel high pressure drawing apparatus, 114*f*
 stress-strain behavior as function of CO_2 pressure, 118*f*
 structure of one-stage drawn fibers, 119
 two-stage drawing, 119–121
 ultrahigh molecular weight, 111
 use of subcritical and supercritical CO_2 as drawing media, 112–113
 WAXD results for CO_2 -treated fibers at various pressures, 116*f*
- Power generation. *See* Combustion, clean
- Precipitation with compressed antisolvents (PCA), recrystallization process, 98
- Process chemistry alteration
 emission reduction technology, 68*t*
 substituting perfluorocompounds with benign chemicals, 64–65
- Process improvement
 adjusting process parameters reducing perfluorocompounds, 65
 emission reduction technology, 68*t*
- Process modeling, quantitative analysis of waste generation, 45–47
- Process waste, electroplating process, 43, 45
- Proton exchange membrane (PEM), fuel cell, 154
- ## Q
- Qualitative analysis
 drag-out minimization, 47
 estimating surface tension based on experience, 48
 example of rule evaluation by fuzzy logic, 49*f*
 fuzzy rules, 47–48
- Quantitative analysis, process modeling, 45–47
- ## R
- Radioactive tank wastes
 separation and recovery of TcO_4^- , 214–215
See also Aqueous biphasic systems
- Radiopharmacy, TcO_4^-/MoO_4^{2-} , ReO_4^-/MoO_4^{2-} , and ReO_4^-/WO_4^{2-} separations, 212–214

- Raschig process, scheme, 170–171
- Recycle system
 perfluorocompound (PFC) capture unit, 72*f*
 performance of Air Liquide system, 71–74
 quantification test, 73–74
See also Perfluorocompounds (PFCs)
- Reductive carbonylation
 differences between oxidative and, 137–138
 reaction steps, 137
See also Oxidative carbonylation of aniline
- Refining of metals
 experimental, 91
 extraction of Pt or Au into CO₂, 91, 93
 liquid-liquid extraction process for platinum group metals (PGM) refining, 89, 91
 phase behavior results of two complexes using identical ligands, 92*f*
 purification of PGM, 89
 triethyl amine (TEA) as ligand, 91
See also Carbon dioxide technology; Metals recovery
- Rheology, magnetic dispersions, 21–22
- Rinsing model, wastewater minimization, 46
- Room temperature ionic liquids (RTIL)
 choice of cation, 216
 correlation of distribution ratios for ¹⁴C-labeled aromatic solutes with 1-octanol/water biphasic systems, 217*f*
 extraction of metal cations from aqueous systems using extractants, 217*f*
 green separation technology, 215
 properties, 215–216
 structural variation in 1-alkyl-3-methylimidazolium-based RTIL including crystal structure of low melting decyl derivative [dmim][PF₆], 216*f*
 studies of partitioning behavior of organic solutes in RTIL, 217
 use of RTIL in separations, 216–217
See also Separations research
- S**
- Safety
 oxidative carbonylation of aniline, 139
 wafer processing, 40
- Salting-out poly(ethylene glycol) (PEG).
See Aqueous biphasic systems (ABS)
- Selective catalytic reduction (SCR)
 NO_x conversions, 163
 operating window for SCR catalyst formulations, 164*f*
- Semiconductor manufacture
 advantages of membrane system, 74
 Applied Material 5000 processes, 72*t*
 basic design parameters, 71
 capture and recycle, 67
 cascaded membrane system, 71*f*
 catalytic combustion, 66
 chemical species present in process exhaust as function of time, 73*f*
 combustion abatement, 65–66
 comparison of different perfluorocompound (PFC) emission reduction technologies, 68*t*
 concentrations of CF₄ and C₂F₆ at inlet and outlet of membrane unit, 73*f*
 destructive abatement, 65–67
 emission reduction options, 64–67
 fiber assembly in pressure vessel, 70*f*
 hollow fiber separation systems, 70
 kinetic diameter of different gas molecules, 70*t*
 nitrogen and oxygen as fast permeating species, 69–70
 performance of Air Liquide PFC recycle system, 71–74
 PFC capture unit, 72*f*
 PFC-containing exhaust gas fed to bore side of fiber, 70*f*
 PFC recycle system: membrane technology, 67, 69–71
 plasma abatement, 67
 process chemistry alteration, 64–65
 process improvement, 65
 quantification test of PFC recovery system, 73–74
 selectivity and flux characterizing membranes, 69
 slow acceptance of new process, 38
 solution/diffusion mechanism governing transport of gas through polymeric membrane, 69
 thermal-chemical abatement, 67
See also Wafer processing
- Separations research
 adsorption for metals recovery, 229–233
 implementation of green separations technologies, 218

- liquid/liquid extraction, 207
 pervaporation for volatile organic compound (VOC) recovery, 223–229
 room temperature ionic liquids (RTIL), 215–217
 ubiquitous in every industry, 207
See also Aqueous biphasic systems (ABS); Metals recovery; Room temperature ionic liquids (RTIL); Volatile organic compound (VOC) recovery
- Silicon wafer
 manufacturing, 29–30, 32
See also Wafer processing
- Silver, Ag-Pd/C catalyst. *See* Oxidative carbonylation of aniline
- Simulations. *See* Electroplating operations
- Solvent-based coatings, superior properties, 8
- Solvent elimination. *See* Wafer processing
- Solventless electron beam-cured process
 comparison of hourly cost of operation, 27*t*
 economics, 26–27
 hourly materials consumption and costs, 27*t*
 magnetic tape manufacturing, 19–20
 preparation, 23, 25–26
 rheology of magnetic coating fluids, 24*f*, 25–26
 silane coupling agent Z-6030, 25
See also Magnetic tape manufacture
- Source reduction, electroplating process, 43, 45
- Spray atomization
 ultrasonic nozzles, 99–106
See also Supercritical carbon dioxide
- Subcritical carbon dioxide, drawing media, 112–113
- Sulfur dioxide
 acid rain, 174
 activity of ceria for SO₂ reduction by CH₄ under wet conditions, 189
 activity/selectivity of Cu- and Ni-Ce(La)Ox catalysts for SO₂ + CH₄, 188
 addition of Cu into Ce(La)Ox, 189
 catalyst characterization, 181, 184
 ceria and La-doped ceria, 177
 ceria-based catalysts, 176
 ceria-based catalysts for SO₂ reduction, 175
 CH₄-TPR (temperature-programmed reduction) of pre-sulfated Ce(La)Ox, 5%Ni-Ce(La)Ox, 5%Cu-Ce(La)Ox, 185*f*
 dry-gas activity of Ce(La)Ox and Cu- or Ni-containing Ce(La)Ox in CH₄-SO₂-He mixtures, 187
 effect of 5 wt% Ni or Cu in Ce(La)Ox under dry conditions, 180*f*
 effect of contact time on SO₂ conversion and sulfur selectivity of 5%Cu-Ce(La)Ox, 180*f*
 effect of Cu or Ni addition on selectivity of Ce(La)Ox, 188
 effect of feed CH₄/SO₂ ratio on SO₂ conversion and sulfur selectivity, 182*f*
 elemental analysis method, 176
 experimental, 176–177
 fluorite oxide-type structure in 5%Cu-Ce(La)Ox and 5%Ni-Ce(La)Ox samples, 182*f*
 formation of COS and CS₂, 188–189
 initial reduction rate measurements, 187
 natural gas reductant of, 175
 O1s and S2p XP spectra of fresh and used catalysts, 183*f*
 performance of Ce(La)Ox with addition of water vapor in feed gas, 177, 178*f*
 physical properties of catalysts, 179*t*
 reaction between SO₂ and CH₄, 175
 reaction tests in packed-bed quartz microreactor, 176
 reducibility of pre-sulfated catalysts at constant temperature, 177
 reduction of pre-sulfated 5%Cu-Ce(La)Ox by CO or CH₄ at 550°C, 186*f*
 reduction of pre-sulfated catalysts by CH₄, 184, 187
 role of metal/metal oxide clusters in working catalyst, 188
 scanning transmission electron microscope/energy dispersive X-ray spectroscopy (STEM/EDS) method, 176
 STEM/EDS of used Ni-Ce(La)Ox, 183*f*
 (SO₂ + CH₄) reaction light-off curves of 750°C-calcined CeO₂ and La-doped CeO₂, 178*f*
 TPR of pre-sulfated catalysts, 176–177
 transition metal-containing ceria catalysts, 179, 181

- use of regenerative sorbent technologies, 175
- water inhibiting methane adsorption on ceria surface, 189
- wide temperature range with or without O₂ forming surface or bulk sulfates, 187–188
- See also* Ceria catalysts
- Supercritical antisolvent (SAS)
- schematic, 100*f*
 - spray process, 98
- Supercritical carbon dioxide
- advantages of CO₂-based coating process over conventional air suspension coating, 106
 - advantages of CO₂-based coating process over conventional fluidized air based coating, 107
 - advantages of gas antisolvent/precipitation with compressed antisolvents (GAS/PCA), 98
 - advantages of scCO₂-powered ultrasonic nozzle, 103, 106
 - aerosol spray extraction system (ASES), 98
 - atomizing spray with ultrasonic nozzle, 99, 100*f*
 - demonstration of coating process, 105*f*
 - drawing media, 112–113
 - gas antisolvent (GAS) recrystallization, 98
 - generation of sound waves, 101
 - helium, supercritical CO₂, or combinations as energizing gas, 101
 - particle formation by rapid expansion of supercritical solutions (RESS), 98
 - particle formation by recrystallization, 98
 - precipitation with compressed antisolvents (PCA), 98
 - producing solvent-free drug micro- and nanoparticles using DMSO, 103
 - recrystallized hydrocortisone as long, thick, whisker-shaped particles, 103, 104*f*
 - schematic of apparatus forming drug nanoparticles, 101, 102*f*
 - schematic of SAS process, 100*f*
 - scanning electron micrograph (SEM) of coated nonpareil sugar bead coated with layer of RG503H micro-particles, 107, 108*f*
 - SEM of hydrocortisone particles recrystallized from dimethyl sulfoxide (DMSO) using capillary zone, 102*f*
 - SEM of hydrocortisone particles recrystallized from DMSO using ultrasonic nozzle and CO₂ as energizing gas, 103, 104*f*
 - SEM of ibuprofen particles recrystallized from DMSO using ultrasonic nozzle and CO₂ as energizing gas, 103, 105*f*
 - supercritical antisolvent (SAS) process, 98
 - suspension coating using scCO₂, 106–107
 - use of ultrasonic nozzles for spray atomization, 99–106
 - See also* Pharmaceutical industry; Supramics® process technology
- Supramics® process technology
- cedar shake look-alike, 130–131
 - economics, 131–133
 - energy efficiency, 131
 - fiberglass-reinforced ceramic wall-board, 131
 - global perspective, 133
 - ground rules for manufacturing, 125–126
 - process, 128, 130–131
 - products, 126–127
 - project test site, 126
 - sample mix designs for precursors, 128*t*
 - schematic of process, 129*f*
 - separating CO₂ for use in manufacturing process, 130
 - supercritical CO₂ for carbonating range of mixtures, 127
 - See also* Cement and cement/fiber composites
- Surfactant
- impact on removal of volatile organic compounds (VOC), 224–225
 - recovery in contaminated groundwater cleanup, 224
- Surfactant/hydrophobe system, miniemulsion polymerization, 9
- Suspension coating process
- using supercritical CO₂, 106–107
 - See also* Supercritical carbon dioxide
- ## T
- Tetrahydrofuran (THF), magnetic tape coating formulations, 19
- Thermal-chemical abatement
- emission reduction technology, 68*t*

- perfluorocompound (PFC) emission reduction, 67
- Thermal combustion
 - catalytic assisted in gas turbine, 155–156
 - turbine generating electricity, 157*f*
- Toluene, magnetic tape coating formulations, 19
- Transportation
 - consuming energy and generating pollutants, 149
 - See also* Combustion, clean
- Turbine, gas
 - catalytic assisted thermal combustion, 155–156
 - electricity generation, 157*f*
- Two-stage drawing
 - poly(ethylene terephthalate) fibers, 119–121
 - See also* Poly(ethylene terephthalate) (PET) fibers

U

- Ultrasonic nozzles
 - spray atomization, 99–106
 - See also* Supercritical carbon dioxide

V

- Vibrational shear enhanced process (VSEP), vibrating membrane module, 227–228
- Vision 2020 for chemical industry, conference theme, 2
- Volatile organic chemicals (VOCs)
 - benefits of alternative technologies to replace, 207–208
 - use of zeolites, 162–163
- Volatile organic compound (VOC) recovery
 - application of novel pervaporation vibratory membrane module, 227–228
 - emerging research direction, 228–229
 - equilibrium partitioning in closed systems (EPICS) method to determine micellar partitioning, 225
 - extramolecular fraction of VOC in system, 225
 - flux across pervaporation membrane, 225
 - impact of surfactant on removal of VOC, 224–225

- model for predicting change in flux, 225
- novel membrane development, 228
- pervaporation background, 223–224
- qualitative illustration of effect of surfactants on VOC concentration in liquid boundary layer and at membrane surface, 226*f*
- software development, 228
- surfactant recovery in contaminated groundwater cleanup process, 224
- vibrational shear enhanced process (VSEP), 227–228
- See also* Separations research

W

- Wafer processing
 - acids, bases, and solvents for computer-chip industry in 1997, 39*f*
 - anisotropic plasma etching defining patterns with finer degrees of dimensional control, 33*f*
 - boiling points of common etch products, 35*t*
 - combining microwave processing with RIE treatment, 34, 36
 - cross-sectional view of CMOS device with fabrication-processing steps, 31*f*
 - dry ashing and isotropic dry etching, 32
 - ENVIRO™ process technology using benign chemicals, 38
 - environmental and monetary concerns, 38, 40
 - evaluating new processes on manufacturing lines, 36, 38
 - evolution of conventional ashing to 1998, 34
 - example of etching of TiN/Al/TiW sandwich metal film, 37*f*
 - filling contact holes, 30
 - fluorine plasmas, 36
 - fundamentals of device manufacturing, 29–30, 32
 - illustrations of deposited polymers, 35*f*
 - introduction to ENVIRO™ processing, 34, 36, 38
 - microwave plasma in ENVIRO™ process, 34
 - potential cost savings for ENVIRO™ process, 40
 - processing in plasma reactor, 37*f*

removing organics without oxidation of contaminating metals, 34
 resist ash and solvent-clean step following each patterned layer, 30, 32
 safety considerations, 40
 shrinking devices and anisotropy in etching, 32, 34
 slow acceptance of new semiconductor manufacturing process, 38
 solventless processes in full production, 38
 solvents and acids removing photore-sist mask, 30
 spin rinsers-dryer, 40
 stripping process of ENVIRO™ process, 36
 typical materials for etching, 33*f*

Waste minimization
 electroplating process, 43, 45
 process waste and source reduction, 43, 45
 source reduction, 42–43
See also Electroplating operations

Water-based coatings, properties and performance characteristics, 8

Water-borne coatings via hybrid mini-emulsion polymerization
 alternative coatings with advantages of water- and solvent-based systems, 8–9
 calculation methods for degrees of grafting and crosslinking, 12
 conversion-time curves for hybrid mini-emulsion polymerization of alkyd and oil-modified polyurethane (OMPU), 13, 14*f*
 degree of grafting and degree of cross-linking, 15
 double bond content analysis by ¹³C NMR, 12
 droplet and particle size by quasi-elastic light scattering, 12
 droplet and particle size for alkyd and OMPU systems, 13
 droplet nucleation mechanism in mini-emulsion, 9
 emulsion preparation and polymerization methods, 10
 experimental materials, 10

factors determining shelf-life stability, 13
 film hardness and adhesion, 15
 film hardness and adhesion testing, 12
 OMPU/acrylate coatings, 9
 particle nucleation and monomer transport, 9
 polymerization mechanism in mini-emulsion, 9–10
 promising role in converting solvent-based coatings to environmentally friendly, 16
 residual double bond content analysis, 15
 shelf-life stability determination, 12
 surfactant/hydrophobe system in mini-emulsion, 9

Water-borne tape coating process, preventing pollution, 19–20

Z

Zeolites

ammoxidation process using hydrogen peroxide, 170–171
 automobile cold start, 165
 catalyst for HC–NO_x reduction in lean environments, 152
 cumene synthesis, 166–168
 cumene synthesis catalysts, 166*t*
 cumene synthesis catalysts, zeolite-based, 168*t*
 faujasite structure, 161*f*
 fine chemical and chemical applications, 165–169
 N₂O as oxidant in direct oxidation of benzene to phenol, 168
 nitrogen oxides (NO_x), 163, 165
 nitrous oxide (N₂O), 165
 operating temperature windows for selective catalytic reduction (SCR) catalyst formulations, 164*f*
 production of flavors and fragrances, 168–169
 properties, 160, 162*t*
 Raschig process, 170–171
 replacing homogeneous catalysts, 169
 use in green technologies, 162–169
 volatile organic chemicals (VOC), 162–163